GCM-derived Climate Change Scenarios and their Impacts on New Zealand Water Resources

This thesis is presented in partial fulfilment of

the requirements of the degree of

Doctor of Philosophy

in

Science

at

Massey University, Palmerston North,

New Zealand

Freddie Simon Mpelasoka

Massey University

2000

Abstract

The derivation of local scale climate information from experiments of coarse-resolution general climate models (GCM) can be addressed with variety of 'downscaling' techniques. 'Downscaling' refers to attempts to address the scale mismatch between information from the GCMs and that at which impacts occur. Methods for downscaling range from simple interpolation of climate model outputs to the use of regional climate models nested within larger-scale simulations. Some methods use statistical representations and interpolations; some use dynamic approaches. All of these methods depend on the quality of the initial simulation. Downscaling models fitted to present climatological records are generally referred to as empirical approaches. In a semi-dynamical approach, regional free atmospheric circulation indices simulated by a GCM were employed in this study to derive local climate variables from cross-scale relationships. The relationships were captured from historical records of simultaneously observed local variables and regional-scale circulation indices. Subsequent climate change scenarios were used in impact case studies of two New Zealand catchments' response and water resources.

The assessment of climate change impacts requires data at the spatial and temporal resolution at which impacts occur. The outputs of the current GCMs cannot be used directly in the development of specific climate change scenarios due to their coarse resolution although semi-empirical downscaling of GCM outputs to desired scales may offer an immediate solution by relating GCM outputs to single-site climate elements. Artificial neural network (ANN) and multivariate statistics (MST) models were adapted to derive the changes to a number of New Zealand site precipitation and temperature characteristics from free atmosphere circulation indices in a comparative study of their potential in downscaling outputs of GCM transient experiments. Both downscaling models capture similar general patterns from free atmosphere circulation indices.

Subsequently the ANN model was used to derive changes of mean monthly precipitation and temperature characteristics from circulation variables projected in a transient climate change experiment performed by the Hadley Centre coupled ocean-atmosphere global climate model (HadCM2). HadCM2 validated well with respect to

the National Centers for Environment Prediction reanalysis for its 'present climate' simulation. The predicted changes in seasonal mean sea level pressure fields over the 'New Zealand' region include an intensified anticyclonic belt coupled with negative pressure tendencies to the southwest, which is expected to squeeze stronger westerly winds over southern and central New Zealand.

Monthly mean precipitation and temperature time series for 18 points on a 0.25°latitude x 0.25°longitude grid over New Zealand were derived from the circulation indices. The indices were defined by anomalies (with respect to 1961-1990) of mean sea level pressure, zonal and meridional mean sea-level pressure gradients, atmospheric geopotential thickness between 850-700 hPa pressure surfaces, and wind speeds at 10 m above the surface over New Zealand for the period 1980-2099. Temperature and precipitation characteristics were examined for four tri-decades (1980-2009, 2010-2039, 2040-2069 and 2070-2099), and changes projected with respect to the pseudo-present tri-decade (1980-2009). An average temperature increase of 0.3-0.4°C per tri-decade is projected. Precipitation distribution was modelled using the Gamma probability function and the precipitation characteristics determined by the 'scale' and 'shape' parameters of the Gamma function. Precipitation is predicted to decrease over the north of North Island while marked precipitation increases are projected over the western, central and southwestern areas of the country. Changes in coefficients of variation of monthly precipitation exhibited both increases and decreases in interannual variability of precipitation over the region. Interannual variability in monthly precipitation increases to 1.2-2.2 and decreases to 0.5-0.9 times the pseudo-present coefficients of variations of monthly precipitation by 2070-2099 are projected. The tri-decade to tri-decade changes however, show no trend and this may be attributed to high frequency variations in monthly precipitation.

A water balance model was adapted to assess the impacts of changes in precipitation and temperature in two case studies of catchment response. Time series of monthly flows were simulated for each tri-decade. Data for each tri-decade were modelled using a lognormal distribution to generate a 3000-year data set, which was used in a risk analysis to determine the reliability, resiliency and vulnerability of the two water resource systems (hydro power and irrigation schemes). For both of these water resource systems, the changes in operational risk-descriptors with respect to the

pseudo-present tri-decade, are within limits in which adjustments can be made, taking into account that traditional design criteria incorporate considerable buffering capacity for extreme events.

Aknowledgements

I am very grateful to my supervisors, Prof. John Flenley, Mr. Richard Heerdegen (Massey University), Dr. Brett Mullan and Dr. James Salinger (National Institute for Water and Atmospheric Research) for their patient supervision. Indeed, I am indebted to Mr. Richard Heerdegen, Dr. Brett Mullan and Prof. John Flenley because I feel privileged to have had such friendly support, encouragement and constructive criticisms and suggestions that have enriched this work. Their time and commitment are highly appreciated.

Many thanks to the Climate Impacts LINK Project, University of East Anglia (Norwich, UK) for providing GCM data from HadCM2 experiments. I am grateful to Mr. Daniele Denaro (Rome, Italy) and Dr. Ping Li (Vancouver, Canada) for support in the neural networks software application and Dr. Ted Drawneek (Massey University Computing Services) for his consultancy time and co-operation. I am also thankful to Dr David Roper (Mighty River Power) for permission to access the Taupo/Waikato hydro scheme hydrological records.

I am also indebted to my wife Bussakorn and our daughter Amy for their patience and encouragement throughout the programme. In a way this thesis belongs to them as much as it does to me.

I would like to take this opportunity to extend my sincere gratitude to all people who assisted me in one way or another during all stages of my PhD. programme.

I dedicate this thesis to our daughter Amy for whom all this seems worthwhile.

Table of Contents

List of Figures

List of Tables

List of abreviations and symbols

A_i	Snow accumulation in month i
alb	Albedo (short-wave radiation reflection coefficient)
ANN	Artificial neural networks model
CFC	chlorofluorocarbons
CH_4	Methane
CLIMPACTS	Climate change, variability and environment effects programme
CO_2	Carbon dioxide
CSIRO	Commonwealth Scientific and Industrial Research Organization
°C	Degrees Celsius
C_p	Specific heat at constant temperature
Cv	Coefficient of variation
DJF	December, January and February
dp_m'	Anomalies of meridional mean sea level pressure gradient
dp_z'	Anomalies of zonal mean sea level pressure gradient
E	Evaporation estimate
E_a	Evaporation estimate which assumes an unlimited availability of energy
E_r	Evaporation estimate that assumes the ability of the system to remove moist air is not limiting
E_{rc}	Reference crop evapotranspiration
E[x]	Expected value
e_d	Vapour pressure
ENSO	El Niño South Oslillation
ETa	Actual evapotranspiration
ETp	Potential evapotranspiration
f	Cloudiness factor
G	Soil heat flux
GCM	Global circulation model
GG	Greenhouse gases
gpm	Geopotential meter

HadCM2	Hadley Centre coupled ocean-atmosphere global climate model
hPa	Hekta pascal
IISA	The International Institute for Applied Systems Analysis database
IPCC	Intergovernmental panel for climate change
IPO	Inter-decadal Pacific oscillations
IR	Infrared radiation
J	Joules
JJA	June, July and August
K_w	Diffusivity
l	Mixing length
LAM	June, July and August
LPIS	Level plains irrigation scheme
m	Meter
mf_i	Snow melt factor in month i
mm	millimeter
Mslp'	Anomalies of mean sea level pressure anomalies
MST	Multivariate Statistics model
μm	Micrometer
N	Total day length
n	Bright sunshine hours per day
NCEP	National centers for environmental prediction
NIWA	National Institute for water and atmospheric research limited
NOAA	National oceanic and atmospheric administration
N_2O	Nitrous oxide
NREBP	Artificial neural networks software package
PgC	Petagram of carbon
O_3	Ozone
P_{eff}	Effective precipitation
P_{effi}	Effective precipitation in month i
Pm_i	Observed precipitation in month i
ppbv	Parts per billion by volume
ppmv	Parts per million by volume
Prin	Principal component

Prob	Probability
Q_o	Observed monthly discharge
Q_p	Modelled monthly discharge
R_a	Extraterrestrial radiation
R_b	Baseflow
R_d	Direct runoff
R_n	Net radiation
R_s	Surface runoff
R_{ss}	Sub-surface runoff
R_t	Total runoff
RMSE	Root mean square error
S_{max}	Maximum storage capacity (depth)
SAS	Statistical analysis software
Sp	Degree of distribution spread
T	Mean air temperature
t	Time
thk'	Anomalies of atmospheric thickness between 700 and 850 hPa pressure surfaces
UK	United Kingdom
UV	Ultraviolet radiation
WBM	Water balance model
Wm^{-2}	Watts per square meter
WMO	World Meteorological Organization
wsp'	Anomalies of wind speed at 10m above surface
$\bar{x}$	Mean
z	Relative storage ($0 \leq z \leq 1$)
α	Reliability; sub-surface runoff proportionality coefficient; relative humidity index
β	Gamma function scale parameter; direct runoff coefficient
γ	Gamma function shape parameter; resiliency; sub-surface runoff exponential coefficient; psychometric constant
Γ	Gamma probability function
ν	Vulnerability

ε	Surface runoff coefficient
Δ	Slope of the saturated vapour pressure curve
σ	Stefan-Boltzmann constant

Chapter One

General Introduction

1.1 General overview

The impact of changes in climate is a problem of crucial and growing importance to society, particularly to planners who are already struggling with other environmental stresses due to growing populations and economies. Predicted climate change induced by global warming presents new challenges, which include uncertainties regarding regional climate change. The uncertainties regarding the magnitude and direction particularly of precipitation are significant and a major limiting factor in impact assessment studies of potential risks that society faces and the chances that these risks will be realised. While the regional patterns of future climate change are poorly resolved, it is clear that the altered patterns of radiative forcing[1] associated with anthropogenic emissions will alter regional climates noticeably, and will have different effects on climate conditions in different regions (Houghton *et al.*, 1997). A capability for producing realistic climatological statistics or time series for future climate conditions would be of great utility for a range of environmental impact studies. For example, hydrological impact assessment often requires a suitable precipitation time series to be generated for input to a hydrological model of a system. At catchment scale, a monthly precipitation and temperature time series for a future climate has to be used with a precipitation-inflow model to simulate future reservoir levels. In urban drainage studies, even a finer time resolution is necessary for use with a hydraulic flow simulation model to predict the frequency of sewer overflow discharges to receiving watercourses.

---

[1] Radiative forcing is a change in net downward radiation (combined solar and infrared) at the tropopouse

Among the expected consequences of global warming are shifts in worldwide weather patterns. These changes will not occur uniformly and may result in greater weather variability and temperature extremes in some regions. Moreover, other unforeseen effects cannot be ruled out and unlike in the past, climate might change rapidly and dramatically over the coming decades and centuries.

The most promising method for predicting climate change is the use of global climate models (GCMs). The term GCM is often used loosely and can be thought of as referring to the more recent term 'global climate model' or to the older term 'general circulation model'. The aim of GCMs is the calculation of the full three-dimensional character of the climate. The solution of a series of equations that describe the movement of energy, momentum and various constituents (e.g. water vapour in the atmosphere and salt in the oceans) and the conservation of mass are formulated. Generally the equations are solved to give the mass movement (i. e. wind field or ocean currents) at the next timestep. Also included are processes such as cloud and sea ice formation, and heat, moisture and salt transport (McGuffie and Henderson-Sellers, 1997).

The first step in obtaining a solution is to specify the initial and boundary conditions at a number of 'grid points' obtained by dividing the Earth's surface into a series of rectangles so that a regular grid results. Initial and boundary conditions are specified at each grid point for the surface and several layers in the atmosphere and ocean. The set of coupled non-linear equations is then integrated with respect to time assuming prescribed changes in atmospheric composition and forcing at each grid point using numerical techniques. Outputs of these model integrations (experiments) then provide projections of plausible future climate.

However, there are still many problems in the presentation of surface climate variables generated via GCMs due to limited understanding of the climate system and computational restraints. It is the mismatch in spatial (and sometimes temporal) scales between GCMs and impact studies that presents the biggest challenge. Important climate elements such as precipitation and temperature have localised characteristics that cannot be resolved with the current resolution of GCMs. Moreover, impact assessment studies

require data at the spatial and temporal resolution at which impacts occur. Hence, a key requirement for the production of climate change scenarios from GCMs is the development of methods to 'downscale' GCM output to scales at which impacts occur.

This study focuses on the use of downscaling methods to bridge the gap between the resolution of GCM outputs and the required climate change information for impacts assessment. Artificial neural networks (ANN) and multivariate statistics (MST) approaches were independently adapted to capture the cross-scale relationships between observed free atmosphere regional circulation indices and local-scale characteristics in precipitation and near-surface air temperature (hereafter referred to as temperature) over a number of New Zealand sites. Subsequently the ANN approach was used to downscale outputs of a transient global climate change experiment (circulation variables) to construct local-scale scenarios of precipitation and temperature changes over New Zealand. The precipitation and temperature change scenarios were constructed for three tri-decades (2010-2039, 2040-2069 and 2070-2099) with respect to the pseudo-present (1980-2009).

Systems and activities that are particularly sensitive to precipitation and temperature changes include aquatic ecosystems; hydrology and water resource management; agricultural production; and human infrastructure. Impacts are not a linear function of the magnitude and rate of climate change. For some species (and hence systems), thresholds of change in temperature, precipitation or other factors may exist, which, once exceeded, may lead to discontinuous changes in viability, structure or function. To demonstrate the applicability of the climate change information derived in this study, and to examine the range of hydrological impacts which can be associated with the predicted changes, a water balance model (WBM) was adapted to simulate the hydrological response of two New Zealand catchments. Two hydrologically different catchments were selected to provide a reasonable range of catchment responses to climate change. The results were translated into water resource systems performance in terms of risk descriptors reliability, resiliency and vulnerability of water systems. These were used as examples to illustrate performance criteria that water managers and planners might need when considering the impacts of climate change.

In this chapter the role of the greenhouse effect in determining global climate and the consequences of an enhanced greenhouse effect are outlined. Observed trends in the mean global temperature and other climate elements in the 20th century are highlighted as possible signals of global changing climate. Also the potential impacts of global warming on water resources are raised to put into perspective the potential risks that society faces and the chances that those impacts might be realised lead to the given research objectives of this study. The importance of extended analysis of climate impacts beyond hydrological values for planning and management purposes is discussed.

1.2 Greenhouse effect and global climate

The physical mechanisms behind the atmospheric warming process are now well understood (Wilby, 1995). The Sun, which is the Earth's only external source of energy, emits solar radiation to the Earth mainly in the form of visible and ultraviolet (UV) radiation. The Earth being much cooler than the Sun, re-emits energy of lower intensity than that emitted from the Sun, in the form of invisible infrared (IR) as depicted in Figure 1.1. These two major energy fluxes must balance i.e. they must be in equilibrium. The Earth's atmosphere, however, affects the nature of this energy balance. The greenhouse gases like water vapour (H_2O), carbon dioxide (CO_2), methane (CH_4), nitrous oxide (N_2O) and other trace greenhouse gases are relatively transparent to the visible and near-infrared wavelengths that carry most of the energy of solar radiation, but they efficiently absorb the infrared emitted by Earth. Due to the downward re-radiation of infrared by greenhouse gases, the temperature in the atmosphere rises like in an actual greenhouse.[2] This is the Earth's natural greenhouse effect and keeps the Earth warmer than it would be without an atmosphere.

[2] In an actual greenhouse temperature, the temperature rise is attributed to limited convection from carrying away heat rather than differential UV/IR transmissivity of the glass.

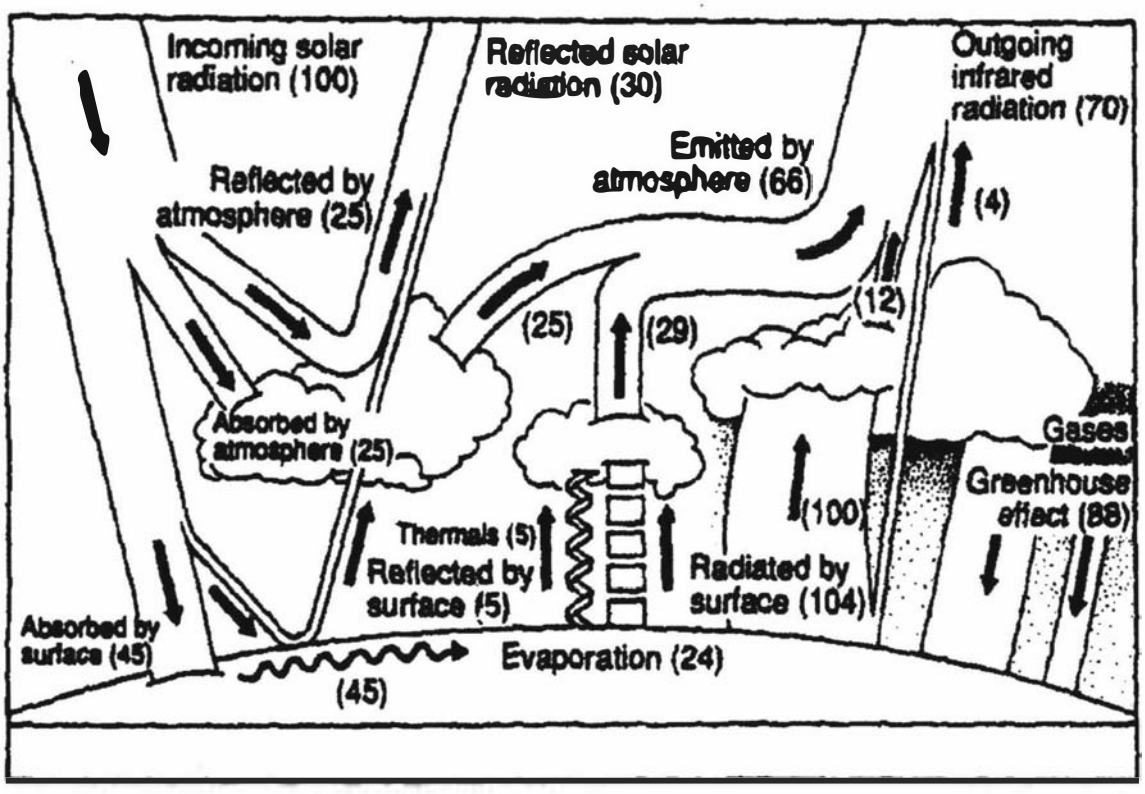

Figure 1.1 The greenhouse effect arises as the Earth's atmosphere tends to trap heat near the surface. The numbers are given in terms of the percentage each arrow represents relative to Earth-averaged solar constant, about 342 Wm^{-2} (Schneider, 1989).

The key to understanding how the Earth's atmosphere regulates surface temperature resides in the greenhouse effect. The solar power per unit area intercepted at the mean Earth-sun distance is the major source of energy that heats the Earth at a rate between 1365 and 1372 Wm^{-2} (Loaiciga *et al.*, 1996). Due to the shape of the Earth's atmosphere, the average solar insolation (about 100 km above the Earth's surface) is approximately 342 Wm^{-2}, about a quarter of the solar irradiance. The solar radiation reaching the Earth is in the wavelength range of 0.15 to 3.00 μm, with maximum intensity at about 0.50 μm. This is short-wave radiation and contains the ultraviolet, visible (0.40 to 0.76 μm), and near-infrared regions of the electromagnetic spectrum (Mitchell, 1989).

Out of 342 Wm^{-2} at the top of the atmosphere, approximately 169 Wm^{-2} is absorbed by the Earth's surface. This absorbed radiation warms the surface of the Earth. The

atmosphere absorbs about 68 Wm^{-2} of the incoming solar insolation, contributing directly to its heating. The remainder of the solar insolation (105 Wm^{-2}) is reflected back to outer space and thus the net input of solar radiation to the surface-atmosphere system is 237 Wm^{-2} (Loaiciga *et al.*, 1996). Without long-term gains or losses of energy, the Earth's surface-atmosphere system can be regarded as a blackbody with an equivalent mean effective radiative temperature of about -18°C. The Earth's surface, however, has a global mean value of approximately 15°C, and the difference of 33°C is due to the greenhouse effect of the atmosphere.

The greenhouse effect occurs as the Earth's surface is warmed up by absorbed solar radiation. The Earth's surface emits radiant energy approximately like a blackbody, with the outgoing radiation between 4 and 60 μm (infrared or long-wave radiation). Since the atmosphere is generally cooler than the Earth's surface, the molecules in the atmosphere absorb more energy than they emit (Stefan-Boltzmann law) thus reducing the efficiency with which long-wave radiation escapes to space. The entrapped long-wave radiation, 153 Wm^{-2} under the current 'equilibrium' conditions, contributes to the maintenance of atmospheric warmth and to long-wave radiation emissions from the atmosphere back to the Earth's surface (Loaiciga et al., 1996).

A latitudinal poleward transport of heat also exists from the tropics to the poles. If this energy transfer did not occur, the equator would be 14°C warmer on average than now, whilst the poles would be 25°C colder. Changes to these fluxes of energy determine the state of our climate and factors that influence them on a global scale may be regarded as causes of global climate change.

1.2.1 The enhanced greenhouse effect

The most recent and comprehensive studies of the global atmosphere indicate that currently climate is changing in ways that mirror the effects of global warming (Hansen and Lebedeff, 1987; Markham *et al.*, 1993). Due to the increasing concentrations of the greenhouse gases, the atmosphere traps more terrestrial radiation in the troposphere, enhancing the natural greenhouse effect.

The 'enhanced' greenhouse effect is the direct result of human activities which have changed and are continuing to change the balance of gases that form the atmosphere (Shine and Forster, 1999). This is especially true of such key 'greenhouse gases' as carbon, methane and nitrous oxide, which act like a natural blanket around the Earth, and have increased above their levels of the last 10,000 years (Houghton, 1996). The problem is that human activity is making the blanket 'thicker'. Carbon dioxide is produced mainly in the burning of fossil fuels such as coal, oil and gas in industry, in electricity generation, in transport and for heating purposes. In the incineration of waste, a great deal of CO_2 is released as well. Methane is released mainly in cattle farming (digestive processes and manure), in waste treatment (fermentation on landfills), through leaks in the distribution of natural gas and in combustion processes. Nitrous oxide is released especially in the burning of fossil fuels (mainly in traffic), in a number of processes in the chemical industry and in agriculture.

1.2.2 Temperature trends

The 20th century has been exceptionally warm in the context of the last millennium, and perhaps many millennia (Bradley, 2000). The global mean surface temperature has risen by between 0.3 and 0.6°C since about 1860, with the four globally-averaged warmest years being in the 1980s and the early 1990s (Folland *et al.*, 1992; Houghton *et al.*, 1996), as depicted in Figure 1.2. Recent analysis indicates that the last years of the decade were even warmer, suggesting a continuance of the warming trend. The warming has been greatest at night over land in the mid-to-high latitudes of the Northern Hemisphere. During the northern winter and spring, the warming has been stronger than during other seasons. In some areas, primarily over continents, the warming has been several times greater than the global average.

Global cooling at the surface and tropospheric cooling of a few tenths of a degree however occurred during 1992 and 1993. This cooling has been attributed to the Mt Pinatubo volcanic eruption in June 1991 (Nicolas *et al.*, 1996), even offsetting an El Niño event persisting throughout this period, which normally causes warmer than average global temperature anomalies.

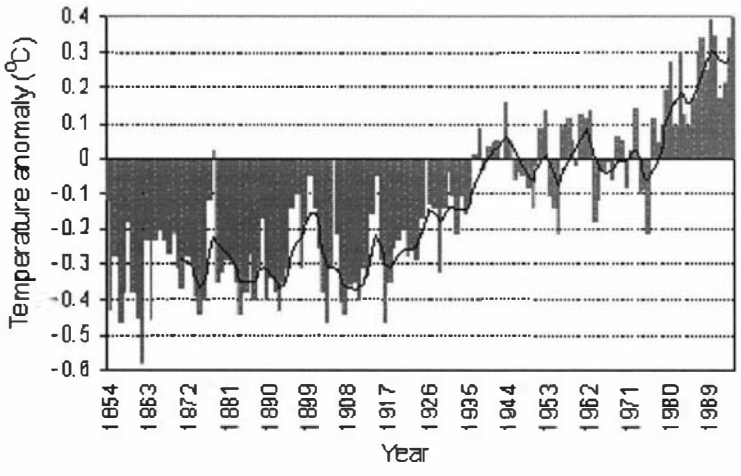

Figure 1.2 Global warming in the 20th century (Houghton *et al.*, 1996).

Combined land and ocean temperature analyses indicate that during the last decade globally averaged surface temperatures have been higher than in any decade in the past 140 years. Global average surface temperatures increased rather differently in the two hemispheres. A rapid increase in the Northern Hemisphere temperature during the 1920s and 1930s contrasts with a more gradual increase in the Southern Hemisphere.

The observed warming over the past several decades is mainly detected by the increase in daily minimum (night-time) air temperature with little contribution from daily maximum (day-time) air temperature (Karl *et al.*, 1993). Data for the period 1951-1990, from continental areas comprising 37% of the global landmass, shows that minimum temperatures increased by 0.84°C compared with an increase of only 0.28°C for maximum temperatures, resulting in a significant reduction in diurnal temperature ranges.

Variations in cryospheric variables, such as snow, ice and glacial extent occur in response to changes in temperature, sunshine amount, precipitation and changes in wind-stress. Snow cover maps have been produced using the USA National Oceanographic and Atmospheric Administration (NOAA) satellite imagery. Consistent with the surface and tropospheric temperature measurements is the decrease in snow cover and extent around 1980. Variations in sea ice extent have also been reported. Considerable interest in retreating sea ice has been generated, in the last few years, by the disintegration of the

Larsen sea ice shelf adjacent to the Antarctic continent. In view of the rapidity with which this retreat is taking place, such an event has been viewed as a signal of global warming (Doake and Vaughan, 1991; Vaughan and Doake, 1996; Rott *et al.*, 1996). A comparison of sea ice data acquired on submarine cruises between 1993 and 1997 with similar data acquired between 1958 and 1976 indicates that the mean ice draft at the end of the melt season has decreased by about 1.3m in most of the deep water portion of the Arctic Ocean, from 3.1m in 1958-1976 to 1.8m in the 1990s (Rothrock *et al.*, 1999).

1.2.3 Global warming uncertainties

While the surface warming is not inconsistent with the climate model predictions, there are other possible explanations for the warming trend: natural mechanisms of climate change such as changes in the degree of volcanic and solar activity, or a changing distribution of ocean temperatures. In addition, the Earth's climate can fluctuate purely at random by as much as 0.3°C over 100 years. These mechanisms may obscure the greenhouse-induced trend which may be less than or greater than the observed warming of around 0.5°C. The temperature rise must surpass the natural variability in the climate before natural changes in climate can be discounted. As acknowledged by the Intergovernmental Panel on Climate Change (IPCC) the most plausible explanation for the warming trend that has occurred since the mid-19th century is the enhancement of the greenhouse effect. The IPCC also stated that, on the balance of evidence, there is a discernible human influence on the global climate (IPCC, 1996a).

1.3 Observed trends in other global climate elements

Associated with the global warming is a chain of reactions of impacts within the climate system as the global 'heat engine' adjusts to new conditions. Changes in atmospheric circulation, which is the main control behind regional changes in wind, precipitation, moisture and other climate variables, trigger their variations. Variations in many climate variables are quite strongly related through large-scale features of the atmospheric circulation. Observed changes in a number of circulation features, including El Niño events in the southeast Pacific, mid-latitude northern hemisphere westerlies and the

location and intensity of the Aleutian low pressure system in the north Pacific, may all be related to the more general global warming of the twentieth century (Trenberth and Hoar, 1996).

Precipitation measurements at thousands of sites over the past hundred years or so have resulted in the compilation of global data sets (Bradley *et al.*, 1987; Diaz *et al.*, 1989). Several large-scale analyses of precipitation changes in both hemispheres demonstrate that during the last few decades precipitation has tended to increase in the mid-latitudes but decrease in the Northern Hemisphere subtropics. A striking precipitation decrease has occurred in the African Sahel during the last four decades. This dramatic desiccation has been linked to ocean circulation changes of the tropical Atlantic and the effect they had on sea surface temperatures.

High frequency (up to inter-annual) trends in precipitation variability have been revealed in regional precipitation data networks over the United States, Europe and Eastern Australia (Karl *et al.*, 1995). Precipitation global data sets for low frequency (decadal to multi-decadal) variability of precipitation show that global mean precipitation has not changed (Tsonis, 1996). The fluctuations about the mean, however, have increased significantly in decadal to multi-decadal time scales; that is, over the past century, during which global warming has occurred, the precipitation field has undergone changes on these scales in which extremes have become more probable.

Increased global cloudiness would be an expected consequence of higher global temperatures as would increase global evaporation and precipitation. Some increases in mean annual cloudiness have been observed over Europe, Australia, the Indian sub-continent and North America (McGuffie and Henderson-Sellers, 1994). Climate variations described as wet or dry summers, or mild, cold or stormy winters have become increasingly common since a few decades ago. In many parts of the world no season is the same as the last nor indeed the same as any previous seasons, nor to be repeated in detail next time round (Houghton, 1994).

1.4 Trends in New Zealand's climate

Whilst globally averaged records offer a means of assessing temperature change, it is important to realize that there are significant latitudinal and regional differences in the extent and timing of the warming. In New Zealand (as well as in Australia and the south Pacific), progressive warming has been detected (Salinger *et al.*, 1996; Whetton *et al.*, 1996).

The magnitude of warming between the decades 1861-1870 and 1981-1990 was 1.1°C. The coldest decade was 1901-1910 (-0.8°C below 1951-1980), and 1981-1990 the warmest (+0.3°C above 1951-1980). The temperatures increased sharply after the 1940s, but the mean annual warming has slowed recently. New Zealand temperature and that of the surrounding ocean surface have warmed by 0.7 ±0.1°C since the beginning of the century. Westerly circulation has increased in the New Zealand region over the last four decades. Areas exposed to this westerly circulation show daily temperature range decreases without significant decrease in sunshine hours except Southland. Precipitation time series show a decreasing trend to the decade 1981-1990, except in the west and south of the South Island, where increases have occurred (Salinger *et al.*, 1996).

A significant shift in the New Zealand climate has occurred during the past 20 years. Climate records (1930-1997) reveal that since 1977 the north and east of the North Island has become 10% drier and 5% sunnier with more droughts. The west and south of the South Island have become 10% wetter and 5% cloudier with more damaging floods. Fewer frosts are occurring nation-wide, the retreat of the west coast glaciers has halted but eastern glaciers continue to shrink and night temperatures continue to rise. Climate records and main weather features in the New Zealand and south Pacific regions show that the changes in average temperature and rainfall totals have impacted dramatically on the number of climate extremes such as frosts, floods and droughts. The changes have resulted from the strengthening of the anticyclonic belt which brings fair weather to northern New Zealand. It has squeezed stronger westerly winds over southern and central New Zealand. This climate shift has prevailed for two decades with variations around this new average since the mid-seventies (Salinger and Mullan, 1999). Climate records also

exhibit variations that could be associated with the ENSO[3]-like Interdecadal Pacific Oscillations (IPO) (Zhang *et al.*, 1997).

1.5 Future climate change

According to current projections, the mean global temperature may stand as much as 2°C above the pre-industrial level by the year 2100. To place this change in climate in context, the temperature rise that brought the planet out of the most recent ice age was only of the order of 4 to 5°C (IPCC, 1996b). Carbon dioxide concentrations in the atmosphere are already higher than at any time during the last 160,000 years. If these concentrations continue to rise at present rates, the Earth's temperature may become warmer than at any time during the last 40 million years (Houghton, 1996).

1.6 Global warming and water resources

Climate change has an effect on water resources through its influence on the 'hydrological cycle', the pathways and storage by which water passes from the atmosphere to the land surfaces, lakes and rivers, and then to the oceans or back to the atmosphere (Figure 1.3). Water falls as rain, snow, hail, and in some areas as fog (all together referred to as precipitation). Some of the precipitation is intercepted by vegetation and evaporates back to the atmosphere. The rest falls onto glaciers and snowfields, directly onto rivers and lakes, or onto the ground surface. From the ground surface water runs off into watercourses, evaporates or infiltrates into the soil where it may be used in transpiration by plants, passes into groundwater and contributes to the maintenance of the perennial flow in rivers and streams. Groundwater finds its way

[3] ENSO (El Niño Southern Oscillation) refers to an abnormal warming of ocean temperatures across the eastern and central tropical Pacific which, during a strong episode, extends from the date line to the west coast of South America. These abnormally warm waters are accompanied by large-scale changes in tropical rainfall, wind patterns and air pressure, which ultimately interact to affect the midlatitude jet streams and weather patterns

eventually into watercourses or direct to sea. Water eventually discharges to the sea, by groundwater and streamflow.

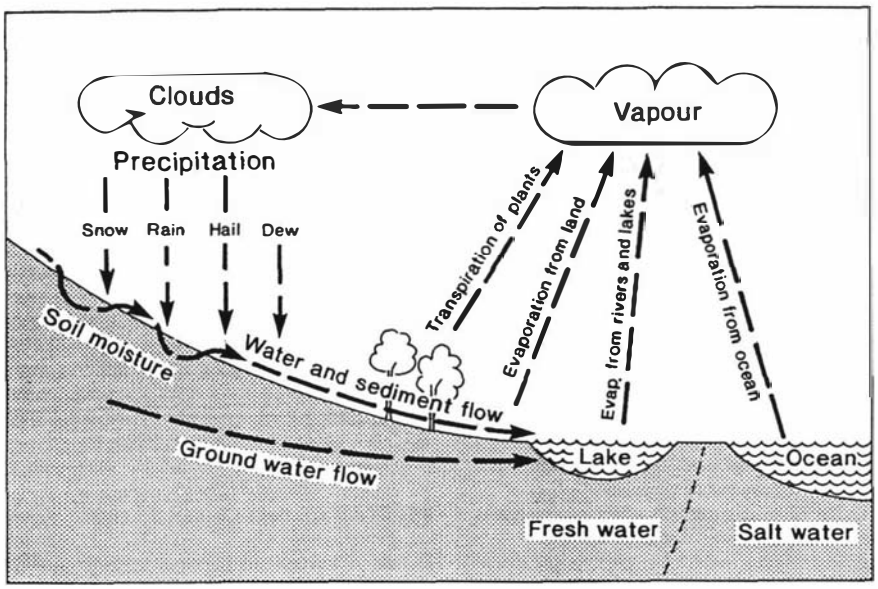

Figure 1.3 The hydrological cycle (after Mosley, 1992).

All these components of the hydrological cycle are of great practical significance. Of the 'storage components', snowfields, glaciers and lakes are major stores of water which provide reliable flows for hydroelectricity and water supply schemes downstream. Rivers themselves are sources of water for consumption or energy generation, habitats for fish and other aquatic life and places for human recreational activities.

As shown in Table 1.1 the rate of turnover within stores varies considerably, from 10,000 to 15,000 years for terrestrial ice to about seven to ten days for atmospheric moisture (Jones, 1997). Turnover is 3-5 times faster in the freshwater stores than in the saline ones, with the exception of ice. The maintenance of freshness is reflected in the rapid turnover. The turnover rates in the table show the importance of exposure at the Earth's surface, which is the most active surface for interchange. The 'surface area to volume ratio' is a rough measure of the relative exposure of the water (in some form) held in each store.

Table 1.1 Storage and turnover in the major hydrological stores (Jones, 1997).

Store	Best estimate volume (10^3 km^3)	Range in estimates (10^3 km^3)	Per cent range	Area (10^6 km^2)	Per cent total	Per cent freshwater	Turnover rate years	Surface area to volume ratio
Oceans	1 350 000	50 000	4	360	97.40	0	3000	0.26
Ice caps/ glaciers	27 500	12 700	81	16	1.98	85.9	8000–15 000	0.67
Terrestrial waters	8477.8			134	0.61			
–groundwater	8200	325 990	7949		0.59	13.5	>5000-deep <330-active	
–inland seas	105	39.6	46		0.008			
–lakes	100	120.0	400		0.007	0.313	10	329.0
–soil moisture	70	133.5	809		0.005	0.219	0.038–0.96	
–rivers	1.7	1.1	110		0.0001	0.005	0.038	
–biota	1.1	49.0	490		0.0001	0.003	0.077	
Atmosphere	13	3.5	33	510	0.001	0.04	0.027	>39 000
Man-made stores								
–reservoirs	5				0.0004	0.016		
–irrigated soil	2				0.0001	0.006		
TOTAL								
global	1 385 990.8							
freshwater	32 000				2.4			

The ratio largely explains why average turnover is so slow in the oceans, despite the ocean surface being the source of 86% of atmospheric moisture and one of the most active exchange interfaces in the whole system. It also demonstrates how exposed terrestrial surface waters are. Deviations from the trend show the importance of (1) the amount of energy available at the interface; (2) the efficiency of energy use; and (3) the ease of exchange. Hence, turnover is relatively slow in ice sheets and glaciers because of the special properties of ice, which inhibit losses, and because of their location in low-energy (cold) climates. Turnover is slow for deep groundwater because of its remoteness from the Earth's surface and because of its depth within a relatively slowly permeable medium.

As acknowledged by the IPCC (Houghton *et al.*, 1996), enhanced greenhouse warming will affect water temperatures, precipitation patterns, evapotranspiration rates, the timing and magnitude of runoff, and the frequency and intensity of storms. In addition, precipitation and temperature changes would affect the demands for irrigation water, hydroelectric power generation and other purposes. For example, irrigation water

demands are particularly sensitive to changes in precipitation and temperature characteristics.

A wide range of hydrological impacts including, for example, changes in timing and magnitude of runoff, soil moisture and evaporation have been intensively examined using a variety of different climate change scenarios (MacCabe and Ayers, 1989; Mimikou and Kouvopoulos, 1991; Bataglin *et al.*, 1993; Wolocket *et al.*, 1993; Nash and Gleick, 1993; Poiani *et al.*, 1995; Chiew *et al.*, 1995; Kirshen and Fennessey, 1995). All of these studies indicate that runoff is very sensitive to changes in precipitation especially in drier catchments. Changes in rainfall have little effect on soil moisture in wet catchments but in drier catchments, the percentage change in soil moisture levels can be greater than the percentage change in rainfall. Compared with precipitation, temperature increase alone, except for snowmelt timing, has negligible impacts on runoff and soil moisture. This suggests that water resources systems could be very vulnerable to changes in precipitation inputs and that a small change in precipitation could lead to a large change in a water resource system's performance.

1.7 Study justification

Improved understanding of how climate affects human society involves development of a framework to analyze complex interactions among biophysical and socio-economic processes. Virtually every natural and managed system is affected by climate, prime examples being the geographic distribution of natural ecosystems-productivity of managed ecosystems such as agriculture, regional water resources, coastal habitation, wetlands and energy generation and demand. Moreover, human alteration of ecosystems and their own natural processes have their own impact on the atmosphere and hence upon the climate system.

Climate impact studies include assessment of the impacts of observed climate and its variability, and potential impacts of climate change. Observed climate data and climate model outputs (e.g., temperature, precipitation, solar radiation) can be used as inputs to

'impact models' to produce regional changes in variables such as crop yields, water availability, and forests.

The impacts of predicted climate change and the atmospheric changes driving it are neither uniform nor limited to one particular part of the globe. New Zealand's geographical isolation, therefore, affords no sanctuary. Actually, the rate of temperature increase has been greater in New Zealand than for the globe in general. Since 1900, the global average surface temperatures for land and sea have increased by 0.45°C but New Zealand's temperature has risen by 0.70°C (Salinger, 1995). Therefore there is need in New Zealand, as elsewhere, to begin putting in place mechanisms that could enhance the coping skills to ensure that the impacts of predicted climate changes on water resources will be managed as effectively as possible. Changes in threshold events like droughts and floods may require both individual and institutional adjustments.

Apart from rain-fed agriculture, water is a managed resource in New Zealand, as it is in most of the industrialized world. Through a system of dams and conveyances, surface water is made available for different uses. The value of New Zealand water resources was estimated to exceed NZ$2,000 million annually (Mosley, 1988), mainly covering water supply, waste disposal, freshwater fisheries, recreation and amenities, and hydro-electricity.

Among the many concerns associated with climate changes due to global warming, the potential effects on water resources are frequently cited as the most worrisome. On the contrary, those who manage water resources have not yet rated climate changes among their top planning and operational concerns (Lins and Stakhiv, 1998). This can be attributed to an important shortcoming of nearly all the water resources impacts studies that have focused exclusively on the hydrological response to climate without consideration of that information which water managers need to adapt to climate change while taking account of basic water management options.

Water resources sensitivity studies have been simplified assessments on how the hydrological regime (usually streamflow) will respond to prescribed or model-simulated

climate conditions (usually temperature, precipitation and evaporation). Results have generally been expressed in terms of changes in the yield of the water system (such as reservoirs) and changes in the water volume.

Simple postulates, for example, that a change in climate could lead to consistently low or high flows in a particular catchment conceal several problems which are inherent in relating climate change to resource impact. In particular, they are the nature of climate change itself, the strength of the relationship between climate changes and the resource systems response, and the availability of (past) climate and sociological data for evaluation. Thus water management agencies find it difficult to justify changing system design features or operating rules on the basis of the currently simulated climate change, given that traditional design criteria incorporate considerable buffering capacity for extreme events. In the face of the predicted climate change, however, frequency and intensity may shift climate risks in ways such that traditional adjustments in water resources may prove less feasible in the future as projects become smaller and new facilities are delayed by economic and other environmental stresses (Riebsame, 1988).

Therefore, changes in catchment hydrological responses should then be evaluated in terms of water resource systems' performances. Such assessment extends analysis of climate impacts beyond hydrological values, which might not fully explain societal implications of populations at risk for any policy decision regarding societal preparation for either short-term or long-term climate change impacts.

1.8 Research objectives

This study addresses three research objectives:

- To develop a semi-empirical approach which can be used with statistical methods (e.g. neural networks or multivariate statistics) to downscale GCM-scale climate change information to scales at which impacts occur;
- To assess changes in catchment response to precipitation and temperature changes via case studies;

- To translate changes in catchment water yield into descriptions of impacts on selected water resources in New Zealand, as an exploration of the use of the current generation of GCM outputs in impact estimation.

In the two case studies, impacts of climate change on the performance of Lake Taupo as a reservoir for the Waikato Hydroelectric Power Scheme in the North Island and the Opihi River as a source of water for the Levels Plain Irrigation Scheme (LPIS) in South Canterbury were quantified using risk descriptors.

1.9 Thesis organisation

This chapter presents a background to science issues regarding the current global warming and the associated climate change. The importance of the greenhouse effect in determining the global climate and the consequences of an enhanced greenhouse effect are outlined. Observed trends in the mean global temperature and other climate elements in the 20th century are highlighted as possible signals of global changing climate. The potential impacts of global warming on water resources are highlighted to put into perspective potential risks that society faces and the chances that those impacts might be realised, leading to the research objectives of this study. The importance of extended analysis of climate impacts beyond hydrological values for planning and management purposes is discussed and feasible approaches proposed.

In Chapter Two climate and the climate system concepts which form the basis of modelling the climate system's response to climate forcings and their feedbacks leading to climate change are reviewed. Projections of global climate changes for the 21st century based on experiments by global climate models are also reviewed. Chapter Three outlines a research framework and the approaches adapted to derive climate change scenarios and to assess the impacts on hydrology and water resources. In Chapter Four a semi-empirical approach to capture cross-scale relationships between local climate variable and free-atmosphere regional circulation variables is presented. In Chapter Five the main features of New Zealand's climate are discussed. Scenarios of precipitation and temperature changes constructed in the study are presented.

Potential impacts of predicted climate change on hydrology and water resources are reviewed in Chapter Six and in Chapter Seven approaches to water resources impact assessment are considered. The state of the natural water environment and pressures imposed on New Zealand water resources are highlighted in Chapter Eight. Two case studies are presented to illustrate the impacts of predicted changes in temperature and precipitation characteristics on New Zealand water resources. A general discussion and conclusions are presented in Chapter Nine.

Chapter Two

Climate and the climate system

The key to climate change studies is first to understand what climate is, and how the global climate system operates. In this chapter a definition of climate is given with a view of giving a clear distinction between weather and climate concepts. Climate system characteristic features are reviewed to put into perspective the mechanisms and physical processes responsible for climate changes.

2.1 Climate

The term 'climate' can have a wide range of meanings (McGuffie and Henderson-Sellers, 1997). Traditionally, to a geologist or geomorphologist, the 'climate' is an external agent which forces many of the phenomena of interest. To an archaeologist, the 'climate' of an earlier time might have had a crucial influence on the people being studied, or might have been of little socio-economic significance but still so strong an environmental feature that it has left a 'signature' which can be interpreted. Agriculturists commonly see the 'climate' as the background 'norm' upon which year-to-year and day-to-day weather is imposed, while to a common person, 'climate' often first suggests temperature, although rainfall and humidity may also come to his mind.

At this point, it is important to make a clear distinction between weather and climate. Weather is concerned with detailed instantaneous states of the atmosphere with the day-to-day evolution of individual synoptic systems. The atmosphere is characterised by relatively rapid fluctuations in time and space so that the weather, identified as the complete state of the atmosphere at a given instant, is continuously changing. For the climate, on the other hand, it is difficult to have a single satisfactory definition because the climate system encompasses so many time- and space-scales (Figure 2.1). Climate can be viewed as existing in at least three domains: time, space and human perception.

In that sense, climate is usually defined as the 'averaged weather' over an agreed time interval, typically three decades as defined by the World Meteorological Organisation (WMO). Defined for the globe or a selected region, climate is completed with some measures of variability of its elements and with information on the occurrence of extreme events. The same variables that are relevant in the weather are also those that are important in characterisation of climate. The quantities are most often surface variables such as temperature, precipitation, and wind, but in a wider sense the 'climate' is the description of the state of the climate system. The distinction of climate from weather is the neglect of details of the daily fluctuations in the state of the atmosphere (Peixoto and Oort, 1993). Instead, climate includes the various statistics produced by considering an ensemble or a sequence of instantaneous states, so that the climate is independent and free from the statistical fluctuations that would characterise any individual realisation. A climate change is the difference between two climate states, and a climate anomaly is the difference between a climate state and the mean state.

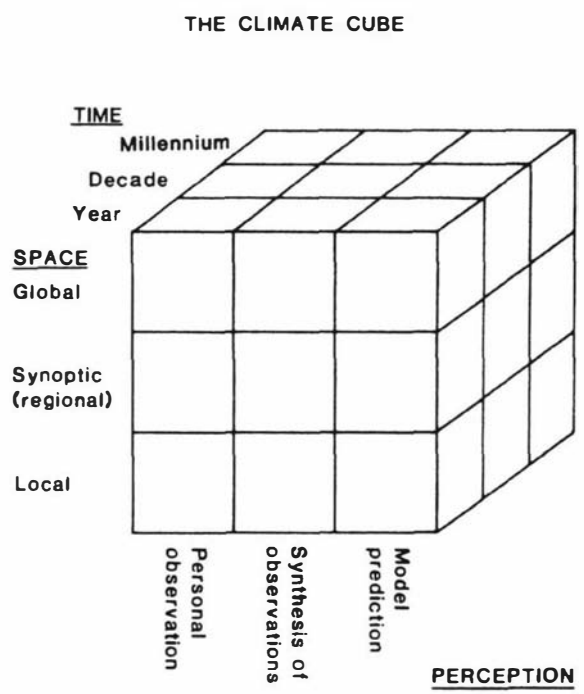

Figure 2.1 The climate cube. Divisions of climate domains depicted here are arbitrary, and many more could exist (after McGuffie and Henderson-Sellers, 1997).

2.2 The climate system

The climate system consists of five major components: (1) the atmosphere; (2) the oceans; (3) the terrestrial and marine biospheres; (4) the cryosphere (sea ice, seasonal snow cover, mountain glaciers and continental scale ice sheets) and (5) the land surface. These components interact with each other, and through this collective interaction, they determine the Earth's climate. These interactions occur through flows of energy in various forms, through exchanges of water, through flows of various other radiatively important trace gases, including CO_2 and CH_4, and through the cycling of nutrients (IPCC, 1997). The climate system is powered by the input of solar energy, which is balanced by the emission of infrared (heat) energy back to space. Solar energy is the ultimate driving force for the motion of the atmosphere and ocean, the fluxes of heat and water, and of biological activity. Figure 2.2 presents a schematic picture of the climate system, showing some of the key interactions between the various components and the component properties which can change.

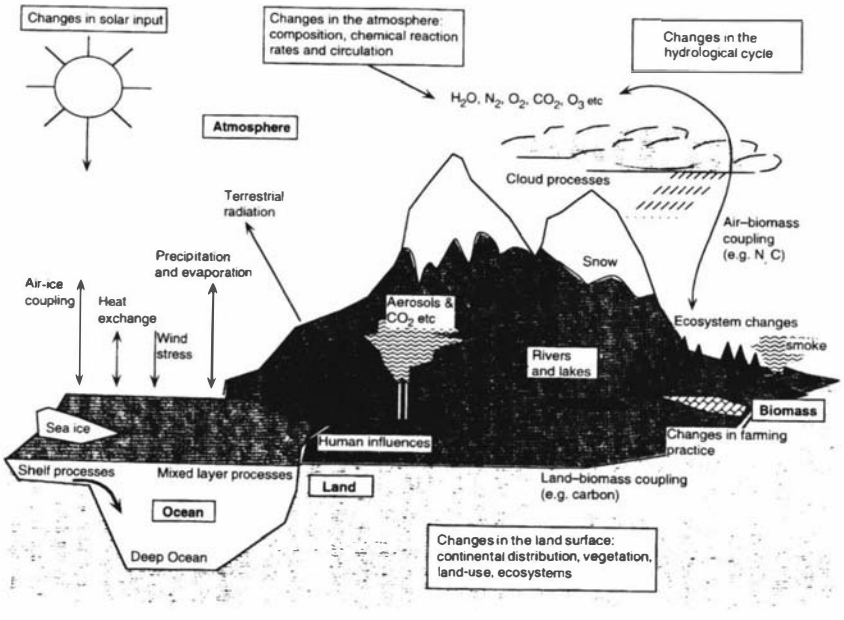

Figure 2.2 Schematic illustration of the components and interactions in the climate system (Houghton *et al.*, 1996).

2.2.1 The Atmosphere

The atmosphere is a mixture of different gases and aerosols (suspended liquid and solid particles) collectively known as air. Although traces of atmospheric gases have been detected well out into space, 99% of the mass of the atmosphere lies below about 25 to 30km altitude, whilst 50% is concentrated in the lowest 5 km. This gaseous mixture remains remarkably uniform in composition, and is the result of efficient biogeochemical recycling processes and turbulent mixing in the atmosphere. The two most abundant gases are nitrogen (78% by volume) and oxygen (21% by volume). Despite their relative scarcity, the so-called greenhouse gases play an important role in the regulation of the atmosphere's energy budget (details given in Chapter One, Section 1.2).

The principal greenhouse gas concentrations that have increased over the industrial period are CO_2, CH_4, N_2O, and chlorofluorocarbons CFC-11 (CCl3F) and CFC-12 (CCl2F2) (Hansen *et al.*, 1998; Schimel *et al.*, 1996). The observed increase of CO_2 in the atmosphere from about 280 ppmv in the pre-industrial era to about 364 ppmv in 1997 (Friedli *et al.*, 1986; Hansen *et al.*, 1998; Keeling and Whorf, 1998) has come largely from fossil fuel combustion and cement production.

These sources amounted to approximately 6.5 Pg C/yr (1 Pg=1015 g) in 1996 (Marland *et al.*, 1999). Land use changes produce a non-negligible but more uncertain contribution of about 1.6 ± 1.0 Pg C/yr (Fan *et al.*, 1998; Schimel *et al.*, 1996). These anthropogenic sources of CO_2 exceed the estimated uptake of CO_2 by the atmosphere and oceans, implying a significant but as yet unidentified terrestrial sink (Enting and Pearman, 1987).

The atmospheric concentration of CH_4 has increased from about 700 ppbv in pre-industrial times to about 1721 ppbv in 1994 (Houghton *et al.*, 1996). Fossil-fuel related sources of CH_4 amount to approximately 70-120 Tg CH_4/yr (1 Tg=1012 g). Increases in CH_4 sources resulting from rice cultivation, animal husbandry, biomass burning, and landfills contribute about 200 - 350 Tg CH_4/yr (Schimel *et al.*, 1996).

The atmospheric concentration of N_2O has increased from about 275 ppbv in pre-industrial times to about 312 ppbv in 1994 (Houghton *et al.*, 1996). Estimated

anthropogenic emissions of N_2O for the 1980s range from 3 to 8 Tg N/yr (Houghton *et al.*, 1996). The main anthropogenic sources are from agriculture and industrial sources including adipic acid and nitric acid production (Schimel *et al.*, 1996).

Chlorofluorocarbons CFC-12 and CFC-11 are manmade compounds that were not appreciably present in the atmosphere before 1950. These compounds have been widely used as refrigerants and in spray propellants and foam blowing. Due to their role in catalyzing decomposition of stratospheric ozone, production of these compounds has been dramatically reduced in response to the Montreal Protocols and subsequent international agreements. Atmospheric concentrations of these compounds are expected to diminish substantially during the next century (Prather *et al.*, 1996).

Prediction of the future persistence of anthropogenic greenhouse gases in the atmosphere is based on mathematical models that simulate future additions and removals. The greenhouse gas concentrations predicted by these models are subject to large uncertainties in the effects of both natural processes and human activities. For some greenhouse gases persistence can be estimated from 'mean residence times', which are obtained with simple linear models and represent the time that would be required for removal of 63% of the anthropogenic excess of the material in the atmosphere, if anthropogenic sources were abruptly diminished to zero (Lasaga and Berner, 1998). This approach yields a rough measure of the persistence in the atmosphere of anthropogenic additions of CH_4 with an estimated mean residence time of 10 years (Prather, 1996, 1998); N_2O, 100 years, (Prather, 1996, 1998); and CFC-11 and CFC-12, 50 and 102 years, respectively (Prather *et al.*, 1995).

The persistence of anthropogenic CO_2 in the atmosphere cannot be estimated with such a simple model because exchange with the ocean and sediments leads to a more complex behavior. Model simulations of oceanic CO_2 uptake provide response times associated with CO_2 gas exchange at the ocean surface of approximately 10 years (Liss and Merlivat, 1986; Toggweiler *et al.*, 1989) and downward mixing of surface waters on the order of decades to centuries (Maier-Reimer and Hasselmann, 1987; Sarmiento *et al.*, 1992). But even when these oceanic CO_2 removal processes are allowed sufficient time in

the models to reach their maximum capacity, they can remove only about 70 to 85% of the anthropogenic CO_2 added to the atmosphere (Archer *et al.*, 1998; Broecker and Peng, 1982; Sarmiento *et al.*, 1992).

Additional CO_2 might be removed by burial in soils or deep sea sediments through mechanisms that, although poorly understood, are generally believed to require times extending to thousands of years (Harden *et al.*, 1992; Schlesinger, 1990; Stallard, 1998). Removing some of the anthropogenic CO_2 by this mechanism may require reactions with carbonate sediments in the deep sea that occur on timescales of thousands of years (Archer *et al.*, 1998; Boyle, 1983; Sundquist, 1990). On the basis of such analyses, it is now generally believed that a substantial fraction of the excess CO_2 in the atmosphere will remain in the atmosphere for decades to centuries, and about 15-30% will remain for thousands of years.

The additional anthropogenic greenhouse gases that have been introduced into the atmosphere increase the IR energy absorbed by the atmosphere, thereby exerting a warming influence on the lower atmosphere and the surface, and a cooling influence on the stratosphere (Peixoto and Oort, 1992; Ramanathan *et al.*, 1985).

The radiative influence resulting from a given incremental increase in greenhouse gas concentration can be quantified and compared as as the radiative forcing. Climate model calculations indicate that to good approximation the global warming influence of the several greenhouse gases is equal for equal forcing (Wang *et al.*, 1991, 1992), lending support to the utility of the concept of climate forcing and response.

Of the several anthropogenic greenhouse gases, CO_2 is the most important agent of potential future climate warming because of its large current greenhouse forcing, its substantial projected future forcing (Houghton *et al.*, 1996), and its long persistence in the atmosphere. Understanding climate response to a specified forcing is one of the major challenges facing the climate research community.

In principle, empirical inferences of climate sensitivity would be of great value, but development of such inferences is confounded by the natural variability of the climate

system (Santer *et al.*, 1996), by local or regional effects that can be different from the global effects, and by the simultaneous working of multiple transient forcings and responses. For these reasons a principal means for understanding climate system response to forcing is by use of computer models of the Earth's climate system.

Since the atmosphere is a thermo-hydrodynamical system, it is characterized by its composition, its thermodynamical state as specified by the thermodynamic variables, and its mechanical state (motion). A complete description of the state of the atmosphere also includes other variables, such as cloudiness, precipitation, and adiabatic heating, which affect the large-scale behaviour of the atmosphere. The atmosphere, as a thermodynamic system, cannot be considered separately from the neighbouring systems (Fig. 2.2). Although these systems are very different in their composition, physical properties, structure and behaviour, they are all linked together by fluxes of mass, energy, and momentum forming a global system, the so-called climate system.

2.2.2 The Oceans

Transfers of energy take place between the atmosphere and the other components of the climate system, the most important of these components include the world's oceans. Surface ocean currents assist in the latitudinal transfer of heat (Figure 2.3). Warm water moves poleward whilst cold water returns towards the equator. Energy is also transferred via moisture. Water evaporating from the surface of the oceans stores latent heat which is subsequently released when the vapour condenses to form clouds and precipitation.

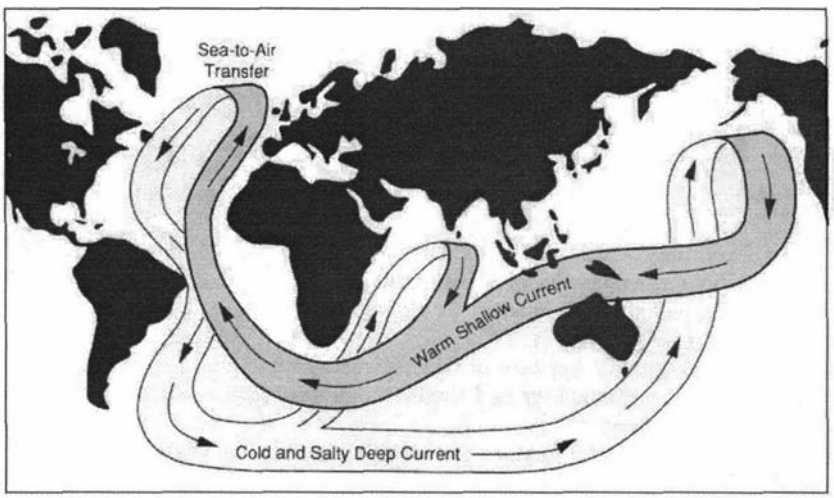

Figure 2.3 The great ocean conveyor belt (Broecker, 1991).

The significance of the ocean is that it stores a much greater quantity of energy than the atmosphere. The upper ocean in contact with the atmosphere alone stores approximately 30 times as much heat as the atmosphere. Thus, for a given change in heat content of the ocean-atmosphere system, the temperature change in the atmosphere will be around 30 times greater than that in the ocean. Small changes to the energy content of the oceans could therefore have considerable effects on global climate. Energy exchanges also occur vertically within oceans between the upper layer and deep water. Sea salt remains in the water during the formation of sea ice in the Polar Regions, with the effect of increased salinity of the ocean. This cold, saline water is particularly dense and sinks, transporting with it a considerable quantity of energy. A global thermohaline circulation exists, which plays an important role in the regulation of the global climate.

2.2.3 The Cryosphere

The cryosphere consists of those regions of the globe, both land and sea, covered by snow and ice. These include Antarctica, the Arctic Ocean, Greenland, Northern Canada, Northern Siberia and most of the high mountain ranges throughout the world, where sub-zero temperatures persist throughout the year. The cryosphere plays another important role in the regulation of the global climate system. Snow and ice have a high albedo

(reflectivity), that is they reflect much of the solar radiation they receive. Without the cryosphere, more energy would be absorbed at the earth's surface rather than reflected, and consequently the temperature of the atmosphere would be higher.

2.2.4 The Biosphere

The biosphere influences the fluxes of certain greenhouse gases such as CO_2 and CH_4. Plankton in the surface oceans utilizes the dissolved carbon dioxide for photosynthesis. This establishes a flux of carbon dioxide, with the oceans effectively 'sucking' down the gas from the atmosphere. On death, the plankton sinks, transporting the carbon to the deep ocean. Such primary productivity reduces by at least four-fold the atmospheric concentration of carbon dioxide, weakening significantly the Earth's natural greenhouse effect. The biosphere also influences the amount of aerosols in the atmosphere. Millions of spores, viruses, bacteria, pollen and other minute organic species are transported into the atmosphere by winds, where they scatter incoming solar radiation, and influence the global energy budget.

2.2.5 The Geosphere

Variations in global climate over hundreds of millions of years are partly due to changes to the Earth's crust. Changes in the shape of ocean basins and the size of continental mountain chains (driven by plate tectonic processes) may influence the energy transfers within and between the other components of the climate system. On much shorter time-scales physical and biological processes affect certain characteristics of the soil, such as moisture availability and water run-off, and the fluxes of greenhouse gases and aerosols into the atmosphere and oceans. Volcanic eruptions replenish the carbon dioxide in the atmosphere, removed by the biosphere, and emit considerable quantities of dust and aerosols.

2.2.6 State of climate

The components of the climate system influence global and regional climate in many of distinct ways:

- by influencing the composition of the Earth's atmosphere, thereby modulating the absorption and transmission of solar energy and the emission of infrared energy back to space;

- through alterations in surface properties and in the amount and nature of cloud cover, which have both regional and global effects on climate; and

- by redistributing heat horizontally and vertically from one region to another through atmospheric motions and ocean currents.

The balance of solar and terrestrial radiation budgets determines the overall state of the global climate. How this energy balance is regulated depends upon the fluxes of energy within the global climate system. Due to its low density and ease of movement, the atmosphere is the most 'nervous' of the climate sub-systems. Therefore, the space- and time-scales of the atmosphere are quite short in terms of both scales for other components. The coupling of the atmosphere and hydrosphere are difficult especially with the oceans due not only to critical space- and time-scales but also because the coupling between these components is strongly latitude-dependent. In the tropics the systems are closely coupled, particularly through temperature; in the mid-latitudes the coupling is weak, predominantly via momentum transfer; but in high latitudes there is a tighter coupling, primarily through salinity, which is closely involved in the formation of oceanic deep bottom water. Biochemical processes controlling the exchange of CO_2 between atmosphere and ocean also vary as a function of geographical location.

The cryosphere component plays an important role in the radiative exchange through high albedo of ice and snow. There is also the insulating effect of the cryosphere which is now known to be at least as important as its albedo effect. The sea ice, especially, decouples the ocean from the overlying atmosphere, causing considerable changes in both components. Snow has a similar, but smaller, effect on land. The biosphere component is associated with the CO_2 content in the atmosphere, which is critically dependent upon the biota.

In the natural state, the various flows between the climate system components are usually very close to being 'exactly' balanced (within measurement error) when averaged over periods of one to several decades. For example, prior to the industrial revolution, the uptake of CO_2 by photosynthesis was almost exactly balanced by its release through decay of plant and soil matter, as evidenced by the near constancy of the atmospheric CO_2 concentration for several millennia prior to about 1800 AD (Houghton *et al.*, 1992). From one year to the next, however, there can be modest imbalances which fluctuate in sign, due to the natural variability of the climate system. Humans can also affect the operation of climate processes, and hence the natural balance of the climate system, through persistent regional to global scale alterations in the composition of the Earth's atmosphere and in the properties of the land surface.

2.3 Causes of climate change

When looking for causes of climate change, one is interested in any process that can disturb the energy balance between incoming radiation from the Sun and outgoing terrestrial radiation from the Earth (the global energy balance), the now well known 'climate forcing'. A climate forcing is a change imposed on the planetary energy balance which, typically, causes a change in global temperature.

The climate system is a dynamic system in transient balance. This concept is vitally important in climate modelling. There are energy fluxes within the system which can be visualized as vectors (they involve movements of some quantity from one place to another, and the direction of flow is important), and net fluxes differ considerably as a function of time period considered. Also, different budgets, the result of the fluxes, are established when the imposed disturbance changes. The most important fluxes in the climate system are fluxes of radiant energy (solar and heat), but the fluxes of water and to a lesser extent mass (matter) also affect climate dynamics.

It is well known that climate is modulated by both external and internal factors. To a modeller 'external' is anything the model cannot predict. The external factors may be grouped into:

- general factors such as the solar radiation, the sphericity of the Earth, the Earth's motion around the sun, its rotation and the existence of continents and oceans;

- regional and local factors, such as distance to the sea, topography, nature of underlying surface, vegetation cover, and proximity to lakes.

Internal factors deal with the intrinsic properties of the atmosphere, such as the atmospheric composition, various instabilities and the general circulation (Peixoto and Oort, 1993).

2.3.1 Orbital Variations

On time-scales of a millennium and longer, changes in the character of the Earth's orbit around the Sun (Figure 2.4) can significantly affect the seasonal and latitudinal distribution of incoming solar energy. The net effect of variations in the orbit eccentricity, obliquity and the Earth's axis precession give rise to the now known 'Milankovitch Cycles' and is an example of external climate forcing. The change in energy receipt can amount to 10% or more in certain locations. The Milankovitch Cycles force the changes between ice age and warmer conditions on Earth, on time-scales of 10,000 to 100,000 years. The last Ice Age occurred 18,000 years ago (Houghton, 1994). Figure 2.5 gives a graphical illustration of calculated variations for 0-800,000 years.

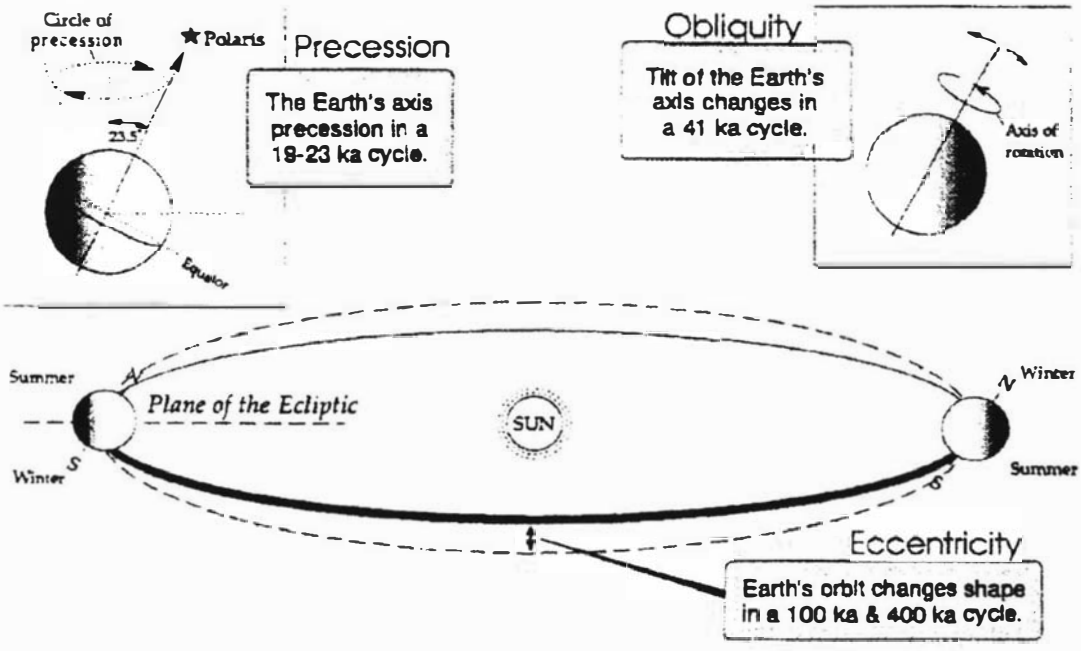

Figure 2.4 Orbit eccentricity, obliquity and precession: the three astronomical cycles involved in solar input and climate variation (Imbrie *et al.*, 1984).

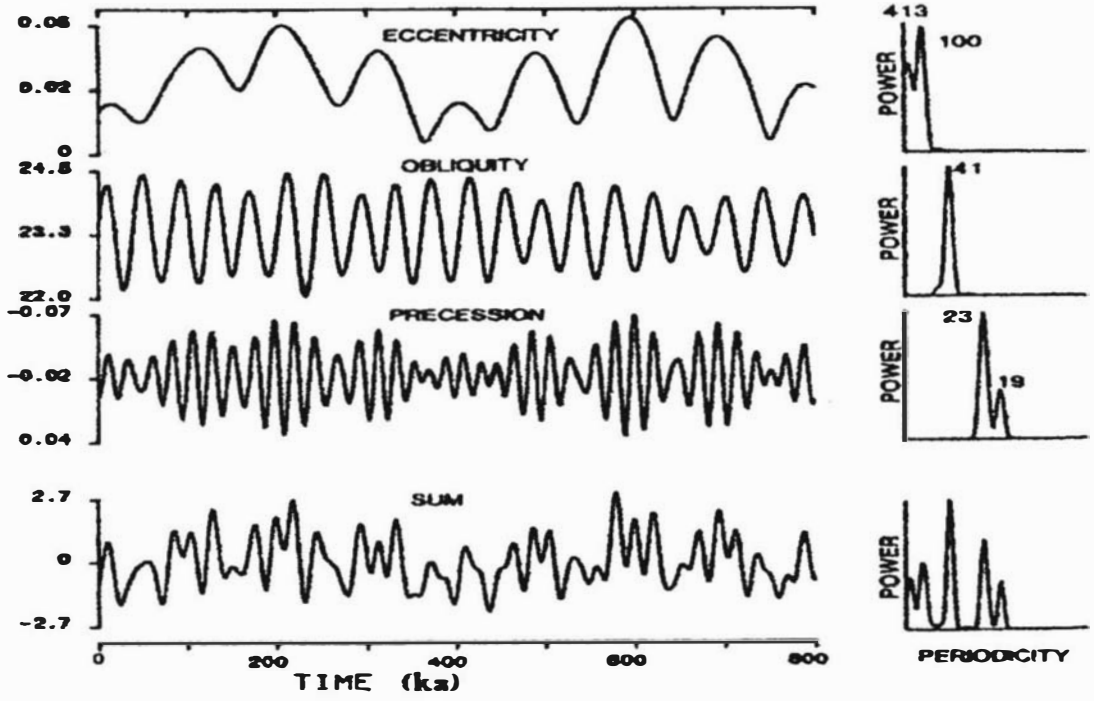

Figure 2.5 Graphical illustration of calculated variations in in eccentricity, obliquity and precession (Imbrie *et al.*, 1984).

2.3.2 Solar Variability

Solar variability is another example of external climate forcing (Bertrand and Ypersele, 1999; Beer *et al.*, 2000). Physical changes within the Sun may alter the intensity or character of the incoming solar energy. There is no doubt that variations do occur in various characteristics of the Sun on a range of time-scales. The 11-year cycle in the number of sunspots on the face of the Sun is well known. But other parameters, including the solar diameter, vary too, and over different time-scales. What is less clear is whether or not these changes produce significant variations in the total solar output. The total solar energy received by the Earth, or solar constant, has only been measured accurately since the advent of the satellite era. In addition, changes which have been detected over the past 20 years are small in magnitude (<<1%), potentially too small to act as a mechanism of climate change. While the change in solar energy may be greater on longer time-scales, this is only a speculative possibility.

2.3.3 Volcanic Activity

Explosive volcanic eruptions can inject large quantities of dust and sulphur dioxide, in gaseous form, into the upper atmosphere, the stratosphere, where the sulphur dioxide is rapidly converted into sulphuric acid aerosols. Whereas volcanic pollution (from smaller eruptions) in the lower atmosphere is removed within days by rain, the volcanic dust and aerosols in the stratosphere may remain for several years, gradually spreading over much of the globe. Volcanic pollution results in a 5 to 10% reduction in the direct solar beam, largely through scattering as a result of the highly reflective sulphuric acid aerosols. Large eruptions, such as the Mount Pinatubo (Philippines) eruption in 1991, can bring about a global cooling of up to 0.3°C lasting for up to two years.

2.3.4 Atmospheric Composition

The changing composition of the atmosphere, particularly its greenhouse gas content, is a well-known climate forcing. A change in the greenhouse gas content of the atmosphere will affect the energy balance of the climate system. For example, if the amount of CO_2 is increased, more out-going radiation will be trapped in the atmosphere. To restore the

energy balance between energy coming from the Sun and energy leaving the Earth, the temperature of the atmosphere rises. Changes in the concentrations of greenhouse gases can occur in numerous ways. Natural changes in the CO_2 content of the atmosphere occurred at the end of the last Ice Age in response to the Milankovitch Cycles.

The most current concern is the impact of human activities, which could operate on relatively short time-scales necessary to create noticeable changes within the next century. These include the emissions of greenhouse gases and aerosols, changes in land use and the depletion of stratospheric ozone. The only natural effects, which could be important on similar time-scales, are volcanic activity and, possibly, oscillations in the deep ocean circulation.

2.4 Modelling climate

The climate of the Earth has undergone large changes in the past as shown from geological evidence, proxy data, and, more recently, historical records (Hendy and Wilson, 1968; Mildenhall and Moore, 1983; Salinger *et al.*, 1996; Whetton *et al.*, 1996). The climate is changing now and will change in the future. As highlighted in Chapter one, these changes have a profound influence on life on Earth as well as on the environment. There are no physical models which can simulate the complex behaviour of the climate system in a laboratory environment in an adequate manner. For example, the non-linear interactions between the various sub-systems are not possible to reproduce, even partially, in any laboratory experiment.

Factors such as the solar radiation, greenhouse gases in the atmosphere, ice cover and the thermo-dynamical quantities that characterise the climate (temperature, density, velocity, moisture content, salinity etc.) are all linked through a set of physical laws expressed by various equations. These equations are based on the general principles of conservation of mass, momentum, and energy. Considered together with the physical and chemical laws that govern the composition of the components of the climate system, they constitute the fundamental theoretical basis for studying climate and its evolution. The variables in these three-dimensional non-linear equations are interrelated. Any change in one of the

variables may induce variations in the others, which in turn will generate a feedback[1] on the original variable.

The set of coupled partial differential equations can, in principle, be solved subject to the solar radiation input and other specified boundary and initial conditions that define an instantaneous state of the climate system. This mathematically closed set of equations constitutes a well-posed mathematical problem and forms the core of the global circulation models (GCMs). GCMs are time-dependent models, which can simulate explicitly, with as much fidelity as possible the many processes that produce the climate. The goal is to understand these processes and to predict the effects of changes and interactions (McGuffie and Henderson-Sellers, 1997). By solving a series of equations expressing these laws it is possible to obtain a clearer picture of past climates by comparison with observational data, and to predict future climate change.

GCMs can be used to simulate climate on different spatial and temporal scales. Due to limited understanding of the climate system and computational restraints, all models simplify what is a very complex climate system. Simplification is achieved in terms of spatial dimensionality, and space and time resolution.

In view of their high level of simulation capacity however, the GCMs constitute a powerful tool for climate research studies since these models have the potential to simulate climate under a great variety of boundary and initial conditions. It is imperative that the model outputs be compared with the large-scale statistics, obtained from the real world. Such comparisons are critical for validation of any GCM.

---

[1] A feedback is a process whereby an initial change in some variable 'A' leads to a change in variable 'B' which then produces further changes in 'A'. A positive feedback tends to amplify the initial change, and a negative feedback acts to diminish the initial change.

2.4.1 Climate system response

Climate models first solve the mathematical equations to determine a 'base' climate. For models estimating future climate change, the 'base' climate would normally be the present climate conditions of the Earth. Estimates of future increases in greenhouse gases, for example, are then input into the model, which then calculates how the climate might 'evolve' or respond in the future. Climate sensitivity is the quantitative measure of the response of the climate system to a forcing factor, for example, doubling of atmospheric CO_2 concentration. The value of the climate sensitivity will be determined by various feedback mechanisms operating, which may act to magnify or diminish the initial response to climate forcing. In the most complex models, the climate sensitivity will be calculated implicitly through simulations of the processes involved. In simpler models this factor is parameterized explicitly by reference to the range of values suggested by the more complex models. Climate models can also be used to model the climate of past ages, for which we have very little observational records.

During the last decade or so, a number of complex climate models have attempted to simulate future human-made climate change. The ability to model the time-dependent nature of the climate system more adequately has allowed investigation of the damping effects of the oceans on climate change. Because the response time of the oceans, in particular the deep ocean, is much longer than for the free atmosphere, they have a regulating or delaying effect on the warming associated with enhanced greenhouse warming. In addition, the more complex models have allowed increased focus on the critical role of climate feedback processes in determining the climate's response to the enhanced greenhouse effect.

2.4.2 Feedbacks

Among the feedbacks considered in the calculation of global mean climate change are the following:

- Water vapour amount: in a warmer climate increased water evaporation will increase the atmospheric concentration of water vapour. Since water vapour is a greenhouse gas, this represents a positive feedback;

- Clouds: changes in clouds are likely to produce a noticeable feedback due to their strong radiative effect. This feedback depends on changes in the amount, altitude and characteristics of the clouds, as well as on the reflectivity of the underlying surface, therefore even the sign of the feedback is uncertain;

- Areal extent of ice and snow: a reduction in the area of sea ice and seasonal snow cover on land as climate warms will reduce the surface reflectivity, thereby tending to produce greater warming (a positive feedback). However, concurrent changes in cloud cover complicate the projections considerably;

- Vegetation: changes in the distribution of different biomes or in the nature of vegetation within a given bionic can also lead to changes in the surface reflectivity, thereby exerting a feedback effect on climate change;

- The carbon cycle: the effect of climate on the terrestrial biosphere and the oceans is likely to alter the sources and sinks of CO_2 and CH_4, leading to changes in their atmospheric concentrations and hence causing a radiative feedback.

- Ocean changes: Ocean warming could lead to changes in marine plankton and their emissions of dimethyl-sulphide (DMS). The consequent effect on cloudiness is potentially a significant negative feedback on global warming.

Of these feedbacks, those involving water vapour and clouds respond essentially instantaneously to climate change, and those involving sea ice and snow respond within a few years. These are referred to as 'fast' feedbacks. Other feedbacks such as some vegetation and carbon cycle processes are relevant on a time-scale of decades, and others such as a reduction in the area of continental ice sheets, dissolution of carbonate sediments in the ocean and enhanced chemical weathering require hundreds to thousands of years to unfold. These are referred to as 'slow' feedbacks.

2.4.3 Regional climate response

Different combinations of forcings involving ozone (O_3), aerosols and well-mixed greenhouse gases will produce substantially different climate changes in any given region. This is especially true for increases in tropospheric aerosols, where regional cooling can occur in the midst of global mean warming, and to a lesser extent for stratospheric and tropospheric O_3 changes (Houghton *et al.*, 1996). Thus, the climate change in a given region associated with a given global mean forcing depends on the specific forcings involved when combining aerosol and ozone forcings with those of well-mixed greenhouse gases, even if the global mean temperature response is roughly the same. Furthermore, when large net negative forcings occur at the regional scale due to the effects of aerosols, the cooling effects will not be restricted to the immediate regions where aerosols occur, due to the effects of heat transport by winds and ocean currents.

There will also be strong regional variations in the climate response to greenhouse gas increases even in the case of well mixed gases, such as CO_2 and CH_4, whose forcing is relatively uniform from one region to the other. This is due to spatial variations in the nature and strength of various feedback processes (such as those involving snow cover, sea ice and clouds) and in atmospheric winds and ocean currents, which can be expected to change in response to overall changes in the global climate (Houghton *et al.*, 1996).

2.5 Climate change in the 21st century

Prediction of climate change over the next 100 to 150 years is based solely on climate model simulations. Understandably, the vast majority of modelling has concentrated on the effects of continued man-made pollution of the atmosphere by greenhouse gases, and to a lesser extent and more recently, atmospheric aerosols. The main concern, at present, is to determine how much the Earth will warm in the near future.

2.5.1 Climate model simulations

During the last decade or so, a number of complex climate models have attempted to simulate future man-made climate change. Significant results indicate the fastest

warming rate of climate change the Earth has experienced since modern civilisation 10,000 years ago (Saunders, 1999):

- a global average warming of 0.3°C per decade, assuming non-interventionist greenhouse gas emission scenarios;
- a natural variability of about 0.3°C in global surface air temperature on time-scales of decades;
- regional variations in the patterns of temperature and precipitation change, with more warming in the higher (polar) latitudes.

The ability to model the time-dependent nature of the climate more adequately has allowed scientists to investigate the delaying effects of the oceans on climate change. The response time of the oceans, in particular the deep ocean is much longer than for the atmosphere; hence they have a regulating or damping effect on the warming associated with the enhanced greenhouse effect, slowing down the rate of global warming. In addition, the more complex models have allowed increased attention to focus on the critical role of climate feedback processes in determining the climate's overall response to the initial enhancement of the greenhouse effect.

2.5.2 Greenhouse feedbacks

Climate models have estimated the temperature change associated with a doubling of atmospheric CO_2 concentrations in the absence of feedback processes to be approximately 1.2°C (the theoretical temperature change associated with a doubling of pre-industrial atmospheric CO_2 concentrations). When feedbacks are included within the model, the CO_2 doubling temperature change is estimated to be 1.5°C - 4.5°C, a number known as 'global equilibrium climate sensitivity'. These estimates show a large range of uncertainty in the model outputs. The additional rise in temperature in the models can be attributed to climatic feedbacks. The most important climatic feedbacks to the enhanced greenhouse effect include the water vapour feedback, the cloud feedback and the ice-albedo feedback.

2.5.3 Water Vapour Feedback

The importance of water vapour feedback in climate change has long been recognised. Water vapour is itself a greenhouse gas. The increase in temperature resulting from higher levels of CO_2, CH_4 and N_2O causes an increase in evaporation and hence the amount of atmospheric water vapour. This in turn enhances the greenhouse effect still leading to further warming, evaporation and more water vapour, which is a positive feedback.

2.5.4 Cloud Feedback

Cloud feedback is the term used to encompass effects of changes in cloud and their associated properties with a change of climate. Although clouds further enhance the greenhouse warming of the climate by absorbing more outgoing infrared radiation (positive feedback), they can also produce a cooling effect through the reflection and reduction in absorption of solar radiation (negative feedback). This uncertainty in cloud feedback, and the different ways GCMs implement them, is the main cause of the wide range in estimates of the global climate sensitivity (Cess *et al.*, 1990).

2.5.5 Ice-Albedo Feedback

The conventional explanation of the amplification of global warming by snow and ice feedback is that a warmer Earth will have less snow cover, resulting in a lower global albedo (reflectivity) and further absorption of more sunlight, which in turn causes a further warming of the climate. Most climate models have simulated this positive surface albedo feedback. The greatest changes in temperature projected to occur in the 21st century are at the high (snow-covered) latitudes.

2.5.6 Expected climate change in the future

Climate change associated with anthropogenic emissions is expected to continue. The IPCC developed a range of scenarios, IS92a to IS92f, of future greenhouse gas and aerosol precursor emissions based on assumptions concerning population and economic growth, land-use, technological changes, energy availability and fuel mix during the

period 1990 to 2100 (IPCC, 1996b). Through understanding of the global carbon cycle and of atmospheric chemistry, these emissions are used to project atmospheric concentrations of greenhouse gases and aerosols and the perturbation of natural radiative forcing.

The increasing realism of simulations of current and past climate by coupled atmosphere-ocean climate models has increased confidence in their use for projection of future climate change. Important uncertainties remain, but these have been taken into account in the full range of projections of global mean temperature and sea-level change.

For the mid-range IPCC emission scenario, IS92a, assuming the 'best estimate' value of climate sensitivity and including the effects of future increases in aerosol, models project an increase in global mean surface air temperature relative to 1990 of about 2°C by 2100 (IPCC, 1996b). This estimate is approximately one-third lower than the 'best estimate' in 1990. This is due primarily to lower emission scenarios, the inclusion of the cooling effect of sulphate aerosols, and improvements in the treatment of the carbon cycle. Combining the lowest IPCC emission scenario (IS92c) with a 'low' value of climate sensitivity and including the effects of future changes in aerosol concentrations leads to a projected increase of about 1°C by 2100. The corresponding projection for the highest IPCC scenario (IS92e) combined with a 'high' value of climate sensitivity gives a warming of about 3.5°C. In all cases the average rate of warming would probably be greater than any seen in the last 10,000 years, but the actual annual to decadal changes would include considerable natural variability. Regional temperature changes could differ substantially from the global mean value. Due to the thermal inertia of the oceans, only 50-90% of the eventual equilibrium temperature change would have been realised by 2100 and temperature would continue to increase beyond 2100, even if concentrations of greenhouse gases were stabilised by that time.

Average sea level is expected to rise as a result of thermal expansion of the oceans and melting of glaciers and ice-sheets. For the IS92a scenario, assuming the 'best estimate' values of climate sensitivity and of ice-melt sensitivity to warming, and including the effects of future changes in aerosol, models project an increase in sea level of about 50

cm from the present to 2100. This estimate is approximately 25% lower than the 'best estimate' in 1990 due to the lower temperature projection, but also reflecting improvements in the climate and ice-melt models. Combining the lowest emission scenario (IS92c) with the 'low' climate and ice-melt sensitivities and including aerosol effects gives a projected sea-level rise of about 15 cm from the present to 2100. The corresponding projection for the highest emission scenario (IS92e) combined with 'high' climate and ice-melt sensitivities gives a sea-level rise of about 95 cm from the present to 2100. Sea level would continue to rise at a similar rate in future centuries beyond 2100, even if concentrations of greenhouse gases were stabilised by that time, and would continue to do so even beyond the time of stabilisation of global mean temperature. Regional sea-level changes may differ from the global mean value owing to land movement and ocean current changes.

Confidence is higher in the hemispheric-to-continental scale projections of coupled atmosphere-ocean climate models than in the regional projections, where confidence remains low. There is more confidence in temperature projections than hydrological changes. All model simulations, whether they were forced with increased concentrations of greenhouse gases alone or together with increased concentrations of aerosols, show the following changes which are associated with identifiable physical mechanisms:

- greater surface warming of the land than of the sea in winter;
- maximum surface warming in high northern latitudes in winter, with little surface warming over the Arctic in summer;
- enhanced global mean hydrological cycle, and increased precipitation and soil moisture in high latitudes in winter.

In addition, most simulations show a reduction in the strength of the north Atlantic thermohaline circulation and a widespread reduction in diurnal range of temperature. These features too can be explained in terms of identifiable physical mechanisms. The direct and indirect effects of anthropogenic aerosols have an important effect on the

projections. Generally, the magnitudes of the temperature and precipitation changes are smaller when aerosol effects are represented, especially in northern mid-latitudes. It is appreciated that the cooling effect of aerosols is not a simple offset to the warming effect of greenhouse gases, but significantly affects some of the continental scale patterns of climate change, most noticeably in the summer hemisphere. The spatial and temporal distribution of aerosols greatly influences regional projections, which are therefore more uncertain. A general warming is expected to lead to an increase in the occurrence of extremely hot days and a decrease in the occurrence of extremely cold days.

Warmer temperatures will lead to a more vigorous hydrological cycle; this translates into prospects for more severe droughts and/or floods in some places and less severe droughts and/or floods in other places. Several models indicate an increase in precipitation intensity, suggesting a possibility for more extreme rainfall events. Knowledge is currently insufficient to say whether there will be any changes in the occurrence or geographical distribution of severe storms e.g. tropical cyclones.

Chapter Three

Research Framework Outline

To derive local-scale climate information, free atmospheric indices were associated to local climate variables. Multivariate statistics and artificial neural networks were techniques adapted in a comparative study for their potential to local climate variables from outputs of GCM transient climate change experiments. Subsequently, the artificial neural networks model was employed in the construction of scenarios for precipitation and temperature changes over New Zealand from one GCM transient run.

A water balance model was adapted to evaluate changes in catchment water yield associated with changes in climate elements. The precipitation and temperature change scenarios were used in hydrological catchment response case studies for two hydrologically different New Zealand catchments, and the results were translated into risk descriptors as an example of information which water managers need to adapt to climate change while taking account of basic management options.

3.1 Research framework

This study forms part of a generalized framework of a model-assisted approach, which constitutes three basic steps, presented as 1, 2 and 3 in Figure 3.1 where:

- Step 1 requires integrated comprehensive long-term in situ observations of land and ocean for a global scale that describe the current and past state of the Earth system. The New Zealand region was considered for this study.

- Step 2 includes investigation of the physical, chemical, biological and geological processes and societal influences that govern Earth-system behaviour and the interactions with the global environment at different spatial and temporal scales.

- Step 3 involves analyses of consequences of change, which include evaluation and interpretation of the resource system's performance under changed climate.

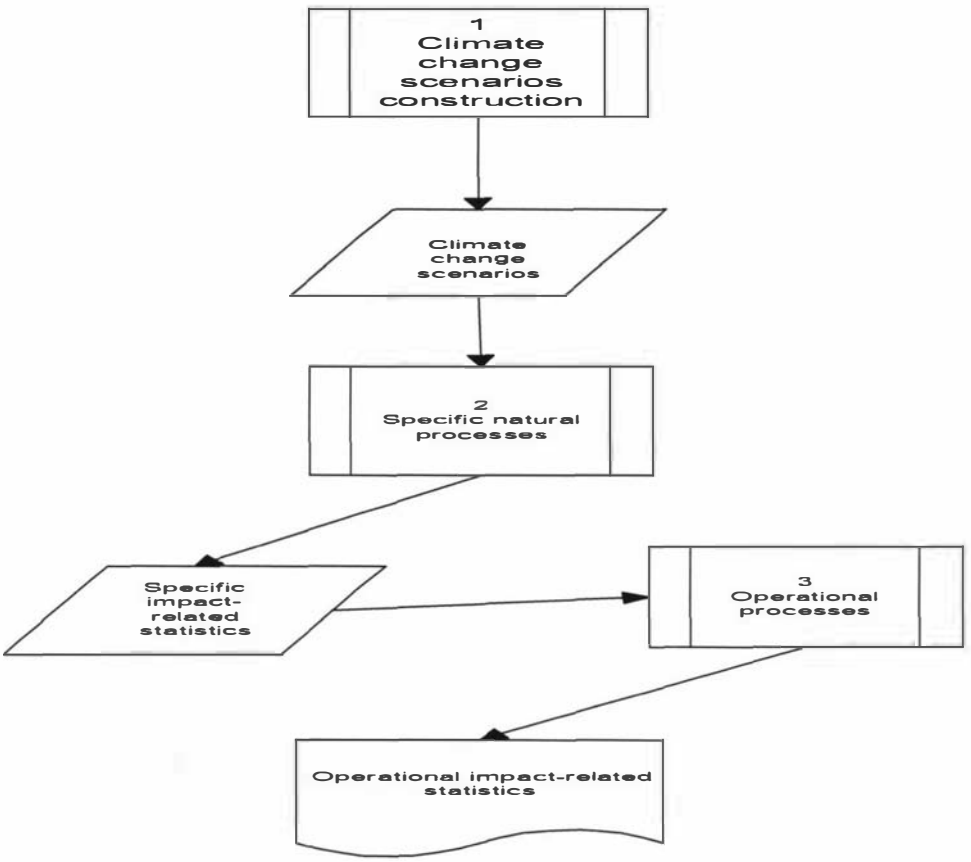

Figure 3.1 Elements of a model-assisted methodology for estimation of the impact of climate change on resource system performance.

3.2 Data

3.2.1 Observed data

Climatological data sets were provided by The National Institute of Water and Atmospheric Research Ltd. (NIWA), through a project supported by New Zealand Foundation for Research, Science and Technology. The basic data sets, which were used, include: -

- 1958-1996 monthly mean temperature and precipitation over New Zealand, from 10 and 19 observation stations, respectively.

- 1958-1996 free-atmosphere circulation variables (monthly mean sea level pressure, 850 and 700hPa geopotential heights) and wind speeds (at 10m). These were extracted from the National Centres for Environmental Prediction (NCEP) reanalysis, on 2.5° latitude x 2.5° longitude grids for New Zealand (35.0-47.5°S and 165-180°E).

The mean sea level pressure data are 12.5°latitude by 15°longitude 'box' averages, centred on New Zealand and to the north, south, west and east. Zonal and meridional mean sea level pressure gradients were determined from the differences between pressure averages of 'boxes' east-west, and north-south for zonal and meridional components, respectively. The geopotential thickness values were determined as differences between respective 850 and 700hPa geopotential heights averaged over New Zealand (35.0-47.5°S and 165-180°E). Similarly wind speeds at 10m were averaged over New Zealand. Precipitation data were gridded on 0.25° latitude x 0.25° longitude for 34.75-47.25°S and 167.25-178.75°E region and eighteen representative grid points were used in the subsequent analysis and the temperature records (most complete) for Chateau, Dunedin, Gisborne, Invercargill, Kaitaia, Milford, New Plymouth, Queenstown, Waipoua, Wanganui, and Wellington were used.

Hydrological data sets (1958-1996) for the Lake Taupo catchment inflows (natural and total), lake levels and the outflows to meet the demands of the Waikato Hydro Scheme were provided by the Mighty River Power authorities. The Opihi River flows and the Level Plains Irrigation Scheme operational water demands from the Opihi River were obtained from the Canterbury Catchment Board and Regional Water Board publication no. 28.

3.2.2 GCM outputs

Projected circulation data were provided by the Climate Impacts LINK Project, University of East Anglia (Norwich, UK) from the output of transient global climate change experiments performed with the Hadley Centre coupled ocean-atmosphere global climate model (HadCM2). The recent experiments used the new Unified Model (Cullen,

1993). These experiments represent a large step forward in the way climate change is modelled by GCMs and raises new possibilities for scenario construction. This experiment has overcome some of the major difficulties that were associated with the previous generations of equilibrium (IPCC, 1990) and cold-start transient (Houghton *et al.*, 1992) climate change experiments.

HadCM2 has a spatial resolution of 2.50° x 3.75° (latitude by longitude) and the representation produces a grid box resolution of 96 x 73 grid cells. This produces a surface spatial resolution of about 417 km x 278km at the equator reducing to 295 x 278km at 45° North and South.

The equilibrium climate sensitivity of HadCM2, that is the global-mean temperature response to a doubling of effective CO_2 concentration, is approximately 2.5°C, although this quantity varies with the time-scale considered. This is somewhat lower than most other GCMs (Houghton *et al.*, 1992).

In order to undertake a 'warm-start' experiment, it is necessary to perturb the model with a forcing from an early historical era, when the radiative forcing was relatively small compared to the present. The Hadley Centre started their experiments performed with HadCM2 with forcing from the middle industrial era, about 1860 (Mitchell *et al.*, 1995 and Johns *et al.*, 1995).

A series of integrations used the combined equivalent CO_2 concentration plus the negative forcing from sulphate aerosols. These integrations simulated the change in forcing of the climate system by greenhouse gases since the early industrial period (taken by HadCM2 to be 1860). The addition of the negative forcing effects of sulphate aerosols represents the direct radiative forcing due to anthropogenic sulphate aerosols by means of an increase in clear-sky surface albedo proportional to the local sulphate loading (Mitchell *et al.*, 1995). The indirect effects of aerosols were not simulated.

The modelled control climate shows a negligible long-term trend in temperature over the first 400 years. The trend is about +0.04°C per century, which is comparable to other

such experiments. HadCM2 represents an improvement over previous generations of GCMs that have been used at the Hadley Centre (Johns *et al.*, 1995; Airey *et al.*, 1995).

The experiments performed have simulated the observed climate system using estimated forcing perturbations since 1860. Johns *et al.* (1995) and Mitchell *et al.* (1995) have established that HadCM2's sensitivity is consistent with the real climate system. The agreement between the observed recent 100-year record of global-mean temperature and that produced in these experiments is better when the greenhouse gases and sulphate aerosols effects are combined than when the effect of greenhouse gases are considered alone.

3.3 Climate change scenarios

In Chapter Four, an artificial neural networks (ANN) and a multivariate statistics (MST) models were calibrated and verified in a comparative study for their potential in downscaling GCM information from transient climate change experiments. In Chapter Five the ANN model was used to derive monthly temperature and precipitation time series (1980-2099) for 18 points on a 0.25°latitude x 0.25°longitude over New Zealand (Figure 3.2).

3.4 Catchments' response

The development of a predictive understanding of how global warming is affecting natural resources is among the most complex of all scientific undertakings. This study focuses on water resources to illustrate the application of transient climate change scenarios in impact assessment. In Chapter Eight, a water balance model (WBM) was calibrated and validated in two case studies of catchment response to predicted climate changes.

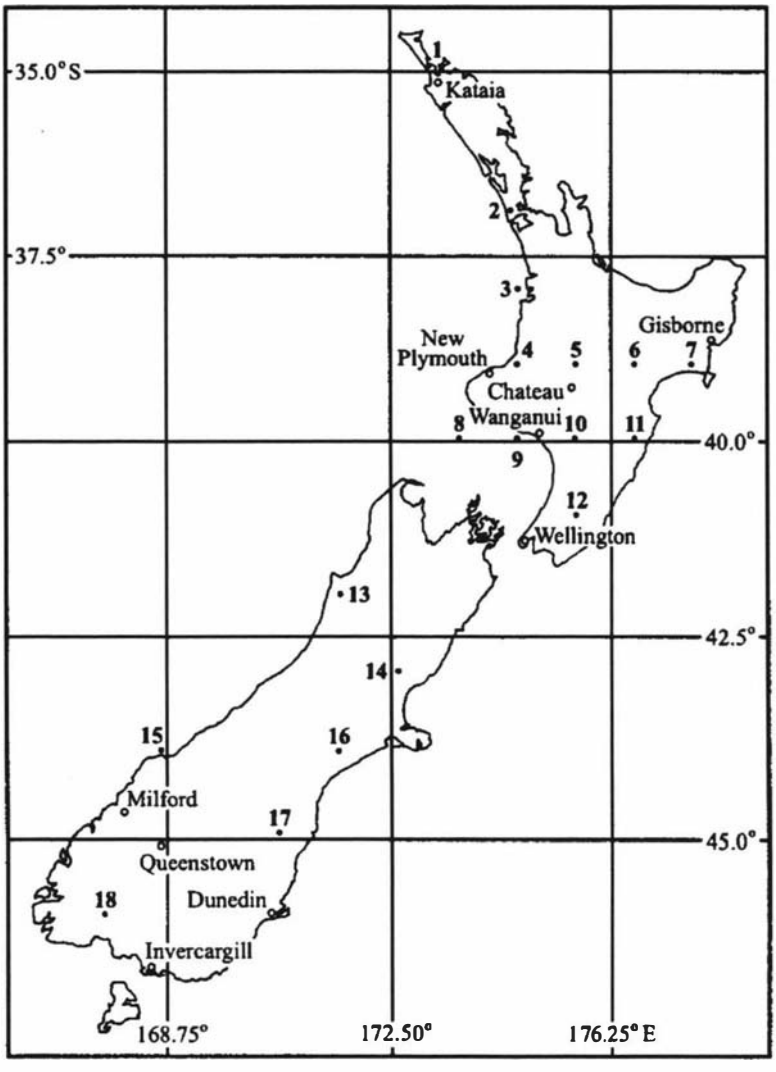

Figure 3.2 Location of selected 18-precipitation study points on 0.25° latitude by 0.25° longitude grid and 10-temperature study sites.

3.5 Assessment of impacts on water resources

Operational risk descriptors that account for water availability (quantities) are mathematically formulated in terms of reliability, resiliency and vulnerability with a view of translating the hydrological changes associated with climate change to quantify water resource systems' performance in chapter Eight.

Chapter Four

Climate change scenarios construction

To assess the impacts of climate change there is a clear need for consistent representations of future changes in climate, in the use of so called 'climate change scenarios'. The first part of this chapter presents an overview of techniques used in the construction of climate change scenario. In the second part, a semi-empirical approach through statistical relationships between local climate variable (predictands) and free-atmosphere regional circulation variables (predictors) was developed to downscale GCM outputs of transient climate change experiments. The artificial neural networks and multivariate statistics techniques were adapted to capture cross-scale relationships using this approach in a comparative study of their potential in downscaling GCM outputs.

4.1 Overview

There are two general techniques for climate change scenarios construction, namely empirical methods and process-based models. The use of general circulation models is the most promising method for predicting global climate changes as acknowledged by the International Panel of Climate Change (IPCC, 1996a).

Empirical methods include the instrumental analogues, palaeo-analogues or spatial analogues for climate change. This approach was used in earlier works by involving the following procedures:

- hypothetical scenarios usually put in the framework of sensitivity analysis by applying an ensemble of potential climates;
- historical scenarios using data from historic periods that 'mimic' a changed climate if available; and
- analogue scenarios where the changed climate in one location is potentially similar to the predicted climate change in another location.

For example palaeo-analogues and analogues drawn from the instrumental record have been used to develop climate change scenarios for New Zealand (Pittock and Salinger, 1982; Salinger and Hicks, 1990).

The process-based models consist of a hierarchy of mathematical models of the climate system. The direct use of GCMs' outputs has the advantage of providing scenarios explicitly from climate change experiments. These scenarios can be used to give a clearer picture of the past climates by comparison with observational data, and to predict future climate change.

Due to the complexity of the climate system processes, however, global climate models are simplifications of the real world. Furthermore, the interaction of the climate system processes with one another produces feedbacks and therefore solutions of model equations have to start from some initialized state and investigate the effects of changes in a particular component of the system. The boundary conditions such as sea surface temperatures, solar radiation or vegetation distributions are set from observational data or independent simulations. These data are mere estimates and rarely of adequate accuracy to completely specify the environmental conditions. As a result, the nature of the boundary conditions is a cause of an inherent uncertainty in the model outputs.

In order to simulate the climate of the globe, general circulation models must integrate all the interactions between the whole climate system. This poses great problems because the various interactions operate on different time scales. For example, the effects of deep ocean overturning may be very important when considering climate averaged over decades to centuries, while local changes in wind direction may be unimportant on these time scales. If, on the contrary, monthly time scales were important, the relative importance of changes would be reversed.

Early climate change scenarios were derived from GCM outputs based on equilibrium conditions (Houghton *et al.*, 1992; Mullan, 1993; Kidson and Watterson, 1995). These GCMs performed experiments to simulate the equilibrium response of the climate system to an instantaneous increase (usually a doubling) of the atmospheric CO_2 concentration.

The major drawback of these experiments is that the resulting equilibrium-doubled CO_2 climate assumed that the components of the climate system were in steady state. In reality, however, this is unlikely to happen since there are unquantifiable and unequal lags between the components of the climate system, particularly when the forcing is not stationary. Furthermore, it is less straightforward to interpret results from equilibrium experiments in terms of calendar years, which limits their use.

Outputs of GCMs for transient climate change experiments are now available. Transient climate change experiments are performed with coupled ocean-atmosphere general circulation models. Due to computational limitations, the first generation of these experiments performed only multi-decadal (up to 100 years) transient climate experiments. Consequently, these experiments lacked long spin-up integrations (required to obtain a steady–state between the ocean and atmosphere systems) and hence suffered the so-called 'cold-start' problem and, in many cases, suffered from serious climate drift. These problems also prevented calendar years from being attached to the results of such experiments and therefore they are treated in much the same way as those from the equilibrium climate change experiments.

Such first generation experiments provided average conditions for January and July and were generated by maintaining a climate forcing appropriate to one particular month and running the model for hundreds of days. These simulations were termed, for example, 'perpetual January' or 'perpetual July' depending on the forcing (McGuffie and Henderson-Sellers, 1997).

Currently, the second generation of transient climate change experiments have been used to examine the response of the climate system to the historic forcing of greenhouse gases and sulphate aerosols that has occurred since the early industrial period. These are 'warm-start' experiments with longer control integrations and longer spin-up periods, therefore, they do not suffer so badly from climate drift. Results from such experiments can be interpreted in terms of calendar years. Nevertheless, low-frequency 'natural' variability in the model, such as that associated with ENSO or IPO fluctuations will have random phase compared to real world. This is because GCMs are not initiated to actual

initial state and the oscillations are unpredictable at extended time range due to the influence of chaotic weather effects.

The GCMs are run for multi-year seasonal cycles, and these are used to produce ensemble averages, e.g. those performed with HadCM2. The predicted conditions apply to an average time period (season), e.g. an average month of July and not to a particular July in the period for which the prediction is made. Ensemble series produced by perturbing initial conditions for each of an ensemble set indeed show that any 'new' climate predicted has variation about the mean, just as with the present climate. The nature of this new variation, however, is of concern when used to estimate the possible impacts of climate change on a regional or local scale.

There are still many problems in the surface climate parameters generated via modelling to support the construction of climate scenarios for a specific impacts model or application. It is the mismatch in spatial (and sometimes temporal) scales between GCMs and impact studies that presents the biggest challenge for successful climate change scenario construction and application. The current high resolution GCMs produce a surface spatial resolution of about 417 km x 278 km reducing to 295 x 278 km at 45° North and South while for the impact assessment for water resources, the minimum desired spatial resolution would be of the order of 10 km. For example, important elements such as precipitation and temperature have localised characteristics that cannot be resolved with the current resolution of current general circulation models. The problem can be partially attributed to scale mismatches, local topography, regional geography and boundary conditions between general circulation models and local climate elements.

Efforts have been made to bridge this gap between the resolution of GCM outputs and the required climate change information, for assessment of their economic and social impact. They have been reviewed by Giorgi and Mearns (1991) and subsequently, in the IPCC report (Houghton *et al.*, 1996). Downscaling approaches ranging from simple to complex techniques are still under development and more work needs to be done in comparing these methods and quantifying their accuracy.

Simple interpolation of coarse GCM grid data to a finer grid has been tried. This approach is simple and easy to use, but lacks reliability. It attracted a lot of criticism for its fundamental assumption of trust in GCM outputs at individual grid points (Wigley *et al.*, 1990; von Storch *et al.*, 1993; Cubasch *et al.*, 1996). There are three key approaches for downscaling GCM outputs (Giorgi and Mearns, 1991):

- dynamical or nesting of high resolution, limited area models within a GCM
- empirical methods
- semi-empirical techniques using transfer functions between scales (Eastering, 1999).

The nesting method uses a regional fine-mesh model referred to as a Limited Area Model (LAM) that is nested in a GCM. In the nesting procedure, the GCM output is used to provide the initial and lateral atmospheric boundary conditions necessary to drive the regional model (Giorgi, 1990; Mearns *et al.*, 1995). In this approach, the GCM is used to simulate realistic large-scale atmospheric behaviour over an area of interest and the LAM is used to describe the effect of local, sub-GCM grid scale forcings (such as topography) on regional patterns of climate variables. While this approach is conceptually consistent with the GCM's representation in terms of the climate system dynamics, it suffers from several limitations including high computing costs and time-consuming processing for developing long-term climate scenarios.

This method has been applied to short periods of a few months (Giorgi 1990; Giorgi *et al.*, 1994) and in examining New Zealand climate for a few years (Renwick *et al.*, 1998). To simulate New Zealand climate a LAM was nested within the output of the Australian CSIRO[1] nine-level generation circulation model. The GCM output was used to derive a regional model run at 125-km grid spacing over the Australian region. The 125-km run was used in turn to derive a simulation at a 50-km resolution over New Zealand. Spatial

[1] CSIRO: Commonwealth Scientific and Industrial Research Organisation

patterns of mean simulated precipitation and surface temperatures improved markedly with increased horizontal resolution of the country's topography (Renwick *et al.*, 1998).

The approach of nesting LAMs in GCMs has potential ability to simulate small-scale atmospheric features such as orographic precipitation (Renwick *et al.*, 1998) and may ultimately provide data that reflect the natural heterogeneity of the climate at regional scales. The success of a dynamic model strongly depends on its horizontal resolution although the computational expenses limit the sample sizes (Cubasch *et al.*, 1996), on top of the inherent errors by the GCM.

Empirical methods typically involve statistically relating observed station or area-average meteorological data to a given weather classification scheme (sometimes coupled with weather generators), which may be either objectively or subjectively derived (Wilby and Wigley, 1997). Objective and/or automated weather classification procedures include principal components, canonical correlation analyses, fuzzy rules and correlation-based pattern recognition techniques such as the 'British Isles Lamb' weather types (Jones *et al.*, 1993).

GCM simulated changes have been commonly 'normalised' or 'scaled' to pattern of change 'per degree global warming'. For example, this approach has been used in some of the IPCC regional climate change projections (Kattenberg *et al.*, 1996) and by the CLIMPACTS[2] programme in New Zealand (Kenny *et al.*, 1994). The scaling approach has a disadvantage of suppressing regional climate dynamics (such as low frequency variations that obscure underlying climate change signal) exhibited in the outputs of the GCMs' transient experiments. Scaling was necessary when only equilibrium model simulations were available, which provided just the 'end-points'. For example, $1xCO_2$ and $2xCO_2$ GCM simulations were used for interpolation with respect to a given absolute time frame.

[2] New Zealand climate change, variability and environmental effects programme

In this study, the semi-empirical approach through statistical relationships may offer a more immediate solution and significantly lower computing requirements (Kidson and Thompson, 1998). A reasonable strategy is to trust the predicted large-scale changes and, whenever possible, to infer local changes by means of sensibly projecting the large-scale information to the local scale. It is widely accepted that the present day GCMs are able to simulate regional-scale, free atmosphere state in a generally realistic manner and with less uncertainty (von Storch *et al.*, 1993). Therefore, transfer functions between observed free atmosphere variables and observed surface climate variables may then be used with free atmosphere variables from transient GCM simulations of individual emissions scenario to generate values for surface-based climate variables for climate change studies.

This technique has the advantage of using inputs from both observed site data and model simulations of climate change, but may also have the disadvantage, such as the variance inflation problem, in which the downscaled values do not contain enough variance. Methods of inflation are required to have the variance artificially increased in some manner (Karl *et al.*, 1990).

Such techniques have their origin in the model output statistics and 'perfect prog' approaches to forecasting surface weather elements (Klein 1982; Glahn 1985). They include use of regression analysis (Kim *et al.*, 1984; Klein and Bloom 1989; Hewitson, 1994), and canonical correlations (von Storch *et al.*, 1993). Kernel techniques have been used to determine distributions for daily precipitation for one location using 500 hPa level heights (Matyasovszk and Bogardi, 1995). To assess regional climate change for New Zealand, statistical techniques have been used with some success (Kidson and Watterson, 1995; Whetton *et al.*, 1996).

A multivariate statistics approach termed 'Climatologic Projection by Model Statistics' (Karl *et al.*, 1990) was introduced using a combination of rotated principal components analysis, canonical correlation analysis and inflated multiple regression. Rotated principal components analysis is used with the atmosphere variables and then the scores of the rotated principal components are used simultaneously with surface climate elements in a canonical correlation analysis. The scores of the canonical correlation analysis are used

as predictors in the inflated multiple regression. The regression equations are then used with the canonical correlation scores derived using free atmosphere variables from a GCM output to generate values of surface climate elements. Artificial neural networks offer an alternative to the regression technique and have been used with some success (Hewitson, 1995; MucGinnis, 1997). Observed circulation data has successfully been related to midday temperature inversions using artificial neural networks.

4.2 Semi-empirical cross-scale relationships

From atmospheric dynamics point of view, local climate characteristics may be linked to regional circulation indices. For example, pressure gradients in the horizontal provide the initial stimulus for air motion and the atmospheric thickness is an important indicator of the heat content of the troposphere. Since the choice of free atmosphere circulation indices is arbitrary, it is important that the variables involved in the cross-scale link explain a great part of the observed variability of local climate variables.

Canonical correlation analysis was used to ascertain the relationships between sets of selected regional circulation variables (predictors) and sets of local-scale climate variables (predictands). The predictors considered in the projections of precipitation and temperature include the anomalies of mean sea level pressure, zonal and meridional mean sea level pressure gradients, atmospheric geopotential thickness between 700 and 850 hPa pressure surfaces and wind speed at 10 m above the ground. From the analytical approach of canonical correlation, the following equations where X and Y are predictor and predictand variables, respectively, were considered.

$$W_1 = a_{11}X_1 + a_{12}X_2 + \ldots\ldots + a_{1p}X_p \qquad (4.1)$$

$$V_1 = b_{11}Y_1 + b_{12}Y_2 + \ldots\ldots + b_{1q}Y_q \qquad (4.2)$$

Equation 4.1 gives a new variable W_1, which is a linear combination of the X variables, and Equation 4.2 gives a new variable V_1, which is a linear combination of the Y variables. If C_1 is the correlation between W_1 and V_1, the objective of canonical correlation is to estimate a_{11}, a_{12}, ...,a_{1p} and b_{11}, b_{12}, ..., b_{1q} such that C_1 is maximum.

Equations 4.1 and 4.2 are the canonical equations, W_1 and V_1 are the canonical variates, and C_1 is the canonical correlation.

Once W_1 and V_1 have been estimated, the next step is to identify another set of canonical variates

- $W_2 = a_{21}X_1 + a_{22}X_2 + ...+ a_{2p}X_p$
- $V_2 = b_{21}Y_1 + b_{22}Y_2 + ...+ b_{2q}Y_q$

such that the correlation, C_2, between them is maximum, and W_2 and V_2 are uncorrelated with W_1 and V_1. That is, the two sets of canonical variates are uncorrelated. This procedure is continued until the m^{th} set of canonical variates is identified such that C_m is maximum.

- $W_m = a_{m1}X_1 + a_{m2}X_2 + ...+ a_{mp}X_p$
- $V_m = b_{m1}Y_1 + b_{m2}Y_2 + ...+ b_{mq}Y_q$

The objective of the canonical correlation is to identify m sets of canonical variates, (W_1, V_1), (W_2, V_2)..... (W_m, V_m), such that corresponding canonical correlations, C_1, C_2..... C_m are maximum and

- Correlation between V_j and $V_k = 0$ for all j not equal to k
- Correlation between W_j, and $W_k = 0$ for all j not equal to k
- Correlation between W_j, and $V_k = 0$ for all j not equal to k

This is a maximisation problem solved by standard mathematical procedures incorporated in statistical software packages such as the 'statistical analysis system software' (SAS). This canonical correlation analysis was carried for the observed precipitation and temperature data sets (predictands) of selected New Zealand locations (Figure 3.2) and five free-atmosphere circulation indices (predictors). The set of predictors based on

NCEP-reanalysis consisted of anomalies of mean sea-level pressure, zonal and meridional pressure gradient, the 850-700 geopotential thickness and wind speed at 10 m above the ground. These variables are presented as X_1, X_2, X_3, X_4 and X_5 in the analysis. The anomalies with respect to 1961-1990 were evaluated over 'New Zealand region' (between latitudes 35-47.5°S and longitudes 165-183.75°E) from 2.5° latitude by 2.5° longitude grid data points. The predictands Y_1, Y_2, Y_3 and Y_4 represent precipitation at points 1, 12, 15 and 17, respectively. The predictand Y_5 represents temperatures for Kaitaia and Y_6 for Dunedin. Canonical correlation analysis outputs for January and July (Tables 4.1 through 4.5) present correlation among predictors and between predictor and predictand variables, canonical correlations and their significance and the explained variances.

From the correlation matrices it can be observed that there are positive and negative correlations among the predictor variables (Table 4.1) indicating multicollinearity among the variables. The correlations between the predictors and predictands also show a varying degree of statistical associations with location and season (Table 4.2). These results suggest that the degree of association of precipitation and temperature with circulation indices is location and season dependent. For both January and July, the first and second canonical correlations of 0.92 and 0.82, respectively, (Table 4.3) are statistically significant at an alpha level of 0.05 as shown in Table 4.4. However, large canonical correlation may not necessarily imply a strong correlation between the raw variables of the two sets because the canonical analysis maximises the correlation between linear composites of the variables in the two sets, without the variance accounted for (Sharma, 1996). Moreover, the correlations among predictor variables indicate the existence of multicollinearity in the raw circulation variables. Therefore to ascertain the cross-scale relationships a measure of how much of the variance in predictand variables is accounted for by the predictor variables was considered from the 'redundancy' measure in the canonical correlation analysis.

Table 4.1 shows that precipitation and temperature are associated with circulation variables and their derivatives. The strength of correlation between circulation indices and the local scale variables, however, varies with location and season. Most importantly,

the correlations in Table 4.2 are consistent with the physics and thermodynamics of the atmosphere. For example, the pressure gradients in the horizontal provide the initial stimulus for air motion. Positive zonal pressure gradient anomalies (X_2), which implies an increase in northerly flow, is positively correlated with warmer temperatures. Similarly, the atmospheric thickness, an important indicator of the heat content of the troposphere anomalies (X_4), is positively correlated with station temperature. Mean sea level pressure (X_1) is negatively correlated with station precipitation because positive pressure tendency is associated with anticyclonic developments (drier conditions) and conversely negative pressure tendency is a signal of cyclonic circulation (wetter conditions). A total 'redundancy' of 0.49 for both cases (January and July) is shown in Table 4.5. That implies the canonical variables of the regional circulation indices account for 49% of the variance in the canonical variables of the precipitation and temperature of the considered locations.

Table 4.1 Correlations among the predictor variables for January (Jan) and July (Jul) of 1961-1990. The predictor variables were regional anomalies of: X_1 = mean sea level pressure; X_2 = zonal mean sea level pressure gradient; X_3 = meridional mean sea level pressure gradient; X_4 = atmospheric geopotential thickness between 700 and 850 hPa pressure surfaces; X_5 = wind speed at 10 m above the ground.

	X_1		X_2		X_3		X_4		X_5	
	Jan	Jul	Jan	Jul	Jan	Jul	Jan	Jul	Jan	Jul
X_1	1.000	1.000	0.045	0.045	-0.237	-0.220	0.695	0.695	-0.380	-0.376
X_2	0.045	0.045	1.000	1.000	-0.298	-0.290	0.219	0.218	-0.217	-0.217
X_3	-0.235	-0.220	-0.297	-0.290	1.000	1.000	-0.137	-0.110	0.823	0.817
X_4	0.695	0.695	0.219	0.218	-0.137	-0.110	1.000	1.000	-0.323	-0.313
X_5	-0.380	-0.376	-0.217	-0.217	0.823	0.817	-0.323	-0.313	1.000	1.000

Table 4.2 Correlations between the predictand variables and the predictor variables for January (Jan) and July (Jul) of 1961-1990. The predictand variables were: Y_1 = precipitation at study point 1; Y_2 = precipitation at study point 12; Y_3 = precipitation at study 15; Y_4 = precipitation at study point 17; Y_5 = temperature at Kaitaia; Y_6 = temperature at Dunedin. The predictor variables were regional anomalies of: X_1 = mean sea level pressure; X_2 = zonal mean sea level pressure gradient; X_3 = meridional mean sea level pressure gradient; X_4 = atmospheric geopotential thickness between 700 and 850 hPa pressure surfaces; X_5 = wind speed at 10 m above the ground.

	X_1		X_2		X_3		X_4		X_5	
	Jan	Jul	Jan	Jul	Jan	Jul	Jan	Jul	Jan	Jul
Y_1	-0.146	0.149	0.344	0.342	-0.371	-0.367	0.133	0.121	-0.380	-0.384
Y_2	-0.366	-0.363	0.448	0.449	-0.341	-0.323	-0.175	-0.167	-0.282	-0.278
Y_3	-0.268	-0.264	0.478	0.477	-0.219	-0.201	0.088	0.095	-0.244	-0.239
Y_4	-0.079	-0.085	-0.119	-0.118	-0.324	-0.346	-0.079	-0.096	-0.429	-0.432
Y_5	0.545	0.547	0.351	0.350	-0.305	-0.280	0.780	0.782	-0.321	-0.314
Y_6	0.292	0.292	0.551	0.551	-0.449	-0.438	0.573	0.571	-0.332	-0.331

Table 4.3 Canonical correlations (January and July 1961-1990).

	Canonical correlation		Adjusted canonical correlation		Approximated standard error		Squared canonical correlation	
	Jan	Jul	Jan	Jul	Jan	Jul	Jan	Jul
1	0.915	0.915	0.884	0.885	0.031	0.031	0.838	0.838
2	0.820	0.820	0.777	0.780	0.062	0.061	0.672	0.673
3	0.583	0.588	0.485	0.497	0.125	0.122	0.340	0.346
4	0.383	0.375	0.308	0.292	0.161	0.160	0.146	0.141
5	0.143	0.162	0.070	0.118	0.185	0.181	0.020	0.026

Table 4.4 Test of H0: The canonical correlations in the current row and all that follow are zero for January and July.

	Likelihood ratio		Approx .F		Num DF		Den DF		Pr > F	
	Jan	Jul	Jan	Jul	Jan	Jul	Jan	Jul	Jan	Jul
1	0.029	0.029	3.49	3.69	30	30	74	78	0.0001	0.0001
2	0.181	0.179	2.15	2.29	20	20	64	67	0.0109	0.0062
3	0.552	0.547	1.11	1.19	12	12	53	56	0.3672	0.3124
4	0.836	0.837	0.65	0.68	6	6	42	44	0.6864	0.6629
5	0.980	0.974	0.23	0.31	2	2	22	23	0.7978	0.7353

Table 4.5 Explained standardised variance of the predictand variables by canonical variables (CV) of their own and of the predictor variables, for January and July (1961-1990). The predictand variables were: precipitation at study points 1, 12, 15, 17; and temperatures at Kaitaia and Dunedin. The predictor variables were regional anomalies of mean sea level pressure, zonal and meridional mean sea level pressure gradients, atmospheric geopotential thickness between 700 and 850 hPa pressure surfaces and wind speed at 10 m above the ground.

CV	Explained variance by							
	Predictand canonical variables				Predictor canonical variable			
	Proportion		Cumulative proportion		Proportion		Cumulative proportion	
	January	July	January	July	January	July	January	July
1	0.3253	0.3228	0.3253	0.3228	0.2725	0.2704	0.2725	0.2704
2	0.2132	0.2132	0.5385	0.5361	0.1432	0.1434	0.4157	0.4138
3	0.1838	0.1779	0.7223	0.7140	0.0625	0.0615	0.4781	0.4753
4	0.0887	0.0984	0.8110	0.8124	0.0130	0.0139	0.4911	0.4892
5	0.1026	0.1016	0.9136	0.9140	0.0021	0.0027	0.4932	0.4919

A potentially important application of the identified cross-scale relationships in the observational record includes the interpretation of the distributions of free-atmosphere circulation indices in perturbed GCM simulations. The relationships between the predictors and predictands change from location to location and season to season. Such differences arise because of changes in solar radiation at the top of the atmosphere, local and regional topography, geography, and other boundary conditions. The question arises whether the relationships will be substantially different in a changed climate or a perturbed GCM simulation. In as much as many of the important factors based on atmospheric dynamics remain relatively constant in a perturbed or changed climate, therefore dynamic-based relationships captured using the current observational records may be quite useful in the construction of future climate scenarios based on downscaling GCM outputs. Different semi-dynamic approaches have been considered in associating circulation indices with local surface climates. For example, precipitation probability and amount were found to be strongly related to vorticity (Conway and Jones, 1998; Conway *et al.*, 1996). Large-scale predictors were evaluated to ascertain their potential to determine daily mean temperatures (Huth, 1999). Seasonal mean regional rainfall is related to large-scale sea-level pressure (von Storch *et al.*, 1993). These relationships depend on the physical and dynamic features of a location.

4.3 Artificial neural networks and Multivariate statistics models

While the primary interest of this study was to project local individual climate elements from regional-scale circulation variables, the objective was to obtain simultaneous values of predictands to ensure consistency in time among the projected climate variables by using identical predictors in the relationships with each of the predictands. To achieve this objective, artificial neural network (ANN) and multivariate statistics (MST) models were considered. The ANN and MST models were independently adapted to capture cross-scale relationships between regional free atmosphere circulation indices and local climates (precipitation and temperature). These techniques have one advantage in common that is the ability to express the relationships between the predictor and predictand variables simultaneously as they occur in nature.

The models were calibrated and verified using observed temperature and precipitation over a number of New Zealand stations and the New Zealand regional circulation variables based on reanalysis by the US National Centers for Environment Prediction (NCEP). Monthly anomalies with respect to 1961-1990, for five circulation indices used as input vectors (predictors), included: mean sea level pressure, zonal and meridional mean sea gradients, atmospheric geopotential thickness between 850 and 700 hPa pressure surfaces and wind speed at 10 m above the ground. Output vectors (predictands) comprised of monthly mean temperature and precipitation. Analysis for New Plymouth, Gisborne, Milford and Invercargill stations is presented.

The data sets were divided into two independent data sets: the calibration data sets which span 1961-1990 period and the validation data sets which combine 1958–1960 and 1991–1996 periods (20% of the historical data). On seasonal bases, the analysis was carried out for summer (December, January and February) and winter (June, July and August).

4.3.1 The ANN model

Modelled on the basic functioning of a biological neuron, an ANN model consists of simple computational structures in a richly connected network (Figure 4.1). The model has the ability to learn, to generalise and to identify key characteristics in data (Shannon and Hewitson, 1996; Mehra and Wah, 1992). This technique has an advantage over other standard methods such as regression by not having the constraints of linearity or prescribed non-linearity. The non-linear mapping is a smooth function which gives plausible generalisations and is easy to use (Shannon and Hewitson, 1996).

As illustrated in Figure 4.1, a neural network consists of several layers, each of which has one or more nodes (processors) connected by weighted links. Typically an ANN has an input (predictor) layer, one or more hidden layers and an output layer, each of which has one or more nodes. Connected units affect each other. The contribution of unit i to the input of a unit j equals $W_{ji}A_i$, where W_{ji} is the weight of the connection from unit i to unit j and A_i denotes the level of activation of unit i. The receptive field of a unit (in a biological sense) denotes a spatially localised set of units that provide input to a cell,

rather than a range of values to which a cell responds. A unit's receptive field comprises units j satisfying W_{ji} not equal to zero.

The net input to a unit is the sum of weighted activations of units in its perceptive field, (possibly) a fraction of its previous activation level, and the external inputs (if any) to that unit. Units with external inputs are called 'input units', those with external outputs are called 'output units' and the rest are known as 'hidden units'.

An ANN model is initially 'untrained' and represents a random function. The neural network has to be trained with some sample of data so that the initial random weights are manipulated to represent the relationship between the input and output. Modification of a network's weights makes it react differently. A pair of units that fire together will have their interconnecting weights made more positive, and those which do not fire together will have their weights made more negative. The direction and amount of the weights' modifications are specified by learning rules that attempt to minimize either a function or an estimate error. In supervised learning, the process of ANN training repetitively presents a set of inputs with known target output until desired networks' output is obtained.

The ANN model was trained with a learning algorithm known as conventional feed-forward multi-layer perceptrons with error back-propagation. The central problem that back-propagation solves is the evaluation of the influence of a parameter on a variable whose computation involves several elementary steps. The solution of this problem is given by the chain rule, but back-propagation exploits the particular form of the functions used at each step (or layer) to provide an elegant and local procedure (Cun, 1988).

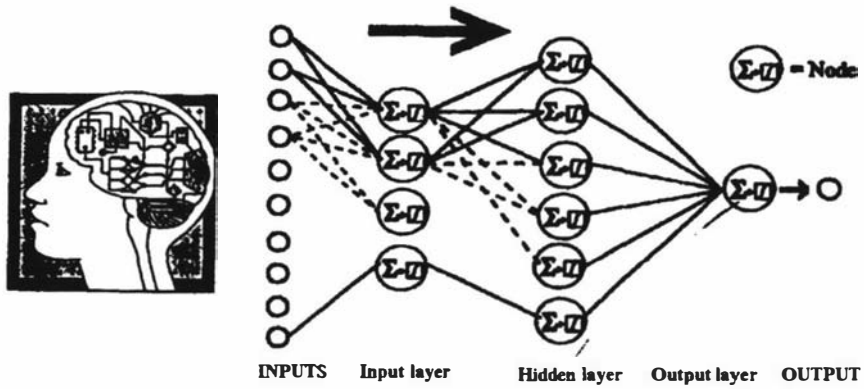

Figure 4.1 A simple artificial neural network (modified after Hewitson and Crane, 1994).

A package of shareware interactive programs (NREBP) for creating, loading, training and computing neural networks was used. The input and output data were scaled to desired ranges by using the following linear transformation:

$$S_{i,p} = a_i X_{i,p} + b_i \tag{4.3}$$

where i is the index which denotes the component of the input vector, p denotes the p^{th} input vector, $S_{i,p}$ is the scaled input, $X_{i,p}$ is the original input, a_i is the scaling factor and b_i is the offset factor.

$$a_i = \frac{(S_i)_{max} - (S_i)_{min}}{(X_i)_{max} - (X_i)_{min}} \tag{4.4}$$

$$b_i = \frac{(X_i)_{max}(S_i)_{min} - (X_i)_{min}(S_i)_{max}}{(X_i)_{max} - (X_i)_{min}} \tag{4.5}$$

where $(S_i)_{max}$ and $(S_i)_{min}$ are respectively the maximum and minimum of the scaled values of the i^{th} component on input, $(X_i)_{max}$ and $(X_i)_{min}$ are respectively the maximum and minimum values of the i^{th} component of the input amongst the available training sets.

Pre-processing of the input data can significantly improve the performance of the network both during training and generalization (Anderson and Rosenfeld, 1988). The transfer function of the hidden and output neurons is a sigmoid. Therefore the network restricts the output variables to the interval [0,1]. This necessitates the scaling of the output variables. To ensure reasonable gradients of a sigmoid, the input data is also scaled to a range of [0,1] (Pao, 1989; Li *et al.*, 1996).

4.3.2 Multivariate statistics model

A multivariate statistics model based on climatological projection by model statistics approach was adapted after Karl *et al.* (1990) to relate regional-scale free-atmosphere indices to station precipitation and temperature observations. The model employs three multivariate statistical techniques:

- principle component analysis
- canonical correlation analysis
- inflated regression analysis

It is acknowledged that each of the above procedures addresses different objectives within the model. The principal component analysis eliminates redundant predictors (or dimensions) which facilitates logical and simple characterisation of climate elements at specific locations and time in terms of predictor variables. Canonical correlation technique provides identical predictors for the relationships with each of the predictands for simultaneous projections, which is important for consistent projections in time among the variables. Since standard multiple regression only seeks to minimise the mean square error between matching observations and predictions, the desired minimum errors in terms of projected distributions in this application can be achieved through reduced errors on month-by-month basis by applying inflation regression.

4.3.2.1 Principal components

Assuming that there are p variables, principal components analysis aims at forming p linear combinations:

$\xi_1 = \omega_{11}x_1 + \omega_{12}x_2 + \ldots\ldots\ldots \omega_{1p}x_p$

$\xi_2 = \omega_{21}x_1 + \omega_{22}x_2 + \ldots\ldots\ldots \omega_{2p}x_p$

.

.

$\xi_p = \omega_{p1}x_1 + \omega_{p2}x_2 + \ldots\ldots\ldots \omega_{pp}x_p$ (4.6)

where: $x_1, x_2, \ldots . x_p$ are variables

$\xi_1, \xi_2, \ldots\ldots\ldots \xi_p$ are the *p* principal components (PCs)

ω_{ij} is the weight of the j^{th} variable of the i^{th} PC for j =1,....., p and i = 1,....., p

The weights ω_{ij}, are determined such that ξ_1, accounts for the maximum variance in the data, ξ_2 accounts for the maximum variance that has not been accounted for by ξ_1, and so on.

$\omega_{i1}^2 + \omega_{i2}^2 + \ldots . \omega_{ip}^2 = 1$ for i = 1, .. ., *p*. (4.7)

$\omega_{i1}\omega_{j1} + \omega_{i2}\omega_{j2} + \ldots\ldots\ldots\ldots + \omega_{ip}\omega_{jp} = 0$ for all $i \neq j$ (4.8)

The condition given by Equation 4.7 requires that the squares of the weights sum to 1 and is somewhat arbitrary. This condition is used to fix the scale of the new variable and is necessary because it is possible to increase the variance of a linear combination by changing the scale of the weights (Sharma, 1996). The condition given by Equation 4.8 ensures that the new dimensions are orthogonal to each other. This is essentially a calculus problem solved by standard mathematical procedures also incorporated in statistical software packages. These weights used for forming the principal component are called eigenvectors (a name derived from the analytical procedure used for estimating the weights).

The variances (eigenvalues) and eigenvectors are determined using standardised data of the predictor variables (e.g. circulation indices) to form 'new' uncorrelated circulation indices without multicollinearity in the predictor variables. The covariance matrix was used to estimate the weights of the linear combinations forming the PCs whose eigenvalues were used to determine the number of PCs to retain for further analysis.

In the atmospheric sciences, numerous procedures have been proposed over the years regarding the number of PCs to retain for analysis (Karl *et al.*, 1990; Richman, 1988). Some of the procedures are informal, while others claim to be more formal. Since the number of initial predictor variables in this application is arbitrary (based on data availability and priori relevance), the question as to the exact number of PCs that should be retained in the analysis is not particularly important. Different selection of predicators can easily lead to a different number of 'statistically significant' PCs. However, if too much information is disregarded the ability to predict local conditions, may be lost.

The PCs are retained by the 'eigenvalue-greater-than-one rule'. This rule is the default option in most of the statistical packages, and its rationale is that for standardised data the amount of variance extracted by each component should, at a minimum, be equal to the variance of at least one variable. As noted by Sharma (1996) this rule is flawed in the sense that, depending on various conditions, this heuristic may lead to a greater or fewer number of retained PCs than necessary and, therefore, should be used in conjunction with other rules. Hence, a 'scree plot' technique (eigenvalues versus the number PCs) was used conjunction with the eigenvalue-greater-than-one rule.

The retained PCs were rotated using 'Varimax' criterion, with an advantage of retaining the orthogonal constraints. This rotation is desirable to maximise the correlation of a few variables with a given PC at the detriment of explaining total variance across the data set (Karl *et al*, 1990). The loadings of the rotated PCs were examined for an indication of the extent to which the original variables are influential or important in forming the principal components. Loadings greater than 0.4 were considered to indicate the influential original variables.

4.3.2.2 Canonical correlation

An overview of the theory and mathematics of canonical correlation is given in Section 4.2. The technique of canonical correlation has been used previously in the atmospheric sciences with some success (e.g. Lawson and Cerveny, 1985). In this application canonical correlation analysis was carried out between the predictands (local scale

climate variables) and the predictors, now in form of scores of the rotated PCs. Canonical variable scores were calculated for each observation and significant canonical variables using standardised scores of the rotated PCs.

Regression equations were developed relating the canonical variable scores to the predictands. A separate regression equation was derived for each predictand, but each equation uses identical canonical variables as predictors. There are several advantages in using canonical correlation instead of regression analysis for capturing the cross-scale relationships. First, the relationships between the predictands and the predictors are simultaneously expressed, as they occur in nature, and yet the concept of common (or explained) variance between the two sets is retained. The interpretation of the relationship between the predictors and predictands can be better understood in this context. In addition to the relationship between the predictors and predictands, the interrelationships among the predictands within each canonical variable are easily assessed. This provides a means to more readily understand why a given local climate may or may not be readily captured by a set of regional free-atmosphere circulation indices under consideration.

4.3.2.3 Inflated multiple regression

The inflated projections are derived from Equation 4.9 after Klein et al. (1958).

$$X_I = \frac{X - \overline{X}}{R} + \overline{X} \tag{4.9}$$

where: X_I is the inflated predictand

X is the projected value of predictand

$\overline{X}$ is the mean of projected predictands over the period under consideration

R is the multiple correlation of the predictand with the predictors

This operation increases the mean square error of estimate but it ensures the reproduction of the mean and variance. Since for climatological purposes the correct mean and

variance of projected data set are more important than the prediction error on any given event, the application of Equation 4.9 was desirable.

From the calibration predictor data sets two PCs were retained for both summer and winter explaining a total variance of 70% in the predictors. In Table 4.6 the 'loadings' of the rotated PCs ($Prin_1$ and $Prin_2$) are presented. The loadings give an indication of the extent to which the original variables are influential or important in forming the principal components score and vice versa. Considering loadings greater than 0.4 to indicate the influential original variables, it is shown that $Prin_1$ is a new dimension that contrasts the anomalies of zonal pressure gradient with the anomalies of meridional pressure gradient and the wind speed 10 m above ground in summer. In winter, $Prin_1$ contrasts mean anomalies of sea-level pressure with meridional pressure gradient and wind speed anomalies. $Prin_2$ complements the anomalies of mean sea-level pressure with the atmospheric thickness in summer. In winter $Prin_2$ complements the anomalies of zonal pressure gradient with the atmospheric thickness anomalies.

Table 4.6 Principal component loadings, where $Prin_1$ and $Prin_2$ represent the first and second rotated PCs respectively. Mslp', dp_z', dp_m', thk' and wsp' are anomalies of mean sea-level pressure, zonal pressure gradient, meridional pressure gradient, 850-700 hPa geopotential thickness, and wind speed at 10 m (above the ground) with respect to 1961-1990.

PC loadings	$Prin_1$		$Prin_2$	
	Jan	Jul	Jan	Jul
Mslp'	-0.147	-0.493	0.909	0.025
dp_z'	-0.506	-0.343	0.046	0.785
dp_m'	0.941	0.825	-0.066	-0.114
thk'	-0.113	0.146	0.912	0.888
wsp'	0.872	0.894	-0.282	-0.027

Canonical correlation analysis between the predictands (precipitation and temperature) and the scores of the rotated PCs for each station and season gave two pairs of canonical variables $\{(W_1, V_1), (W_2, V_2)\}$, where W and V refer to predictor and predictand canonical variables, respectively. As reported in the SAS outputs, both pairs of canonical variables were statistically significant at an alpha level of 0.05 from the approximation of F-test for assessing the significance of the Wilks' Λ (Equation 4.10) and the likelihood ratio of the ^{r}th canonical correlation.

$$\Lambda_r = \prod_{i=r}^{m}(1 - C_i^2) \qquad 4.10$$

where Λ = Wilks value

m = number of canonical variables

i = 1,....., m

C = canonical correlation

The correlations between the canonical variables and the rotated PCs ($Prin_1$ and $Prin_2$) indicated $Prin_1$ to be strongly related to W_1, as much $Prin_2$ is related to W_2. Similarly, strong the correlations were exhibited between V_1 and temperature as well as V_2 and precipitation. As an example of relationships between canonical variables and the scores of the rotated PCs, and the predictands at New Plymouth is given in Table 4.7. By implication, $Prin_1$ can be related to the thermometric variables (temperature) and $Prin_2$ to be associated to moisture-related variables (precipitation).

Table 4.7 Correlations between canonical variables $\{(W_1, V_1)$ and $(W_2, V_2)\}$ and their respective standardised rotated principal components' scores ($Prin_1$_scores and $Prin_2$_scores); and predictands at New Plymouth during winter (June-August) over the calibration period.

Variables	Canonical variables			
	Predictors		Predictands	
	W_1	W_2	V_1	V_2
$Prin_1$_scores	0.971	-0.238	-	-
$Prin_2$_scores	0.289	0.957	-	-
Temperature	-	-	-0.997	0.084
Precipitation	-	-	0.299	0.954

4.3.1 Comparison of model reproduction of means and standard deviations

Modelled and observed mean and standard deviation values of precipitation and temperature over the validation data sets are shown in Tables 4.8 and 4.9. Relatively high root mean square error (RMSE) values are shown in Table 4.8 compared with those in Table 4.9 for the reproduced precipitation. These seasonal differences in RMSE values suggest that the models can capture precipitation characteristics (means and variability) better over winter than over summer. This can be attributed to the fact that winter precipitation events are more associated with large-scale circulation features (e.g. frontal systems) than summer precipitation which can easily be associated with local scale features (e.g. thermal lows).

Similarly, Table 4.8 shows relatively lower RMSE values than Table 4.9 does for the reproduced temperature means and standard deviations for both models illustrating that the models capture summer temperature variability slightly more consistently than in winter. This suggests that summer temperature variability is more of a large-scale atmospheric circulation phenomenon compared with winter temperature variability.

Table 4.8 Observed (Obs) and modelled, artificial neural networks (ANN) and multivariate statistics (MST), precipitation means ($\bar{x}$) and standard deviations (σ) for summer (December - February) using independent data sets. RMSE represents Root mean square error.

Location	Precipitation (mm)						Temperature (° C)					
	Obs.		ANN		MST		Obs.		ANN		MST	
	$\bar{x}$	σ	$\bar{x}$	σ	$\bar{x}$	σ	$\bar{x}$	σ	$\bar{x}$	σ	$\bar{x}$	σ
New Plymouth	90	54	104	57	97	68	17.4	1.1	17.5	1.2	17.6	1.4
Gisborne	51	26	53	48	59	55	19.2	0.8	19.3	0.9	19.5	1.3
Milford	789	346	746	498	665	465	14.5	1.1	14.5	1.4	14.5	1.7
Invercargill	108	54	120	70	110	72	13.9	0.8	13.9	1.1	13.9	1.4
	RMSE		23	77	62	62	RMSE		0.07	0.20	0.18	0.50

Table 4.9 Observed (Obs) and modelled, artificial neural networks (ANN) and multivariate statistics (MST), precipitation means ($\bar{x}$) and standard deviations (σ) for winter (June - August) using independent data sets. RMSE represents Root mean square error.

Site	Precipitation (mm)						Temperature (° C)					
	Obs.		ANN		MST		Obs.		ANN		MST	
	$\bar{x}$	σ	$\bar{x}$	σ	$\bar{x}$	σ	$\bar{x}$	σ	$\bar{x}$	σ	$\bar{x}$	σ
New Plymouth	142	68	149	41	155	68	9.4	0.5	9.4	0.9	9.7	2.2
Gisborne	91	39	89	43	102	57	9.4	0.6	9.5	0.8	9.4	0.7
Milford	421	232	450	165	422	206	5.0	0.8	5.1	0.9	5.2	0.8
Invercargill	83	43	84	39	84	37	4.5	1.4	4.9	1.0	5.2	1.1
	RMSE		15	36	9	16	RMSE		0.2	0.3	0.4	0.9

4.3.2 Comparison of model distribution of modelled and observed anomalies

Quantile-quantile plots (q-q plots) were used to compare distributions of observed and modelled monthly anomalies. If a modelled variable y and observed variable x are

identically distributed then the plot of y-quantiles versus x-quantiles will be a straight-line configuration with slope=1, pointing towards the origin (Wilk and Gnanadesikan, 1968). An elementary property of q-q plots is that if y is a linear function of x then the corresponding q-q plot will always be linear, only with possible changes of line location and slope in case of any transformations of y relative to x values. This linear invariance property makes the use of q-q plots valuable, as linearity is a geometric configuration which can be perceived very easily. Moreover, departures from linearity are sensitively appreciated. The modelled versus observed anomalies for temperature and precipitation were plotted in Figures 4.2 through 4.5. The slope of the q-q plots exceeding one indicates a larger spread of anomalies of modelled variable compared to the observed and suggests that the model errors are not uniform within the distribution. It is shown that both models over estimates or under estimates the observed variables either in the lower or upper end of the distribution.

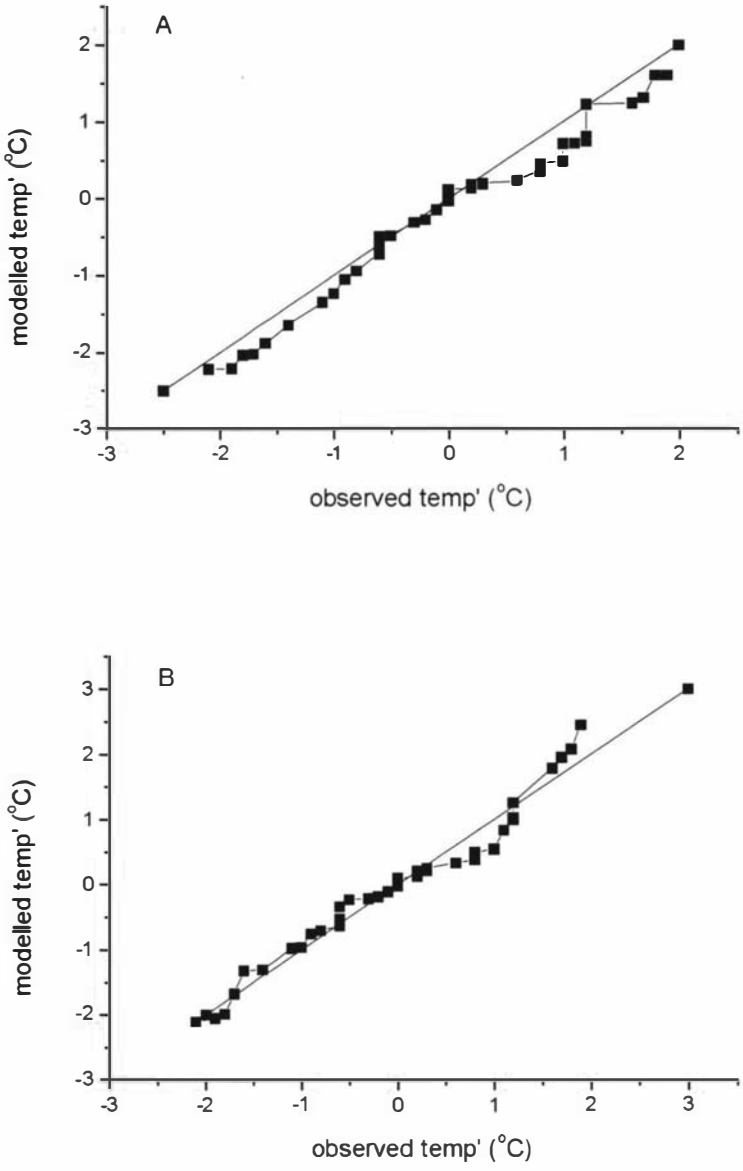

Figure 4.2 New Plymouth: modelled versus observed temperature anomalies (temp') during summer with respect to 1961-1990, where (A) and (B) refers to neural networks and multivariate statistics models respectively.

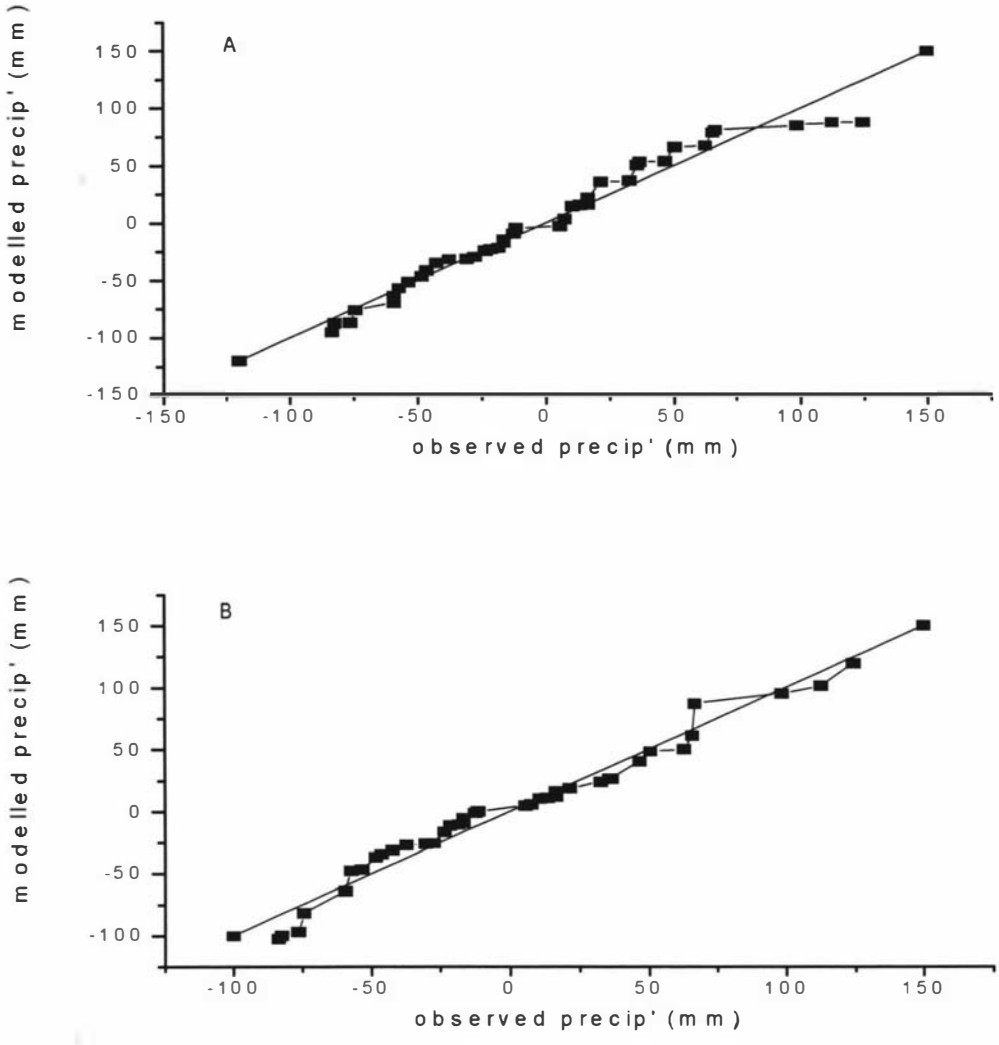

Figure 4.3 New Plymouth: modelled versus observed precipitation anomalies (precip') during summer (December – February) with respect to 1961-1990, where (A) and (B) refers to neural networks and multivariate statistics models, respectively.

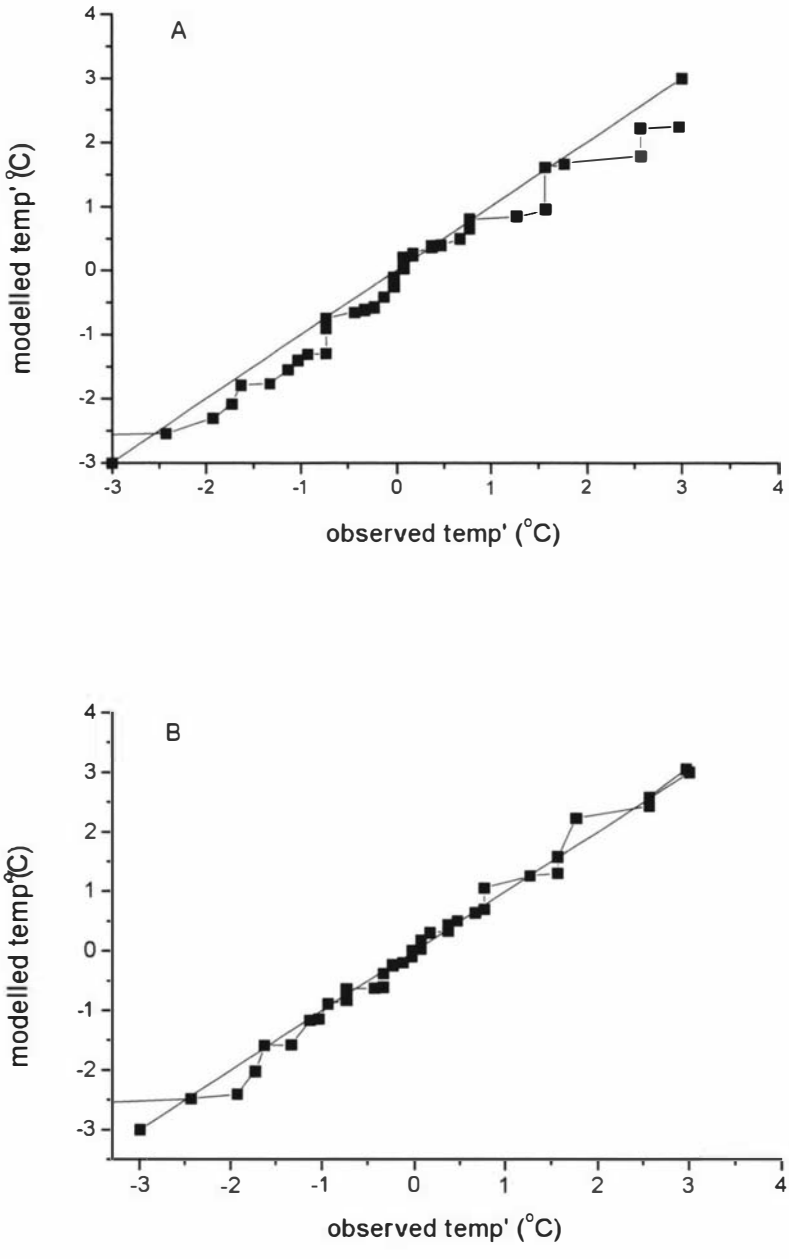

Figure 4.4 Invercargill: modelled versus observed temperature anomalies (temp') during winter (June-August) with respect to 1961-1990, where (A) and (B) refers to neural networks and multivariate statistics models, respectively.

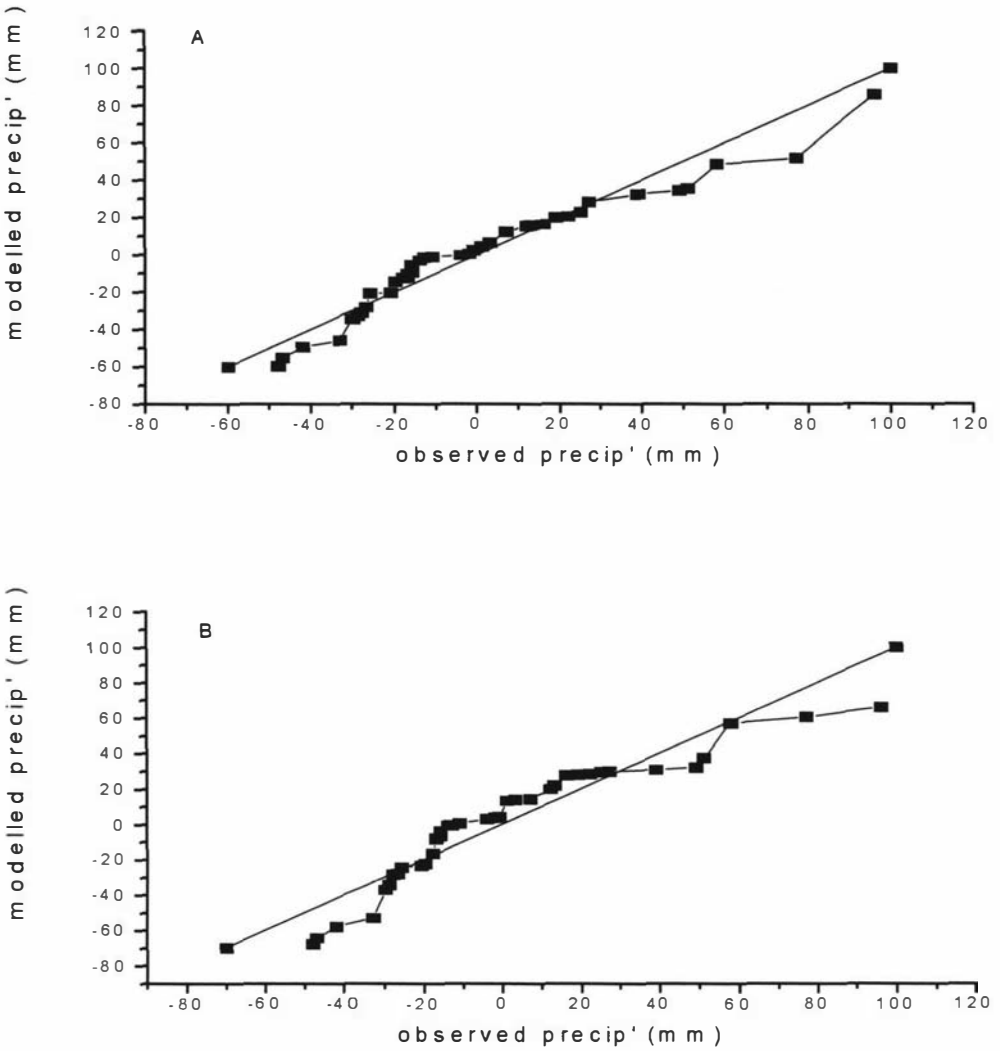

Figure 4.5 Invercargill: modelled versus observed precipitation anomalies (precip') during winter (June-August) with respect to 1961-1990, where (A) and (B) refers to neural networks and multivariate statistics models, respectively.

4.4 Conclusion

Regional circulation indices over New Zealand defined by anomalies of mean sea level pressure, zonal and meridional pressure gradients, atmospheric geopotential thickness for 850-700 hPa pressure surfaces, and wind speed at 10 m above the ground demonstrated significant association (link) with temperature and precipitation events. The results show the atmospheric dynamics point of view, that the pressure gradients in the horizontal

provide the initial stimulus for air motion. For example, positive zonal pressure gradient, which implies an increase in northerly flow, is positively correlated with warmer temperatures. The atmospheric thickness as shown by the strong positive correlation between the 850-700 hPa thickness and temperature anomalies is an important indicator of the heat content of the troposphere.

The artificial neural networks and multivariate statistics approaches were independently adapted to capture the cross-scale relationships between these free atmosphere circulation indices and the local climate characteristics. The output from both the artificial neural networks and multivariate statistics models based on circulation variables from the NCEP reanalysis, verified generally well with the observed mean monthly temperature and precipitation over New Zealand. This was illustrated by the mean and variance reproduction of the observed values by the models.

However, the quantile-quantile plots illustrated some differences between the modelled and observed distributions of anomalies of precipitation and to a lesser extent for temperature in the extreme tails. These discrepancies with respect to the observed anomalies can be attributed to the fact that the time-means features of the circulation variables are not in themselves the causal mechanisms for weather events. For example, precipitation is a discrete process that takes place in short period events. These features only represent the associated mean large-scale climatic environment that encourages or discourages the system responsible for a given local climate condition and therefore the values in the extreme tails tend to blur the captured relationships.

Based on these results, the artificial neural networks and the multivariate models were both proved to be versatile tools in the construction of climate change scenarios by downscaling regional-scale circulation information with semi-empirical approaches. Subsequently, the artificial neural networks model was used in Chapter 5 to downscale precipitation and temperature change scenarios for New Zealand from HadCM2 global climate change transient experiments.

Chapter Five

New Zealand present and future climate

While the regional patterns of future climate change are poorly resolved by GCMs, it is clear that the altered patterns of radiative forcing will alter regional climates noticeably, and will have different effects on climate conditions in different regions. An outline of the main features of New Zealand's present climate is given together with precipitation and temperature change scenarios constructed in this study to put into perspective the potential risks that society faces if these scenarios are realised.

5.1 Present climate

New Zealand is situated between latitudes 34° S and 47° S, narrow and mountainous, with a set of major ranges. The orientation of the main mountain divide (Southern Alps in the South Island and a number of ranges in the North Island) run along a line of 220°. Wind blowing from west of 220° is effectively blocked from the east of the divide, while that from east of 220° (which includes southerlies) is blocked from reaching the western parts of the islands.

The country covers an area of 267,000 km^2 with 1,930 km distance from the extreme north to the extreme south and 400 km from west to east at the widest point. Surrounded by an extensive water body, the nearest landmasses are Australia (1,600 km to the west) and Antarctica (2,200 km to the south). No part of New Zealand lies further than 130 km from the sea. The north of the country protrudes into the subtropical belt of anticyclone, experiencing relatively dry weather with an average temperature of 16°C. The south of the country lies in the westerly wind belt. Average temperature in the south is around 10°C.

5.1.1 Precipitation

As summarised by Maunder (1971), New Zealand climate is largely maritime, except in Central Otago where climate is more 'continental' with hot, dry summers and cold winters. There is a strong west-east gradient in precipitation, especially over the South Island. The mean annual precipitation over the country ranges from over 8000 mm in the Southern Alps to 350 mm in Central Otago, east of the Alps. Most of the country receives 800 to 1600 mm of precipitation on average except those areas in the east of both islands which experience frequent dry spells and droughts. Precipitation above 3200 mm is mostly over mountainous areas which are generally unoccupied by people.

Annual precipitation totals are least variable in the southwest of the country becoming more variable in the east and north. The annual precipitation totals are almost normally distributed with coefficients of variation usually falling in the range of 0.12 to 0.25. Totals in individual years rarely exceed 175% or fall below 50% of the station average. These limits are exceeded only in low precipitation areas from South Canterbury to East Cape.

In this region, troughs with associated depressions and fronts are the major precipitation producing mechanisms. A broad scale ascent of air takes place in areas of strong low-level convergence accompanying transient waves in the upper-level westerly flow. Such conditions usually develop most strongly beneath the zone of maximum wind speed in the upper westerlies. The baroclinic instability due to strong horizontal temperature gradients leads to a rapid increase in the amplitude of the upper level wave with a corresponding increase in cyclonic circulation around a deepening low-pressure centre at the surface. These large-scale cyclonic systems also produce fronts which in turn give birth to smaller waves and depressions.

Occasionally, the westerly pattern breaks down giving way to southerly 'cold snaps' bringing snow to lowlands in winter, or they give way to tropical depressions moving from the north, bringing warm, moist air into the region (November-March). A few indirectly affect New Zealand and they can make a significant contribution to the

precipitation and its relatively high variability in summer in the northern and northeastern areas of the country.

Convective activity in unstable air-mass conditions also contributes significantly to rainfall in many parts of the country. Non-frontal convective activity accounts for 14-20% of the annual precipitation over the three North Island hydro-catchments of Taupo, Waikato and Rangitaiki (Hurnard and Coulter, 1979).

Winter precipitation predominates in the North Island where twice as much precipitation falls in winter as in summer. On the other hand, much of the southern half of the South Island winter is the season of least precipitation where a summer maximum is found inland, partly due to convective showers. Spring precipitation is generally greater in the western parts of the islands and less in the eastern parts corresponding to a seasonal maximum in the westerlies during October and November.

In general, seasonal and monthly precipitation distributions are skewed and can be represented by a 'gamma' frequency curve. The coefficient of variation of seasonal totals ranges from 0.2 in winter and spring in western areas to about 0.5 in summer in northern and eastern North Island districts. Similarly for monthly totals, coefficients of variation of 0.8 to 0.9 have been found for stations in the north and east of the North Island in late summer and 0.3 to 0.5 in western and southern districts in the winter and spring. In the North Island, variability tends to be greatest in summer and least in winter whilst in the South Island it is greatest in summer and autumn and least in spring (Coulter, 1969).

A slight persistence in monthly precipitation is apparent such that for a typical station, the probability of any month having below average precipitation is about 0.55 if the preceding month was 'wet' and 0.60 if it was 'dry'. Runs of 'dry' months are more common than runs of 'wet' months (Coulter, 1969).

5.1.2 Wind and temperature regime

The wind blows from the northwest, west, or southwest for 39% of the time in northern areas, 41% in the central areas and 37% in southern areas. Northerly flow prevails for

11% and 8% of the time in northern and eastern areas respectively. In central and southern areas northerlies prevail for 16-17% of the time (Hurnard and Coulter, 1979).

At the same latitude, the eastern areas are 0.5-1.0°C warmer than the western areas of the country, with a latitudinal gradient of about 1°C per 2°latitude. The change in temperature with altitude approximates the environmental lapse rate of 6.5°C per 1000m and inland areas experience quasi-continental influences to the temperature regime.

Temperature extremes also tend to occur in the drier areas i.e. east of the main mountain ranges. These areas are vulnerable to drought or severe dry spell and widespread flash floods. These events could probably be associated to periodic influence of the El Nino-South Oscillation.

5.2 Climate change scenarios

Preliminary projections of New Zealand climate change were based on early outputs of GCM experiments and qualitative understanding of relationships between regional atmospheric circulation and local climate in 1988 (Mullan *et al.*, 2000), and palaeo-analogues and analogues drawn from the instrumental record (Salinger and Hicks, 1990). Based on New Zealand's previous period of maximum warmth 8-10,000 years ago, this assumes a 1.5°C increase by 2050. Westerly winds would decline by 10%, bringing fewer precipitation days to the western regions, with an increase of 10-15% in precipitation in the west and a decrease of 5-10% in the east. Another scenario assumes a temperature rise of 3°C with more frequent precipitation in the north associated with moist northerlies from the cyclone belt and less precipitation in the south. Under both scenarios, precipitation extremes are expected to be more frequent and widespread. Drought would increase in the east, particularly, in parts of Otago, Canterbury and Hawke's Bay.

First detailed climate change scenarios for New Zealand were constructed in 1990 based on statistical downscaling of GCM and were updated over the next few years (Mullan, 1994; Whetton *et al.*, 1996). These scenarios were still based on outputs of GCMs equilibrium simulations with models which contain 'slab oceans'. Regional climate modelling nested in equilibrium GCM was carried out based on the CSIRO-9 global

circulation model (Renwick *et al.*, 1998, 1999). Projected temperature changes were broadly consistent with those predicted by the statistical downscaling, with the largest increases in the south of the country. Projected changes in the large-scale circulation brought about by an equilibrium doubling of CO_2 concentration indicate a general weakening of the westerly winds over New Zealand. Rainfall is predicted to increase in the eastern regions in most seasons, notably in Canterbury in winter and spring, when the decrease in westerly wind force is largest. In winter, rainfall is simulated to decrease slightly in the west of the North Island. There is a general increase expected in summer, especially over the ocean to the north and east of the country, partly attributed to the extra moisture transport associated with the anomalous northwest flow from the region of the Coral Sea. These regional projections differ somewhat from the results of the statistical downscaling approach, especially the projected increases in rainfall over Canterbury. A review of the most recent changes in Australasia suggests a reduction in snow and a shorter snow season in the Southern Alps (Basher *et al.*, 1998).

With the rapidly growing body of information relevant to the assessment of climate change, previous scenarios of New Zealand climate change have inevitably been superseded. In particular, GCM transient experiments may offer significantly different scenarios. Simulations of broad scale atmospheric circulation by a fully coupled ocean-atmosphere GCM at current resolution are reasonably realistic (Whetton *et al.*, 1996). This is due to the fact that ocean circulation plays an important role in promoting the storage of heat by the deep ocean during climate change. Moreover, the ocean circulation itself changes in response to the changes in the surface fluxes of heat, water, or momentum received from the atmosphere e.g. the bi-decadal Pacific Oscillations.

Transient simulations generally predict an increase in Southern Hemisphere meridional temperature gradient (higher warming rates near the equator than the southern oceans) and consequently strengthening of westerly flow across New Zealand region are projected (Whetton *et al.*, 1996). However, at the current horizontal resolution of GCMs, the local scale climate characteristics over New Zealand like anywhere else, are still not adequately resolved, and therefore the outputs of the GCM transient experiments cannot be used directly to present the country's future climate. Initial work on downscaling from a transient run with one GCM outputs (HadCM2) was undertaken (Mpelasoka *et al.*, 2000) and forms part of this study.

5.3 HadCM2 climate change information

Since 1997, the Climate Impacts LINK Project (UK), has disseminated results of climate change experiments performed with the most recent version of the Hadley Centre's GCM (HadCM2) to a broad cross-section of the international climate-change research community, of which this work forms part. HadMC2 is a state-of-the art coupled ocean-atmosphere GCM, which has provided the platform for a wide range of climate-change simulations over the past 5 to 6 years. HadCM2 has proved to be a particularly successful model, with many characteristics that give confidence in its global scale performance (Johns *et al.*, 1997). However, in common with other models, it has some deficiencies which contribute significantly to uncertainties in the model predictions on top of those due to incomplete knowledge of anthropogenic forcings and the range of possible future emissions scenarios.

In these experiments the model first investigated the response of the climate system to the historic forcing of greenhouse gases and sulphate aerosols that has occurred since the early industrial period. The greenhouse and sulphate aerosols forcings were gradually increased to represent the observed changes in forcings due to all the greenhouse gases and the aerosols from 1860 to 1990. Then from 1990 to 2099 HadCM2 experiments used a 1% per year-compounded increase in concentrations of greenhouse gases and a scenario of sulphate aerosol concentrations derived from the sulphur emissions in the IS92a scenario. The IS92a scenario prepared by the IPCC assumes the world population to be a little over double its present level by 2100 and moderate economic growth. The increasing concentrations in the atmosphere of greenhouse gases alone should have produced a larger warming than observed in recent decades (e.g. Salinger *et al.*, 1996).

The burning of fossil fuels, which also leads to the release of sulphur that oxidises to form hydrated sulphate aerosols (Mitchell and Johns, 1997), has moderated the warming. Sulphate particles scatter the incoming radiation and also act as cloud condensation nuclei, which may lead to more cloud-droplet formation and hence brighter clouds. Then by contrast, sulphate aerosols may produce a global-scale cooling, being greatest in the northern mid-latitudes, where the aerosol loading is the greatest, and in high latitudes in

winter due to feed-backs between sea-ice and temperature (Mitchell and Johns, 1997). The inclusion of sulphate aerosol effects in the general circulation models significantly improves the agreement between GCM predictions and observed global mean and large scale patterns of temperature in recent decades (Mitchell *et al.*, 1995).

5.3.1 Mean sea level pressure fields

A comparison of HadCM2 simulated circulation variables with NCEP reanalysis circulation data over the 'New Zealand region' (latitude 35.0-47.5°S and longitude 165-180°E) was made. HadCM2 validated well with respect to NCEP reanalysis for its 'present climate' simulation at least for the tested free atmospheric variables. For example, a t-test of the mean of 1980-1989 monthly mean sea-level pressure over the 'New Zealand region' shows no significant difference at $p \leq 0.01$. In Figure 5.1 the pattern of HadCM2 and NCEP reanalysis monthly mean sea-level pressure are matched fairly well, and the quantile-quantile plot of the pressure anomalies averaged over the region suggests comparable anomaly distributions from the two data sets.

Figure 5.2 depicts the differences of mean sea-level pressure distributions between 22.5-60 ° S and 150-195 ° E for summer (DJF) and winter (JJA) for the pseudo-present tri-decade and 2070-2099. The 'normal' seasonal circulation variables were determined from the monthly mean values for the tri-decades 1980-2009 (pseudo-present), and 2070-2099.

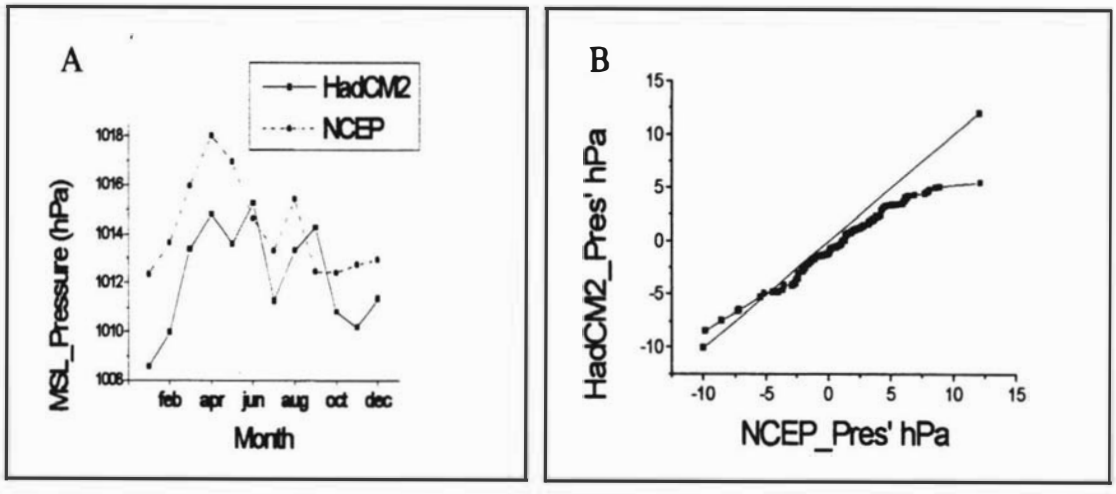

Figure 5.1 'A' Plot of monthly mean sea level pressure (MSL_Pressure) simulated by HadCM2 versus NCEP-reanalysis values over 'New Zealand region' 'B' quantile-quantile plot of HadCM2 and NCEP monthly MSL pressure anomaly distribution (Pres') based on data for the period 1980-1989 for both NCEP and HadCM2.

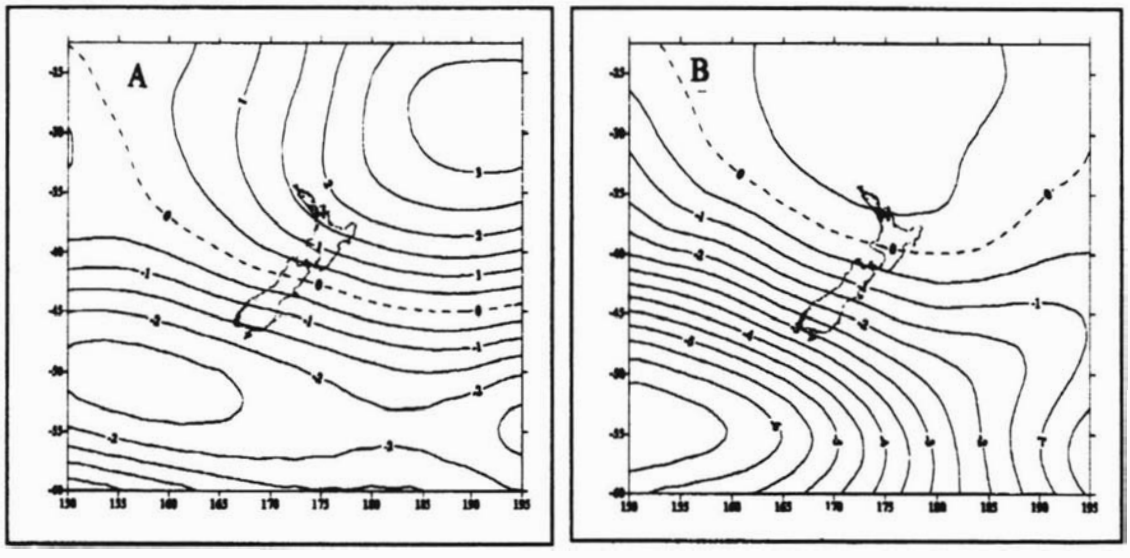

Figure 5.2 HadCM2 mean sea level pressure difference (hPa) between 1980-2009 and 2070-2099 tri-decades for summer (A) and winter (B) respectively.

The differences between mean pressure fields of the pseudo-present tri-decade and 2070-2099 indicate pressure build up in the north-eastern sector coupled with falls centred to the south-west. These pressure field changes will have effects on pressure gradients over the region, as presented in Table 5.1. Mean sea level pressure gradients were calculated from the HadCM2 grid-points for northern, central and southern sectors of New Zealand (areas between latitudes 32.5-37.5; 37.5-42.5; and 42.5-47.5°S, respectively), for January, April, July and October for four tri-decades (1980-2009, 2010-2039, 2040-2069 and 2070-2099). An increase of 30 to 80% with respect to the gradients of the pseudo-present were predicted for the northern sector, with greatest increases in October (spring) and diminishing increases in July (winter) over the tri-decades. In the central sector, the increase in pressure gradients of 12 to 50% were demonstrated with greatest and least increases in winter and summer, respectively. Similarly, over the southern sector pressure gradient increases of between 2 and 45% were predicted showing least increases in summer.

Cyclotrophic mean wind directions calculated from the zonal and meridional pressure gradient components (Table 5.2) showed more of northwesterly winds than of southwesterlies over the northern sector during summer. Westerlies are expected over the central and southern sectors with a tendency to become northwesterlies during the 2070-2099 tri-decade. In other seasons southwesterlies were demonstrated except over the southern sector where a more westerly flow is projected.

Table 5.1 HadCM2 model mean sea level pressure gradients over northern, central and southern sectors of New Zealand (latitudes 32.5-37.5°S; 37.5-42.5°S; and 42.5-47.5°S, respectively) for January, April, July and October during the four tri-decades (1980-2009, 2010-2039, 2040-2069 and 2070-2099).

Tri-decade	Magnitude of mean sea level pressure gradient (hPa per degree of latitude/longitude)											
	January			April			July			October		
	North	Central	South	North	Central	South	North	Central	South	North	Central	South
1980-2009	0.385	0.986	1.574	0.315	0.868	1.617	0.531	0.896	1.395	0.514	0.940	1.560
2010-2039	0.514	1.183	1.710	0.439	1.201	1.980	0.855	1.342	1.645	0.694	1.420	2.167
2040-2069	0.486	1.105	1.617	0.512	1.206	1.967	0.780	1.346	1.737	0.759	1.452	2.133
2070-2099	0.576	1.286	1.821	0.493	1.268	2.066	0.671	1.155	1.663	0.929	1.637	2.249

Table 5.2 HadCM2 model mean derived-wind directions over northern, central and southern sectors of New Zealand (latitudes 32.5-37.5°S; 37.5-42.5°S; and 42.5-47.5°S, respectively) for January, April, July and October during the four tri-decades (1980-2009, 2010-2039, 2040-2069 and 2070-2099).

Tri-decade	Derived- wind direction (degrees)											
	January			April			July			October		
	North	Central	South	North	Central	South	North	Central	South	North	Central	South
1980-2009	266	271	272	254	264	266	263	268	272	269	269	271
2010-2039	273	272	272	259	265	267	269	272	273	269	268	268
2040-2069	272	273	273	259	265	267	268	271	273	264	266	267
2070-2099	277	274	274	259	266	268	266	272	275	265	266	267

5.3.2 Atmospheric thickness

Trend in the atmospheric geopotential thickness was demonstrated by the thickness between 850 and 700 hPa pressure surfaces ($\Psi_{850\text{-}700}$) in geopotential metres (gpm). An average increase of 0.15 and 0.10 gpm per year for January (summer) and July (winter), respectively, is shown in Figure 5.3.

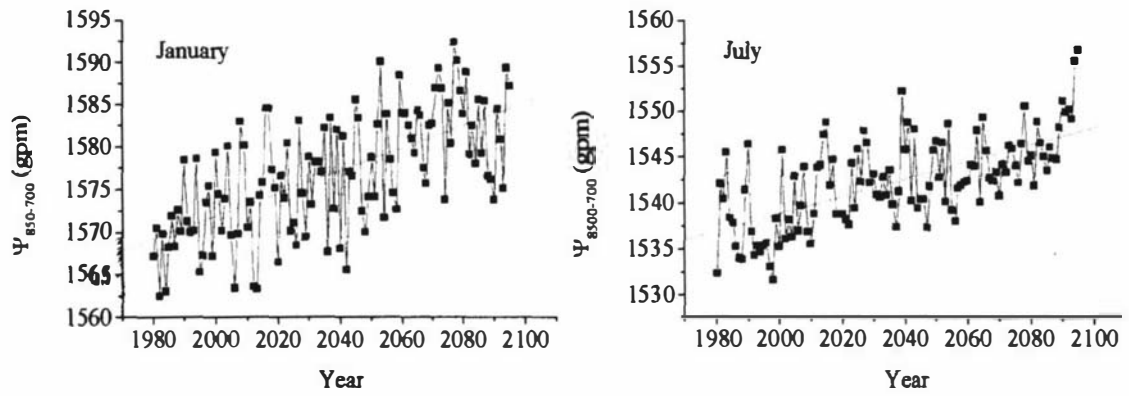

Figure 5.3 HadCM2 model atmospheric thickness between 850 and 700 hPa pressure surfaces ($\Psi_{850\text{-}700}$) in geopontential metres (gpm) for the months of January (left-hand panel) and July (right-hand panel) in the period 1980-2099.

5.4 HadCM2-derived scenarios

Downscaled projections of New Zealand temperature and precipitation changes have been calculated from outputs of the HadCM2 transient simulations forced by emissions IS92a scenario of sulphate aerosol concentration and 1% compounding CO_2 concentration. Projected changes are presented for three tri-decades (2010-2039, 2040-2069 and 2070-2099) with respect to the pseudo-present tri-decade (1980-2009). It is important to appreciate that these scenarios of change are based on only a single emissions scenario.

The downscaled changes for 18 (13 for temperature) (Figure 3.2) locations over New Zealand are contoured to give an idea of the pattern of change across the country. With such a small number of points, the appearance of the maps will depend considerably on how the contouring package works.

What was done here is to use a starting 'guess' value over a fine 0.5x0.5 degree mesh covering NZ, and successively correct this according to available downscaled data with the Cressman interpolation approach widely used in meteorology for ingesting unevenly spaced data. (Cressman, 1959; Seaman and Hutchinson, 1985). Several iterations are made through the data, successively narrowing the radius of influence within which downscaled data are allowed to affect the grid-point value.

The starting guess can be critical with a small number of data points. The guess is assumed to be equal to the value of the data point closest in latitude. This results in contours that tend to run along latitude circles in the absence of further data. On the whole, this assumption tends to give a better pattern than assuming every point has the same starting value (e.g., zero change, or the data average change). If there are two points within one degree latitude, then the start guess is that for the point closer in longitude (thus one could get a 'jump' across NZ if there is a data point on the west coast and a second on the east coast showing rather different changes).

5.4.1 Mean temperature

HadCM2-model derived mean temperatures from the HadCM2 outputs for the pseudo-present tri-decade (1980-2009) range from 14°C in cooler central areas to 18°C in Northland and Auckland during summer. Mean temperatures range from 4°C to 12°C during winter. Changes in mean air surface temperature with respect to the pseudo-present for January (summer), April (autumn), July (winter) and October (spring) are presented in Figures 5.4 through 5.6.

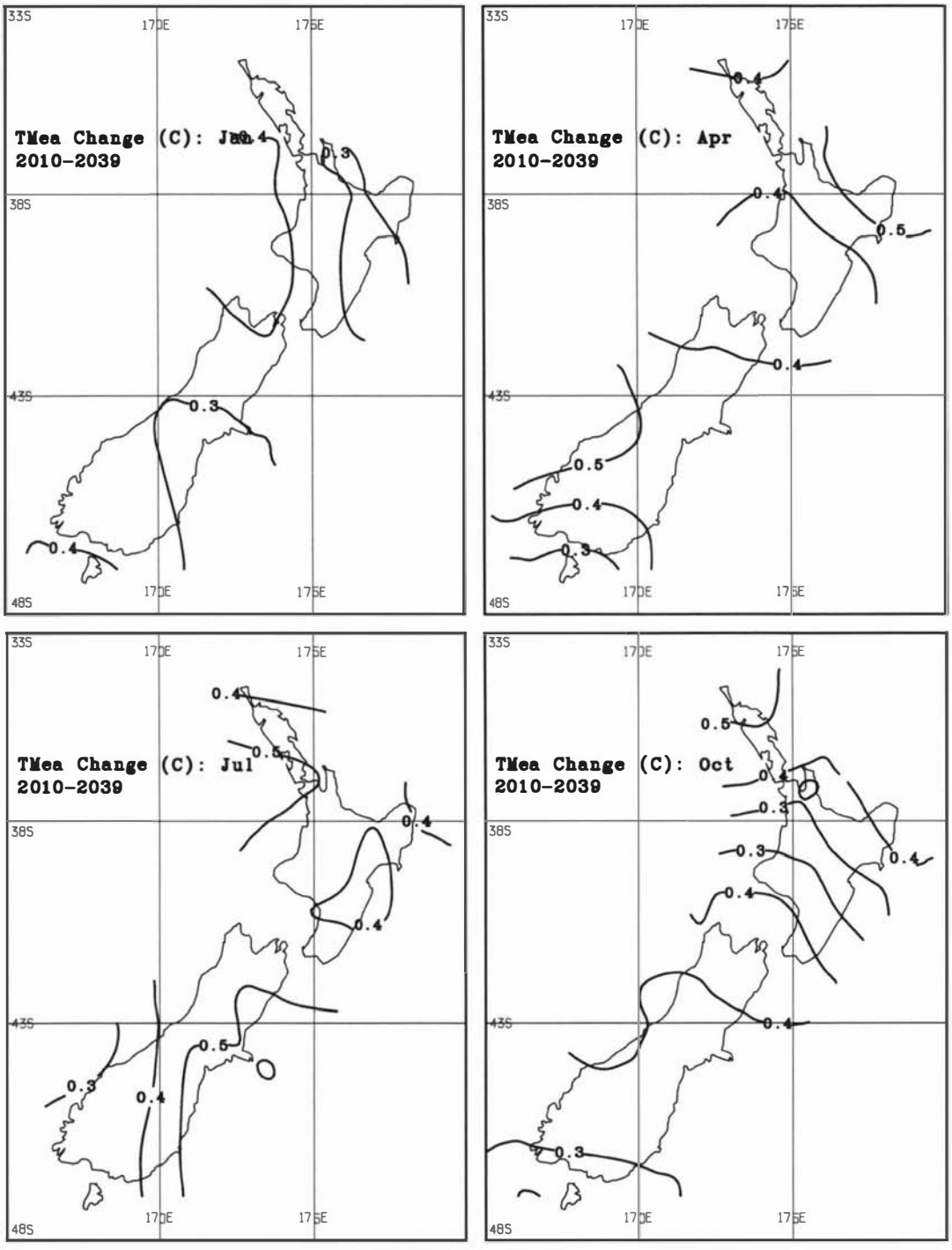

Figure 5.4 HadCM2-model derived mean temperature (Tmean) changes for 2010-2039 with respect to 1980-2009, contours every 0.1°C. Upper panels: left-hand for January (summer) and right-hand for April (autumn). Lower panels: left-hand for July (winter) and right-hand for October (spring).

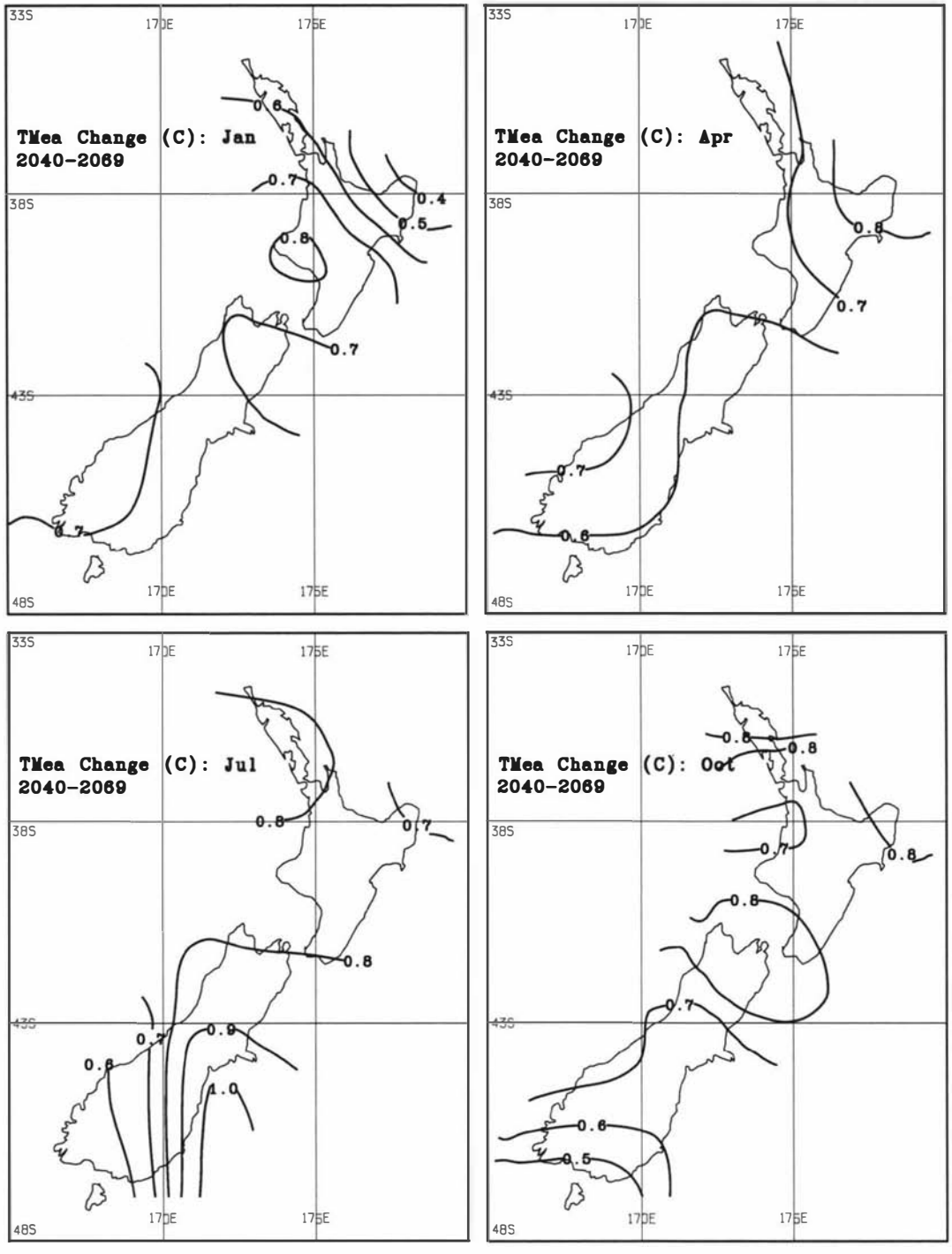

Figure 5.5 HadCM2-model derived mean temperature (Tmean) changes for 2040-2069 with respect to 1980-2009, contours every 0.1°C. Upper panels: left-hand for January (summer) and right-hand for April (autumn). Lower panels: left-hand for July (winter) and right-hand for October (spring).

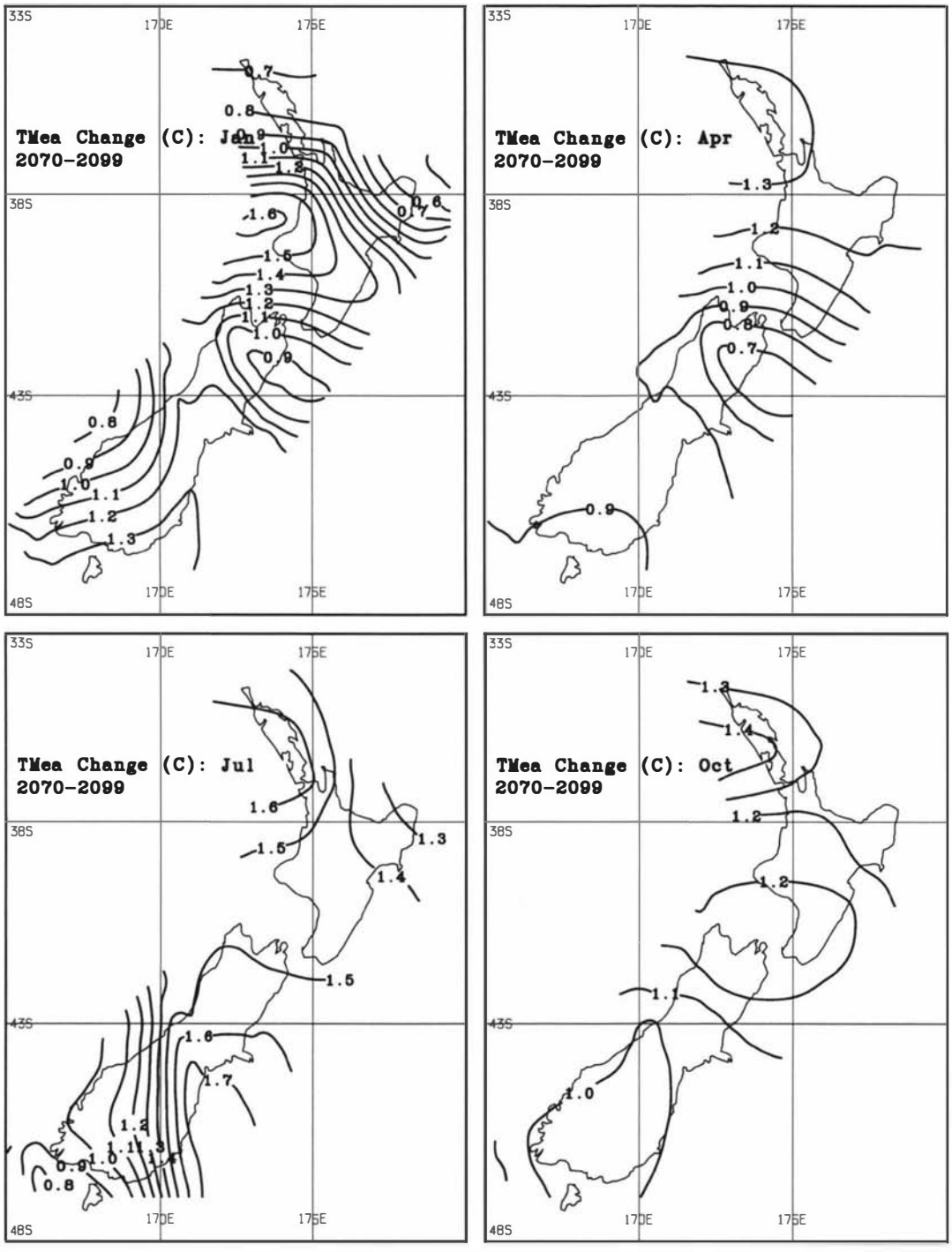

Figure 5.6 HadCM2-model derived mean temperature (Tmean) changes for 2070-2099 with respect to 1980-2009, contours every 0.1°C. Upper panels: left-hand for January (summer) and right-hand for April (autumn). Lower panels: left-hand for July (winter) and right-hand for October (spring).

These temperature change scenarios suggest a general warming of 0.3-0.4°C per tri-decade. Although there is no strong warming gradient over the country for most of the time, a pattern of temperature change is exhibited in the north-south direction. Slightly greater warming is projected for winter than in summer particularly in the North Island. Over the South Island, a west-east warming contrast is projected and can be attributed to stronger westerlies driving land temperatures closer to offshore seas surface temperatures which increases at a relatively lower rate. In the tri-decade 2010-2039, greatest warming of about 0.5°C is over the northeastern areas during April (autumn). In most areas a warming of 0.7-0.8°C is projected in the tri-decade 2040-2069 and 1.5-1.7°C for 2070-2099.

5.4.2 HadCM2-derived precipitation scenarios

HadCM2-derived mean precipitation for the pseudo-present tri-decade ranges from 300 mm/month in the southwest of the South Island to 50 mm/month in the southeastern areas of North Island during summer. During this season the South Island is relatively wetter than the North Island. Winter precipitation distribution shows an overall greater precipitation amount over the North Island ranging from 100 mm/month to 200 mm/month. In the South Island there is a big contrast in monthly precipitation amounts between the western and the eastern areas. Precipitation in the South Island ranges from 300 mm/month in the west to 50 mm/month in the east. A spatial analysis of mid-season month precipitation changes for the tri-decades 2010-2039, 2040-2069 and 2070-2099 is given in Figures 5.7 through 5.9.

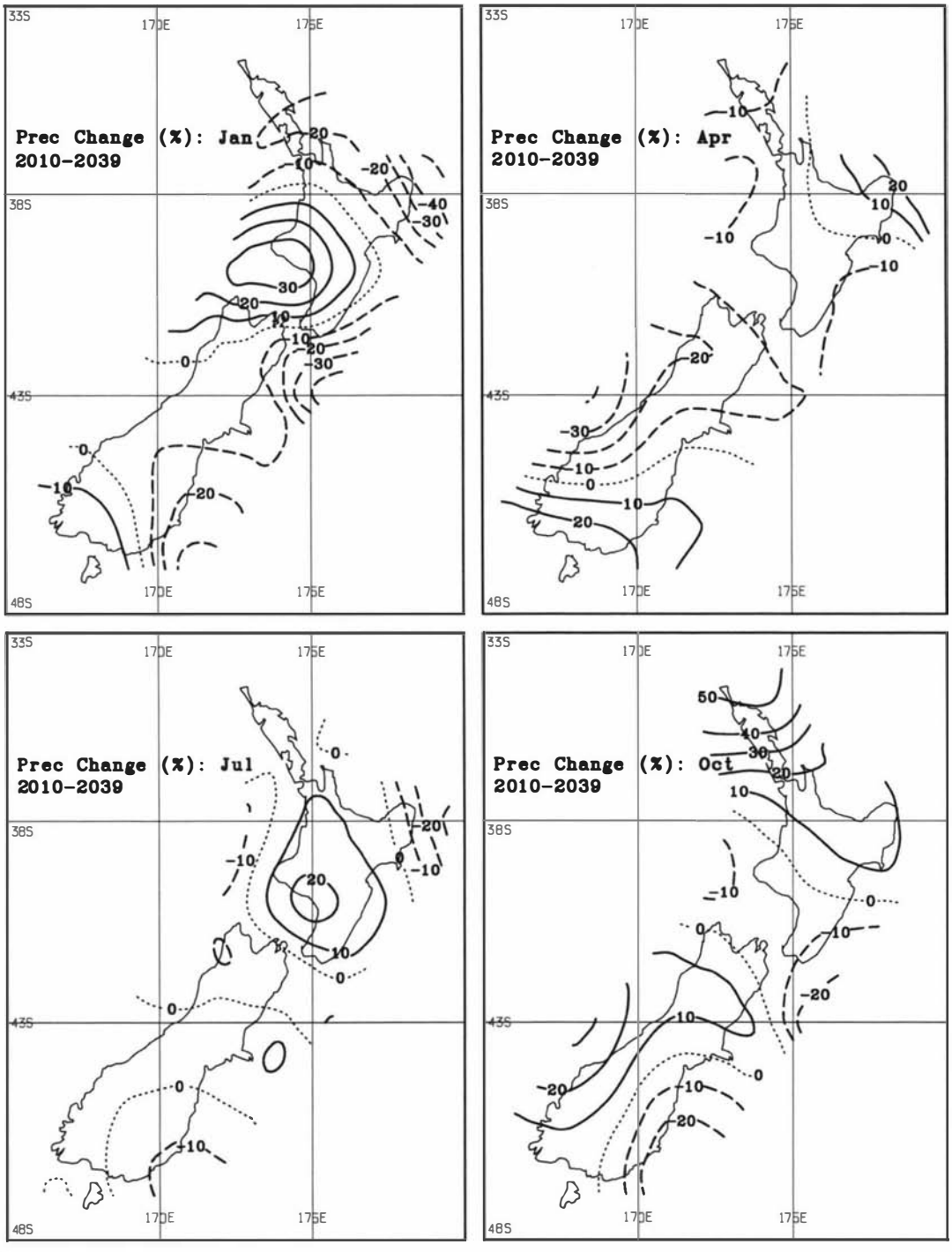

Figure 5.7 HadCM2 model derived precipitation (Prec) changes for 2010-2039 with respect to 1980-2009, contours every 10%. Upper panels: left-hand for January (summer) and right-hand for April (autumn). Lower panels: left-hand for July (winter) and right-hand for October (spring).

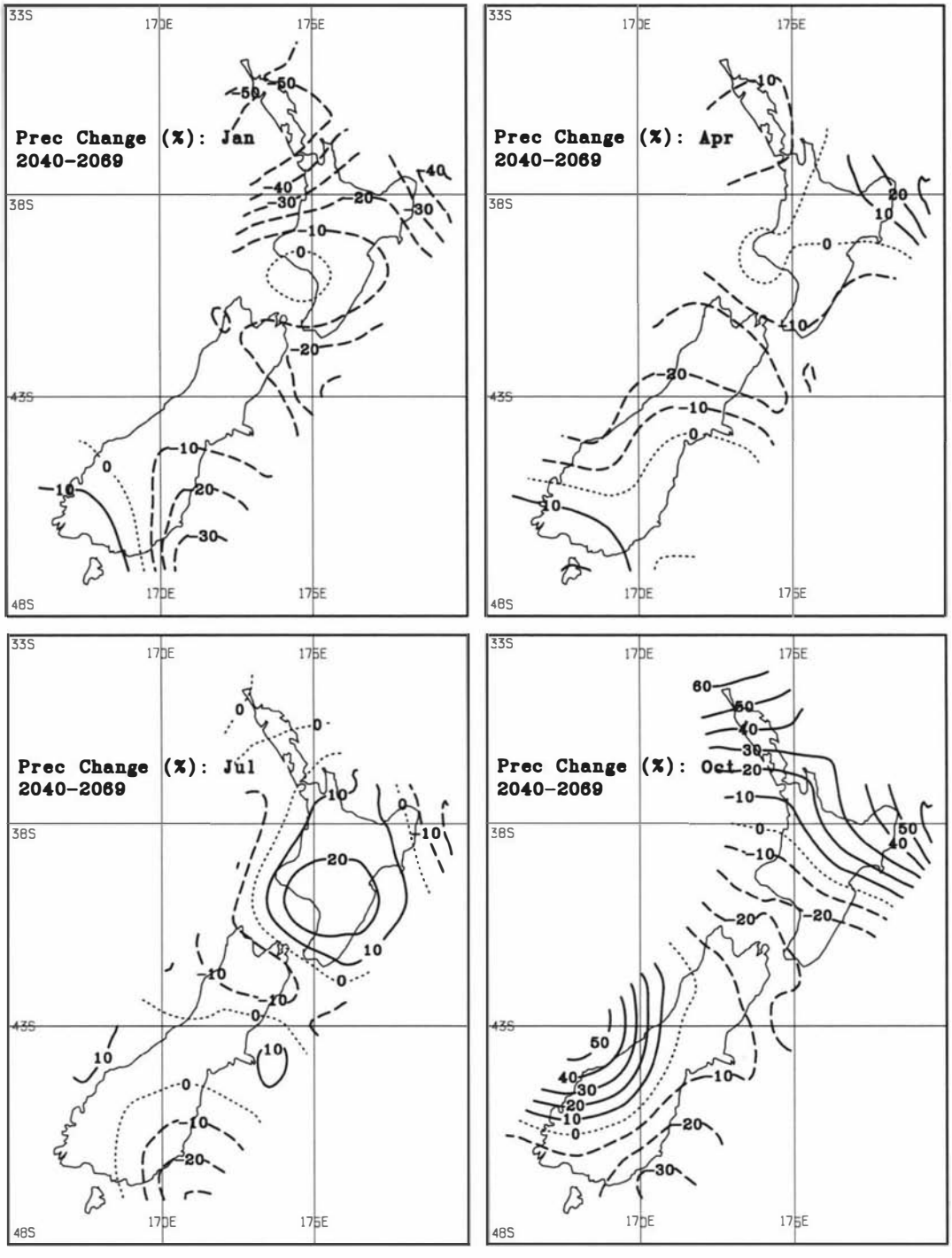

Figure 5.8 HadCM2 model derived precipitation (Prec) changes for 2040-2069 with respect to 1980-2009, contours every 10%. Upper panels: left-hand for January (summer) and right-hand for April (autumn). Lower panels: left-hand for July (winter) and right-hand for October (spring).

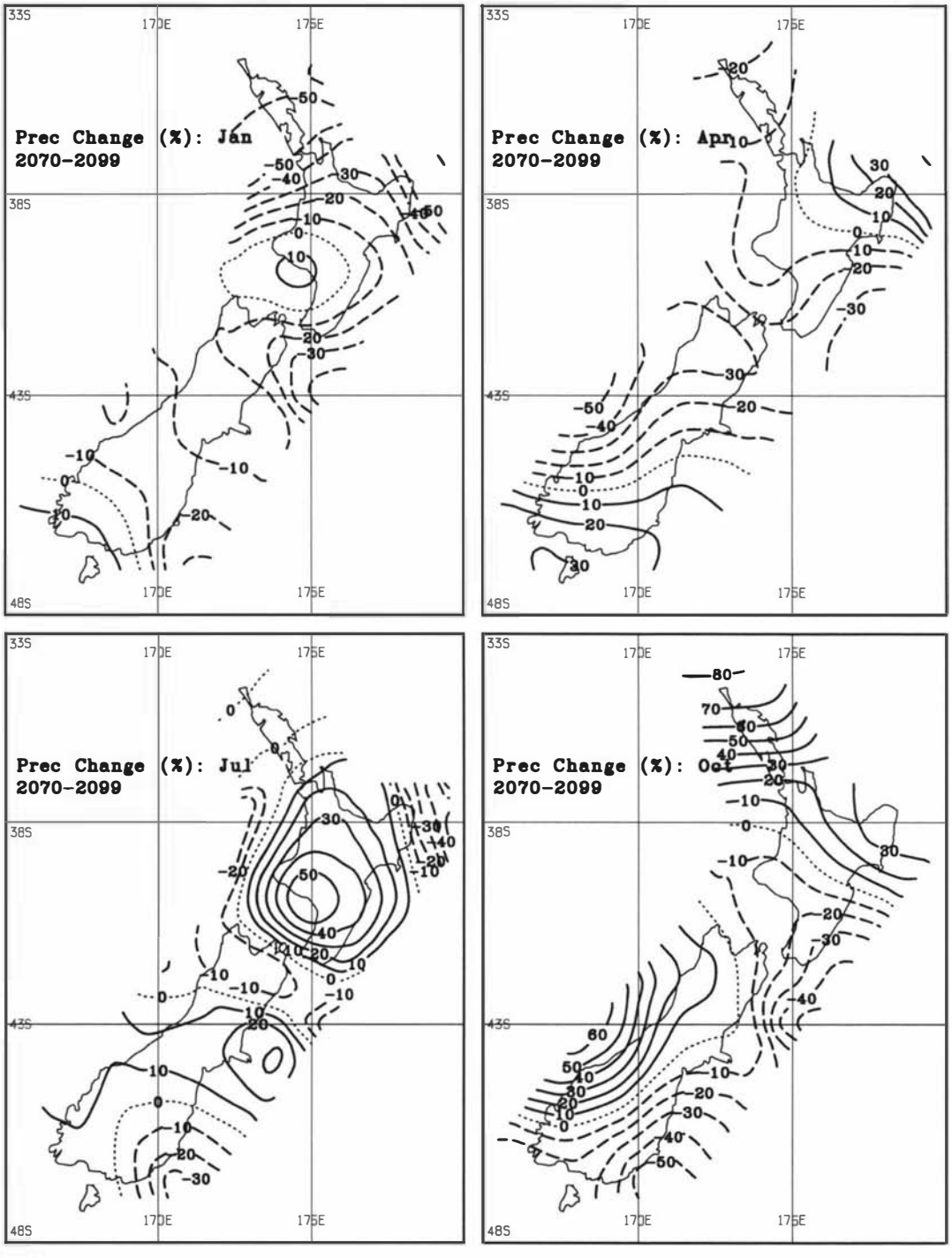

Figure 5.9 HadCM2 model derived precipitation (Prec) changes for 2070-2099 with respect to 1980-2009, contours every 10%. Upper panels: left-hand for January (summer) and right-hand for April (autumn). Lower panels: left-hand for July (winter) and right-hand for October (spring).

Precipitation changes derived from the HadCM2 regional free atmosphere circulation indices demonstrate a pattern with a general precipitation decrease over northern New Zealand and an increase over the central and southern areas mainly to the western side. A west to east progression of precipitation increases over the three tri-decades is projected in the central areas, particularly in winter. The increased westerlies magnify precipitation increases in the southwest and decreases in the central eastern areas.

In the tri-decade 2010-2039, summer precipitation over the northern sector is projected to have decreases of up to 20%. Decreases of up to 40% in 2040-2069 are demonstrated to slow down and maintain the same decreases over the 2070-2099 tri-decade. Western areas of the North Island are expected to get wetter by 20-70%, and these increases are predicted to progress gradually to the central North Island. Marked precipitation increases from the southwest of South Island are expected to extend to southern South Island for increases of up to 70% except for the southeast coast, which has a decrease of up to 10%. It is acknowledged that the 'bull eyes' in the pattern of precipitation changes can be attributed to the noise in the monthly data of the predictor variables coupled with spatially scarce data points.

It can be noted that precipitation changes do not exhibit trends on monthly basis over the three tri-decades. This could be attributed to the multi-decadal climate variability consistent with the demonstrated variability in the HadCM2 predicted circulation indices. High frequency climate variability in the region, including inter-decadal variability, is likely to influence on the general climate change pattern over the region.

5.5 Precipitation characteristics

Although climate change has commonly been expressed in terms of the change of mean values, it is acknowledged that the variability and occurrence of extreme events may have a greater impact than changes in the mean climate itself (Katz and Brown, 1992). Generally, GCM simulations indicate that a warmer climate could result in a decrease in temperature variability, an increase in precipitation variability and the number of extreme events. Direct identification of climate variability and extreme events from model outputs

is difficult due to the scale complexity. Deductions may be made indirectly by examining the distributions of climate elements and their changes over time.

Precipitation data exhibit high spatial and temporal variability that makes identification of trends from direct analyses of the time series very difficult. Since precipitation characteristics are key inputs for water resources impact assessment, changes in precipitation characteristics were considered in the study. Modelling with the gamma distribution provides an alternative to detecting signals from the actual data. It allows the detection of changes in the precipitation field by monitoring changes in the less variable parameters of the distribution. A two-parameter gamma probability function fits precipitation data well (Tsonis, 1996). The gamma distribution is given by:

$$f(x) = \beta^{-\gamma} x^{\gamma-1} e^{-(x/\beta)} / \Gamma(\gamma) \quad \beta > 0,\ \gamma > 0 \tag{5.1}$$

where:

x is the random variable

Γ is the gamma function

β and γ are the scale and shape parameters, respectively.

As investigated by Thom (1958), the maximum likelihood estimates for β and γ from a sample of N values are given by:

$$\gamma = (1+\sqrt{1+4A/3})/4A \tag{5.2}$$

and $$\beta = \frac{\bar{x}}{\gamma} \tag{5.3}$$

where: $A = \ln \bar{x} - \dfrac{\sum \ln x}{N}$

$\bar{x}$ is the sample mean.

The gamma function properties of interest are:

- the expected value $\bar{x} = \beta\gamma$; and

- variance $s^2 = \gamma \beta^2$.

Estimates of β and γ are reliable from a sample size N ≥ 30 (Kendall and Stuart, 1961).

Gamma distribution parameters are calculated from the derived precipitation time-series for the four tri-decades (1980-2009, 2010-2039, 2040-2069 and 2070-2100 over the 18 study points (Figure 3.2). Most importantly, the spatial variations and trends in the gamma distribution parameters suggests localised changes in precipitation characteristics over time.

Precipitation distribution over a given tri-decade can be characterised by the mean, variance and the degree of spread (the range between the first and the ninth percentiles of a distribution) as indicators of expected precipitation amounts, variability and the likelihood of extreme events, respectively. The direction of change of precipitation characteristics with respect to the precipitation of the pseudo-present tri-decade can be detected in the trends of the gamma function over time.

Changes in precipitation distribution characteristics were examined in a randomly generated values for 300 years using gamma distribution over each tri-decade. Precipitation distribution characteristics were defined in terms of spread (Sp), coefficient of variation (CV) and expected precipitation amounts (E[x]). For sensitivity illustration (Table 5.3), hypothetical changes in the gamma parameter were applied to the pseudo-present precipitation at study point 2 (see Figure 3.2). It is also depicted in Figure 5.10 that an increase in the 'scale' parameter is associated with increases in the expected magnitude of precipitation amount, variability and the chances of extreme events (below and above 10 and 90 percentile, respectively), and vice versa. Similar projections could be made for the 'shape' parameter, but with less sensitivity to variability and number of extreme events. A spatial analysis of CV ratios to the pseudo-present for three tri-decades starting from 2010 is presented in Figures 5.11 through 5.13

Table 5.3 Degree of distribution spread (Sp), coefficient of variation (CV) and expected magnitude (E[x]) in response to the gamma distribution parameter hypothetical changes at study point 2.

scale (β)	shape (γ)								
	2 x γ =2.46			1 x γ =1.23			0.5 x γ =0.615		
	E[x]	CV	Sp	E[x]	CV	Sp	E[x]	CV	Sp
2 x β=128	308	0.086	63	157	0.098	39	78	0.087	18
1 x β=64	153	0.128	49	79	0.125	27	40	0.118	12
0.5 x β=32	78	0.177	37	38	0.179	18	20	0.180	9

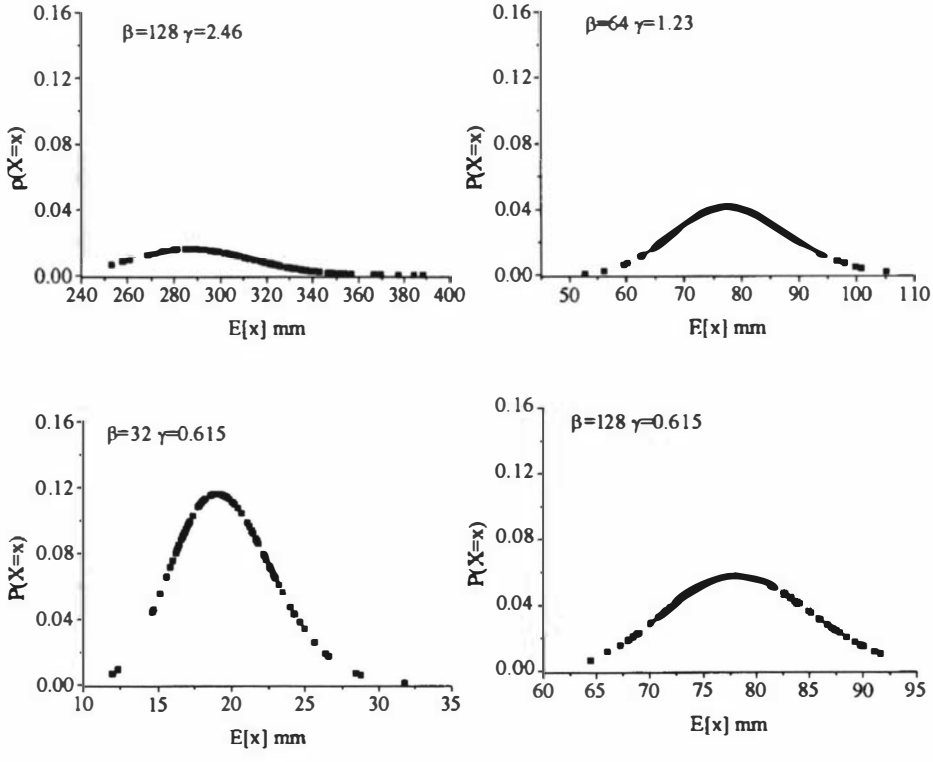

Figure 5.10 Distribution characteristics of precipitation to demonstrate the sensitivity of changes in the gamma scale (β) and shape (γ) parameter at study point 2, where P(X=x) is the probability of x units of precipitation.

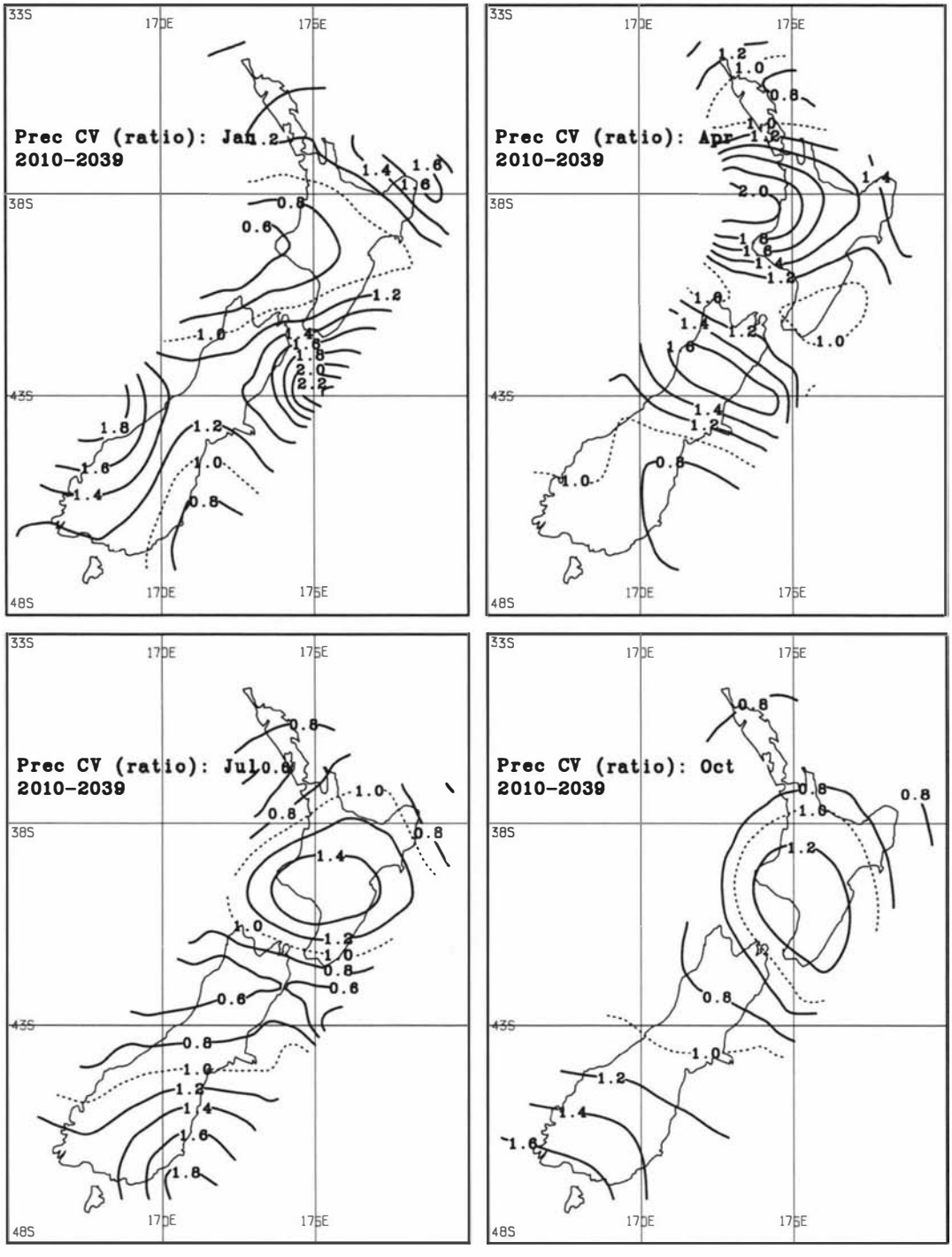

Figure 5.11 HadCM2-model derived precipitation coefficient of variation (Prec CV) ratios for 2010-2039 to 1980-2009; contours every 0.2 (ratio). Upper panels: left-hand for January (summer) and right-hand for April (autumn). Lower panels: left-hand for July (winter) and right-hand for October (spring).

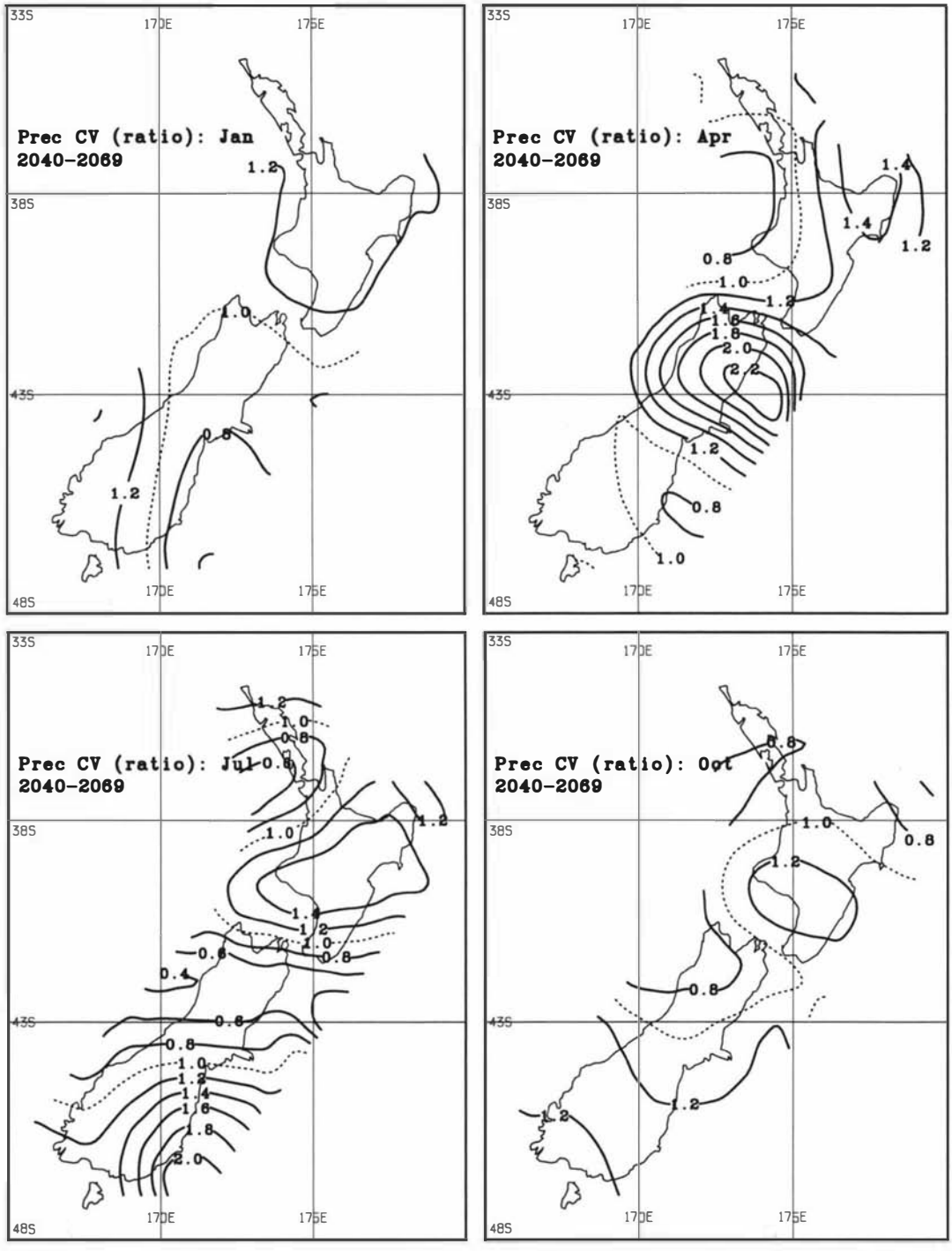

Figure 5.12 HadCM2-model derived precipitation coefficient of variation (Prec CV) ratios for 2040-2069 to 1980-2009; contours every 0.2 (ratio). Upper panels: left-hand for January (summer) and right-hand for April (autumn). Lower panels: left-hand for July (winter) and right-hand for October (spring).

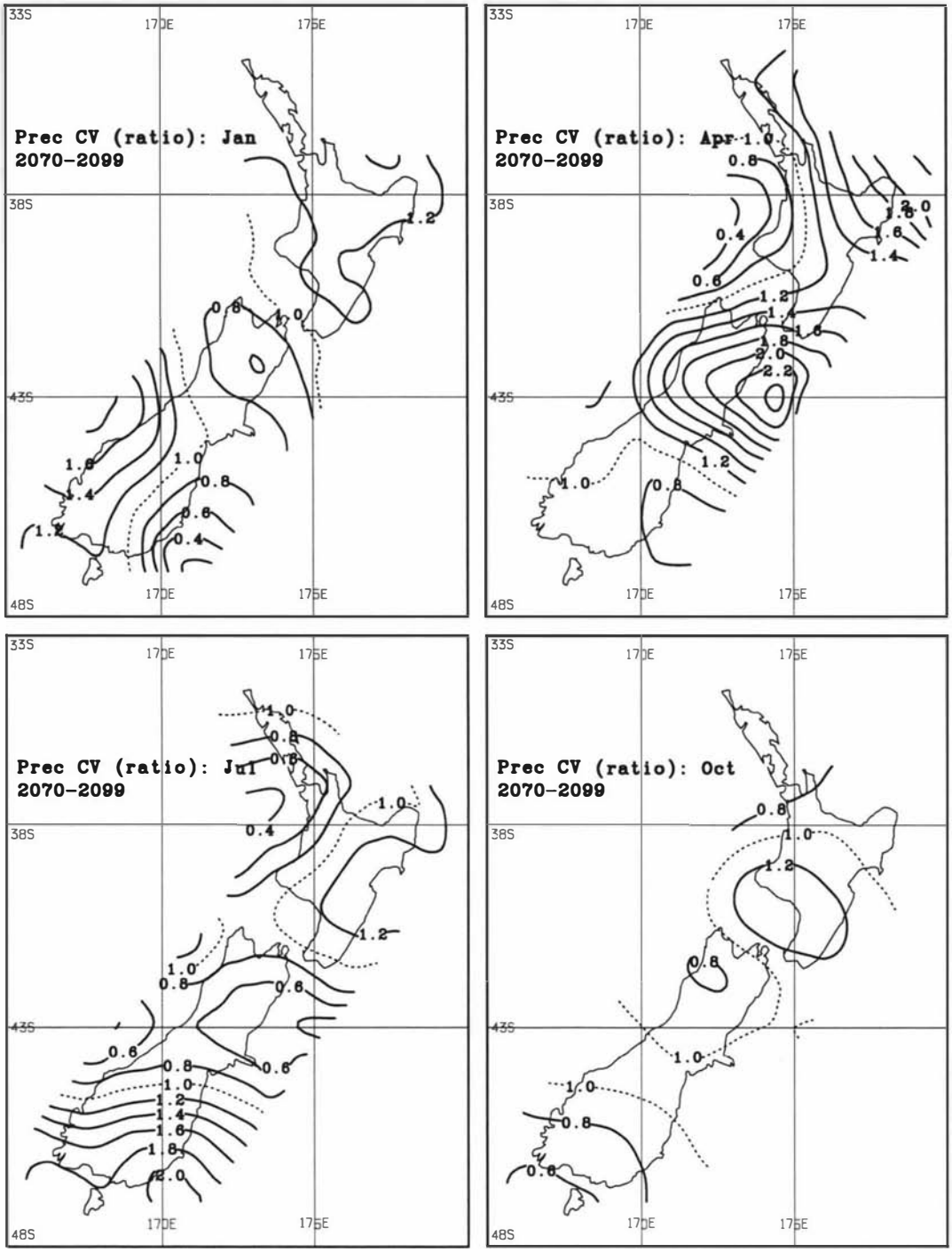

Figure 5.13 HadCM2-model derived precipitation coefficient of variation (Prec CV) ratios for 2070-2099 to 1980-2009; contours every 0.2 (ratio). Upper panels: left-hand for January (summer) and right-hand for April (autumn). Lower panels: left-hand for July (winter) and right-hand for October (spring).

A general increase in precipitation coefficients of variation is demonstrated over the country, particularly over the northeastern and southeastern areas. The coefficients of precipitation variation of 1.2-1.7 times the pseudo-present coefficients of variation are expected over the north and northeastern parts of the North Island and the southeastern areas in the South Island during summer. Marked increases in variability of 1.2-2.2 times are projected for the eastern and central North Island and southeastern South Island during winter. Decreases to 0.6-0.8 are projected over the western, central and eastern South Island in winter.

5.6 Conclusions

Due to the location and topographical features of New Zealand, the main control of climate is the strength and orientation of the westerly wind regime, and to a lesser extent, the occasional northerly and southerly winds associated with the passage of troughs, depressions and fronts over the region. Consequently, besides north-south contrast in climate, there is a strong west-east gradient in precipitation, particularly over the South Island.

The HadCM2 transient climate change experiments outputs have reasonably demonstrated realistic simulations of the mean sea level pressure field. The monthly mean pressure patterns from the HadCM2 simulations validated well with respect to NCEP-reanalysis for its 'present climate' simulation over the New Zealand region. In the simulations, differences between mean pressure fields of the pseudo-present and the future tri-decades indicate pressure build up in the northeastern sector coupled with pressure falls centred to the southwest. The predicted changes suggest strengthening of the anticyclonic belt which brings fair weather to northern New Zealand. Coupled with pressure falls to the southwest the anticyclonic belt will squeeze stronger westerly winds over southern and central New Zealand. These changes in the pressure fields and hence stronger westerly winds contrast with previously projected changes based on GCM equilibrium experiments. Importantly, the pattern of change in the mean sea level pressure gradients enhances westerly winds over the central and southern sectors of the

country. Except for the areas to the east of the Alps, an eastward progression of precipitation increases is projected over the South Island, particularly in the central areas.

Chapter Six

Impacts on hydrology and water resources

6.1 Introduction

The impacts of climate change are transmitted via their effects on the physical environment, and particularly on those factors which are at the base of our 'hierarchy of needs' - air, water and secure habitation. This calls for a special emphasis to be placed on the response of water resources to climate change. Without water, life itself is impossible; without adequate water for agriculture, industrial and domestic use, electric power generation, and waste disposal, organised life in society would be impossible. Because water is fundamental to so many aspects of present-day society and economy, any possible changes in its availability must be anticipated and planned for.

Climate change will lead to an intensification of the global hydrological (water) cycle through increases in surface temperature and rates of evapotranspiration, and in some regions, increases in precipitation. Changes in the total amount of precipitation and its frequency and intensity directly affect the magnitude and timing of run-off and the intensity of floods and droughts. Such changes will have significant impacts on regional water resources. This chapter reviews the impacts of climate change on the hydrological cycle, and by implication, the management of water resources. Particularly, the effects of changes in temperature, precipitation, carbon dioxide, and sea levels on water resources are outlined along with the impacts of these climate variables on water for irrigation and for domestic, industrial, and electric power uses.

6.2 Impacts on the hydrological cycle

The effects of future climate change on hydrological patterns can be estimated by combining hydrological models (which simulate water catchments and run-off) and climate models (which simulate the climate effects of enhanced greenhouse effect in the atmosphere). A number of conclusions have been proposed with a considerable amount

of certainty based on models in simulating the environment (Hurd *et al.*, 1999). An increase in air temperature would increase potential evapotranspiration, but the magnitude of increase also depends on changes in sunlight, humidity, wind speed, rainfall and vegetation characteristics. Actual evapotranspiration may increase or decrease according to the availability of soil moisture.

It is not certain how individual catchment areas will respond to changing evapotranspiration rates and precipitation. It is likely, however, that those drier hydrological regimes will be more sensitive to changes in climate. Relatively small changes in temperature and precipitation could cause relatively large changes in run-off. Arid and semi-arid regions will therefore be particularly sensitive to reduced rainfall and to increased evaporation and plant transpiration. An increase in the duration of dry spells will not necessarily lead to an increased likelihood of low river flows and groundwater levels, since increases in precipitation may be experienced during other seasons. More probably, increased rainfall will lead to an increased likelihood of river flooding. Changes in seasonal patterns of rainfall may affect the regional distribution of both ground and surface water supplies.

Hydrological regimes in high latitude or mountain areas are often determined by winter snowfall and spring snowmelt. Most climate models predict that global warming will reduce the amount of precipitation falling as snow in these regions, increasing the rate of water runoff and enhancing the likelihood of flooding.

There will, however, be regional variations. Freshwater ecosystems, including lakes, streams and non-coastal wetlands will be influenced by changes to the hydrological cycle as a result of climate change. These influences will interact with other changes influenced by land use, waste disposal and water extraction. Freshwater ecosystems will respond to new flood regimes and water levels. Changes in water temperatures could affect the survival and growth of certain organisms, and the diversity and productivity of freshwater ecosystems. Changes in runoff, groundwater flows, and precipitation directly over lakes and streams would affect nutrients and dissolved organic oxygen, and therefore the quality and clarity of the water.

6.3 Hydrological sensitivity to climate change

The effects of climate change and CO_2 enrichment on evapotranspiration, the effects of the climate change on river flows and the impacts of river flows on available supplies have been evaluated. Also the impacts of climate change on floods and drought, irrigation requirements, water quality, recreation, wildlife, urban water, and electricity generation have been examined (Waggoner, 1990).

The range of likely changes in average annual precipitation associated with an equivalent doubling of atmospheric CO_2, for any given region might be of the order of ± 20%. The corresponding ranges of likely changes in regional runoff and soil moisture are suggested to be in the order of ± 50% (Schneider, *et al.*, 1990).

Changes in runoff are the direct result of changes in precipitation and evaporation (which is strongly influenced by temperature). For example, a catchment with an annual effective precipitation of 1,000 mm and actual evaporation of 600 mm will have a runoff of 400 mm. For the same level of actual evaporation, if the effective precipitation is reduced by 10% to 900 mm, runoff will be 300 mm, which is a 25% reduction.

River flow sensitivity to climate variables differs widely for different locations and climates (Schaake, 1990). Schaake's estimates of the 'elasticities' of runoff with respect to precipitation and temperature (i.e. the percentage change in runoff resulting from a 1% change in precipitation and temperature) range from less than 1% to as high as 10%. The runoff 'elasticities' are higher for drier climates and the elasticity with respect to precipitation is greater than that of evapotranspiration. Thus, a warming alone will decrease runoff much less than a warming accompanied by a decrease in precipitation.

Estimated impacts of alternative temperature and precipitation changes on annual runoff in several semiarid rivers suggest that relatively small changes in temperature and precipitation can have large effects on runoff (Frederick and Major, 1997). For example with no change in precipitation, estimated runoff declines by 3 to 12 percent with a 2°C increase in temperature and declines by 7 to 21 percent with a 4°C increase in temperature. These results are consistent with other studies (e.g. Schaake, 1990; and Karl

and Riebsame, 1989) which concluded that runoff is more sensitive to changes in precipitation than changes in to temperature. Nevertheless, a 10 percent increase in precipitation does not fully offset the negative impacts on runoff attributable to a 4°C increase in temperature in three of the five rivers for which the climate scenario was studied.

Many of the climate impact studies highlight the vulnerability of water resource systems to climate variables (Watson *et al.*, 1997) and suggest that small changes in these variables could lead to large changes in system performance. Most notably, isolated single-reservoir systems in arid and semiarid regions are extremely sensitive and less able to adapt to climate impacts that could vary from decreases in reservoir yields in excess of 50% to seasonal flooding,

Uncertainties as to how the climate will change and how societies will adapt to these changes are challenges that all climate impact studies confront. However, one of the more likely impacts of global warming on regional hydrology involves areas where winter snowfall is the primary source of precipitation and spring and summer snowmelt are the primary sources of streamflow. Such regions are likely to see a distinct shift in the relative amounts of snow and rain and in the timing of snowmelt due to higher temperatures. The resulting changes in runoff patterns could greatly alter the likelihood of flooding and the availability of water during peak demand periods such as the irrigation season (Frederick and Major, 1997).

6.4 Sea level rise

Impacts on water resources will also come from rising sea levels due to thermal expansion of the oceans and increased melting of glaciers and land ice. Global sea level has increased some 10 to 20 cm during the past century, largely due to the melting of land-based ice sheets and glaciers (Frederick and Major, 1997). The most recent IPCC results suggest average sea level might rise another 15 to 95 cm by the year 2100, with the best guess of about 50 cm (Houghton *et al.*, 1996).

Higher sea levels and increased storm surges could adversely impact freshwater supplies in some coastal areas. Saline water profiles in river mouths and deltas would be pushed farther inland, and coastal aquifers would face an increased threat of saltwater intrusion. The intrusion of saltwater into current freshwater supplies could jeopardise the quality of water for some domestic, industrial, and agricultural users. For example, sea level rise would aggravate water-supply problems in coastal areas.

6.5 Carbon dioxide effects

A growing body of research suggests that atmospheric CO_2 levels may affect water availability through its influence on vegetation. Controlled experiments indicate that elevated CO_2 concentrations increase the resistance of plant stomata to water vapour transport, resulting in decreased transpiration per unit of leaf area. Some experiments suggest that a doubling of CO_2 will increase stomatal resistance and reduce transpiration by about 50 percent on average (Rosenberg *et al.*, 1990). On the other hand, CO_2 also has been demonstrated to increase plant growth, leading to a larger area of transpiring tissue and a corresponding increase in transpiration. Other factors that might offset any potential increases in plant water-use efficiency are a potential increase in leaf temperatures due to reduced transpiration rates and species changes in vegetation communities (Rosenberg *et al.*, 1990). The net effect of opposing influences on water supplies would depend on the type of vegetation and other interacting factors, such as soil type and climate.

Use of a generic crop simulator originally developed to model runoff, soil erosion, crop productivity and the interactions among them, including detailed hydrological processes, suggests that the increased stomata resistance would increase runoff, especially from land in perennial crops such as alfalfa (*Medicago sativa*) and wheatgrass (*Elymus apricus*). This positive CO_2 effect, however, would offset only a small fraction of the decrease in streamflows resulting from the higher temperature and lower precipitation rates that may characterise the climate change scenario.

6.6 Water demand

Precipitation, temperature, and CO_2 levels can affect the demand for, as well as the availability of, water. This section considers how changes in these climate variables might affect the demand for various uses of water.

6.6.1 Irrigation water use

Generally irrigation is the largest use of water in terms of withdrawals and percentage-wise consumptive use. Irrigation is also the most climate-sensitive water use. The profitability of irrigated farming relative to dryland farming tends to increase as conditions become hotter and drier and crop yields produced under dryland conditions decline. In areas with available and affordable water supplies, hotter and drier conditions would likely lead both to an increase in the land under irrigation and to an increase in the amount of water applied per irrigated acre (Frederick and Major, 1997). As already noted, CO_2 enrichment would tend to increase both the water-use efficiency of the plants and the growth of the plant, with less certain impacts on water use per unit of land.

When allowance is made for the impacts of higher levels of atmospheric CO_2 on transpiration rates, these increases in irrigation water use are dampened somewhat. An increase in CO_2 from 350 to 450 parts per million reduced estimated water use for irrigation by an average of 7% (Frederick, 1991).

Studies of effects of hypothetical change in temperature, precipitation, and stomatal resistance on annual plant water use in a humid-temperate climate (McCabe and Wolock, 1992), suggest that increases in mean annual water use are strongly associated with increases in temperature and less strongly associated with decreases in precipitation. When temperature and precipitation are the only changes, water use increased with 20% more precipitation and a 2°C warming. Results also suggest that plant water use is even more sensitive to changes in stomatal resistance than to temperature. Decreases in water use resulting from greater stomatal resistance results in less water use for all scenarios except those with the smaller (20%) increase in stomatal resistance and temperature increases of at least 4°C.

6.6.2 Domestic water use

Domestic use, especially outdoor use for watering lawns and gardens, is somewhat sensitive to changes in temperature and precipitation. The estimated temperature and precipitation 'elasticities' of the demand for water varies widely depending on the region, season, and whether the estimates differentiated between indoor and outdoor urban and suburban uses. The elasticity estimates suggest that a 1% rise in temperature would increase residential water use from 0.02% to 3.8% and a 1% decrease in precipitation would increase residential water use between 0.02% and 0.31 %.

Studies of urban water use suggested that potential evapotranspiration and precipitation best explain changes in residential water attributable to the climate. For example, higher evapotranspiration attributable to a temperature rise of 2.2°C and 4.4°C increased residential water demand by an estimated 2.8% and 5% respectively during the summer season (Hughes *et al.*, 1994).

Herrington (1996) found that the impacts of climate change on the water demand in England and Wales would be significant on showering, lawn sprinkling, and other garden uses. His projections for the year 2021 indicated that a 1.1°C increase in temperature would increase water demand by 12% for showers, 35% for lawn sprinkling, and 19% for other garden use.

6.6.3 Industrial and thermoelectric power water uses

Industrial use includes water for purposes such as processing, washing, and cooling in facilities that manufacture products. Thermoelectric power use includes water used for cooling to condense the steam that drives the turbines in the generation of electric power with fossil fuel, nuclear, or geothermal energy. Global warming could have important implications for these water uses. A rise in water temperature would reduce the efficiency of cooling systems and, therefore might result in an increased demand for cooling water. If aquatic ecosystems were threatened by higher water temperatures resulting from either global warming or returnflows of cooling water, these uses might be subjected to more stringent environmental regulations.

A possible response to the imposition of stricter regulations on returnflows would be to switch from once-through cooling systems to cooling towers and cooling ponds that return little or no water to the source. While the water withdrawals would drop sharply as a result of such a switch, there is little difference in the consumptive use of water for these cooling technologies. The evaporation losses occur on site with cooling towers and ponds. In a once-through system more of the evaporation occurs off-site and is attributable to the increased temperature of the receiving water body (Miller, 1990).

Global warming would also have indirect effects on industrial thermoelectric power uses. Summer energy use for air conditioning would rise, and winter demand for space heating would decline. Changes in the temporal and perhaps the spatial demand for energy would alter the demand for cooling water.

6.6.4 Instream water uses

The impacts of global warming on the quantity, quality, and timing of runoff would affect instream water uses such as aquatic ecosystem maintenance, instream water quality, hydroelectric power generation, navigation, and recreation. They might also affect, either directly or indirectly, water demands. For example, changes in streamflows would affect actual and potential hydroelectric power generation, which in turn would affect the demand for substitute sources of electricity. Since the alternative electric power source (thermoelectric) is one of the largest users of water (for cooling), shifts in hydroelectric power production could have a significant impact on the demand for water within a catchment.

6.6.5 Non-climate factors influencing future water availability and demand

Climate is only one of many factors that will affect the future availability and demand for water. Population, technology, economic conditions, social and political factors, and the values society places on alternative water uses are important determinants of supply and demand conditions and, indeed, may be more important determinants than those attributable to climate change (Houghton *et al.*, 1996).

A wide range of non-climate factors affects the quantity and quality of freshwater supplies. Groundwater stocks are depleted when pumping exceeds recharge rates, and both surface and groundwater supplies are degraded when the capacity of an aquatic system to assimilate pollutants is exceeded. On the other hand, the effective supply of water can be augmented by investments to develop, protect and restore supplies. Investments in infrastructure such as dams and canals can capture water that otherwise would be unavailable for use.

Population growth will be a major, if not the most important, determinant of future water demand and availability. Countries with high population growth rates will experience sharp declines in per capita water availability regardless of the assumed climate scenario

The ability to foresee how non-climate factors will influence the future supply and demand for freshwater is probably not any better than our current ability to foresee how a global-warming-induced climate change will affect water supplies. Indeed, if the past record of forecasting water use is any guide, great uncertainties are likely to stem from the non-climate variables, and those uncertainties may be greater than those associated with climate variables (Frederick and Major, 1997).

The difficulties of projecting changes in water use a decade or two in the future is a bottleneck to projections over periods that might be useful in climate impact studies. The populations, incomes and life styles that create demands for water are likely to change substantially over the time horizon within which climate change will have significant impacts. The additional change from climate change must be added to these largely unknown changes.

6.7 Summary and conclusion

As acknowledged by the IPCC Working Group II there is evidence regarding the impacts on water resources (IPCC, 1996a) as summarised below:

- The timing and regional patterns of precipitation events will change, and more intense precipitation events are likely.

- Even in areas with increased precipitation, higher evaporation rates may lead to reduced runoff. More annual runoff due to increased precipitation is likely in the higher latitudes. Some lower latitude catchments, however, may experience reductions in runoff due to a combination of increased evaporation and decreased precipitation.

- Although potential evapotranspiration rises with air temperature, actual evapotranspiration may increase or decrease according to the availability of moisture.

- GCMs and hydrological impact studies provide evidence of an increase in flood frequencies with global warming. The amount of increase for any given climate scenario is uncertain, and impacts will vary among catchments. Floods may become less frequent in some areas.

- The frequency and severity of droughts could increase in some areas as a result of a decrease in total rainfall, more frequent dry spells, and higher evapotranspiration. The hydrology of arid and semiarid areas is particularly sensitive to climate variations.

- Seasonal disruptions in water supplies of mountainous areas, where snowmelt is an important source of spring and summer runoff, might result if more precipitation falls as rain rather than snow and the length of the snow storage season is reduced. Water quality problems are likely to increase where streamflow declines.

Water availability is an essential component of human welfare and productivity. Much of the world's agriculture, hydroelectric power production, water needs and water pollution control is dependent on the hydrological cycle, and the natural recharging of surface and groundwater resources. Changes in the natural water availability, as a result of global warming, will result in impacts which are generally most detrimental in regions already under existing climatic stresses.

Changes in surface water availability and run-off will influence the recharging of groundwater supplies and, in the longer term, aquifers. Water quality may also respond to changes in the amount and timing of precipitation. Rising seas could invade coastal freshwater supplies. Coastal aquifers may be damaged by saline intrusion as salty groundwater rises. Reduced water supplies would place additional stress on people, agriculture, and the environment.

Water resource management consequently needs to focus on demand management and the implementation of regulatory controls to adapt to these changes. Long-term management strategies might also need to be revised accordingly. However, more specific information is required at geographic scales of particular relevance for water resource planning.

Chapter Seven

Water resources impacts assessment

Water resources and the hydrological cycle are largely controlled by climate factors including precipitation, temperature, wind speed, and solar radiation. Water supplies and control systems (reservoirs, spillways, storm sewers, flood protection structures) and rules and protocols defining their management, are dependent on local climate and hydrological patterns. Changes in climate conditions can therefore affect surface water and ground water availability, quality, and value of such diverse uses as electric power production, support of aquatic ecosystems and irrigation.

A number of modelling approaches have been developed and previous models modified for studying the effect of climate change on hydrological catchment responses and water yield. In this Chapter, potential techniques for impact assessment are considered and an approach to translate changes in catchment water yield into descriptions of impacts on water resources is proposed.

7.1 Hydrological Models

Hydrological modelling is concerned with the accurate simulation of the partitioning of water among the various pathways of the hydrological cycle (Dooge, 1992). This partitioning in its simplest form is expressed by the water balance equation:

$$Q = P - ET \pm \Delta S \tag{7.1}$$

where: Q is runoff, P is precipitation

ET is evapotranspiration

ΔS is change in system storage.

Equation 7.1 is common to all hydrological models. The variety and number of hydrological models developed to solve Equation 7.1 reflect the wide range of modelling purposes, data constraints, and spatial and temporal scale that have influenced the

conceptualization and parameterization of the processes in the equation (Leavesley, 1994). Models can be classified using a number of different schemes (Becker and Serban, 1990; Dooge, 1992). Classification criteria include purpose of model application (e.g. real-time application, long-term prediction, process understanding), model structure (models based on fundamental law of physics, conceptual models reflecting these laws in a simplified approximate manner, black-box or empirical analysis), spatial discretization (lumped parameter, distributed parameter), temporal scale (hourly, daily, monthly, annual) and spatial scale (point, field, catchment, region, global).

7.1.1 Empirical models

An empirical representation of Equation 7.1 considers only the statistical relations among the components of the water balance. Empirical models do not explicitly consider the governing physical laws of the processes involved, but only relate input to output through some transfer function. As such, empirical models reflect only the relations between input and output for the climate and catchment conditions during the time period in which they were developed. Extension of these relations to climate or catchment conditions different from those used for development of the function is questionable.

7.1.2 Water balance models

Water balance models originated with the work of Thornthwaite (1948) and Thornthwaite and Mather (1955). These models are basically bookkeeping procedures used with Equation 7.1 to account for the movement of water from the time it enters a catchment as precipitation to the time it leaves the catchment as runoff. The models vary in their degree of complexity based on the detail with which each component of Equation 7.1 is considered. Most models account for direct runoff from rainfall and lagged runoff from catchment storage in the computation of total runoff (Q). In addition, most models compute the ET term as some function of potential ET and the water available in storage (S). While water balance models can be applied at a daily, weekly, monthly, or annual time step, in climate studies they have been applied most frequently at the monthly time step.

A simple three-parameter monthly water balance model was applied by Arnell (1992) to 15 catchments in the United Kingdom to estimate changes in the monthly river flow regimes and to investigate the factors controlling the effects of climate change on river flow regimes in a humid temperate climate. The three parameters, which were fitted to each individual catchment, represent (1) the fraction of precipitation that contributes directly to runoff; (2) the maximum storage capacity of the catchment; and (3) the catchment lag for converting the water available for runoff to streamflow. Arnell (1992) also compared the water balance model with four different empirical models for the assumed climate changes. No one empirical formulation gave a consistently closer match to the water balance model estimates of climate change effects, and differences among empirical models for the same scenario were large. He noted that the results suggest that estimates of possible change based on annual empirical models should be treated with extreme caution.

Gleick (1987) developed a monthly water balance model for application to the Sacramento River catchment in California. He began with a basic model similar to that used by Arnell (1992) but varied the parameter representing the fraction of precipitation that contributes to direct runoff by season. A snow accumulation and melt component was developed to account for the seasonal storage and release of water by a snowpack. A monthly water balance model that also accounts for snow processes was developed and applied by Mimikou *et al.* (1991) for evaluating the regional hydrological effects of climate change in the central mountainous region of Greece. Schaake (1990) developed a nonlinear monthly water balance model for the evaluation of regional changes in annual runoff associated with assumed changes.

Water balance models provide the ability to simulate average runoff for given precipitation over a range of catchment conditions and to simulate the year-to-year variation in runoff as precipitation varies. Limitations include the need to calibrate parameters to observed conditions and the inability to adequately account for possible changes in individual storm runoff characteristics at the time steps they are applied.

7.1.3 Conceptual lumped-parameter models

Conceptual lumped-parameter models are developed using approximations or simplifications of fundamental physical laws and may include some amount of empiricism. They attempt to account for the linear and nonlinear relations among the components of the water balance equation. As with water balance models, conceptual lumped parameter models attempt to account for the movement of water from the time it enters the catchment until it leaves as runoff. However, flow paths and residence times of water are considered in much greater detail and normally at time steps of the order of minutes, hours, or one day. Vertical and lateral flow processes may be considered. Vertical processes may include interception storage and evaporation, infiltration, soil moisture storage, evapotranspiration, ground-water recharge, and snow pack accumulation and melt. Lateral flow processes may include surface runoff, subsurface flow, ground-water flow, and streamflow. In addition, some models include the capability to simulate some associated sedimentary, chemical, and biological processes.

Processes usually are parameterised at the scale of an entire catchment area. This area often has a heterogeneous mix of vegetation, soils, and land use. Consequently, parameters are assumed to be effective values that are representative of the mix of conditions and normally must be calibrated using historic information. Some applications attempt to account for spatial variability in the catchment characteristics by making sub-area delineations based on considerations such as land use or vegetation. The effect of elevation on climate characteristics such as temperature and precipitation are considered by dividing a catchment into elevation bands.

One of the more frequently used models in this group is the Sacramento Soil Moisture Accounting Model (Burnash *et al.*, 1973). The Sacramento model simulates the movement and storage of soil moisture using five conceptual storage zones. The model has 17 parameters that define the capacities and flux rates to and from the storage zones. Nemec and Schaake (1982) used the Sacramento model to evaluate the effects of a moderate climate change on the sensitivity of water resource systems in an arid and a

humid catchment in the United States. Sensitivity was evaluated by simulating the variation in storage-yield relations of hypothetical reservoirs located in each catchment.

Several other models having a similar structure to the Sacramento but with different process conceptualisations have been used to assess the effects of climate change on many regions of the globe (Bultot and Dupriez, 1976; Bultot *et al.*, 1992; Nathan *et al.*, 1988). The more detailed process simulation capabilities and higher temporal resolution permitted by conceptual lumped-parameter models permits a more detailed assessment of the magnitude and timing of process responses to climate change. For example, increased resolution of precipitation timing and form (rain or snow) permit the estimation of streamflow timing and the frequency and magnitude of flood peaks. However, these capabilities are accompanied by an increase in the number of process parameters that must be determined, and in the amount and type of data needed to characterise the catchments used as input to run the simulations.

7.1.4 Process-based distributed-parameter models

These models are firmly based on the understanding of the physics of the processes that control catchment response. Process equations involve one or more space coordinates and have the capability of forecasting the spatial pattern of hydrological conditions in a catchment as well as catchment storages and outflows (Beven, 1985). Spatial discretization of a catchment to facilitate this detail in process simulation may be done using a grid-based approach or a topographically based delineation. In each case, process parameters are determined for each grid cell or topographic element.

The ability to simulate the spatial patterns of hydrological response within a catchment make this approach attractive for the development of models that couple hydrological processes with a variety of physically based models of biological and chemical processes. The applicability of models of this type to assess the effects of climate change has been recognized (Beven, 1989).

Major limitations to the application of these models are the availability and quality of catchment and climate data at the spatial and temporal resolution needed to estimate

model parameters and validate model results at this level of detail. These data requirements may pose a limit to the size of the catchment in which these models can be applied.

7.2 Modelling aspects

Most of the current modelling approaches have been built upon existing operational models with modifications as needed to extend the application to a wider range of catchment conditions and to account for limited knowledge of catchment and climate characteristics. While for most there is some measure of success and applicability of the methods developed, each also has a number of qualifying assumptions and limitations that affect the interpretation of model results (Leavesley, 1994).

7.2.1 Parameter estimation

The variety of modelling approaches used reflects a number of factors, including assessment objectives, data constraints, and the spatial and temporal scales of application. While these models differ in their degree of complexity, they share a common problem. Each has a number of parameters that must be estimated or calibrated for model application. Some parameters are defined as being physically based and are assumed to be measurable from catchment and climate characteristics. Many of the parameters are less well defined and are optimized or fitted.

Problems with the use of fitted parameters include limited length of historical data record, minimal or no information on reasonable values or acceptable ranges of values, incorporation of model and data errors in parameter values, and the effects of parameter. Intercorrelation can produce compensating errors that inadvertently improve the simulation (Leavesley, 1994). Underestimation in one parameter may be compensated for by overestimation in another parameter resulting in the right answer for the wrong reason.

7.2.2 Scale

A major factor in the development of more physically based models (lumped- or distributed-parameter), is the consideration of scale. Interests in the assessment of hydrological impacts range spatially from the local, regional to global scale, and temporally from minutes and hours to days, months, years, and longer. As noted by Klemes (1983), as one moves from small plots and hillslopes to large catchment systems, different sets of physical laws dominate at each major scale. Physical laws at a larger scale tend to express averages or integrals of those dominants at smaller scales. For a given model, parameters estimated or fitted for small catchments may not be representative for larger catchments. Likewise, time is a consideration in parameter estimation in that parameters estimated for a daily flow simulation may not be representative for different simulation intervals. A variety of models and modelling approaches will be needed to address the large number of modelling objectives and scales of application.

7.2.3 Model validation

Models used to assess the effects of climate change are evaluated on their ability to reproduce historical time series of observed hydrological variables (e.g. streamflow). However, for conditions that are representative of a potential climate change, observations will not be available in advance, and the climate, as well as the physical characteristics of a catchment, may be significantly different from those used in the parameter calibration procedure. The problem of defining quantitative measures of model performance in terms of its ability to adequately simulate new conditions is formidable.

Klemes (1985, 1986) suggests a hierarchical scheme for the systematic testing of climatic and geographic transferability in hydrological simulation models. This scheme presents two tests for application under stationary conditions and two tests for nonstationary conditions. The nonstationary tests are those designed for testing models developed for climatic and geographic transferability.

The first test for nonstationary conditions is a differential split sample test and is used to

evaluate climate transferability. In this test, two periods with different values of the climate parameter of interest are identified. For example, a wet and a dry period are identified if precipitation is being considered. If the model is to be used to simulate a wetter climate, it should be calibrated using the dry period and validated using the wet period. If the intended model application is a dry period, the procedure is reversed.

The second test is intended to evaluate both climatic and geographic transferability and is a proxy-catchment differential split-sample test. Two catchments within a region are selected and, as in the previous test, two periods with different values of a climate parameter of interest are identified. Using the wet and dry example, the model would be calibrated on the wet period of each catchment and evaluated on the dry period of the opposite catchment. Calibration on the dry period and testing on the wet period using the same paired catchment scheme provides an alternative application of this test. Acceptance in the nonstationary tests is based on model performance using the alternative climate and catchment conditions.

7.2.4 Model suitability

There are numerous models and modelling approaches being used to assess the impacts of climate change on water resources. Model choice is normally a function of problem objectives, data constraints, and the spatial and temporal scales of application. Empirical and water-balance type models have generally been applied to large-basin and regional analyses at time-scales of months to seasons to years. More detailed conceptual lumped parameter and process-based distributed-parameter models have generally been applied to smaller catchments at time-scales of 24 hours or less.

Empirical models have minimal data requirements but have questionable transfer value to catchment and climate conditions different from those used to develop the input-output relations of the model. An increased range of simulation capabilities is provided as one moves from water-balance models to conceptual lumped-parameter models to process-based distributed parameter models. This is accompanied, however, by an increase in the number of model parameters and the number and types of data needed to

support parameter estimation and model operation. Limited knowledge of the relations between parameter values and measurable catchment and climate characteristics often results in many of the parameters being calibrated to measured data. The use of calibrated parameters provides a large degree of uncertainty in the ability of these types of models to be climatically and geographically transferable as well.

Although there are no agreed upon bases for credibility of a model because of the many different types of models and model applications, it is logical to compare various characteristics of the differences between simulated and observed flows. For example, means of maximum and minimum flows, seasonal flows, and so on (WMO, 1975).

Since no simulation model is intended merely to show how it fits the data used for its development, performance characteristics derived from the calibration data set are insufficient evidence for its satisfactory performance. The data used for model validation (verification) must represent a situation similar to that in which the model will be used, as it is recognized that data from the actual situation to be simulated are not available.

There are, however, certain tests that can be applied to provide at least some measure of confidence that the initial model calibration is still valid. Spilt sample tests can easily be applied to water balance models and this is a significant advantage over many other deterministic conceptual models (WMO, 1975).

Such physically based models may also be designed so that the adequacy of individual structural components can be tested separately. For example, proper evaluation of evapotranspiration is an important component of the hydrological cycle, as evapotranspiration is a key 'link' between the atmosphere and the soil matrix within the hydrological cycle. The importance of this link has been observed by Dooge (1992) who states that any estimate of climate change impacts on water resources depends on the ability to relate changes in actual evapotranspiration (ETa) to predicted changes in precipitation and potential evapotranspiration (ETp).

The water balance model approach proves to be one of the versatile tools for evaluating the effects of changes in temperature and precipitation on water availability at catchment

level, and has proved over the years to be flexible and easy to use for studying a wide range of water resource problems. The application of such models may provide considerably more information on hydrological effects and the vulnerability of water resource systems to climate change than is currently available.

7.3 A water balance model (WBM) adapted to assess catchment response

This is a simple water balance model in a long line of hydrological models. A number of modelling approaches have been developed and previous models modified for studying the impacts of a potentially altered climate on catchment responses (Nemec and Shaake, 1982; Gleick, 1987; Lettenmaier and Gan, 1990; Mimikou and Kouvopoulos, 1991; McCabe and Wolock, 1992; Nash and Gleick, 1993; Reibsame, 1994; Skiles and Hanson, 1994; Xu *et al.*, 1995).

More sophisticated models developed over the past thirty years are not advantageous from the computational point of view and only result in over-parameterisation that leads to difficulty in the calibration procedure (Franchini and Pacciani, 1991). Three to five parameters should be sufficient to reproduce most of the information in a hydrological record (Beven, 1989).

The ability to relate changes in actual evapotranspiration to predicted precipitation changes and potential evapotranspiration is the main factor in estimation of catchment response(Dooge, 1992). The WBM attempts to use simple yet widely accepted assumptions regarding the water balance. The model uses a small number of parameters and incorporates a physically sound and widely accepted method for computing potential evapotranspiration as a simple approach appropriate for climate change impact assessment. It is capable of simulating flow response of a catchment as well as changes in other variables such as storage and actual evapotranspiration.

7.3.1 Modelling elements within WBM

There are essentially two main modelling components within the WBM. The first component uses continuous functions to describe water movement into and out of a conceptualised catchment. The second component calculates potential evapotranspiration.

To describe water movement, the common link in water balance approaches is the computation of a mass balance within the soil moisture zone. There are many ways of representing the infiltration, storage behaviour of the soil moisture zone and discharge (Eagelson, 1978; Shaw, 1982; Chow *et al*., 1988, Todini, 1988). The WBM accounts for changes in the soil moisture by taking into account precipitation, outflow and actual evapotranspiration while using potential evapotranspiration to drive the extraction of water from the soil moisture store (Figure 7.1).

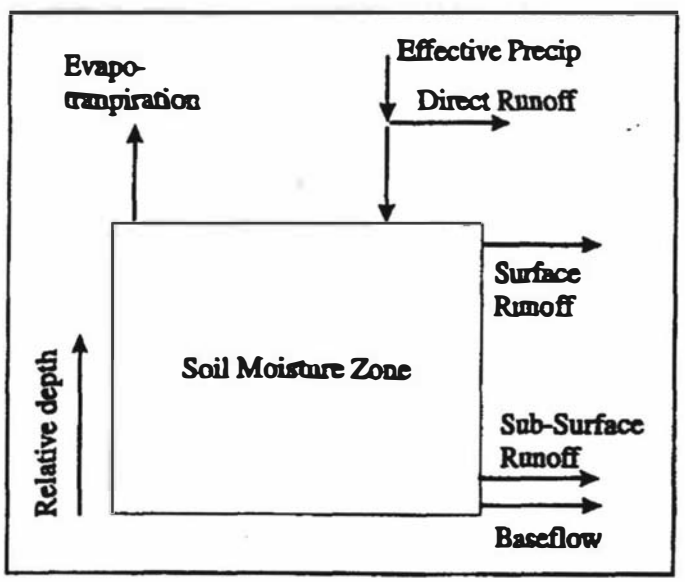

Figure 7.1 Conceptualisation of the water balance model (Yates and Strzepek, 1994).

Elements of this model approach are adapted from a water balance model framework developed by Kaczmarek (1991). Potential evaporation is calculated by using the well-known Priestly-Taylor radiation approach within the WBM. The uniqueness of this lumped conceptual model in representing water balance is the use of continuous functions of relative storage to represent surface outflow, sub-surface outflow, and

evapotranspiration. The mass balance is written as a differential equation and storage is lumped as a single, conceptualised 'bucket' (Figure 7.1) with the components of discharge and infiltration being dependent upon the state of the relative storage (Equation 7.2). The water balance component of the model contains five parameters related to:

- direct runoff (R_d);
- surface runoff (R_s);
- subsurface runoff (R_{ss});
- maximum soil water-holding capacity and
- baseflow.

Owing to the differential approach of the model, varying time steps can be used depending on data availability and basin characteristics. For larger basins with long times of concentration, longer time steps are recommended. For the computation of effective precipitation in regions where snowmelt makes up a substantial portion of the runoff water, a temperature index model is used with the upper and lower temperature bounds determined by trial and error.

7.3.1.1 The soil moisture balance

Soil moisture balance can be described by the following equqtion:

$$S_{max}\frac{dz}{dt} = (P_{eff}(t)(1-\beta)) - R_s(z,t) - R_{ss}(z,t) - ETa(ETp,z,t) - R_b \qquad (7.2)$$

where:

S_{max} = Maximum storage capacity (depth)
z = relative storage ($0 \le z \le 1$)
t = time
P_{eff} = Effective precipitation (depth/time)
β = direct runoff coefficient
R_s = Surface runoff (depth/time)
R_{ss} = Sub - surface runoff (depth/time)
ETa = Evaporation (depth/time)
ETp = potential evapotranspiration
R_b = baseflow (depth/time)

7.3.1.2 Direct runoff (R_d)

Direct runoff, which is synonymous with Horton overland flow is:

$$R_d = \beta P_{eff} \tag{7.3}$$

7.3.1.3 Actual evapotranspiration (ETa)

Actual evapotranspiration is a function of potential evapotranspiration (ETp) and the relative catchment soil moisture storage status. A number of expressions have been given that describe evapotranspiration as a function of the soil moisture status (Kaczmarek, 1991). Shown are a linear and a non-linear expression. A simple-linear expression might be given by:

$$ETa(z, ETp, t) = zETp \tag{7.4}$$

A non-linear relationship has been used to describe evapotranspiration (Kaczmarek, 1993).

$$\mathrm{ETa}(z, \mathrm{ETp}, t) = \mathrm{ETp}\left(\frac{5z - 2z^2}{3}\right) \begin{cases} \mathrm{ETp}(z) & \text{albedo is a function of soil mositure} \\ \mathrm{ETp_c} & \text{fixed albedo} \end{cases} \tag{7.5}$$

Potential evapotranspiration is modelled using the Priestley-Taylor method (described below). This method was chosen due to its simplicity and the evidence supporting such an empirical relationship on a regional basis, which is the case for river basin modelling (Shuttleworth, 1993). The Priestley-Taylor method is a radiation-based approach to modelling ET_p, where the net radiation is taken from observed data (in equivalent water depth, mm/day) or is computed based on analytical methods. The albedo, a measure of surface reflectivity incorporated into the computation of net radiation, can be given as monthly mean values, or can be computed based on the soil moisture content of the soil as well as the predominant surface cover (grass or forest, snow, and fraction of bare ground).

7.3.1.4 Surface runoff (R_s)

A variation of the surface runoff term has been used in the WBM approach. Surface runoff is described in terms of the storage status, z, the effective precipitation, P_{eff}, and the baseflow. If the precipitation is exceeded by the predefined baseflow, then surface runoff is zero (Kaczmarek, 1993). Surface runoff is defined as:

$$R_s(z,P,t) = \frac{\varepsilon}{1+\varepsilon-z}(P_{eff} - R_b) \tag{7.6}$$

where: ε = surface runoff coefficient

Investigation of this expression led to a reformulation that gave a more robust solution to catchments with large variations in storage due to extreme seasonality. The above expression has been changed to

$$R_s(z,P,t) = \begin{cases} z^{\varepsilon}(P_{eff} - R_b) & \text{for } P_{eff} > R_b \\ 0 & \text{for } P_{eff} \le R_b \end{cases} \tag{7.7}$$

Equation 7.7 allows the surface runoff term to approach zero, as the relative storage becomes very small. If there is a large contribution from direct runoff, then this can be described with the parameter β (Equation 7.2).

7.3.1.5 Sub-surface runoff (R_{ss})

Sub-surface runoff is a function of the relative storage status (z) times a sub-surface runoff coefficient of 'proportionality' (α) given in Equation 7.8.

$$R_{ss} = \alpha z^{\gamma} \tag{7.8}$$

In most cases, the value of the sub-surface runoff 'exponential' coefficient (γ) is 2.0. Although it was observed for some catchments, that γ the value appeared to be smaller than 2.0. As γ approaches 1.0 the sub-surface discharge responds more linearly with

relative storage, indicating a decrease in the holding or retention capacity of the soil. A value of $1.0 > \gamma < 2.0$ might be more appropriate for gravel-dominated catchments.

The 4th model parameter is the maximum catchment holding capacity, S_{max}. The storage variable, z, is given as the relative storage status: $0 \leq z \leq 1$. Referring to Figure 7.1, S_{max} is defined as the maximum storage volume, so when S_{max} is multiplied by z, the current storage volume for the period is given.

7.3.1.6 Total runoff (R_t)

Total runoff, for each time step, is the sum of the four components:

$$R_t = R_s + R_{ss} + R_b + R_d \tag{7.9}$$

The differential equation (7.2) is solved using a predictor-corrector method (Carnale and Chapra, 1988). The model is calibrated using an unconstrained heuristic algorithm which finds an optimal set of model parameters while meeting the criteria of minimising the root mean square error between the observed and predicted monthly runoff value. The direct runoff coefficient, β, and the sub-surface runoff 'exponential' coefficient, γ, are not part of the optimisation routine.

Time series inputs to this model include effective precipitation (adjustments for seasonal interception, elevation adjustments, and gauge error must be predefined using the worksheet), potential evapotranspiration, and for calibration and validation purposes, an outflow in the units of depth/time. Potential evapotranspiration can be estimated using the Priestly-Taylor sub-component in which case a temperature time-series is also required.

For catchments with a large portion of outflow from snowmelt, a temperature index snowmelt model is used with temperature thresholds for melting and freezing, creating an 'adjusted' effective precipitation. The snowmelt model is also used to calculate winter albedo in those catchments where winter precipitation in the form of snow is significant (Equation 7.12).

7.3.2 Effective precipitation

A sub-component of the WBM is the computation of an 'adjusted' effective precipitation based on snowmelt processes. Precipitation must first be corrected for elevation effects, gauge error, seasonal interception, etc.; the snowmelt model will then compute an 'adjusted' effective precipitation to the water balance component. The following relationships are used to derive this 'adjusted' effective precipitation based on the snowmelt process.

$$Peff_i = mf_i(A_{i-1} + Pm_i) \tag{7.10}$$

where

$$mf_i = \begin{cases} 0 & \text{for } T_i \le T_s \\ 1 & \text{for } T_i \ge T_l \\ \dfrac{(T_i - T_s)}{(T_l - T_s)} & \text{for } T_s < T_i < T_l \end{cases} \tag{7.11}$$

where: mf_i = melt factor in month i

T_i= mean temperature of month i

T_s= freezing threshold temperature

T_l= melting threshold temperature

and snow accumulation is written as

$$A_i = (1 - mf_i)(A_{i-1} + Pm_i) \tag{7.12}$$

where: A_i = snow accumulation in month i

mf_i = melt factor in month i

Pm_i = observed precipitation in month i

$Peff_i$ = effective precipitation in month i

7.3.3 Priestley Taylor method for potential evapotranspiration

Penman (1948) was the first to describe evaporation in terms of the two main micrometeorological components: energy for the conversion of water to a vapour phase and aerodynamic processes for the removal of saturated air away from the surface. The Penman equation is the most widely known combined method of estimating evaporation.

$$E = \frac{\Delta}{\Delta+\gamma} E_r + \frac{\gamma}{\Delta+\gamma} E_a \qquad (7.13)$$

where: E .= Combined evaporation estimate (mm/day)

Δ = slope of the saturated vapour pressure curve

γ = psychometric constant = $C_p \frac{pK_h}{0.622lK_w}$

where: C_p = specific heat at constant temperature K_h,

K_w = diffusivity (L^2/t)

l = mixing length

E_r = Evaporation estimate that assumes the ability of the system to remove moist air is not limiting.

E_a = Evaporation estimate which assumes an unlimited availability of energy.

Priestley and Taylor (1972) found that for very large areas the second term of the Penman equation is approximately thirty percent that of the first. Thus an approximation to the Penman equation which gives an estimate of reference crop evapotranspiration (E_{rc}) may be written as:

$$E_{rc} = \alpha \frac{\Delta}{\Delta+\gamma} (R_n - G) \qquad (7.14)$$

where: α = 1.26 in humid climates (relative humidity greater than 60% in the month with the maximum evaporation) and 1.74 for arid climates (relative humidity less than 60% in the month with the maximum evaporation).

G = soil heat flux which for regional estimates can be assumed to be zero; all other terms carry their definitions.

This reference crop evapotranspiration estimate (referred to in this application as potential evapotranspiration) should show lower values than similar estimates, which give free surface evapotranspiration.

7.3.4 Radiation

Net radiation data can be estimated using Equation 7.15. Aside from temperature, the equation uses two additional climate variables; relative humidity and bright sunshine hours per day (Leemans and Cramer, 1992). Assuming relative humidity and sunshine hours to be functions of precipitation and temperature, estimates of their projections can be based on temperature and precipitation scenarios.

$$R_n = \left((1 - alb)\left(0.25 + 0.5\frac{n}{N} \right) Ra \right) - (f)(0.34 - 0.14\sqrt{e_d})\sigma\,(T + 273.2)^4 \qquad (7.15)$$

where: R_n = net radiation (MJ $m^{-2}day^{-1}$)

alb = albedo (short-wave radiation reflection coefficient)

n = bright sunshine hours per day (h)

N = total day length (h)

R_a = extraterrestrial radiation (Mj $m^{-2}day^{-1}$)

f = cloudiness factor, given by

$$f = \left(a_c \frac{b_s}{a_s + b_s} \right) \frac{n}{N} + \left(b_c + \frac{a_s}{a_s + b_s} a_c \right) \qquad (7.16)$$

where: a_s = 0.25 and b_s = 0.50

a_c = 1.35 and b_c = -0.35 (arid climates) or

a_c = 1.00 and b_c = 0.00 (humid climates)

σ = Stefan-Boltzmann constant (4.903×10^{-9} Mj m^{-2} $^oK^{-4}day^{-1}$)

e_d = vapor pressure (kPa)

T = mean air temperature (°C)

If it is assumed that the density of water is constant (1000 kg m^{-3}) then R_n (Equation 7.15) can be converted from $MJm^{-2}day^{-1}$ to mm day^{-1} by dividing R_n by the latent heat of vaporisation (in MJ kg^{-1}). Actual vapour pressure is estimated by multiplying mean monthly relative humidity values with saturated vapour pressure taken from the IISA database (Leemans and Cramer, 1992). To compute the extraterrestrial radiation and total day length the following equations are used.

$$R_N = 15.392 d_r (w_s \sin f \sin d + \cos f \cos d \sin w_s) \tag{7.17}$$

$$N = \frac{24}{\pi} \omega_s \tag{7.18}$$

$$dr = 1 + 0.033 \cos(2pJ / 365) \tag{7.19}$$

$$w_s = arc \cos(-\tan f \tan d) \tag{7.20}$$

$$d = 0.4093 \sin(2pJ / 365 - 1.405) \tag{7.21}$$

where: R_N = extra-terrestrial radiation (mm/day)

d_r = relative distance earth-sun

w_s = sunset hour angle (radians)

f = latitude of site (+ for northern hemisphere, - for southern hemisphere)

[radians]

d = solar declination [radians]

N = maximum possible daylight hours

J = Julian day

7.3.5 Albedo

The albedo is a measure of the surface's capacity to reflect incoming short-wave solar radiation. Albedo can be given exogenously as monthly mean values or it can be computed, based on land cover conditions as well as the soil moisture status. Two broad land cover classes are used within the WBM, where one is forest and the other is grass and pasture. Shuttleworth (1993) suggested the following albedo values (Table 7.1) and these are used within the WBM to compute albedo based on equation (7.22)

$$alb_i = \begin{cases} ([1-mf_i)0.8] + mf_i[(1-GC)(a_1-(z*a_2)) + GC(a_d-(z*a_w))] & \text{if } mf_i < 1.0, \text{ new snow} \\ [(1-mf_i)0.2] + mf_i[(1-GC)(a_1-(z*a_2)) + GC(a_d-(z*a_w))] & \text{if } mf_i < 1.0, \text{ old snow} \\ (1-GC)(a_1-(z*a_2)) + GC(a_d-(z*a_w)) & \text{if } mf_i = 1.0 \end{cases} \quad (7.22)$$

where for each month I

alb_i = albedo

GC = ground cover index ($0.0 < GC < 1.0$; GC = 0.0 completely covered, GC = 1.0 completely bare)

mf_i = melt factor; ($0.0 < mfi < 1.0$), (Equation 7.20)

z_i = relative soil moisture; ($0.0 < z_i < 1.0$), (Equation 7.2)

a_1, a_2 = albedo bounds based on land cover type (grass/pasture or forest)

a_d, a_w = albedo bounds for bare soil (dry and wet)

Table 7.1 Albedo values for different land covers included within WBM Shuttleworth (1993).

Land cover class	Albedo values, alb
Forest	0.11-0.16
Grass and pasture	0.20-0.26
Bare soil	0.10 (wet) – 0.35 (dry)
Snow and ice	0.20 (old) – 0.80 (new)

7.4 Impact on water resource systems performance

A number of indicators can be used to describe the possible performance of water resource systems. Simple and frequently used measures of system performance are the mean and variance of system outputs as performance indices. While the mean and variance are useful statistics, they are often not sufficient. In particular, the mean and variance describe the average level and average squared deviation from the mean of the parameters in question. These statistics provide a very vague description of just how poorly a system might behave in an extreme situation when a failure occurs. For example, the availability of water for hydroelectric power generation may be satisfactory 360 days a year. The primary concern is for the 5 days when the water is unavailable and when the operations might be seriously affected.

Figure 7.2 illustrates the inability of the mean and variance to define how severe and how frequent periods of poor performance may be. The figure contains a time history of performance of two possible systems. The mean and variance of the performance parameter is the same in both cases over the time period shown. In fact, the curves are mirror images about their mean level. However, the performance history on the left hand side in Figure 7.2 displays two periods where performance clearly fell below the performance standards while the performance history on the right hand side shows no failure.

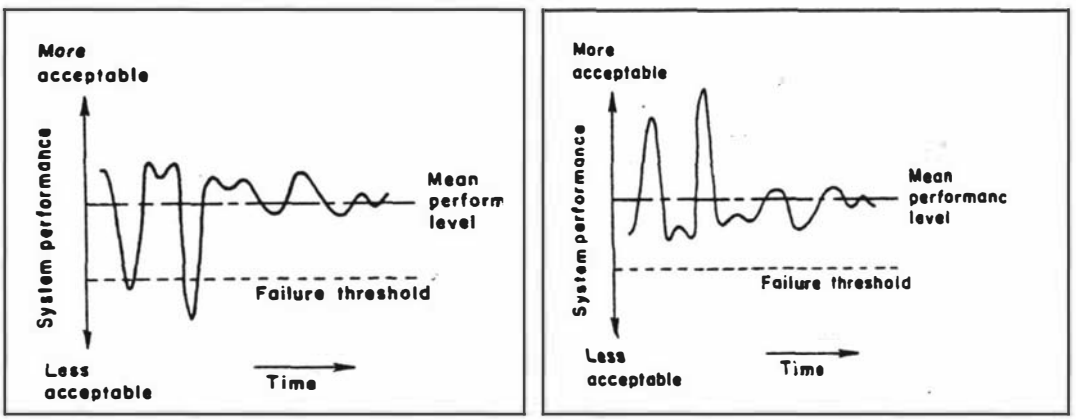

Figure 7.2 Variable system performance with infrequent failures (left) and without failures (right) (Hashimoto *et al.*, 1982)

When summarizing the values of performance parameters by their mean and variance, it is also difficult to determine if an improvement in the mean accompanied by an increase in the variance is an overall improvement. However, if performance is highly variable or if the consequences of poor performance are severe then it is appropriate and desirable to employ risk descriptors, which (unlike the mean and variance of a parameter) describe in clear and meaningful terms what the character of failure might be.

Performance of water resources has been commonly described in terms of means and variances of some hydrological operating variables (e.g. streamflow). In many cases the focus has been exclusively on the hydrological response to climate change without addressing the sensitivity of the resource systems performance to changes in hydrological characteristics. In this study attempts were made to translate catchment water yield into information which water managers may need to adapt to change while taking account of basic water management options. Operational risk descriptors in terms of water availability were formulated to illustrate the quantification process of a resource system performance in the wake of climate change.

Reliability, resiliency and vulnerability performance criteria were tested for their potential to capture and quantify possible system performance, which are especially important for extreme events that might be associated with climate change. These

performance risk measures may be useful in the selection of water resource system capacities, configurations, operating policies and targets (Hashimoto *et al.*, 1982).

In this approach the analysis of system performance focuses on the system failure, defined as any output value in violation of a performance threshold (such as a performance standard or contractual obligation). System performance is described from three viewpoints:

- how often the system fails (reliability);
- how quickly the system returns to a satisfactory state once a failure has occurred (resiliency); and
- how significant the likely consequences of failure may be (vulnerability).

Mathematical definitions of these criteria are adapted after (Hashmoto *et al.*, 1982) assuming that a stationary stochastic process can describe the performance within at least three decades (a typical period over which climate is defined by WMO). Therefore, the probability distributions that describe the output time series are constant within that period. Of course, this is only an approximation of reality as, for instance, the probability distribution of streamflows at a particular site may change over time due to land use changes in the drainage area. Still, it is both convenient and satisfactory in many cases to assume that streamflows are a stationary process within three decades of defining a climate driving such flows.

7.4.1 Reliability

A system's output state or status, denoted by the random variable x, at time t, where t takes on discrete values 1, 2, 3, ..., can be partitioned into two sets: a set of all satisfactory outputs, **S**, and a set of all unsatisfactory (failure) outputs, **F**. At any time t, the system output is assumed to be in a state which is an element of one of these sets. The reliability of a system can be described by the frequency or probability, α, that a system is in a satisfactory state:

$$\alpha = \text{Prob}(x_t, \in S) \tag{7.23}$$

Reliability is a widely used concept in water resources planning. Reliability is sometimes taken to be the opposite of risk. That is, the risk or probability of failure is simply one minus the reliability, α. Both reliability and this definition of risk do not describe the severity or likely consequences of a failure. The possible severity of failures can be described by other criteria, such as resiliency and vulnerability.

7.4.2 Resiliency

Resiliency describes how quickly a system is likely to recover or bounce back from failure once a failure has occurred. If failures are prolonged events and system recovery is slow, this may have serious implications for system performance. A good system should be able to recover and return to a satisfactory state rapidly.

Resiliency may be given a mathematically precise definition. Let T_F be the length of time a system's output remains unsatisfactory after a failure. The resiliency of a system can be defined as the inverse of the expected value of T_F. To derive a mathematical expression for that expected value, let z_t be a parameter such that: $z_t = 1$ for $x_t \in S$ and $z_t = 0$ for $x_t \in F$. Then $\frac{1}{n}\sum_{1}^{n} Z_t$ is the fraction of the time from period $t = 1$ to $t = n$ that the system output or performance is satisfactory. In the long run this fraction approaches the probability of the performance being satisfactory, and hence equals system reliability:

$$\lim_{n \to \infty} \frac{1}{n} \sum_{t=1}^{n} z_t = \alpha \tag{7.24}$$

Let a parameter W_t indicate a transition from a satisfactory to an unsatisfactory state,

where: $W_t = 1$ for $x_t \in S$ and $x_{t+1} \in F$; and $W_t = 0$ otherwise.

In the long run the mean value of W_t will equal the probability ρ of the system being in the set S in some period t and going to the set **F** in the following period given by:

$$\rho = \{\text{Prob } x_t \in S,\ x_{t+1} \in F\} = \lim_{n \to \infty} \frac{1}{n} \sum_{t=1}^{n} W_t \tag{7.25}$$

The average sojourn time in the unsatisfactory or failure states ($\overline{T}_F$) during an n-period experiment is:

$$\overline{T}_F = \frac{A}{B} \tag{7.26}$$

where A is the total time in **F** and B is the number of times the process went into **F**. Hence

$$\overline{T}_F = \frac{1}{n} \sum_{t=1}^{n} (1 - Z_t) \left(\frac{1}{n} \sum_{t=1}^{n} W_t \right) \tag{7.27}$$

As n approaches infinity, the average sojourn time $\overline{T}_F$ will approach its mean value $(1-\alpha)/\rho$. Thus the expected length of time that the system's output or performance remains unsatisfactory once it becomes unsatisfactory equals:

$$\mathrm{E}[T_F] = \frac{1-\alpha}{\rho} \tag{7.28}$$

$\mathrm{E}[T_F]$ defines the average number of time periods a failure is expected to last once it has occurred. The inverse of this is the system's average recovery rate (γ) and is the measure of resiliency:

$$\gamma = \frac{\rho}{1-\alpha} = \frac{\text{Prob } \{X_t \in S \text{ and } X_{t+1} \in F\}}{\text{Prob } \{X_t \in F\}} \tag{7.29}$$

7.4.3 Vulnerability

Here vulnerability refers to the likely magnitude of a failure, if one occurs. Even when the probability of failure is small, attention should be paid to the possible consequences

of failure. Holling (1978) discusses the idea of safe-fail as opposed to fail-safe. Attempts to maximise system reliability are attempts to make a system's operation failure-free. Still, few systems can be made so large or so redundant that failures are impossible. Even when it is possible to raise levees high enough or make water supply reservoirs large enough that failure is hard to imagine, it is often not economic to do so.

Efforts to maximise system efficiency and reliability can increase a system's vulnerability to costly failure should failure occur. For example, transformation of traditional agricultural systems to high yield single-species crops sets the stage for disaster should a new crop disease or pest develop. Likewise, flood control reservoirs and levees that control small floods create an image and sense of security; as a result, unwise development in partially protected areas can occur. This creates the potential for large losses should a large flood occur or a levee break (Adams and Gemmell, 1980).

It is important that decision-makers be aware of the vulnerability of a system to severe failure should a failure occur. This should be an important criterion in water resource system design and selection. To construct a mathematical index of system vulnerability, assume that the system performance variable x, can take discrete values x_1, ... ,x_n. To construct a quantitative indicator of system vulnerability to severe failure should a failure occur, a numerical indicator of the severity of that state, denoted s_j is assigned to each discrete failure state $x_j \in$ **F**. Furthermore, let e_j be the probability that x_j, corresponding to s_j, is the most unsatisfactory and severe outcome that occurs in a sojourn into the set of unsatisfactory states **F**. Then e_j equals the probability that x_j, corresponding to s_j, is the most severe outcome in a sojourn in **F**. One reasonable overall system vulnerability, (ν), would be the expected maximum severity of a sojourn into the set of unsatisfactory states. This does not emphasise how long failure may persist but how bad things may become.

$$\nu = \sum_{j \in F} s_j e_j \tag{7.30}$$

The catchment response and water resource systems performance approaches were linked in two case studies to illustrate their potential in exploration of the use of the current generation of GCM outputs in impact estimation in Chapter 8.

Chapter Eight

New Zealand water resources

Water, seen in terms of the 'conservation ethic', Maori spiritual values, or the Judaeo-Christian view of water as a source of life, is beyond evaluation. Nevertheless, water is a fundamental economic resource, for which a value in money terms can in principle be estimated. An overview of the main features of New Zealand's water environment and the pressures imposed on it is presented with two case studies to quantify the impacts of predicted climate change on New Zealand hydrology and water resources.

A water balance model (WBM) was calibrated and verified for the Lake Taupo and the Opihi River catchments' responses to climate changes. Subsequently, the model was used to simulate water yields over four tri-decades (1980-2009, 2010-2039, 2040-2069 and 2070-2099). Potential impacts associated with changes in catchment yields were evaluated in terms of water resource systems' performance by formulating operational risk descriptors for the Waikato Hydro Scheme (Lake Taupo outflows) and the Level Plains Irrigation Scheme (Opihi River flows).

8.1 Value of New Zealand

A formal analysis of the value of New Zealand's water resource has not been carried out, but Mosley (1988) suggested total of about $2000 million per annum. Values of water in terms of money were estimated for water irrigation and water supply, power generation, recreation, commercial freshwater fisheries, waste disposal, gravel extraction, transportation, flood damage, erosion and sedimentation.

Existing irrigation schemes cover over 200,000 ha, and the potentially irrigable area exceeds 800,000 ha. The total cost of schemes presently under consideration or recently completed (1988) is $420 million; the value of resulting increases in agricultural production cannot be calculated. The total annual cost of water (Mosley, 1988), which averages $0.25 per cubic metre m^3, is:

- Agriculture $286 million
- Industry $112 million
- Domestic $78 million

The value of electricity generation in twelve months of 1984/85 water year was $827 million (200,000 GWh for hydro and 6,000 GWh for thermal stations). All types of electric power stations require water, either as the source of power itself, or for coolant or waste discharge. Hydro stations use 8% of the total river flows.

There are 160,000 fishing licence holders, paying $4 million annually in licence fees, and an unknown number of jetboaters, canoeists and other river recreationists. The Rakaia River, for example, received 70,000 visitors for jetboating and canoeing alone, and its value for recreation was assessed at $4.7 million in 1984. Rivers and lakes are a huge asset to the New Zealand public for recreation, and a major attraction for overseas tourists, but are readily degraded by reduced flows, either by abstraction or naturally.

Recreational and fresh-water fishing is an expanding industry which was projected, in 1984, to generate $25 million in 1988. Its survival is dependent on adequate flow in the rivers to allow fish passage and to prevent river mouth closure.

Rivers are used to treat 120 tonnes per day of BOD[1] (a measure of organic waste). The capital value of municipal sewage treatment systems, which treat 80 tonnes per day of BOD, is $3,000 million (an annual cost). Waste assimilation capacity, of course, varies with flows, particularly low flows.

---

[1] Biochemical Oxygen Demand is an indicator of microbial contamination. It measures the amount of oxygen in water sample that is consumed over a five-day test period by the micro-organisms and biochemical processes that break down rotting organic matter.

Rivers are a major source of aggregate for construction purposes, railway ballast and road material. Permissible extraction rates are governed by river stability and sediment transport, which in turn are controlled by the sequence of flows, particularly flood flows. In 1984/85, a total of over 800,000 m^3 was removed from the major rivers in Hawkes Bay alone; the Hawkes Bay Catchment Board (Now the Hawkes Bay Regional Council) charged extractors a fee of 56c/ m^3. The value of the aggregate resource in the Manawatu is estimated to exceed $2 million annually.

A major cost of maintaining the road and rail network is in constructing and replacing bridges, and repairing or replacing bridges and embankments damaged by floods. The cost of a bridge is highly dependent on the size of the waterway required (i.e., number of spans, height of piers), which in turn depends on expected flows. The current cost of bridge reconstruction and replacement approximates $25 million per annum.

As flood plains have been increasingly heavily developed for residential and agricultural purposes, flood damages have increased to an average of $90 million per year. The national land estate has an assessed value of $50,500 million per annum. However, hill country research demonstrated that erosion of hillsides by slips might reduce farm productivity by almost 10% and profitability by even more. The economic and social costs of such individual erosion features are immense. Annual expenditure on catchment works and river control schemes to deal with more widespread erosion and also to combat flood damage averaged almost $40 million per year.

8.2 Natural water environment

New Zealand's natural water environment consists of four main components: rainfall (which also includes other forms of precipitation, such as snow and hail); surface water (which includes streams, rivers, lakes and wetlands); groundwater (which includes both ambient and geothermal underground water); and the marine water into which they all drain (which includes estuaries, coastal waters and the open sea). Interwoven with these is an unnatural, but highly important, fifth component - the piped (or reticulated) drinking

water and drainage systems that supply clean water to, and remove dirty water from, most households.

8.3 Water from precipitation

The total annual precipitation in New Zealand is estimated to be between 300,000 million and 600,000 million m^3 of water. Most parts of the North Island have a mean annual precipitation between 1200 and 2400mm. In the South Island precipitation has greater regional variations. Generally, the west is wetter and the east is drier, with the most extreme variations in the southern South Island.

Central Otago (east of the Southern Alps) is the driest area, with an average annual precipitation of about 350mm, while Fiordland and Westland (west of the Southern Alps) have annual precipitation of more than 6000 mm. The uneven distribution of precipitation is attributed to the effect of the high mountain ranges (details discussed in Chapter Five).

A considerable proportion of winter precipitation falls as snow in the mountains of New Zealand, and water delayed contributes to lake storage and river flows during spring and summer (Fitzharris *et al.*, 1992).

8.4 Surface water

Despite its relatively small size, New Zealand is well endowed with freshwater resources such as rivers, lakes, and wetlands. On a national scale, streams and rivers occupy approximately 294,600 ha, lakes 339,800 ha, and wetlands 311,300 ha (Scott, 1996). Surface water which includes streams, rivers, lakes and wetlands, provides about 60% of the surface water and 40% comes from underground. Rivers also provide 75% of the country's electric power, and they are home to more than 50 species of fish as well as freshwater invertebrates and plants.

8.4.1 Streams and Rivers

Due to the mountainous terrain of both main islands, there are many comparatively small catchments with fast-flowing stony streams and rivers. The North Island has 36 major river catchments (Figure 8.1) and the South Island has 40 (Figure 8.2).

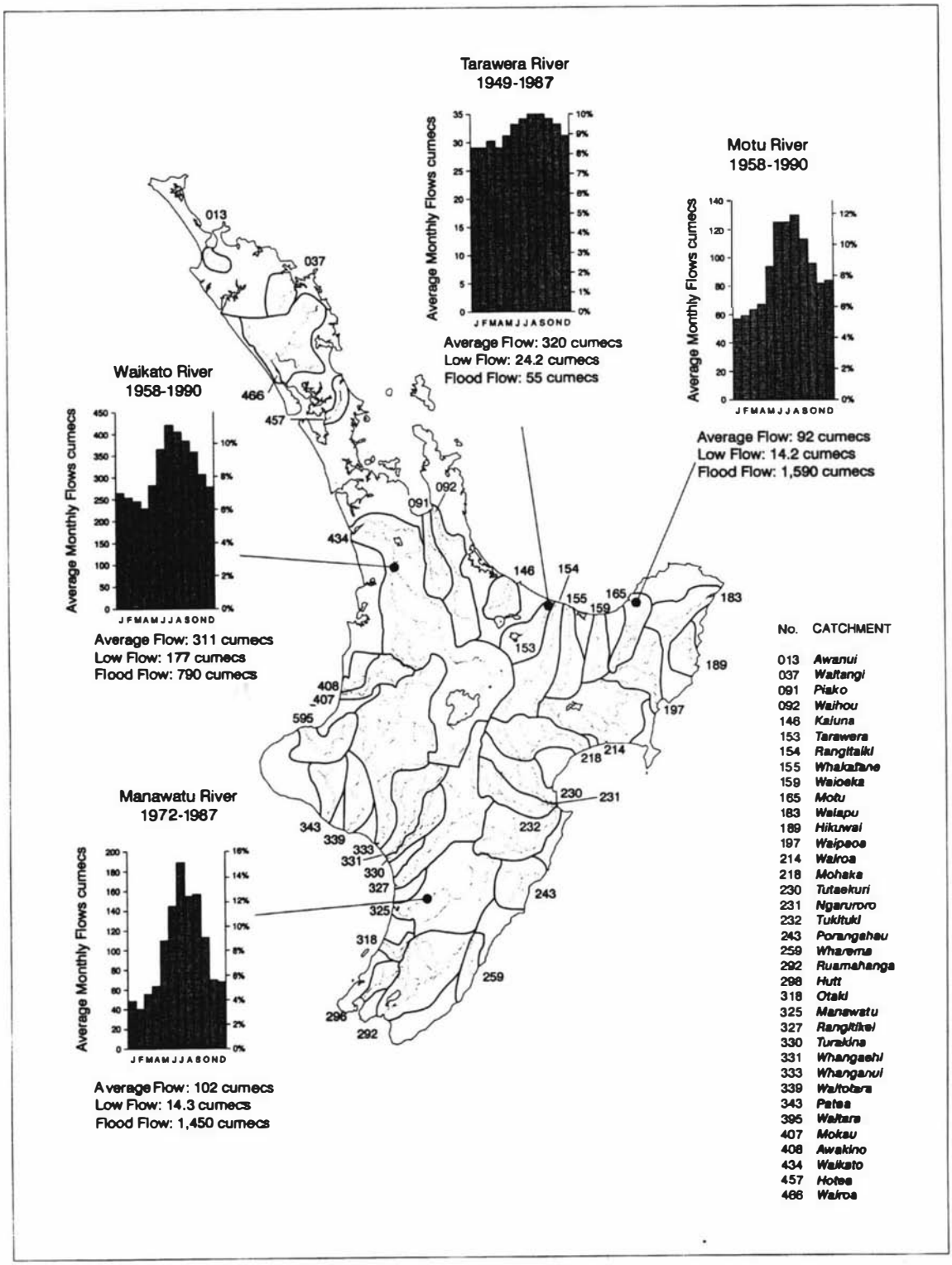

Figure 8.1 Catchments and typical flows in cumecs (m^3/s) of the main rivers in the North Island. Adapted from Taylor *et al.*, 1997 (after Duncan, 1992).

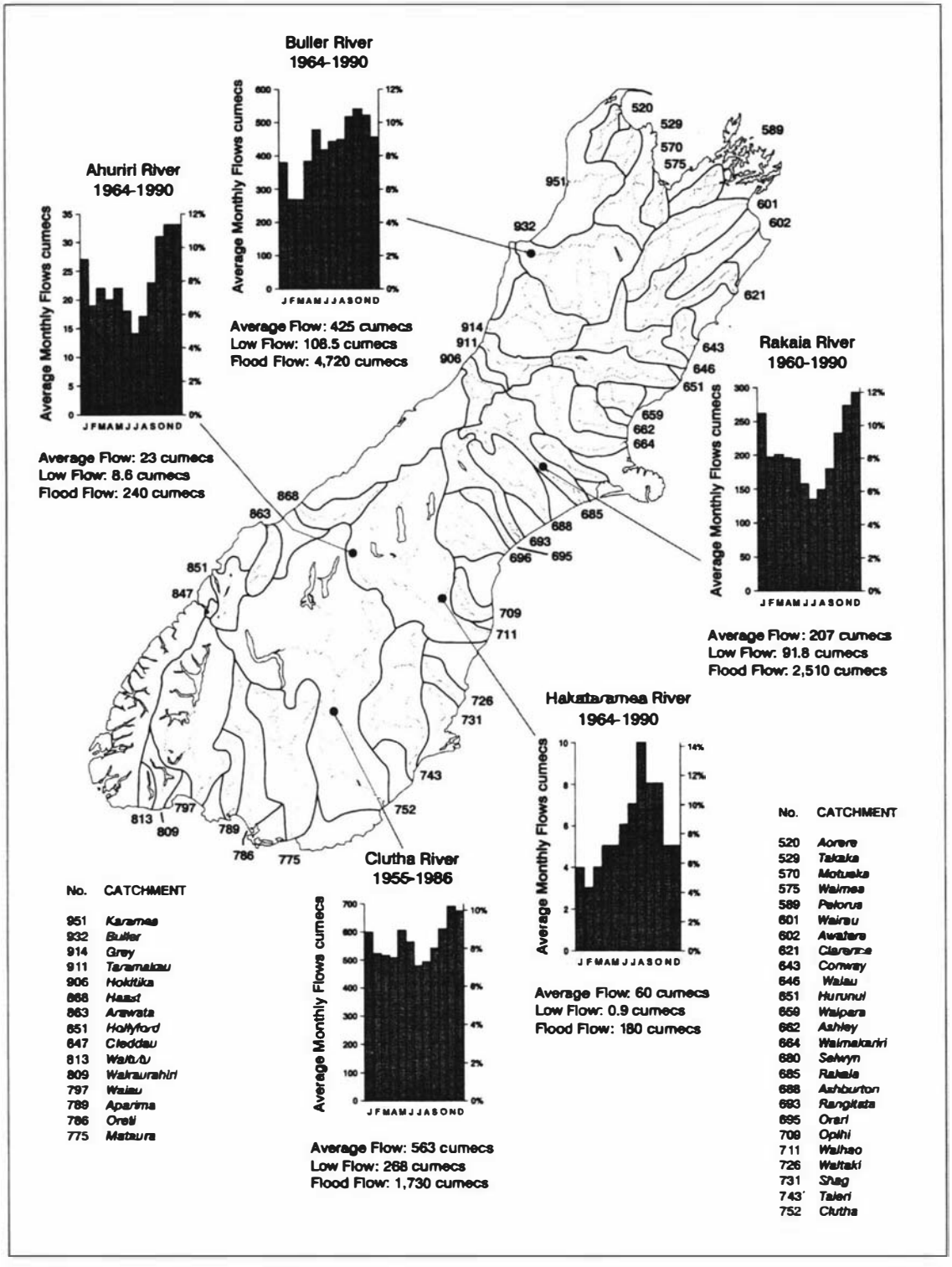

Figure 8.2 Catchments and typical flows in cumecs (m^3/s) of the main rivers in the South Island. Adapted from Taylor *et al.*, 1997 (after Duncan, 1992).

The largest river in New Zealand is the South Island's Clutha which drains a catchment area of 20,580 km^2. The Clutha River has an average flow of 570 cumecs. The Waikato River in the North Island is the longest river (425 km) and has a catchment area of 11,400 km^2 and an average flow of 327cumecs.

Seasonal variations in rainfall and evapotranspiration cause river flows to change through the year (i.e. lower flows in summer and autumn and higher flows in winter and spring). This variation is more extreme in the east coast of both islands where summers are relatively dry. In some rivers such as the Rakaia and the Ahuriri, however, the summer flows are relatively high because water from the melting snow is augmented by increased rainfall from the seasonal northwest winds (Duncan, 1992).

In some places, river flow is also augmented by groundwater which may enter from springs and openings in hillsides and cliffs or seep from sloping ground. In some of the central North Island rivers, the contribution from groundwater is large enough to reduce the seasonal flow variation caused by rainfall, as is demonstrated by the relatively constant flow of the Hamurana Stream near Rotorua (Taylor *et al.*, 1997).

8.4.2 Lakes

New Zealand has at least 770 lakes with a combined surface area of about 3,340 km^2 ha (Molloy, 1980). Most of the lakes are small with surface areas of less than 0.5 km^2. Many of them are shallow lakes only several metres deep and surrounded by farmland. Only 40 lakes have areas greater than 50 ha (Lowe and Green, 1987).

New Zealand's lakes were formed by three broad processes, namely:

- volcanic eruptions created the hollows for most of the larger North Island lakes;
- glacial ice gouged out the basins for most of the South Island lakes;

- land barriers formed by accumulated sediment, sand bars, and earth movements, blocked off river channels, creating a large number of shallow lakes in floodplains and coastal areas.

Lake Taupo in the North Island is the largest lake in New Zealand, with an area of about 620 km^2 and a maximum depth of 163 m. Its size is the legacy of several vast ancient eruptions. Lake Wairarapa is the second largest in the North Island with an area of almost 80 km^2 and is shallow with a maximum depth of less than 3 m. Drainage for farmland has greatly reduced Lake Wairarapa's area. The deepest (and probably least modified) North Island lake is Waikaremoana, which formed when a landslide blocked a valley 2,000 years ago. Its maximum depth is 248 m. Apart from Taupo and Waikaremoana, only one other North Island lake (Rotomahana) is deeper than 100 m (Spigel and Viner, 1992).

The South Island's largest lake is the glacial Lake Te Anau, with an area of around 350 km^2 and a maximum depth of 417 m, and Lake Wakatipu, with an area of 290 km^2 and a maximum depth of 380 m and the third largest is Ellesmere (or Waihora). The later is also the country's largest shallow lake with an area of 180 km^2 reduced from 300 km^2 by drainage and a maximum depth of less than 3 m. The deepest lake in the South Island and also the deepest lake in New Zealand, is the glacial Lake Hauroko in Southland which has a maximum depth of 462 m. Apart from Te Anau, Wakatipu and Hauroko, 12 other South Island lakes have depths greater than 100 m (Spigel and Viner, 1992).

At least 16 artificial lakes have been created for hydro-electric power stations, the largest of which is the South Island's Lake Benmore (69 km^2) and the smallest of which is the North Island's Lake Aratiatia (0.34 km^2).

8.4.3 Wetlands

Wetlands are areas of shallow water containing specially adapted plant and animal communities (e.g. rushes, sedges, reeds, flax, water birds, eels, mudfish and aquatic invertebrates). They occur on land-water margins, or on land that is temporarily or permanently wet. Although they are found at all altitudes, from coastal estuaries and sand

dunes to alpine tarns, wetlands mainly occur in valley floors and on flood plains, often in association with former river courses and ponding areas, lake margins and dune hollows.

Wetlands are a major habitat for at least eight species of indigenous freshwater fish as well as frogs, birds and invertebrates. Coastal wetlands are more biologically productive than virtually any other ecosystem, providing habitat, breeding areas, and food for shellfish, crustaceans, inshore fish and birds. A fifth of New Zealand's indigenous birds use wetlands as their primary habitat. Wetlands also support other ecosystems by absorbing floodwaters and filtering wastewater. They regulate water flows, recharge ground aquifers, maintain water quality, and limit coastal erosion.

Freshwater wetlands covered at least 6,700 km^2 before European settlement, but have now been reduced by drainage for pasture to around 1,000 km^2. Although several thousand wetlands still survive, most are very small and have been modified by human activities and invasive species. It is likely that, in the last 100 years, some characteristic New Zealand wetland types have been lost completely, while very few examples are left of others, such as Kahikatea swamp forest and some kinds of flax swamp and salt marsh (Cromarty and Scott, 1996).

8.4.4 Groundwater

After rainfall soaks into the ground as soil moisture it may seep into streams as delayed flow, plants may absorb it, or it may seep further into the ground and become groundwater. The underground areas in which groundwater collects are called aquifers. Aquifers take many geological forms, including caverns, deep rock fissures, and porous gravel beds. The most extensive New Zealand aquifers composed of alluvial gravel overlaid with fine-grained marine sediments formed during the Pleistocene.

New Zealand's groundwaters range in temperature from less than 10°C to more than 300°C, depending on how close they are to active faultlines or volcanic zones. The Resource Management Act (1991) defines groundwater of 30°C or more as geothermal, whereas groundwater cooler than this is considered to be within the range of ambient land and surface water temperatures (Taylor *et al.*, 1997).

8.4.5 Ambient groundwater

Extensive aquifers of ambient groundwater occur in many parts of the country, including the Canterbury Plains, Marlborough and Tasman Districts, Hutt Valley, Manawatu, Hawke's Bay, the Bay of Plenty, the Waikato and Hauraki Lowlands, and South Auckland. In areas prone to surface water shortages or seasonal fluctuations in river flows and rainfall, these groundwater reserves have become an important source of water supply. Aquifers can satisfy heavy summer demand with water stored during the winter and can smooth out the effects of wet and dry years. Approximately 40% of New Zealand's freshwater supplies are now drawn from groundwater.

Aquifers vary in their depth and in the extent to which they are 'confined' or 'unconfined'. Unconfined aquifers are surrounded by porous rock or sediment, while confined ones are surrounded by impermeable materials. Water flows easily through unconfined aquifers, but is often trapped or reduced to very low flows in confined aquifers. Because they are more exposed to surface water and leachate, unconfined aquifers are more vulnerable to pollution, particularly if they are shallow and close to the land surface.

Places with unconfined aquifers include parts of the Aupouri peninsula in Northland, the Pauanui spit on the eastern Coromandel coast, the Hamilton basin, and much of the Wairarapa and Canterbury plains. Areas with confined aquifers include the Kaawa shellbeds between Manukau harbour and Pukekohe, the Rangitaiki Plain, and much of the Heretaunga Plain of Hawke's Bay (Thorpe, 1992).

8.4.6 Geothermal groundwater

Geothermal groundwater occurs where aquifers have been heated in volcanic zones, along faultlines, or in deep fissures (5 km or more underground). These heated groundwaters are usually referred to as geothermal fields or systems. New Zealand's geothermal fields are classified as low temperature if they are below 100°C and high temperature if they are above 100°C (Hunt and Bibby, 1992).

Low temperature geothermal systems are generally associated with faultlines or deep groundwater circulation (Cave *et al.*, 1993). They are found in the centre and north of the North Island from Taranaki and Hawke's Bay northwards. In the South Island they are associated with the Alpine and Hope faultlines, and so run in a band from Hanmer Springs to the Copland River in Westland and on down to western Fiordland. When low temperature geothermal systems breach the surface, they appear as hot springs. Often, however, they remain underground until discovered by drilling.

High temperature geothermal systems are associated with volcanic activity. All 24 high temperature fields are in the North Island, where their total surface area has been estimated at around 30 to 40 km^2 (Cave *et al.*, 1993; Bibby, 1995). Nine have temperatures ranging from 100°C to 180°C, and most of the rest are in the 200°C to 300°C range. The high temperature fields display themselves at the surface in a variety of ways, ranging from warm ground to spectacular geysers of steam and boiling water. In between these extremes are hot springs, sinter deposits, fumaroles, and hot mud pools.

Except for one high temperature field at Ngawha, in Northland, which is not associated with recent volcanism, all the others occur in the Taupo Volcanic Zone. This zone extends from Mount Ruapehu in the centre of the North Island to the Bay of Plenty. It incorporates Lakes Taupo, Rotorua and Tarawera, the upper reaches of the Waikato and Tarawera Rivers, and the significant townships of Taupo and Rotorua.

8.5 Floods and drought in New Zealand

Flooding can occur in any season and in all regions, although the steep, mountainous, catchments of the South Island's West Coast have the highest frequency. Even drought-stricken Auckland was afflicted by flood damage in the midst of its 1994 water supply crisis. It is likely that flooding increased after New Zealand's two main episodes of forest clearance following Maori and European settlement (Duncan, 1994).

Flood trends since 1920 are also difficult to establish, partly because the definition of a flood event often depends on whether serious property damage occurred. Even if rainfall and river flows had been constant since 1920, we might expect the amount of property

damage to increase simply because of population growth and urban and farm development in flood-prone areas. A recent review of river flow data found no overall trends in the frequency of high or low flows (Pearson, 1992), nor has it been possible to draw a firm conclusion about national trends in damaging floods (Ericksen, 1986). A total of 820 damaging flood events were recorded from 1920 to 1953 (averaging 25 events per year), but only 118 were recorded from 1955 to 1985 (averaging 4 per year). The two sets of records are not comparable, however, because the latter refers only to floods affecting towns.

Across the nation, the yearly cost of flood damage was estimated in 1986 at $90 million (around $125 million in 1997 terms). These costs were in addition to the $30 million spent annually on flood protection, and millions more spent on insurance (Ministry of Environment, 1992; Ministry of Civil Defence, 1994). Typical flood damage includes erosion, deposits of sediment over vegetation, reduced farm production, and damaged crops, roads, bridges and buildings. Flooding also causes ecological damage, eroding river banks and depositing sediment which can destroy coastal seaweed and shellfish communities as well as freshwater fish habitat and populations (Jowett, 1992; McDowall, 1993).

8.6 Drought

Periods of low rainfall in New Zealand are shorter but they can have significant impacts on urban and rural water supplies, hydroelectricity generation, and agricultural production. The areas most prone to periods of water shortage are in the east of the country and in some 'rain shadow' enclaves on both main islands. The impacts on farms are sometimes made worse by the style of farm management. Hill country pastoral properties in drought-prone areas, for example, can be severely affected because they tend to be marginally economic and so carry the maximum possible stock numbers.

Some dry spells are also made worse by the climatic phenomenon known as El Niño, which alters weather patterns over large areas of the Southern Hemisphere. El Niño brings more frequent south-westerly winds to New Zealand, intensifying the rain shadow

effect so that eastern and northern parts of New Zealand become drier than normal, and the country as a whole becomes a little cooler.

8.7 Pressures on New Zealand water environment

The total amount of water harnessed each year for electricity production, crop and livestock production, industrial production, and normal household activities has been estimated at almost 102,000 million cubic metres (Taylor *et al.*, 1997). With such a variety of water uses, there is a lot of impact on water flows and quality. Some of the heaviest impacts, however, have not come from water use, but from land use. The greatest single source of pressure has probably been the removal of forests for pastoral agriculture. This has increased erosion, sedimentation and flooding.

Another heavy pressure on the water environment is from urban populations and industry. The increased urban water demand has reduced the levels of some rivers and aquifers, and the demand for electricity has led to river flows being disrupted by dams. Dams alter the flows of rivers and streams, and create barriers to fish movement. Large dams have flooded valleys, raised lake levels and reduced the flows of some major rivers to residual trickles. New Zealand has thousands of dams, most of which are small water-supply dams on farms. However, more than 400 dams have storage capacities greater than 18,500 m^3. Some of these large dams were built to store water for irrigation, others for power generation, and others for domestic and industrial supply or floodwater control (Freestone, 1992).

The largest dams are for power generation. In fact, 98% of the water which is harnessed for human use in New Zealand is used to generate electricity. The controlled release of large torrents of water from dams provides the raw energy to spin the electricity-generating turbines at some 80 power stations around the country. The two main areas are the six stations on the Waikato River and those stations supplied by runoff from the eastern side of the Southern Alps.

The impact of a dam on river flows varies with the size of both the dam and the river. Most hydroelectric dams in New Zealand are 'run of the river' schemes, with enough storage for only a few hours or days of generation. This means they do not modify the seasonal flow patterns but may cause large day-night fluctuations in response to varying power demands. For example,

daily flows in the Clutha River vary from 200 to 600 cumecs as the Roxburgh power station responds to changing demand for power. Such disturbance of the flow regime can affect river channel stability and reduce fish habitat and spawning areas.

Large dams have dramatically altered the flows of some of New Zealand's rivers and lakes. They include Otago's Clutha, Waitaki and Waipori rivers, and the North Island's Waikato River. Other rivers have been affected by diversions of water, such as Southland's Waiau River whose flow was halved when water was diverted to the Manapouri power station, and the Whanganui River in the central North Island. In the South Island's Waitaki River catchment, the diversion of flows into a system of canals and power stations reduced the flows in the Tekapo, Pukaki and Ohau rivers to 'residual' levels.

8.8 Impacts case studies

Two hydrologically different catchments were considered to provide a contrast of catchment responses to climate change. The Lake Taupo catchment in the North Island is in a relatively wet climate with a winter maximum of precipitation while the Opihi River catchment in the South Island is in a relatively dry region with no marked seasonality.

8.8.1 Lake Taupo catchment

The Lake Taupo catchment is located near the geographical centre of the North Island about latitude 39°S, at an altitude ranging from 357 m to 2800 m above sea level and has a natural land catchment area of 2,660 km^2. The lake itself occupies a 600 km^2 depression of volcano-tectonic origin. To the west and north of the lake rhyolite domes and ignimbrite sheets with pumiceous ash-filled valleys characterise the landscape. In the east, from the Kaimanawa Ranges to the lake edge, the topography comprises pumiceous breccia on easy rolling interfluves separating deeply entrenched streams. The slopes of the greywacke Kaimanawa Ranges are typically steep and mountainous. Towards the south of the basin topography is dominated by the Tongariro- Ruapehu volcanic complex. The basin is bounded to the east by the Kaimanawa Range (1372 m) and to the west by

the Hauhungaroa Ranges (914 m). Apart from relatively small areas of recent volcanic soil and skeletal hill soils on the ranges yellow-brown pumice soils mantle the basin.

Precipitation ranges from 1000 mm to over 5000 mm on the higher ranges and mountains and is generally of short duration but of high intensity. The catchment has average sunshine of 5.87 hours per day, average relative humidity of 79.7% and a mean temperature between 10°C and 19°C. In Figure 8.3 the Lake Taupo natural inflows, the catchment mean monthly precipitation and evapotranspiration are presented for the 1961-1998 historical data. Precipitation is evenly distributed over the year with relatively higher values over winter months during which the potential evapotranspiration is minimal. As shown in the figure precipitation and evapotranspiration drive the scale and pattern of the lake inflows respectively.

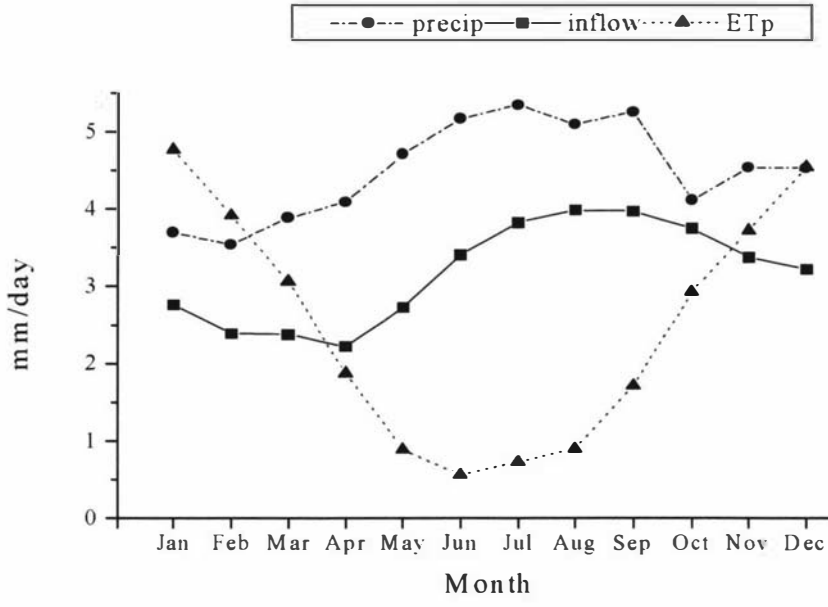

Figure 8.3 Mean monthly precipitation (precip), natural inflow (inflow) and potential evapotranspiration (ETp) for the Lake Taupo catchment, 1961-1998.

8.8.2 Opihi River catchment

The Opihi River is situated in the central eastern portion of the South Island and has a catchment area of 1,680 km^2 at Saleyards Bridge at latitude of about 44°S. The catchment occupies four hydrological regions of different topography, climate, geology and vegetation characteristics.

- The Canterbury Foothills region, typically of moderately steep ranges with alpine vegetation (bare rock and scree) above 1200 m.
- The Waitaki region of steep ranges up to 1800 m with snow-grass and tussock cover.
- The Canterbury Plains region characterised by flat coalescing shingle fans with a cover of short tussock grasses and intensive land use pattern.
- The Timaru Downlands region extending from sea level to an altitude of 460m and is characterised by flat plains and rolling hills that have been developed for pasture and crops.

The catchment annual precipitation is about 860mm and ranges from 1400mm along the Two Thumb Range to 550mm at the Opihi River mouth. Precipitation tends to show a distinct seasonal trend with less precipitation during winter months. The proportion of precipitation in the form of snow increases with altitude and is a major form of precipitation above 1200m. The catchment has average sunshine of 5.16 hours per day, average relative humidity of 83.5% and a mean temperature between 7°C and 16°C. In Figure 8.4 the mean monthly precipitation, potential evapotranspiration and runoff at Saleyards Bridge are depicted for 1965-1979. This is a catchment of relatively low precipitation with high rates of evapotranspiration during the summer.

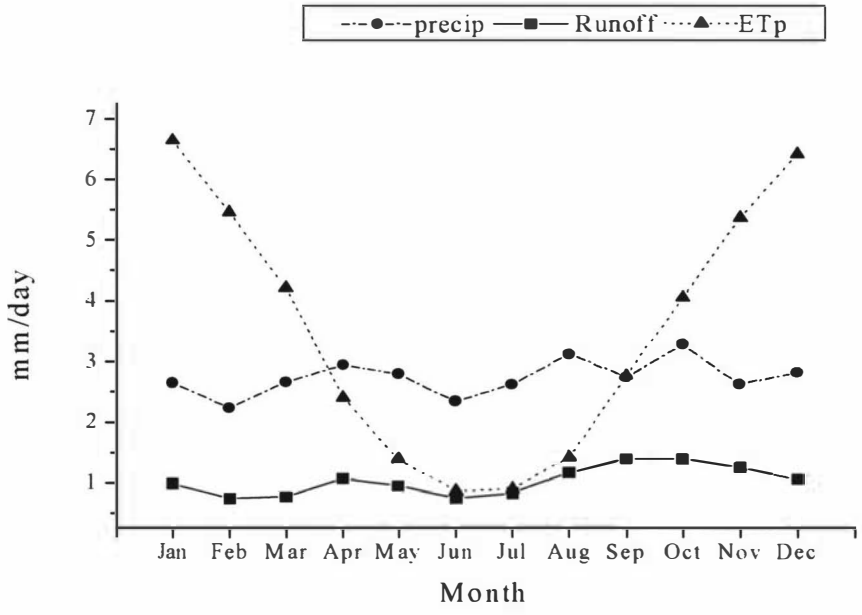

Figure 8.4 Mean monthly precipitation (precip), runoff and potential evapotranspiration (ETp) of the Opihi River catchment at Saleyards Bridge, 1965-1979.

8.9 Catchment response modelling

A split sample test is used in both catchments to evaluate the hydrological model. In this test the historical record is broken into two parts, one used for calibration and the other for validation. If the statistical values (correlation coefficient and monthly error) derived from the calibration and validation procedure are similar then the model is deemed acceptable. For a lumped model like WBM it is possible to achieve similar calibration results with significantly different parameters, although parameters can lose some of their physical meaning. For example, a large soil moisture holding capacity, combined with a large value sub-surface flow parameter will give similar results to smaller values of these parameters.

The correlation coefficient is given by:

$$\rho_{Q_o Q_p} = \frac{Cov(Q_o, Q_p)}{\sigma_{Q_o} \sigma_{Q_p}} \qquad (8.1)$$

where: $Cov(Q_o, Q_p)$ is the covariance of the observed and modelled discharge

σQ_o and σQ_p are the standard deviation of the observed and modelled series

The average monthly error ($E_{p,o}$) between the modelled and observed discharge is given by:

$$E_{p,o} = \frac{\sum abs(Q_p - Q_o)}{n} \tag{8.2}$$

where: $abs(Q_p-Q_o)$ = absolute value of the difference between modell (Q_p) and observed (Q_o) monthly discharge.

8.9.1 Calibration and validation of WBM for the Lake Taupo inflows

Hydroclimatological records for the years 1961-1990 were used for the WBM calibration and 1991-1996 records were used for model validation. The following are model parameters determined in the model calibration:

Surface inflow coefficient, $\varepsilon = 0.588$

Sub-surface 'exponential' coefficient, $\gamma = 2.0$

Sub-surface' proportionality' coefficient, $\alpha = 2.061$

Maximum storage, $S_{max} = 837$ mm

Initial relative storage, $z_i = 0.30$

Direct inflow coefficient, $\beta = 0.15$

Latitude = 38°S

Upper temperature, $T_l = 3.0$°C

Lower temperature, $T_s = -3.0$°C

Priestly Taylor coefficient, P.T. = 1.26

Ground index cover, GC = 0.50 (forest)

Base inflow (5 percentile low inflow)
= 1.6 mm/day

The model reproduced the observed inflow series reasonably well (appendix, Figure A1). The statistical association between the observed and modelled monthly inflows given in Table 8.1 demonstrates the model performance in the simulation of the lake inflows. In Figure 8.5, the reproduction of observed mean monthly lake inflows for the calibration and validation series is depicted. The observed and modelled lake inflows are highly

correlated for both calibration and validation series. Consistency in the average error is exhibited between calibration and validation modelled series.

Table 8.1 Calibration (1961-1989) and validation (1990-1996) statistical association between the observed and modelled monthly Lake Taupo inflows.

	Correlation	Average error (mm/day)
Calibration	0.86	0.39
Validation	0.83	0.41

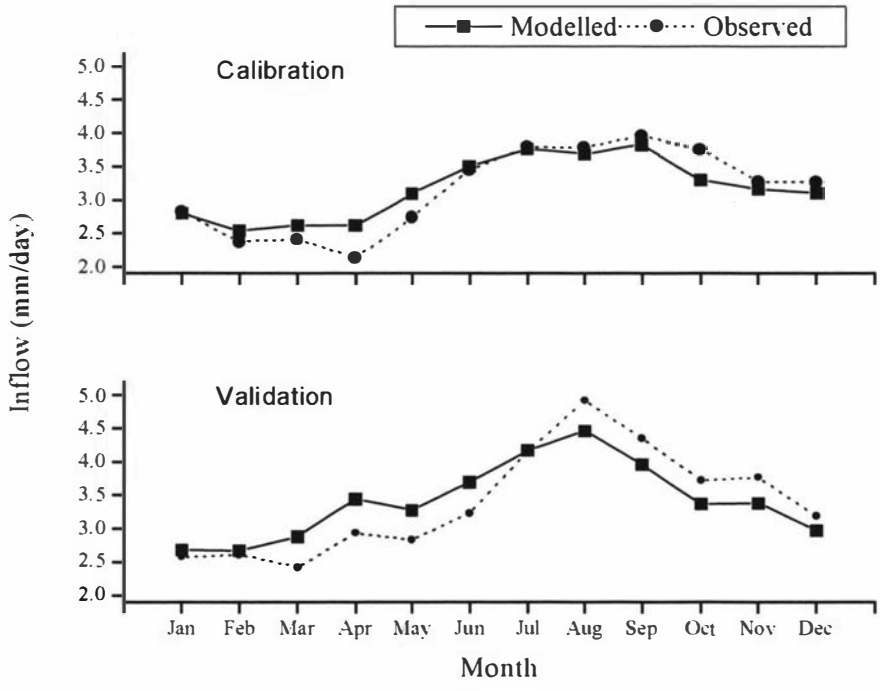

Figure 8.5 Observed versus modelled Lake Taupo monthly mean inflows for calibration and validation series.

8.9.2 Calibration and validation of WBM for the Opihi River runoff

The Opihi River catchment data at Saleyards Bridge for 1965-1974 were used in model calibration and the model was validated over the 1974-1979 period. The following are the model parameters determined in the model calibration:

Surface inflow coefficient, $\varepsilon = 0.8125$

Sub-surface exponential coefficient, $\gamma = 2.0$

Sub-surface proportionality coefficient, $\alpha = 3.605$

Maximum storage, $S_{max} = 1430$ mm

Initial storage, $z_i = 0.40$

Direct inflow coefficient, $\beta = 0.15$

Latitude = 44°S

Upper temperature, $T_l = 3.0$°C

Lower temperature, $T_s = -6.0$°C

Priestly Taylor coefficient, P.T. = 1.26

Ground index cover, G C = 0.40 (forest)

Base inflow (5 percentile low runoff)
= 0.20mm/day

The model reproduced the observed runoff series fairly well (appendix, Figure A2). The statistical association between the observed and modelled monthly runoff given in Table 8.2 demonstrates the model performance in simulating runoff of the Opihi River. In Figure 8.6, the reproduction of observed mean monthly runoff for the calibration and validation series is depicted. The observed and modelled runoff are fairly correlated for both calibration and validation series. Consistency in the average error is exhibited between calibration and validation modelled series.

Table 8.2 Calibration (1965-1973) and validation (1974-1979) of statistical association between the observed and modelled mean monthly runoff for the Opihi River at Saleyards Bridge.

	Correlation	Average error (mm/day)
Calibration	0.55	0.41
Validation	0.49	0.44

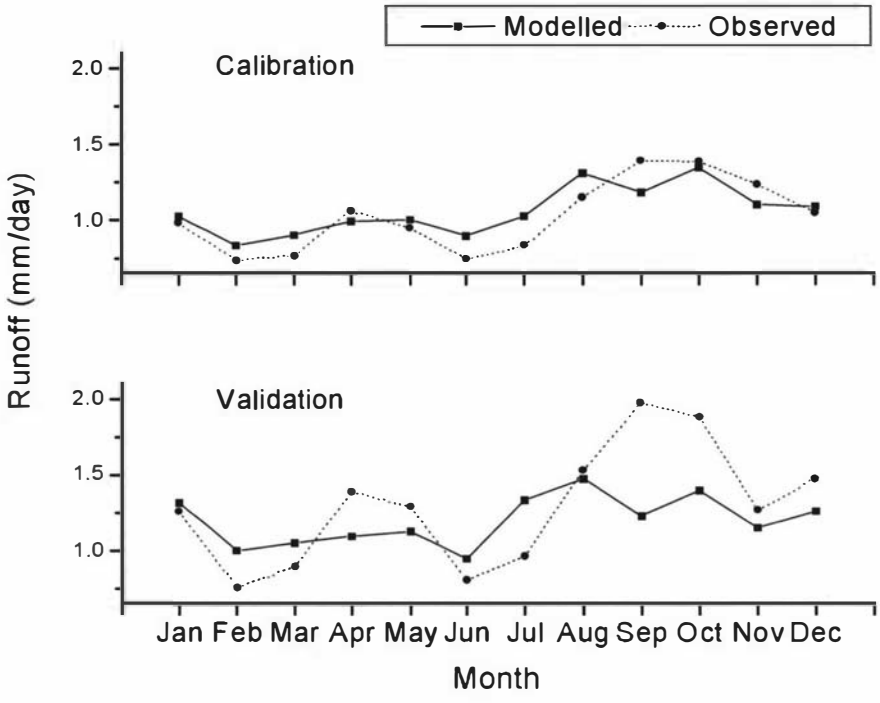

Figure 8.6 Modelled versus observed mean monthly runoff for calibration and validation series of the Opihi River catchment at Saleyards Bridge.

8.9.3 The WBM performance

The WBM proved to be consistent in simulating the flows in both study catchments, as demonstrated in the cross validation. The model performance, however, was relatively better for the Lake Taupo catchment than for the Opihi. In a catchment with high variability in precipitation like the Opihi, a lumped model tends to smooth out the associated variability in runoff (Figure 8.6). The model also proved to be sensitive to the definition of effective precipitation in the Opihi River catchment, where a variation of 1 or 2°C (T_l and T_s) was significant in the representation of snow melt, which was used to derive the effective precipitation.

A likely weakness of a lumped model approach such as that used in WBM is the inadequate representation of the seasonal variability in the soil moisture holding capacity. For instance, in a winter dominated precipitation regime like Taupo, in soils with less

moisture holding capacity than the summer dry soils, a single maximum soil-moisture holding capacity causes the model to over-estimate inflows in March to June at the expenses of under-estimated inflows in August to November (Figure 8.5).

8.10 Evaluation of catchment response to predicted climate change

In order to examine the catchment response to climate change, climate change scenarios at catchment level, in terms of mean monthly temperature, precipitation, humidity and sunshine hours together with vegetation for four tri-decades starting from 1981, were inputs of the WBM. The precipitation and temperature changes were based on the scenarios constructed in Chapter 4 from a realisation of the global warming environment by the HadCM2 global climate change transient experiments. Seasonal precipitation and temperature changes are summarised in Tables 8.3 through 8.6.

Seasonal precipitation change scenarios over the three periods indicate a general increase in mean precipitation over the Lake Taupo catchment except for summer in the second and third tri-decades where a decrease of 5-10% is projected. Increase of 0-25%, 0-35% and 5-65% with respect to the pseudo-present tri-decade is projected for 2010-2039, 2040-2069 and 2070-2099 respectively (Table 8.3). A gradual increase of 0.5-1.5°C in mean temperature is projected (Table 8.4). Increase of in mean precipitation over the Opihi River catchment is projected for winter and spring and a tendency of decrease (0-5%) in summer and autumn. Increase of 0-10%, 5-10% and 10-25% is projected for 2010-2039, 2040-2069 and 2070-2099 respectively (Table 8.5). Also a gradual warming over the Opihi catchment is projected to increase mean temperatures by 0.3-1.7°C with greatest warming in winter (table 8.6).

Table 8.3 Seasonal precipitation change scenarios for the Lake Taupo catchment with respect to pseudo-present tri-decade (1980-2009).

Period	Change in seasonal precipitation (%)			
	summer	autumn	winter	spring
2010-2039	+5	+0	+25	+15
2040-2069	-10	+0	+35	+10
2070-2099	-5	+5	+65	+5

Table 8.4 Seasonal temperature change scenarios for the Lake Taupo catchment with respect to pseudo-present tri-decade (1980-2009).

Period	Temperature change (°C)			
	summer	autumn	winter	spring
2010-2039	+0.25	+0.40	+0.43	+0.20
2040-2069	+0.69	+0.73	+0.76	+0.67
2070-2099	+1.33	+1.20	+1.47	+1.17

Table 8.5 Seasonal precipitation change scenarios for the Opihi River catchment with respect to the pseudo-present tri-decade (1980-2009).

Period	Change in seasonal precipitation (%)			
	summer	autumn	winter	spring
2010-2039	-5	-5	+10	+5
2040-2069	-5	+5	+10	+5
2070-2099	-0	-10	+25	+10

Table 8.6 Seasonal temperature change scenarios for the Opihi River catchment with respect to the pseudo-present tri-decade (1980-2009).

Period	Temperature change ($\delta T^{o}C$)			
	summer	autumn	winter	spring
2010-2039	+0.31	+0.48	+0.49	+0.44
2040-2069	+0.72	+0.63	+0.72	+0.86
2070-2099	+1.17	+0.89	+1.68	+1.02

Relative humidity and sunshine hours at a location are assumed to be functions of temperature and precipitation and therefore, from the long-term records, empirical relationships (multiple regression) were used to estimate monthly mean values of these variables. Equations 8.1 and 8.2 give estimates of monthly mean relative humidity using monthly mean temperature and precipitation tri-decade projections for the Lake Taupo and Opihi River catchments. Similarly, monthly mean sunshine hours were estimated using Equations 8.3 and 8.4. Tables 8.7 through 8.10 show the estimated monthly mean relative humidity and sunshine hours for 1980-2009, 2010-2039, 2040-2069 and 2070-2099.

$$RH_{Taupo} = 114\text{-}3.11Precip - 1.44Temp \quad (8.1)$$

$$RH_{Opihi} = 100\text{-}6.78Precip - 0.903Temp \quad (8.2)$$

$$Sn_{Taupo} = -3.78 + 0.635Precip + 0.478Temp \quad (8.3)$$

$$Sn_{Opihi} = 2.48 + 0.471Precip + 0.166Temp \quad (8.4)$$

where: RH = monthly mean relative humidity (%)

Precip = monthly mean precipitation (mm)

Temp = monthly mean temperature (^{o}C)

Sn = monthly mean sunshine hours.

Relative humidity tends to decrease slightly over the three tri-decades relative to the pseudo-present for both catchments except for Lake Taupo during autumn. The general decrease in relative humidity for Lake Taupo catchment is about 2% with an increase of 1% during autumn (Table 8.7). Over the Opihi catchment the decrease in relative humidity is up to 4% (Table 8.9). In contrast to relative humidity, sunshine hours show a tendency to increase over the three tri-decades, except during autumn in the Lake Taupo catchment (Tables 8.8 and 8.10). These changes, however, are too small to have significant effect on the hydrology of either catchment.

Table 8.7 Estimated mean monthly relative humidity (%) for the pseudo-present tri-decade (1980-2009) and the following three tri-decades for the Lake Taupo catchment.

Tri-decade	Summer			Autumn			Winter			Spring		
	Dec	Jan	Feb	Mar	Apr	May	Jun	Jul	Aug	Sep	Oct	Nov
1980-2009	75.4	75.9	76.5	77.2	80.2	82.0	83.5	84.0	83.7	81.1	82.1	78.2
2010-2039	74.9	75.2	75.8	77.3	80.3	82.1	82.9	83.4	83.1	80.9	81.8	78.0
2040-2069	74.1	74.4	75.0	77.5	80.5	82.4	82.6	83.2	82.9	81.0	81.8	78.0
2070-2099	75.0	75.1	75.7	78.1	81.1	83.0	82.2	82.8	82.5	80.6	81.4	77.6

Table 8.8 Estimated mean monthly sunshine hours/day for the pseudo-present tri-decade (1980-2009) and the following three tri-decades for the Lake Taupo catchment.

Tri-decade	Summer			Autumn			Winter			Spring		
	Dec	Jan	Feb	Mar	Apr	May	Jun	Jul	Aug	Sep	Oct	Nov
1980-2009	7.39	7.54	7.41	7.03	5.96	5.14	4.46	4.20	4.41	5.20	5.33	6.45
2010-2039	7.66	7.84	7.72	7.03	5.96	5.13	4.66	4.40	4.61	5.29	5.43	6.54
2040-2069	7.96	8.16	8.04	7.01	5.93	5.09	4.78	4.51	4.73	5.32	5.47	6.58
2070-2099	7.78	8.02	7.90	6.91	5.83	4.96	4.97	4.70	4.93	5.48	5.64	6.74

Table 8.9 Estimated mean monthly relative humidity (%) for the pseudo-present tri-decade up to the tri-decade 2070-2099 for the Opihi River catchment.

Tri-decade	Summer			Autumn			Winter			Spring		
	Dec	Jan	Feb	Mar	Apr	May	Jun	Jul	Aug	Sep	Oct	Nov
1980-2009	70.2	69.8	72.4	70.7	71.6	75.9	81.5	80.2	75.5	76.0	70.6	73.1
2010-2039	68.1	67.9	70.6	70.0	70.8	75.2	80.3	78.9	74.1	75.6	70.2	72.6
2040-2069	67.1	66.9	69.7	69.7	70.5	74.9	79.7	78.3	73.4	74.3	68.7	71.3
2070-2099	66.1	66.0	69.0	69.5	70.3	74.7	78.2	76.7	71.5	73.0	67.2	70.1

Table 8.10 Estimated mean monthly sunshine hours per day for the pseudo-present tri-decade up to the tri-decade 2070-2099 for the Opihi River catchment.

Tri-decade	Summer			Autumn			Winter			Spring		
	Dec	Jan	Feb	Mar	Apr	May	Jun	Jul	Aug	Sep	Oct	Nov
1980-2009	5.80	5.99	5.84	5.82	5.44	4.76	4.09	4.11	4.58	4.79	5.37	5.42
2010-2039	6.00	6.19	6.02	5.89	5.52	4.84	4.22	4.25	4.73	4.86	5.44	5.50
2040-2069	6.15	6.33	6.16	5.93	5.55	4.87	4.28	4.31	4.79	5.00	5.60	5.63
2070-2099	6.21	6.39	6.21	5.94	5.57	4.88	4.42	4.46	4.96	5.13	5.73	5.75

8.11 Future flow regime

As depicted in Figure 8.7, the Lake Taupo inflows in winter are projected to increase most markedly suggesting more favourable conditions for the hydro-electricity generation by the Taupo-Waikato hydro scheme to meet its high winter demand. Lake Taupo inflows are projected to increase in winter by 21, 26 and 57% in the 2010-2039, 2040-2069 and 2070-2099 tri-decades respectively. Inflow increase of about 15% during summer in 2010-2039 and a slight decrease in the 2040-2069 and 2070-2099 tri-decades can be associated with the projected variability ANN-derived precipitation from the HadCM2 model outputs over the catchment. Inflow increases of 10-15% are also expected during spring. These simulations of 3000 years over each tri-decade suggest an increase of about 10% in the lake inflow coefficient of variation (the standard deviation divided by the mean).

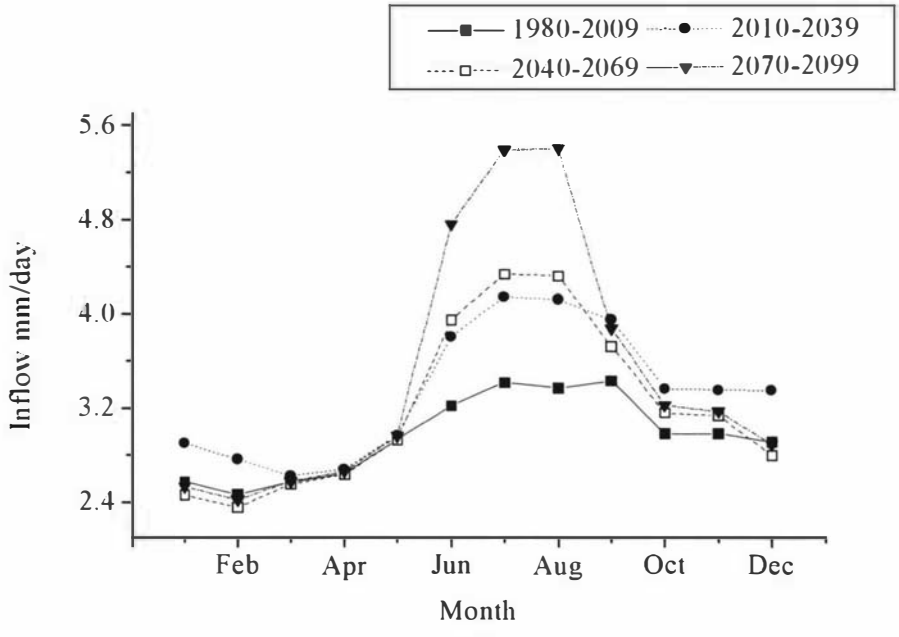

Figure 8.7 Simulated mean monthly Lake Taupo inflows for the pseudo-present tri-decade (1980-2009) and the following three tri-decades.

For the Opihi River the simulated mean monthly runoff at Saleyards Bridge depicted in Figure 8.8 shows that a gradual overall increase of 3, 5 and 10% is expected over the three tri-decades for the months of June to November. Except for the tri-decade 2040-2069, a general decrease of about 6% in runoff is predicted over the tri-decades reflecting the multidecadal variability in precipitation projected for the catchment.

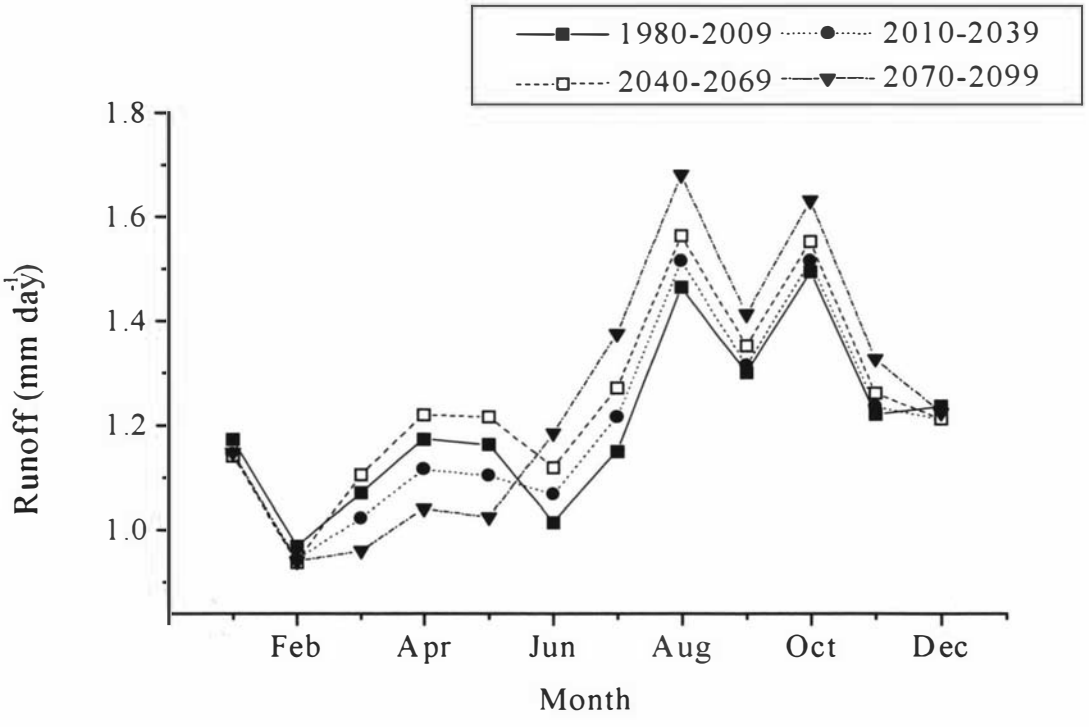

Figure 8.8 Simulated mean monthly runoff at Saleyards Bridge (Opihi River) for the pseudo-present tri-decade (1980-2009) and the following three tri-decades.

8.12 Performance of water resource system: Case studies

The expected changes in catchment hydrological response as a result of climate change may have pronounced impacts on the ability of some of the existing and proposed water resource systems to operate satisfactorily. For a water supply system of a given capacity, the operating policy determines the reliability, resiliency and vulnerability of water availability. In operational decision-making sense, it is of interest to see how a water

resource will perform for representative future hydrological inputs associated with climate change. This requires hydrological time series based on climate change scenarios.

Hydrological data inputs were generated for 3000 years to provide data sets which are big enough for the proposed risk analysis. These generated time series may differ from the observed time series but will retain many of its properties, e.g. events have the same probability of occurrence as in the simulated/observed sequence. It has been found through extensive experience that the lognormal probability function fits a large number of distributions in hydrology, as they are mainly asymmetrical (Yevjevich, 1972) and, therefore, the simulations were based on the lognormal distribution. The potential of three risk-descriptors, namely reliability, resiliency and vulnerability (Chapter 7, Section 7.4) to translate the projected hydrological catchment responses was examined.

8.12.1 The Lake Taupo water resource

The Waikato hydro scheme operation is a function of the Lake Taupo water outflow which in turn depends on the lake water storage. The Lake Taupo natural inflows are supplemented with water gathered in a complex system of river and stream diversions (the Eastern and Western Diversions), tunnels and canals to increase the lake storage. The scheme has its control gates at Lake Taupo for eight hydro stations along the Waikato River which generate around 4400 GWh of electricity a year. This represents about 17% of the electricity supplied to the whole country.

The Lake Taupo operating maximum control level for January to March is 357.10 m and is 357.25 m for April to December. The operating minimum control level is 355.85m (lake levels are measured in terms of their height above sea level). Water between the minimum and maximum operating levels is the water available for electricity generation purposes, under normal conditions. Exactly how and why water levels change at any particular time is the result of a complex interplay of three major variables:

- the supply of water from rainfall and melting snow
- the demand for electricity

- the operating conditions set by the consents

The hydro scheme operates each station efficiently by using as much of the available water as possible within the allowable limits to generate electricity. The river and lake levels are kept within the minimum and maximum permitted levels while meeting the immediate demand for electricity and planning for likely inflows. The hydro scheme shares this water resource with many other users. There are a number of resource consents that manage the effects of the operations on the natural and physical environment, and set boundaries between the hydro scheme with many other users including professional and recreational fishers, tourism operators such as boat companies and fishing guides, water skiers, yachts, power boat users, rowers, canoeists, farmers and landowners. The generation of electricity at a hydro power station results in changes in river water levels and flows upstream and downstream of a station.

8.12.1.1 Lake Taupo storage (levels)

The lake water level at a given time is a function of inflows and outflows (mass balance). In order to determine the lake levels from the natural flows, the monthly supplementary inflows (water diversions) were expressed in terms of percentage of natural inflows based on the 1980-1998 records. A neural networks approach was then used to capture a relationship between the lake natural inflows and outflows (releases) as predictors, and the lake levels as predictands. Data records spanning the period 1951 to 1998 were used for the neural networks model training and validation. A correlation of 0.85 was attained in the model validation run.

Natural inflows for the 1980-2009, 2010-2039, 2040-2069 and 2070-2099 tri-decades were simulated for 3000 years from the flow characteristics (mean and variance) determined in the catchment response evaluation, based on the climate change scenarios for each tri-decade. The inflow duration curves over the four tri-decades are depicted in Figure 8.9.

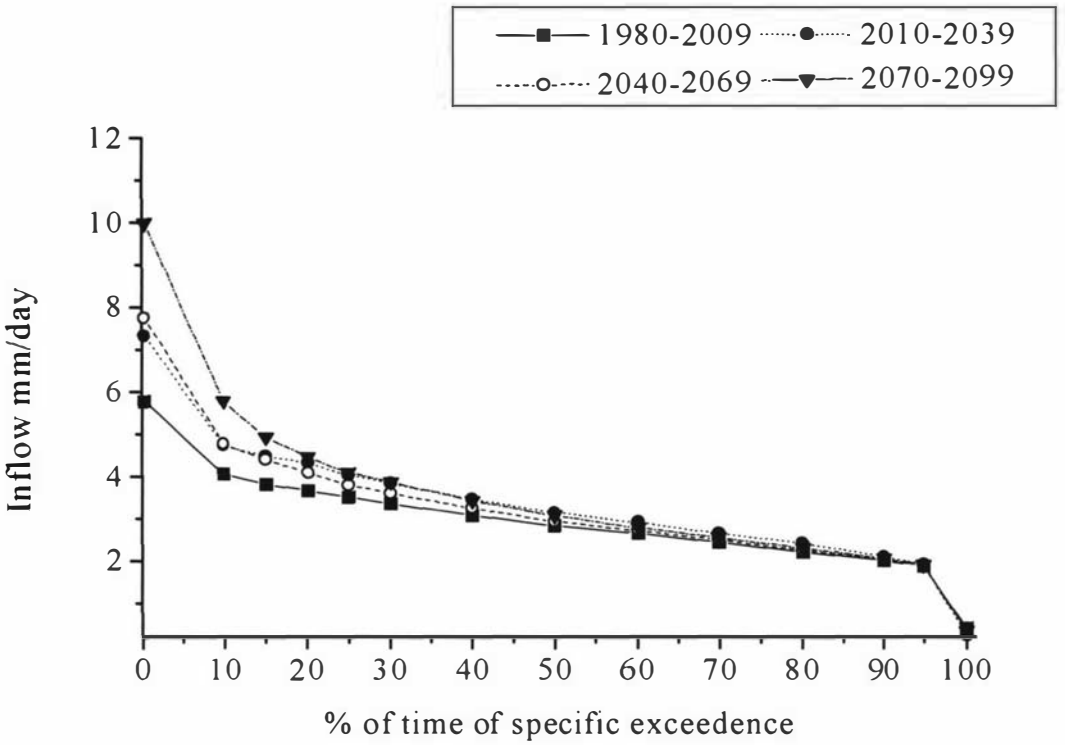

Figure 8.9 Lake Taupo natural inflow duration curve for the pseudo-present tri-decade (1980-2009) and the following three tri-decades.

The pattern of the projected specific exceedence of natural inflows presented in Table 8.11 suggest that, in terms of high magnitude flows, there will be a continually larger increase. A general increase in natural lake inflows is expected, consistent with the predicted eastward progression of increases in precipitation over the catchment in the three tri-decades under study.

Table 8.11 Lake Taupo projected specific exceedence of natural inflows in a given percentage of time.

Tri-decade	Specific exceedence (mm/day)								
	1%	5%	10%	25%	50%	75%	90%	95%	99%
1980-2009	5.36	4.46	4.04	3.50	2.82	2.35	2.00	1.87	1.75
2010-2039	6.62	5.14	4.72	4.03	3.14	2.51	2.09	1.91	1.77
2040-2069	6.79	5.38	4.76	3.79	2.93	2.37	2.03	1.89	1.74
2070-2099	8.60	6.56	5.78	4.08	3.06	2.40	2.06	1.90	1.75

8.12.1.2 Performance of Lake Taupo as a reservoir

Using the present policy of water releases (outflows) at the control gates in terms of mean monthly outflows, the water releases from Lake Taupo were randomly generated for each month for 3000 years using the normal distribution with the mean and standard deviation of the 1980-1998 records. The generated data set formed the monthly 'target' water demands under the present operation policy and were used with the simulated lake natural inflows to determine the corresponding lake levels (using the artificial neural networks) to examine the reservoir performance in meeting the permitted lake level limits in terms of risk descriptors, namely:

- the reliability (α) with which the outflow policy is met
- the resiliency (γ) of the system equal to the reciprocal of the average length of sequences of failure months, and
- vulnerability (ν) of the system equal to the expected maximum severity of a sojourn into a set of unsatisfactory states.

Failure (unsatisfactory) events are defined as occurrences of monthly mean lake levels, which are either above or below permitted levels. The counts of satisfactory and unsatisfactory events were made and from the definitions (Equations 7.23, 7.29 and 7.30)

the three risk descriptors were determined (Table 8.12).

The results in Table 8.12 show no significant changes in the tested performance criteria. However, there are signals of change, for example a tendency of gradual increase in reliability over the 2010-2039 and 2040-2069 tri-decades, and a decrease in 2070-2099. Resiliency was considered in three aspects. Resiliency to failures associated with flooding and drought considered together (general) or separately for excess or deficit. A tendency of decrease in resiliency is demonstrated for the general and excess failures, while resiliency to water deficit failures remains unchanged except in 2070-2099 when a slight decrease is shown.

Vulnerability values suggest a change towards increased severity of flooding. This is consistent with predicted increases in catchment precipitation while the water droughts tend to lessen in severity. The sequences of failure events due to excess water levels remain at a maximum of two months and deficit failure events at one month.

Table 8.12 Reliability, resiliency and vulnerability (severity s and sequence {x}) of Lake Taupo levels as a reservoir system for the Waikato hydro scheme with respect to the current operation policy of water releases.

Tri-decade	Risk descriptor							
	Reliability	Resiliency			Vulnerability			
		general	excess	deficit	excess		deficit	
					s (m)	{x} (month)	s (m)	{x} (month)
1980-2009	0.973	0.972	0.943	1.000	0.40	2	0.44	1
2010-2039	0.974	0.959	0.941	1.000	0.53	2	0.52	1
2040-2069	0.975	0.953	0.931	1.000	0.50	2	0.39	1
2070-2099	0.967	0.961	0.956	0.988	0.62	2	0.41	1

8.12.2 The Opihi River water resource

The water of the Opihi River is used for many diverse purposes including irrigation, stock and domestic supply, effluent disposal, industrial use and recreation. Since the construction of the Level Plains Irrigation Scheme (LPIS) by the Ministry of Works in the late 1930s, irrigation and recreational users have continually contested the available surface water resource of the Opihi River below the Tengawai confluence (de Joux, 1981). The Regional Council issues water rights and restricts water use in times of shortage under the Water and Soil Conservation Act (1967).

Irrigation of pasture, crops and berry fruit is widespread throughout the coastal plains from Geraldine to Timaru and also on suitable river valley flats in the Tengawai, Opihi and Opuha Rivers. Irrigation accounts for 70% of all registered water users in South Canterbury. The LPIS abstracts water at the Butlers Road intake during the irrigation season (September through April).

8.12.2.1 The Opihi River system

The Opihi River system consists of the Tengawai, Opihi, Opuha and Temuka Rivers. The Tengawai River drains the southern catchment and has its headwaters in the Rollesby Range. The Opihi River drains the central catchment and has its headwaters in the Rollesby and Two Thumbs Ranges. The Opuha River joins the Opihi River at Raincliff and extends back to the Two Thumbs Range. The Temuka River consists of the combined flows of the Kakahu, Hae Hae Te Maona and Wahi Rivers and drains the northern part of the Opihi catchment, joining the Opihi some 3.2 km from its mouth.

Figure 8.10 is a flow duration curve for the Opihi River at Saleyards Bridge during the irrigation season, based on simulations of catchment response in four tri-decades starting in 1980.

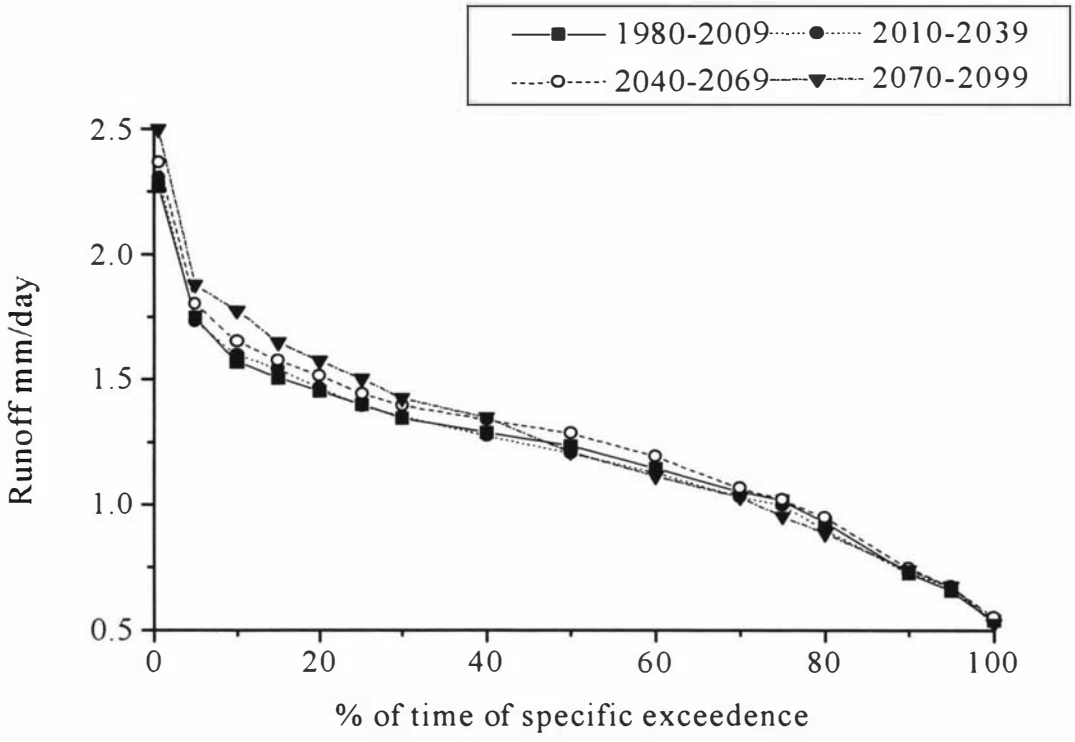

Figure 8.10 The Opihi River runoff duration curves at Saleyards Bridge based on monthly data for the four tri-decades starting in 1980.

The projected specific exceedence values of the Opihi River runoff at Saleyards Bridge presented in Table 8.13 also suggest that in terms of high magnitude flows, there will be a continually larger increase. Specific exceedence of low flows exhibits no trend over the three tri-decades under study.

Table 8.13 Specific exceedence runoff in a given percentage of time for the Opihi River at Saleyards Bridge.

Tri-decade	Specific exceedence (mm/day)								
	1%	5%	10%	25%	50%	75%	90%	95%	99%
1980-2009	2.25	1.75	1.57	1.40	1.24	1.02	0.69	0.66	0.58
2010-2039	2.29	1.73	1.60	1.39	1.21	1.00	0.70	0.67	0.56
2040-2069	2.36	1.80	1.65	1.44	1.28	1.02	0.73	0.67	0.58
2070-2099	2.49	1.88	1.77	1.50	1.21	0.95	0.71	0.67	0.57

8.12.2.2 The Opihi River system performance

There are different peak water demands from the Opihi River during the various months of the irrigation season. The following potential water demands for irrigation, water supplies and recreational flow estimated for the year 2000 (de Joux, 1981) were used in the performance assessment of the Opihi River system:

- September and April: 10.208$m^3 s^{-1}$ (0.525 mm/day)
- October and March: 11.048$m^3 s^{-1}$ (0.568 mm/day)
- November and February: 12.738$m^3 s^{-1}$ (0.655 mm/day)
- December and January: 14.418$m^3 s^{-1}$ (0.742 mm/day)

The system performance in meeting the above potential water demands was assessed using 3000-years generated random monthly data sets of the Opihi River runoff for four tri-decades (1980-2009, 2010-2039, 2040-2069 and 2070-2099). For the irrigation seasons, counts of satisfactory and unsatisfactory events in each tri-decade were used to calculate the system performance in terms of reliability, resiliency and vulnerability, presented in Table 8.14. A tendency of dropping reliability is indicated and resiliency values suggest no marked increases in recovery time. System's vulnerability increases are projected and the results also show a change in pattern of sequences of failure events

increasing from 2 months in the pseudo-present tri-decade to 3 and 4 months in the following tri-decades.

Table 8.14 Reliability, resiliency and vulnerability (severity s and sequence of occurrence {x}) of the Opihi River water available for LPIS irrigation purposes while meeting the other users' demands.

Tri-decade	Risk descriptors			
	Reliability	Resiliency	Vulnerability	
			s (mm/day)	{x}
1980-2009	0.953	0.945	0.83	2
2010-2039	0.948	0.908	0.98	3
2040-2069	0.951	0.922	1.06	4
2070-2099	0.948	0.911	0.96	4

8.13 Conclusions

The WBM is one of the simple models designed for assessing catchment response to climate change. The two case studies show that the model performs fairly well in simulating catchment response given its simplicity. The model revealed the sensitivity of catchment response to precipitation and temperature changes. There are systematic mismatches between the observed and the WBM-modelled flows as demonstrated by the calibration and validation series that can be attributed to the seasonal variation in the maximum soil moisture-holding capacity. In this application, these discrepancies may be unimportant because it is the difference between modelled catchment responses for different time intervals that are important for the impact assessment, other than their absolute values.

Simulations of Lake Taupo inflows under HadCM2-derived precipitation and temperature scenarios demonstrated a general increase of inflows consistent with the predicted eastward progression of increases in precipitation over the catchment over the

three tri-decades under study. The projected specific exceedence values of both catchments suggest that in terms of high magnitude flows, there will be a continually larger increase, while specific exceedence of low flows exhibits no trend.

Operational risk descriptors, that were tested to account for water availability in quantification of water resource systems' performance, in additional to the mean and variance of operating variables, showed low sensitivity to changes. Since the changes in catchment water yield in response to climate change scenarios are acknowledged, the slow sensitivity demonstrated by the risk descriptors can be attributed to the robustness of the systems considered. These results give an indication of the direction of change in both case studies and may be used to capture particular aspects of a water resource system performance associated with periods of extreme events such as drought, peak demands, or extreme climate conditions.

Although the reliability for Lake Taupo reservoir system being in a satisfactory state tends to increase over the tri-decades, severity of flooding (above permitted lake levels) and slower recovery rates were projected. On the contrary, the Opihi River system exhibits a tendency of decrease in reliability. Vulnerability increases are expected and also changes in pattern of sequences of failure events increase from 2 months in the pseudo-present tri-decade to 3 and 4 months in the subsequent tri-decades, a factor which could lead to increased likelihood of on-farm losses.

These two case studies illustrate the potential of operational descriptors in the translation of the impacts of climate change on resources by quantifying system performance under changed climate. Water managers and decision-makers could use this information to supplement other standard operational evaluation criteria including various social and environmental impacts.

Chapter Nine

General discussion and conclusions

Climate change impact assessment studies require consistent representations of future changes in climate at the spatial and temporal resolution at which impacts occur. The most promising method for predicting climate change is the use of Global Climate Models (GCMs). However, as acknowledged by the Intergovernmental Panel for Climate Change (IPCC), confidence is higher in hemispheric-to-continental scale projections of climate change than in regional projections from GCMs (IPCC, 1996b). For an immediate solution to the dilemma of providing predictions in an uncertain world is the use of scenarios. The outputs of the most 'complete' models of the climate system cannot be used directly in construction of climate change scenarios for impact assessment due mainly to resolution limitations associated with our limited and poor understanding of the climate system as well as with computational restraints. The GCMs operate at very coarse spatial scales (typically some 300 km x 300 km).

It is the mismatch in spatial (and sometimes temporal) scales between GCMs and impact studies that presents the biggest challenge. Simple interpolation of coarse GCM grid data to a finer grid is simple and easy to use but lacks reliability for its fundamental assumption of trust in GCM outputs at individual grid points. The current high resolution GCM outputs on 2.5°latitude x 3.75°longitude grids present 15 grid points over the New Zealand region, with only three on land grid-points. This seriously limits the use of GCM information. For example, for climate change impact assessment of water resources, the minimum desired spatial resolution would be of the order of 10 km and monthly for a specific year temporal resolution.

Important climate elements such as precipitation and temperature have localised characteristics that cannot be resolved with the current resolution of GCMs. It is even more difficult for regions like New Zealand with an area of only 267,000 km^2

surrounded by an extensive water body and yet with large contrasts in topographic features across the country. The latitudinal range produces a range in average temperatures from 16°C in the north to 10°C in the south while the topography produces a strong west-east gradient in precipitation, especially over the South Island.

Among key approaches for downscaling GCM outputs, semi-empirical techniques using transfer functions between scales may offer a more immediate solution and significantly lower computing requirements, and in particular, methods which can relate GCM output to single-site climate variables. Before these methods may be applied to the future climate, they must first be developed and validated for the present climate. This study has adopted a simple approach to relate point precipitation and temperature characteristics to free atmospheric regional circulation variables, such as those output from GCMs. Artificial neural networks (ANN) and multivariate statistics techniques (MST) were independently adapted to capture the cross-scale relationships between observed free atmosphere circulation indices and local-scale characteristics in precipitation and temperature. Regional circulation indices over New Zealand were defined by anomalies of mean sea level pressure, zonal and meridional pressure gradients, atmospheric geopotential thickness between 850-700hPa pressure surfaces and wind speeds at 10m above the ground.

Canonical correlation analysis was carried out between the sets of regional-scale free atmosphere circulation indices (predictors) and precipitation and temperature (predictands) at representative sites. Since the choice of the free atmosphere circulation indices is arbitrary the interest was to ascertain the existence of cross-scale link between the two sets, which is the basis of the semi-dynamic downscaling approach.

Positive and negative correlations among the predictor variables and between the predictors and predictands were demonstrated. The results are consistent with the atmospheric dynamics point of view. For example, that the pressure gradients in the horizontal provide the initial stimulus for air motion and in this case positive zonal

pressure gradient, which implies an increase in northerly flow, is positively correlated with warmer temperatures. The atmospheric thickness as shown by the strong positive correlation between the 850-700hPa thickness and temperature anomalies is an important indicator of the heat content of the troposphere. The results also suggest that the degree of association of precipitation and temperature with the circulation indices is location dependent.

The likelihood ratio test indicated that the first and second canonical correlations of 0.92 and 0.82 for both January (summer) and July (winter) were statistically significant at an alpha level of 0.05. However, large canonical correlation may not necessarily imply a strong correlation between the raw variables of the two sets because the canonical analysis maximises the correlation between linear composites of the variables in the two sets, without the variance being accounted for (Sharma, 1996). Moreover, the correlations among predictor variables indicated the existence of multicollinearity in the raw circulation variables. Therefore, to ascertain the cross-scale relationships, a measure of how much of the variance in predictands is accounted for by the predictor variables was considered from the 'redundancy' measure in the canonical correlation analysis. A total 'redundancy' of 0.49 was determined for both January and July, suggesting that regional circulation indices accounted for 49% of the variance in the precipitation and temperature. This confirms the importance of using free atmosphere circulation indices in regional climate change studies.

In a comparative study of their potential in deriving local climate information from regional circulation variables, both ANN and MST models generally verified well with observed mean monthly surface temperature and precipitation over New Zealand derived from the USA National Centres for Environmental Prediction (NCEP) reanalysis data. This was illustrated by the mean and variance reproduction of the observed values by the models.

There are seasonal differences in the root mean square error values, showing relatively higher error values for summer precipitation and winter temperature

respectively. This shows seasonal difference in the ability of this approach to capture precipitation and temperature characteristics (means and variability). Both models performed better in reproducing winter precipitation and summer temperature, and vice versa. This can be attributed to the fact that winter precipitation events are associated more with large-scale circulation features (e.g. frontal systems) than summer precipitation which can easily be associated with local scale features (e.g. thermal lows). Conversely, summer temperature variability is more of a large-scale atmospheric circulation phenomenon compared with the variability of winter temperature.

The performance of the two models was further verified using Quantile-quantile (q-q) plots. The q-q plots of the simulated versus observed anomalies of precipitation and temperature illustrated the two distributions in each case to be similar. This test uses a property that if a modelled variable y and observed variable x are identically distributed then the plot of y-quantiles versus x-quantiles will be a straight-line configuration with slope equal to 1, pointing towards the origin. This linear invariance property makes the use of q-q plots valuable, as linearity is a geometric configuration which can be understood easily. Moreover, departures from linearity are visually easy to detect.

Subsequently the ANN (for its ease of use over the MST) was used to downscale changes in local precipitation and temperature over New Zealand (land based sites) from outputs of the recent transient climate change experiments (HadCM2) circulation variables. In this approach a reasonable strategy was to take the predicted large-scale changes in free atmosphere circulation variables (e.g. mean sea level pressure and geopotential heights of standard atmospheric surfaces), and whenever possible, to infer local/regional changes of sensible projections of the large-scale information to the local scale. In transient climate change experiments the current GCMs such as HadCM2 are able to simulate the large scale, free atmosphere state in a generally realistic manner but with 'random' noise.

Transfer functions between observed free atmosphere variables and observed surface climate variables may then be used with simulated free atmosphere variables from HadCM2 experiments. This technique has the advantage of using inputs from both observed site data and GCM simulations of climate change. However, due to the 'random noise' in the simulations, a different model may give a different pattern of change (Mullan *et al.*, 2000).

In HadMC2 experiments the model first investigated the response of the climate system to the historic forcing of greenhouse gases and sulphate aerosols that has occurred since the early industrial period. The greenhouse and sulphate aerosols forcings were gradually increased to represent the observed changes in forcings due to all the greenhouse gases and the aerosols from 1860 to 1990. Then from 1990 to 2100 HadCM2 experiments used a 1 per cent per year-compounded increase in concentrations of greenhouse gases and a scenario of sulphate aerosol concentrations derived from the sulphur emissions in the IS92a scenario.

HadCM2 validated well with respect to NCEP reanalysis for its 'present climate' simulation of free atmospheric variables (mean sea level-pressure fields). Q-q plots of monthly means and anomalies of the mean sea-level pressure values of HadCM2 versus NCEP-reanalysis data over New Zealand region depicted comparable distributions of both mean sea-level pressure monthly means and anomalies. Statistical tests of the monthly means for 1980-1989 mean sea-level pressure over the New Zealand region shows no significant difference at $\alpha \leq 0.01$ between the HadCM2 and NCEP-reanalysis data. These results suggest potential plausible scenarios of climate change based on HadCM2 outputs over the region.

Among the important features in the HadCM2 predictions to New Zealand future climate is the mean sea-level pressure tendency predicted for the region. Significant pressure build up in the north-eastern sector coupled with pressure falls centred to the south-west of the region are projected. HadCM2-derived mean sea level pressure gradients over the northern, central and southern sectors of New Zealand during the months of January, April, July and October exhibit gradient increases across the

region. Increases of 30 to 80% are predicted over the northern sector, with greatest increases in October (spring) and diminishing increases in July (winter) over the tri-decades. In the central sector, the increase in pressure gradients of 12 to 50% are demonstrated with greatest increases in winter and least increases in summer. Similarly, over the southern sector pressure gradient increases of between 2 and 45% are predicted with least increases in summer.

These changes suggest strengthening of the anticyclonic belt which will squeeze stronger westerly winds over southern and central New Zealand. The calculated cyclotrophic mean wind directions from the zonal and meridional pressure gradient components demonstrated this. The calculations showed more northwesterly winds than southwesterlies over the northern sector during summer. Westerlies are expected over the central and southern sectors with a tendency of becoming northwesterlies during the 2070-2099 tri-decade. In other seasons southwesterlies were likely except over the southern sector where a more westerly flow was projected.

The strengthening of the westerly flow over the region is contrary to previously projected changes based on palaeo-analogues and GCM equilibrium climate change experiments. The difference could be attributed to a major drawback of equilibrium experiments in which the resulting equilibrium-doubled CO_2 climate assumed that the components of the climate system were in a steady state. In reality, however, this is unlikely to happen since there are unquantifiable and unequal lags between the components of the climate system. Following recent developments in climate change experiments by GCMs, previous scenarios of climate change have inevitably been superseded. In particular, GCM transient experiments may offer significantly different scenarios of which the impact assessment community should keep itself aware.

Another feature in the HadCM2 predictions of regional interest is the trend in the atmospheric thickness, defined by the difference between 850 and 700 hPa pressure surfaces' geopotential heights. Average positive trends of 0.15 and 0.10 gpm per year were shown for summer and winter respectively. These trends can be attributed to the

global warming. Based on these HadCM2 projections of New Zealand regional circulation indices, mean monthly near-surface air temperature and precipitation change scenarios with respect to the pseudo-present tri-decade were constructed. A general warming of 0.3-0.4°C per tri-decade is expected over the country. A prominent pattern of temperature change is exhibited in the north-south direction with interruptions of relative greatest warming over the central North Island and southeastern South Island, associated with localised features. For example, over the central North Island and the southern South Island, a west-east warming contrast is projected. The analysis also indicates a southward increase in warming magnitudes (southward increases in contour gradients). In the tri-decade 2010-2039 greatest warming of about 0.5°C takes place over the northeastern areas during April (autumn) and October (spring). A warming of 0.7-0.8°C is expected in the tri-decade 2040-2069 in most areas and the greatest warming of 1.5-2.0°C could be reached in 2070-2099.

Precipitation changes scenarios demonstrate a pattern of a general decrease in precipitation over northern New Zealand and an increase over the central and southern areas, mainly to the west. A west-to-east progression of precipitation increases over the three tri-decades is projected in the central areas, particularly in winter.

In the tri-decade 2010-2039 a decrease of up to 10% in summer precipitation over the northern sector is projected. Decreases of up to 40% in 2040-2069 are demonstrated and expected to slow down in 2070-2099 tri-decade. Western areas of the North Island are expected to get wetter by 20-70% and these increases are predicted to progress eastward to the central North Island. Similarly marked precipitation increases over the southwest of the South Island are projected to progress to the eastern central areas. Areas east of the Southern Alps are likely to experience a decrease of up to 10% in precipitation.

Precipitation characteristics were modelled using a two-parameter gamma probability function (assumed to fit the precipitation data over tri-decades). Precipitation

distribution over a given tri-decade was characterised by the mean, variance and the degree of spread as indicators of expected precipitation amounts, variability and the likelihood of extreme events respectively. The direction of change of precipitation characteristics with respect to the precipitation of the pseudo-present period were detected in the trends of the gamma function 'scale' and 'shape' parameters. For example, if for a given location the 'scale' parameter of the pseudo-present precipitation distribution tends to increase with time, then increased precipitation amount, variability and number of extreme precipitation events would be expected, and vice versa. Similar projections occurred for the 'shape' parameter, but with less sensitivity to variability and number of extreme events.

A general increase in precipitation coefficients of variation is demonstrated over the country, particularly over the northeastern and southeastern areas. Marked summer precipitation variability increases are projected for the North Island. Reduced winter precipitation variability is projected over the South Island except for the southeastern parts where variability increases are predicted by this model (HadCM2) and downscaling (ANN) aproach.

Scenarios of monthly precipitation and mean temperature changes were applied in studies of impact assessment to illustrate the potential of the adopted downscaling approach in bridging the gap between the GCMs' spatial resolution of climate change information and that required for impact studies. The impacts of climate change are transmitted via their effects on the physical environment, and particularly on those factors which are at the base of our 'hierarchy of needs' - air, water and secure habitation. This calls for a special emphasis to be placed on the response of water resources to climate change. Because water is fundamental to so many aspects of present-day society and economy, any possible changes in its availability must be anticipated and planned for.

While some of the potential impacts of global warming may be positive for the New Zealand water resources environment (e.g. extended growing seasons and new crops), others are likely to be negative and pose additional pressures on water resources.

Two case studies of catchment response were carried out, to examine the range of hydrological impacts by applying the changes to catchments in relatively different climatological zones, on top of demonstrating the applicability of the climate change information derived in this study. They were the Lake Taupo catchment and the Opihi River, which is situated, in the central eastern part of the South Island.

A water balance model (WBM) was adapted for modelling catchment response to prescribed climate change (temperature and precipitation). The application of such models provide considerably more information on hydrological effects and the vulnerability of water resource systems to climate change than is currently available. The two case studies showed that the model performs fairly well in simulating catchment response given its simplicity and the limitations of a lumped model. Systematic mismatches between the observed and the WBM-modelled flows, demonstrated in the calibration and validation series, were attributed to the seasonal variation in the maximum soil-moisture holding capacity (the lumped model assumes one value). However, for this application, these discrepancies were considered unimportant, for it is the difference between modelled catchment responses for different time intervals which are important for the impact assessment, rather than their absolute values.

Simulations of Lake Taupo inflows under HadCM2-derived precipitation and temperature scenarios demonstrated a general increase of inflows consistent with the predicted eastward progression of increases in precipitation across the catchment over the three tri-decades under study. The projected specific exceedence inflows of Lake Taupo and the Opihi River runoff at Saleyards Bridge both suggest that in terms of high magnitude flows, there will be a continually larger increase while specific exceedence of low flows exhibits no trend over the three tri-decades. However, these results may conceal some of the problems which are inherent in relating climate change to water resources impacts. Therefore, changes in catchment hydrological responses were evaluated in terms of water resource systems' performances. Such assessments extend the analysis of climate impacts beyond hydrological values to fully explain societal implications of resource systems at risk. It is important to realise

that both components are needed for a comprehensive evaluation of the consequences of any policy decisions regarding societal preparation for climate change impacts. All previous water resources impact studies lack this component and thus water management agencies find it difficult to justify changing system design features or operating rules on the basis of the currently simulated climate change.

Operational risk descriptors that account for water availability were adapted to quantify water resource systems performance in terms of reliability, resiliency and vulnerability. Additional to the mean and variance of operating variables, these performance criteria may capture particular aspects of a water resource system performance particularly during periods of extreme events such as drought, peak demands, or extreme climate conditions.

Flow data for each tri-decade were modelled using the lognormal distribution to generate a 3,000-year data set, which was then used in risk analysis for reliability, resiliency and vulnerability of respective existing water resource systems (hydro power and irrigation schemes) in terms of water availability. These operational risk descriptors were used as an example of performance criteria. Additional to the mean and variance of operating variables, these performance criteria better capture particular aspects of a water resource system performance for extreme climate conditions so as to identify changes beyond natural variability.

Although the signals of global warming are weakly perceived by these risk descriptors, the results illustrate the use of operational descriptors in translation of the impacts of climate change on water resources by quantifying system performance under predicted climate change. Water managers and decision-makers could use this information to supplement other standard operational evaluation criteria including various social and environmental stresses. For the Waikato Hydro Scheme and the Level Plains Irrigation Scheme, the changes in operational risk-descriptors with respect to the pseudo-present are within limits in which adjustments can be made, taking into account that traditional design criteria incorporate considerable buffering

of capacity for extreme events. However, there are likely to be many other water resource systems that exhibit far less robustness to change.

The particular mathematical definitions adapted in this study for reliability, resiliency and vulnerability should be viewed as illustrative examples. Every planning situation is in some way unique and calls for creativity in the definition of appropriate performance descriptors such as resiliency, reliability, and vulnerability. It is unlikely that a single mathematical definition of these concepts will be appropriate or useful in all situations. However, recognition and description of the possibility of low-probability but undesirable consequences of alternative plans should be an important component of the planning process. Hence, engineers and planners need to develop appropriate quantitative risk criteria that describe the undesirable events that individuals may experience as a consequence of climate change in relation to operating policy decisions. However, meaningful impact assessment studies require realistic climate change scenarios that can provide information at a resolution at which impacts occur.

The semi-empirical approach adopted in the study has demonstrated the potential in providing an immediate solution. The method is capable of deriving fine scale predictions based on cross-scale relationships of coarse resolution data with observed local climate characteristics. This is important because the most 'complete' climate models (GCMs), which are used in climate change experiments, generally simulate synoptic and larger scale circulation features more accurately than sub-grid scale surface features. Non-monotonic increases in the characteristics of derived precipitation changes over New Zealand demonstrate the potential of this approach in downscaling outputs of transient climate change experiments, in which a number of circulation features, including Interdecadal Pacific Oscillations (IPO) events may not be ruled out. This is an advantage over the traditional scaling approach that suppresses climate dynamics (such as low frequency variations that obscure underlying climate change signal) exhibited in the outputs of the GCMs' transient experiments.

Such changes in atmospheric circulation, which is the main control behind regional changes in wind, precipitation, and other climate variables, trigger variations that cannot be reflected in scenarios based on the traditional scaling approaches. Additional studies with other GCM transient climate change experiments are recommended to provide further insight into the range of possible climate change scenarios over the region, as well as uncovering possible limitations of this approach.

References

Adams, B.J. and R.S. Gemmell, 1980. Water quality evaluation of regional wastewater management. Journal of Environmental Engineering Division, American Society of Civil Engineers, 106:437-450.

Anderson, J.A. and E. Rosenfeld, 1988. Neuralcomputing: Foundations of research. The MIT Press, Cambridge, MA.

Archer, D., H. Kheshgi, and E. Maier-Reimer, 1998. Dynamics of fossil fuel CO_2 neutralization by marine $CaCO_3$. Global Biogeochemical Cycles, 12:259-276.

Arnell, N.W., 1992. Factors controlling the effects of climate change on river flow regimes in a humid-temperate environment. Journal of Hydrology, 132:321-342.

Basher R.E., A. B. Pittock , B. Bates, T. Done , R.M. Gifford , S.M. Howden, R. Sutherst , R. Warrick, P. Whetton, D. Whitehead, J.E. Williams, and A. Woodward, 1998. Australasia. In: IPCC 1998 Regional Impacts Report

Battaglin, W.A., L.E. Hay, R.S. Parker, and G.H. Heavesley, 1993. Applications of GIS for modelling the sensitivity of water resources to alterations in climate in the Gunnison River basin, Colorado. Water Resource Bulletin, 25:1021-1028.

Becker, A. and P. Serban, 1990. Hydrological models for water-resources system design and operation. World Meteorological Organization, Operational Hydrology Report no. 34, WMO no. 740.

Beer, J., W. Mende, and R. Stellmacher, 2000. The role of the sun in climate forcing. Quaternary Science Reviews, 19:403-415.

Bertrand, C. and J.P. Ypersele, 1999. Potential role of solar variability as an agent for climate change. Climatic Change, 43:387-411.

Beven, K., 1985. Distributed models. In: M.G. Anderson and T.P. Burt (eds), Hydrological forecasting, J. Wiley and Sons, Chichester, England.

Beven, K., 1989. Changing ideas in hydrology–The case of physical based models. Journal of Hydrology, 105:157-172.

Bibby, H.M., T.G. Caldwell, and T.H. Webb, 1995. Geophysical evidence of structure of the Taupo volcanic zone and its hydrothermal circulation. Journal of Volcanology and Geothermal Research, 68:1-3.

Boyle, E. A., 1983. Chemical accumulation variations under the Peru Current during the last 130,000 years. Journal of Geophysical Research, 88:7667-7680.

Bradley, R.S., 2000. Past global changes and their significance for the future. Quaternary Science Reviews, 19:391-402.

Bradley, R.S., H.F. Diaz, J.K. Eisched, P.D. Jones, P.M. Kelly, and C.M. Goodness, 1987. Precipitation fluctuations over Northern Hemisphere land areas since the mid-19th century. Science, 237:171-175.

Broecker, W. S. and T.-H. Peng, 1982. Tracers in the Sea. Eldigio Press, Palisades, New York.

Broecker, W. S., 1991. The great ocean conveyor belt. Oceanography, 4:79-89

Budyko, M.L., 1980. The earth's climate: past and future. (English Translation, Academic press, New York, 1982.

Bultot, F., D. Gellens, M. Speafico, and B. Schadler, 1992. Repercussions of CO_2 Doubling on the Water Balance –A case study in Switzerland. Journal of Hydrology, 137:199-208.

Bultot, F. and G.L. Dupriez, 1976. Conceptual hydrological model for an averaged-sized catchment area: I. Concepts and relationships. Journal of Hydrology, 29:251-272.

Burnash, R.J.C., R.L. Ferral, and R.A. McGuire, 1973. A generalised streamflow simulation system, conceptual modelling for digital computers. US Department of Commerce, National Weather Service and State California, Department of water Resources, Sacramento, CA.

Carnale, K.P and S.C. Chapra, 1988. Numerical methods for engineers, second edition. McGraw Hill, New York.

Cave M.P., J.T. Lumb, and L. Clelland, 1993. Geothermal resources of New Zealand. Ministry of Commerce, Wellington.

Cess, R.D., G.L. Potter, J.P. Blanchete, G.J. Boer, A.D. Del Genio, M. Deque, V. Dymnikov, V. Galin, W.L. Gates, S.J. Ghan, J.T. Kiehl, A.A. Lacis, H. Le Treut, Z.-X. Li, B.J. McAvaney, V.P. Meleshko, J.F.B. Mitchell, J.-J. Morcrette, D.A.

Randall, L.Rikus, E. Roeckner, J.F. Royer, U. Schlese, D.A. Sheinin, A. Slingo, A.P. Sokolov, K.E. Taylor, W.M. Washington, R.T. Wetherald, I. Yagai, and M.-H. Zhang, 1990. Intercomparison and interpretation of climate feedback processes in 19 atmospheric general circulation models. Journal of Geophysical Research, 95:16601-16615.

Chiew, F.H.S., P.H. Whetton, T.A. MeMahon, and A.B. Pittock, 1995. Simulation of impacts of climate change on runoff and soil moisture in Australian catchments. Journal of Hydrology, 167:121-147.

Chow, V.T., D.R. Maidment, and L.W. Mays, 1988. Applied hydrology. McGraw Hill, New York.

Conway, D. and P.D. Jones, 1998. The use of weather types and air flow indices for GCM downscaling. Journal of Hydrology, 213:348-361

Conway, D., R.L. Wilby, and P.D. Jones, 1996. Precipitation and air flow indices over the British Isles. Special issue of Climate Research, 7:169-183.

Coulter, J.D., 1969. On rainfall variations in New Zealand. N. Z. Meteorological Service Technical Information Circular No. 132.

Cressman, G.P., 1959. An operational objective analysis system. Monthly Weather Review, 87:367-374.

Cromarty, P. and D.A. Scott (compilers), 1996. A directory of wetlands in New Zealand. Department of conservation, Wellington.

Cubasch, U., H. von Storch, J. Waszkewitz, and E. Zorith 1996. Estimates of climate change in Southern Europe derived from dynamical climate model output. Climate Research, 7:129-149.

Cullen, M.J.P., 1993. The Unified forecast/climate model. The Meteorological Magazine, 122:81-95.

de Joux, R.T., 1981. The water resources of the Opihi and Temuka Rivers. South Canterbury Catchment Board and Regional Water Board publication no. 28.

Diaz, H.F., R.S. Bradley, and J.K. Eisched, 1989. Precipitation fluctuations over global land areas since the late 1800's. Journal of Geophysical Research, 94:1195-1210.

Doake, C.S.M. and D.G. Vaughan, 1991. Rapid disintegration of the world ice shelf in response to atmospheric warming. Nature, 350:328-330.

Dooge, J.C.I., 1992. Hydrologic models and climate change. Journal of Geophysical Research. 97:2677-2686.

Duncan, M.J., 1992. Flow regimes of New Zealand rivers, p.13-26. In: M. P. Mosley (ed), Waters of New Zealand. New Zealand Hydrological Society, Wellington.

Duncan, M.J., 1994. Hydrological impacts of planting pines. Water & Atmosphere, 2:19-20.

Eagleson, P.S., 1978. Climate soil and vegetation: Parts 1-7. Water Resources Research, 14:705-776.

Eastering, D.R., 1999. Development of regional climate scenarios using a downscaling approach. Climatic change, 41:615-634.

Enting, I. G. and G. I. Pearman, 1987. Description of a one-dimensional carbon cycle model calibrated using techniques of constrained inversion, Tellus, 39B, 459-476.

Ericksen, N.J., 1986. Creating Flood Disasters? New Zealand's need for a new approach to urban flood hazard. Water and Soil Miscellaneous, Publication no. 77, Ministry of Works, Wellington.

Fan, S., M. Gloor, J. Mahlman, S. Pacala, J. Sarmiento, T. Takahashi, and P. Trans, 1998. A large terrestrial carbon sink in North America implied by atmospheric and oceanic carbon dioxide data and models, Science, 282:442-446.

Fitzharris, B., I. Owens, and T. Chinn, 1992. Snow and Glacier Hydrology, p.75-93. In: M. P. Mosley (ed), Waters of New Zealand. New Zealand Hydrological Society, Wellington.

Folland, C.K., T.R. Karl, N. Nicholls, B.S. Nyenzi, D.E. Parker, and K. Ya. Vinnikov, 1992. Climate Change, p.135-170. In: J.T. Houghton, B.A. Callandar, and S.K. Verney (eds), The IPCC scientific assessment. Cambridge University Press, Cambridge, UK.

Franchini, M. and M. Pacciani, 1991. Comparative analysis of several conceptual rainfall runoff models. Journal of Hydrology, 122:161-219.

Frederick, K.D., 1991. Processes for identifying regional influences of and responses to increasing atmospheric CO_2 and climate change. –The MINK project, report IV– water resources, DOE/RL/01830T-H10, Office of Energy Research, U. S. Department of Energy, Washington, DC.

Frederick, K.D. and D.C. Major, 1997. Climate change and water resources. Climatic Change 37:7-23.

Freestone, H.J., 1992. Hydrology and large water projects p.409-421. In: M. P. Mosley (ed), Waters of New Zealand. New Zealand Hydrological Society, Wellington.

Friedli, H., H. Lotscher, H. Oeschger, U. Siegenthaler, and B. Stauffer, 1986. Ice core record of $^{13}C/^{12}C$ ratio of atmospheric CO_2 in the past two centuries. Nature, 324:237-238.

Gates, W.L., Y.J. Han, and M.S. Schlesinger, 1995. The global climate simulated by a coupled atmosphere ocean general circulation model. Preliminary results, p. 131-151. In: J.C.J. Nihoul (ed), Coupled ocean-atmosphere models. Series 40, Elsevier Oceangr.

Giorgi, F., 1990. Simulation of Regional climate using a limited area model nested in a general circulation model. Journal of Climate, 3:941-963.

Giorgi, F., C.S. Brodeur, and G.T.A. Bates, 1994. Regional climate change scenarios over the United States produced within a nested regional climate model: Spatial and seasonal characteristics. Journal of Climate, 7:375-399.

Giorgi, F. and L.O. Mearns, 1991. Approaches to simulation of regional climate change. Reviews of Geophysics and Space Physics, 29:191-216.

Glahn, H.R., 1985. Yes precipitation forecast has improved. Bulletin of American Meteorological Society, 66:820-830.

Hansen, J., M. Sato, A. Lacis, R. Ruedy, I. Gegen, and E. Matthews, 1998. Climate forcings in the industrial era, Proceedings of the National Academy of Sciences, 95: 12,753-12,758.

Hansen, J. and S. Lebedeff, 1987. Global trends of measured surface air temperature. Journal of Geophysical Research, 92:3345-3372.

Harden, J. W., E. T. Sundquist, R. F. Stallard, and R. K. Mark, 1992. Dynamics of soil carbon during deglaciation of the Laurentide ice sheet. Science, 258:1921-1924.

Hashimoto, T., J.R. Stedinger, and D.P. Loucks, 1982. Reliability, resiliency and vulnerability criteria for water resource system performance evaluation. Water Resources Research, 18:14-20.

Hendy, C.H. and A.T. Wilson, 1968. Palaeoclimatic data from speleothems. Nature, 219:48-51.

Herrington, P., 1996. Climate change and demand. Water. Department of Environment, HMSO, London.

Hewitson, B.C., 1994. Regional climates in general circulation model: surface air temperature. Journal of. Climate, 7:283-303.

Hewitson, B.C., 1995. The development of climate downscaling: techniques and applications. In reprints of the 6th International Meeting on Statistical Climatology, Galway, I.R., p.33-36.

Hewitson, B.C. and R.G. Crane, 1994. Precipitation controls in southern Mexico, p121-143. In: B.C. Hewitson and R.G. Crane (eds.), Neural Nets: Applications in Geography. Dordrecht: Kluwar Academic Publishers.

Holling, C.S., 1978. Myths of ecological stability: Resilience and the problem of failure. In: C.F. Smart and W.T. Stanbury (eds.), Studies on Crisis Management, Butterworth, Montreal.

Houghton, J.T., 1994. Global warming: the complete briefing. Oxford, Lion Publishing.

Houghton, J.T., 1996. Danger signal. Our planet. UNEP:Nairobi, p.9-11.

Houghton, J.T., B.A. Callander, and S. K Varney (eds.), 1992. The Supplimentary Report to the IPCC Scientific Assessment. Cambridge University Press.

Houghton, J.T., F.L.G. Meira, B.A. Callander, N. Harris, A. Kattenberg and K. Maskel (eds.), 1996. Climate Change 1995. Contribution of Working Group I to the Second Assessment Report of the International panel of Climate Change. Cambridge University Press, Cambridge.

Houghton, J.T, F.L.G Meira, D.J.Griggs, and Maskell K. (eds.). 1997. Stabilisation of atmospheric greenhouse gases: physical, biological and socio-economic implications. IPCC Technical Paper III, Geneva, Switzerland.

Hughes, T., Y.M. Wang, and R. Hansen, 1994. Impacts of projected climate change on urban water use: An application using the Wasatch water demand and supply model. U. S. Bureau of Reclamation, Provo, Utah.

Hunt, T.M. and H.M. Bibby, 1992. Geothermal hydrology, p147-166. In: M.P. Mosley (ed). Waters of New Zealand. New Zealand Hydrological Society, Wellington.

Hurd, B., N. Leary, R. Jones, and J. Smith, 1999. Relative regional vulnerability of water resources to climate change. Journal of the American Water Resources Association, 35:1399-1409.

Hurnard, S.M. and J.D. Coulter, 1979. Rainfall in New Zealand, p.10-22. In: S.M. Murray and P. Ackroyd (eds) Physical hydrology: the New Zealand experience. New Zealand Hydrological Society, Wellington.

Huth, R., 1999. Statistical downscaling in central Europe: evaluation of methods and potential predictors. Climate Research, 13:91-101.

Imbrie, J. and K.P. Imbrie, 1984. Ice ages: solving the mystery. London Macmillian.

IPCC, 1990. Climate change. The IPCC scientific assessment. J.T. Houghton, G.J. Jenkins, and J.J. Ephrauns (eds.), Cambridge University Press, Cambridge, United Kingdom.

IPCC, 1996a. Climate Change 1965: Impacts, adaptations, and mitigation: Contribution of Working Group II to the second assessment report of the Intergovernmental Panel on Climate Change, Cambridge University Press.

IPCC, 1996b. Climate Change 1995: The science of climate change. Summary for policy makers and technical summary of the Working Group I report, IPCC, Geneva.

IPCC, 1997. An Introduction to simple climate models used in the IPCC second assessment report. IPCC, Geneva.

Johns, T.C., R.E. Crossley, J.F. Gregory, J.M. Mitchell, J.F.B. Senior, C.A. Tett, and R.A. Wood, 1997. The second Hadley Centre model ocean-atmosphere GCM: Model description, spinup, and validation, Climate Dynamics, 13:103-134.

Jones, J.A.A., 1997. Global Hydrology: processes, resources and environmental management. Longman, Singapore.

Jones, P.D., M. Hulme, and K.R. Briffa, 1993. A comparison of Lamb circulation type with an objective classification scheme. International Journal of Climatology, 13:655-663.

Jowett, I., 1992. River hydraulics and instream habitat modelling for river biota, p.249-264. In: M.P. Mosley (ed), Waters of New Zealand. New Zealand Hydrological Society, Wellington.

Kaczmarek, Z., 1993. Water balance model for climate impact analysis, ACTA Geophysica Polonica, 41:1-16.

Kaczmarek, Z. and D. Krasuski, 1991. Sensitivity of water balance to climate change and variability. IIASA Working Paper, WP-91-047, Laxenburg, Austria.

Karl, T.R, P.D. Jones, R.W. Knight, G. Kukla, N. Plummer, V. Ruzuvayev, K.P. Gallo, J. Lindseay, R.J. Charleson, and T.C. Petersen, 1993. Asymmetric trends of daily maximum and minimum temperature: empirical evidence and possible causes. Bulletin of the American Meteorological Society, 74:1007-1023.

Karl, T.R., R.W. Knight, and N. Plummer, 1995. Trends in high-frequency climate variability in the twentieth century. Nature, 377:217-220.

Karl, T.R., W.C. Wang, M.E. Schlesinger, R.W. Knight, and D. Portman, 1990. A method of relating general circulation model simulated climate 1: Seasonal Statistics. Journal of Climate, 3:1053-1079.

Karl, T.R. and W.E. Riebsame, 1989. The impacts of decadal fluctuations in mean precipitation and temperature on runoff: a sensitivity study over the United States. Climatic Change, 15:423-447.

Kattenberg, A., F. Giorgi, H. Grassl, G.A. Meehl, J.F.B. Mitchell, R.J. Stoufer, T. Tokioka, A.J. Weaver, and T.M.L. Wigley, 1996. Climate models-projections of future climate In: J.T. Houghton, L.G. Meira, B.A. Callander, N. Harris, A. Katternberg, and K. Maskell (eds.), Climate change 1995: The science of climate change. Cambridge University Press Cambridge.

Katz, R.W. and B.G. Brown, 1992. Extreme events in a changing climate: variability is more important than averages. Climatic Change, 21:289-302.

Keeling, C. D. and T. P. Whorf, 1998. Atmospheric CO2 records from sites in the SIO air sampling network. Trends: A compendium of data on global change, Carbon Dioxide Information Analysis Center, Oak Ridge National Laboratory, Oak Ridge.

Kendall, M.G. and A. Stuart, 1961. The advanced theory of statistics Vol. 2. Griffin, London.

Kenny, G.J., R.A. Warrick, N.D. Mitchell, A.B. Mullan, and M.J. Salinga, 1994. CLIMPACTS: An integrated model for assessment of the effects of climate change on New Zealand environment. Journal of Biogeography, 22:883-895.

Kidson, J.W. and C.S. Thompson, 1998. A comparison of statistical and model-based downscaling techniques for estimating local climate variations. Journal of Climate, 11:735-753.

Kidson, J.W. and I.G. Watterson, 1995. A synoptic Climatological Evaluation of the Changes in the SCIRO nine-level model with doubled CO_2 in the New Zealand region. International Journal of Climatology, 15:1179-1194.

Kim, J.W., J.T. Chang, N.L. Baker, D.S. Wilks, and W.L. Gates, 1984. The statistical problem of climate inversion: Determination of relationships between local and large-scale climate. Monthly Weather Review, 112:2069-2077.

Kirshen, P.H. and N.M. Fennessey, 1995. Possible climate-change impacts on water supply of Metropolitan Boston. Journal of Water Resources Planning and Management, 121:61-70.

Klein, W.H., 1982. Statistical weather forecasting on different time scales. Bulletin of American Meteorological Society, 63:170-177.

Klein, W.H. and H. Bloom, 1989. An operational system for specifying monthly precipitation amounts over the United States from the field of concurrent 700mb heights. Weather Forecasting, 4:51-60.

Klemes, V., 1983. Conceptualization and scale hydrology. Journal of Hydrology, 65:1-23.

Klemes, V., 1985. Sensitivity of water-resource systems to climate variations. WCP Report no. 98, World Meteorological Organization, Geneva, Switzerland.

Klemes, V., 1986. Operational testing of hydrological simulation models. Hydrological Sciences Journal, 31:13-24.

Lasaga, A. C. and R. A. Berner, 1998. Fundamental aspects of quantitative models for geochemical cycles, Chemical Geology, 145:161-175.

Leavesley, G.H., 1994. Modelling the effects of climate change on water resources - A review. Climatic Change, 28:159-177.

le Cun, Y., 1988. A theoretical framework for back-propagation. Reprint from the Proceedings of the connectionist models summer school, University of Toronto, Ontario, p.21-28.

Leemans, R. and W.P. Cramer, 1991. The IISSA database for mean monthly values of temperature, precipitation, and cloudiness on a global terrestrial grid. IIASA Research Report, RR-91-18.

Lettenmaier, D.P. and T.Y. Gan, 1990. Hydrologic sensitivities of Sacramentao-San Joaquin River basin, California, to global warming. Water Resources Research, 26:69-86.

Li, P., M.T.C. Fang, and J. Lucas, 1997. Modelling of submerged arc weld beads using self-adaptive offset neural networks. Journal of Materials Processing Technology, 71:288-298.

Lins, H.F. and Z.S. Eugene, 1998. Dialogue on water issues -Water resources and climate change -Managing the nation's water in a changing climate. Journal of the American Water Resources Association, 341:255-1264.

Liss, P. and L. Merlivat, 1986. Air-sea gas exchange rates, introduction and synthesis, p.113-128. In P. Buat-Menard (ed), The role of air-sea exchange in geochemical cycling. D. Reidel, Hingham, Mass.

Loaiciga H.A., J.B. Valdes, R.Vogel, and J. Garvey. 1996. Global warming and the hydrological cycle. Journal of Hydrology, 174:83-127.

Lowe D.J. and J.D. Green, 1987. Origins and development of lakes, p.1-64. In: M.P. Mosley (ed), Inland waters of New Zealand. Department of Scientific and Industrial Research, Wellington.

Maier-Reimer, E., and K. Hasselmann, 1987. Transport and storage of CO_2 in the ocean - an inorganic ocean-circulation carbon cycle model. Climate Dynamics, 2:63-90.

Markham A., N. Dudley, and S. Stolton, 1993. Some like it hot. WWF International, CH-1196 Gland, Switzerland.

Marland, G., R. J. Andres, T. A. Boden, C. Johnson, and A. Brenkert, 1999. Global, regional, and national CO_2 emission estimates from fossil fuel burning, cement production, and gas flaring: 1751-1996, CDIAC, Carbon Dioxide Information Analysis Center, Oak Ridge National Laboratory, Oak Ridge.

Matyasovszk, I. and I. Bogardi, 1995. Simulating probability distribution of surface climatic variables from free-atmosphere quantities. In reprints of the 6th International Meeting on Statistical Climatology, Galway, I.R., p.49-52.

Maunder W.J., 1971. The climate of New Zealand–physical and dynamic features, p.213-127. In: J. Gentilli. (ed), Climates of Australia and New Zealand. Elsevier Pub. Co.

McCabe, G.J. and D.M. Wolock, 1992. Effects of climatic change and climatic variability on the Thomthwaite moisture index in the Delaware River Basin. Climate Change, 20:143-159.

McCabe G.J. and D.M. Wolock, 1992. Sensitivity of irrigation demand in humid-temperate region to hypothetical climatic change. Water Resources Bulletin, 28:535-543.

McCabe G.J. and M.A. Ayers, 1989. Hydrologic effects on climate change in the Delanare River Basin. Water Resources Bulletin, 25:1231-1242.

McDowall R.M., 1993. Floods savage the Grey River fish fauna. Water & Atmosphere, 4:16-17.

McGlone, M.S., 1988. New Zealand Handbook of Vegetation Science, 7. B. Huntley and Webb (eds).

McGuffie K. and A. Handerson-Sellers, 1994. Cloudness trends this century from surface observations. Proceedings of the international Minimax workshop College Park, Maryland, U.S. Department of Energy, CON- 9309350, p.231-234, Washington D.C.

McGuffie, K. and A. Henderson-Sellers, 1997. A Climate modelling primer. John Wiley & Sons. Second Edition, New York.

Mearns, L.O., F. Giorgi, L. McDaniel, and C. Shields, 1995. Analysis of daily variability of precipitation in a nested regional climate model: comparison with observations and doubled CO_2 results. Global Planet Change, 10:55-78.

Mehra, P. and B.W. Wah, 1992. Artificial neural networks, p.1-12. In: P. Mehra and B.W. Wah (eds.), Artificial neural networks: concepts and theory: Los Alamitos, Calif. IEEE Computer Society Press.

Mildenhall, D.C. and P.R. Moore, 1983. A late Holocene sequence at Turakirae Head, and climatic and vegetational change in Wellington area in the last 10,000 years. New Zealand Journal of Science, 26:447-459.

Miller, K.A., 1990. Water, Electricity, and Institutional Changes, p.376-393. In: P. E. Waggoner (ed), Climate Change and U.S. Water Resources, 367-393. John Wiley and Sons, New York.

Mimikou, M.A. and Y.S. Kouvopoulos, 1991. Regional climate change impacts: impacts on water resources. Hydrologic Science Journal, 36:247-258.

Ministry of Civil Defence, 1994. National report. Tephra, 13:1-48.

Ministry of Environment, 1992. Water Quality Guidelines no.1. Guidelines for control of undesirable biological growths in water. Ministry of Environment Wellington.

Mitchell, J..F.B, 1989. The 'greenhouse effects' and climate. Reviews of Geophysics and Space Physics, 27:115-139.

Mitchell, J.F.B., R.A. Davis, W.J. Ingram, and C.A. Senior, 1995. On surface temperature, greenhouse gases, and aerosols: Models and observations. Journal of Climate, 8:2364-2386.

Mitchell, J.F.B. and T.C. Johns, 1997. On Modification of Global Warming by Sulphate Aerosoils. Journal of Climate, 10:245-267.

Molly, L.F. (compiler), 1980. Land alone endures: Land use and the role of research. Department of Scientific and Industrial Research, Wellington.

Mosley, M.P., 1988. Climatic change impacts on water resources. In: Climate Change: The New Zealand Response. Ministry for the Environment: Wellington.

Mosley, M.P. (ed), 1992. New Zealand waters. The Hydrological Society, Wellington.

Mpelasoka, F. S., A.B. Mullan, and R.G. Heerdegen, 2000. New Zealand climate change information derived by multivariate statistical and artificial neural network approaches. International Journal of Climatology (accepted).

MucGinnis, D.L., 1997. Estimating climate-change impacts on Colorado Plateau Snowpack using Downscaling methods. Professional Geographer, 49:117-125.

Mullan, A.B., 1993. Current status of climate change modelling in New Zealand. National science strategy committee for climate change, The Royal Society of New Zealand.Information Series 3.

Mullan, A.B., 1994. Climate change scenarios for New Zealand: Statement for Greenhouse '94. NIWA Climate Internal Report No. 94-004, August 1994

Mullan, A.B., D.S. Wratt, and J.A. Renwick, 2000. Transient model scenarios of climate change for New Zealand. Weather and Climate (submitted).

Nash, L.L. and P.H. Gleick, 1993. The Colorado River Climate Change. The sensitivity of streamflow and water supply to variations in temperature and precipitation. U.S. EPA 230-R-93-009.

Nathan, R.J., T.A. McMahon, and B.L. Finlayson, 1988. The impact of greenhouse effect on catchment hydrology and storage-yield relationships in both winter and summer rainfall zones. In: G.I. Pearman, (ed), Greenhouse, planning for climate change. Division of Atmospheric Research, CSIRO, East Melbourne, Australia.

Nemec, J. and J. Schaake, 1982. Sensitivity of water resource systems to climate variation. Journal of Scientific Hydrology, 27:327-243.

Nicollas, N., G.V. Gruva, J. Jouzel, T.R. Karl, L.A. Ogallo and D.E. Parker, 1996. Observed variability and change. In: J.T. Houghton, F.L.G. Meira, B.A. Callander, N. Harris, A. Kattenberg, and K. Mashall (eds), Climate Change 1995. The Science of Climate Change. Cambridge University Press, Cambridge, UK.

Pao, Y. H., 1989. Adaptive Pattern Recognition and Neural Networks. Addison-Wesley, Reading, MA.

Pearson, C.P., 1992. Analysis of floods and low flows, p.95-116. In: M.P. Mosley (ed), Waters of New Zealand. New Zealand Hydrological Society, Wellington.

Peixoto, J.P. and A.H. Oort, 1993. Physics of Climate. American Institute of Physics, New York.

Penman, H.L., 1948. Natural evaporation from open water, bare Soil and grass. Proc. R. Soc. Longdon, vol A193, p.120-145.

Pittock, A.B. and M.J. Salinger, 1982. Towards regional scenarios for a carbon dioxide warmed earth. Climate Change, 4:23-40.

Prather, M., P. Midgley, F. S. Rowland, and R. Stolarski, 1996. The ozone layer: The road not taken. Nature, 381:551-554.

Prather, M. J., 1996. Time-scales in atmospheric chemistry: Theory, GWP's for CH and CO, and runaway growth. Geophysical Research Letters, 23: 2597-2600.

Prather, M. J., 1998. Time scales in atmospheric chemistry: Coupled perturbations to N2O, NOy, and O3. Science, 279:1339-1341.

Priestley, C. and R. Taylor, 1972. On the assessment of surface heat flux and evaporation using large scale parameters. Monthly Weather Review, 100:81-92.

Ramanathan, V., R. J. Cicerone, H. B. Singh, and J. T. Kiehl, 1985. Trace gas trends and their potential role in climate change. Journal of Geophysical Research, 90:5547-5566.

Renwick, J.A., J.J. Katzfey, J.L. McGreor, and K.C. Nguyen, 1999. On regional model simulations of climate change over New Zealand. Weather and Climate, 19:3-14.

Renwick, J.A., J.J. Katzfey, K.C. Nguyen, and J.L. McGreor, 1998. Regional model simulation of New Zealand climate. Journal of Geophysical Research, 103:5973-5982.

Richman, M.B., 1988. A cautionary note concerning a commonly applied eigen analysis procedure. Tellus, 40B, p.50-58.

Riebsame, W.E, 1988. Adjusting water resources management to climate change. Climatic Change, 13:69-97.

Riebsame, W.E., 1994. Rivers. Climatic Change, 13:69-97.

Rosenberg, N.J., B.A. Kimball, P. Martin, and C.F. Cooper, 1990. From Climate and CO_2 Enrichment to Evapotranspiration, p.151-175. In: P. E. Waggoner (ed), Climate change and U.S. water resources. John Wiley and Sons, New York.

Rothrock, D.A., Y. Yu, and G.A. Maykut, 1999. Thinning of the Arctic sea-ice cover. Geophysical Research Letters, 26:3469-3472.

Rott, H., Skvarca P., and Nagler T., 1996. Rapid collapse of the northern Larsen ice shelf. Antarctica. Science, 271:788-792.

Russo J.M. and J.W. Zack, 1997. Downscaling GCM output with mesoscale model. Journal of Environmental Management, 49:19-29.

Salinger, M.J., 1995. Forthcoming. Proceedings of Greenhouse '94', a conference on greenhouse gases and climate issues. National Institute of Water and Atmosphere Research (NIWA), Wellington.

Salinger, M.J. and A.B. Mullan, 1999. New Zealand climate: temperature and precipitation variations and their link with atmospheric circulation 1930-1994. International Journal of Climatology, 19:1049-1071.

Salinger, M.J. and D.M. Hicks, 1990. The scenarios, p.12-18. In: Climate change: impacts on New Zealand. Ministry of Environment, Wellington.

Salinger, M.J., R. Allan, N. Bindoff, J. Hannah, B. Lavery, Z. Lin, J. Lindesay, N. Nicholls, N. Plummer, and S. Torok, 1996. Observed variability and climate change and sea level in Australia, New Zealand and the South Pacific, p.100-127. In: W.J. Bourma and G.I. Pearman (eds), Green house: coping with climate change. CSIRO, Australia.

Santer, B. D., T. M. L. Wigley, T. P. Barnett, and E. Anyamba, 1996. Detection of climate change and attribution of causes, p.407-443. In: J. T. Houghton, L. G. M. Filho, B.A. Callander, N. Harris, A. Kattenberg, and K. Maskell (eds), Climate Change 1995: The Science of Climate Change. Cambridge University Press, Cambridge, UK.

Sarmiento, J. L., J. C. Orr, and U. Siegenthaler, 1992. A perturbation simulation of CO_2 uptake in an ocean general circulation model. Journal of Geophysical Research, 97:3621-3645.

Saunders, M.A., 1999. The Earth's future climate. A-Mathematical, Physical and Engineering science, 357:3459-3480.

Schaake, J., 1990. From Climate to Flow, p. 177-206. In: P. E. Waggoner (ed), Climate change and U.S. water resources. John Wiley and Sons, New York.

Schimel, D., D. Alves, I. Enting, M. Heimann, F. Joos, D. Raynaud, T. Wigley, M. Prather, R. Derwent, D. Ehhalt, P. Fraser, E. Sauhueza, X. Zhou, P. Jonas, R. Charlson, H. Rodhe, S. Sadasivan, K. P. Shine, Y. Fouquart, V. Ramaswamy, S. Solomon, J. Srinivasan, D. Albritton, R. Derwent, I. Isaksen, M. Lal, and D. Wuebbles, 1996. Radiative forcing of climate change, p.65-131. In: J. T. Houghton, L. G. M. Filho, B. A. Callander, N. Harris, A. Kattenberg, and K. Maskell (eds), Climate Change 1995: The Science of Climate Change. Cambridge University Press, Cambridge, UK.

Schlesinger, M. E. and N. Ramankutty, 1994. An oscillation in the global climate system of period 65-70 years. Nature, 360:330-333.

Schneider, S.H., 1989. The greenhouse effect: Science and policy. Science, 243:771-781.

Schneider, S.H., P.H. Gleik and L. O. Mearns, 1990. Prospects for Climate Change, p. 41-73. In: P.E. Waggoner (ed), Climate change and U.S. water resources. John Wiley and Sons, New York.

Scott, D.A. (ed), 1996. A directory of wetlands in New Zealand. Department of Conservation, Wellington.

Seaman, R.S. and M.F. Hutchinson, 1985. Comparative real-data tests of some objective analysis methods by withholding observations. Australian Meteorological Magazine, 33, 37-46.

Shannon, D.A. and B.C. Hewitson, 1996. Cross-relationships regarding local temperature inversions at Cape Town and global climate change implications. South African Journal of Science, 92:213-216.

Sharma, S., 1996. Applied multivariate techniques. John Wiley and Sons, New York.

Shaw, E.M., 1983. Hydrology in Practice. Van Nostrand Reinhold (UK) Co. Ltd.

Shine, K.P. and P.M. D. Forster, 1999. The effects of human activity on radiative forcing of climate change: a review of recent developments. Global & Planetary Change, 20:205-225.

Shuttleworth, W.J., 1993. Evaporation, p.4.1-4.53. In: D.R Maidment,. (ed.) Handbook of hydrology. McGraw Hill Book Company, New York.

Skiles, J.W. and J.D. Hanson, 1994. Responses of arid and semi-arid watersheds to increasing carbon dioxide and climate change as shown by simulation studies. Climatic Change, 26:377-397.

Spigel, R.H. and A.B. Viner, 1992. Lakes, p.305-334. In: M.P. Mosley (ed), Waters of New Zealand. New Zealand Hydrological Society, Wellington.

Stallard, R. F., 1998. Terrestrial sedimentation and the carbon cycle: Coupling weathering and erosion to carbon burial. Global Biogeochemical Cycles, 12:231-257.

Sundquist, E. T., 1990. Long-term aspects of future atmospheric CO_2 and sea-level changes p.193-207. In: R. Revelle (ed), Sea-level change. National Academy Press, Washington, DC.

Taylor, R., P. Cochrane, B. Sptephenson, and N. Gibbs, 1997. The state of New Zealand's environment. I. Smith, A. Saunders, D. Swain, and B. Wall (eds), Ministry of the Environment, Wellington.

Thom, H.G.S., 1958. A note on the Gamma distribution. Monthly Weather Review, 88:117-122.

Thornthwaite, C.W., 1948. An approach towards a rational classification of climate. Geographical Review, 38:55-94.

Thornthwaite, C.W., and J.R. Mather, 1955. The water balance. Drexel Inst. Lab. Climatol. Centerton, N.J., Publication in Climatology.

Thorpe, H., 1992. Groundwater-the hidden resource, p.167-186. In: M. P. Mosley (ed), Waters of New Zealand. New Zealand Hydrological Society, Wellington.

Todini, E., 1988. Rainfall runoff modeling past, present, and future. Journal of Hydrology, 100:341-352.

Toggweiler, J. R., K. Dixon, and K. Bryan, 1989. Simulations of radiocarbon in a coarse-resolution, world ocean model, II, Distributions of bomb-produced ^{14}C, Journal of Geophysical Research, 94:8243-8264.

Trenberth, K.E. and T.J. Hoar, 1996. The 1990-1995 El Niño-southern oscillation event: longest on record. Geophysical Research Letters, 23:57-60.

Tsonis, A.A., 1996. Widespread increases in low-frequency variability of precipitation over the past century. Nature, 382:700-702.

United Nations Environmental Programme, 1997. Understanding climate change. UNEP/IUC, Châtelaine, Switzerland.

Vaughan, D.G. and Doake C.S.M., 1996. Recent atmospheric warming and retreat of ice shelves on the Antarctic peninsula. Nature, 379:328-330.

Viner, D. and M. Hulme, 1997. The climate impacts LINK Project: Applying results from the Hadley centre's climate change experiments for climate impacts assessments. Climatic Research Unit, UEA Norwich, UK.

von Storch, H., E. Zorita, and U. Cubasch, 1993. Downscaling of global climate change estimates to regional scales: An application to Iberian rainfall in wintertime. Journal of Climate, 6:1161-1171.

Waggoner P. E. (ed), 1990. Climate change and U.S. water resources. John Wiley and Sons, New York.

Wang, W.-C., M. P. Dudek, and X.-Z. Liang, 1992. Inadequacy of effective CO_2 as a proxy in assessing the regional climate change due to other radiatively active gases. Geophysical Research Letters, 19:1375-1378.

Wang, W.-C., M. P. Dudek, X.-Z. Liang, and J. T. Kiehl, 1991. Inadequacy of effective CO_2 as a proxy in simulating the greenhouse effect of other radiatively active gases. Nature, 350:573-577.

Watson, R.T., M.C. Zinyowera, R.H.Moss (eds), 1997. The Regional Impacts of climate change: An assessment of vulnerability. A special report of IPCC Working group II, Cambridge University Press.

Whetton, P., A.B. Mullan, and A.B. Pittock, 1996. Climate-change scenarios for Australia and New Zealand, p.145-168. In: W. J. Bourma and G. I. Pearman (eds), Green house: coping with climate change. CSIRO, Australia.

Wigley, T.M.L., P.D. Jones, K.R. Briffa, and G. Smith, 1990. Obtaining sub-grid-scale information from coarse-resolution general circulation model output'. Journal of Geophysical Research, 95:1943-1953.

Wilby, R.L., 1995. Greenhouse hydrology. Progress in Physical Geography, 19:351-369.

Wilk, M.B. and R. Gnanadesikan, 1968. Probability plotting methods for the analysis of data. Biometrika, 55:1-17.

Wolocket, D.M., G.J. McCabe, G.D. Tasker, and M.E. Moss, 1993. Effects of climate change on water resources in the Delawere River basin. Water Resources, Bulletin, 29:475-486.

World Meteorological Organization (WMO), 1975. Intercomparison of conceptual models used in operational hydrological forecasting. Operational. Hydrology Report no.7, WMO, Geneva, Switziland.

Xu, C.-Y., J. Seffiert, and S. Halldin, 1995. Regional water balance modelling in the NOPEX area: development and application of monthly water balance models. Journal of Hydrology, 180:195-210.

Yates, D.N. and K.M. Strzepek, 1994. Comparison of models for climate change assessment of river runoff. IIASA working paper, WP94-45, Laxenburg Austria.

Yevjevich, V., 1972. Probability and statistics in hydrology. Water Resources Publications Fort Collins, Colorado, U.S.A..

Zhang, Y., J.M. Wallace, and D.S. Battisti, 1997. ENSO-like interdecadal variability: 1900-93. Journal of Climate, 9:1004-1020.

Appendices

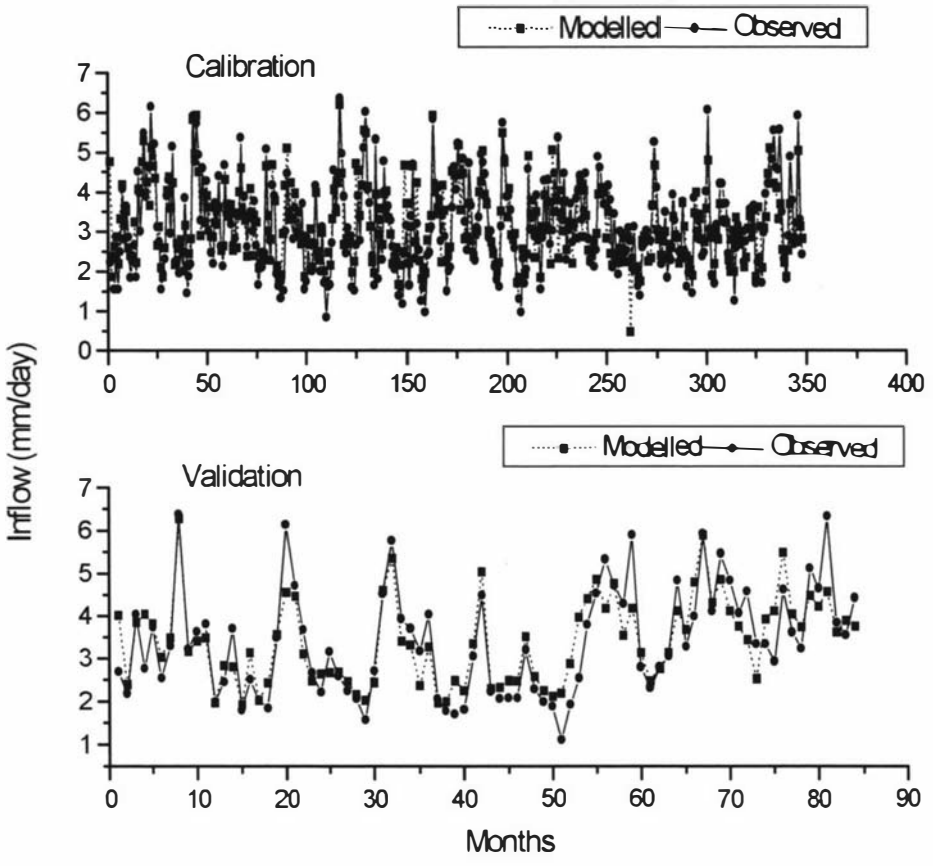

Figure A1 Observed versus modelled monthly Lake Taupo inflows for calibration (1961-1990) and validation (1991-1996) periods.

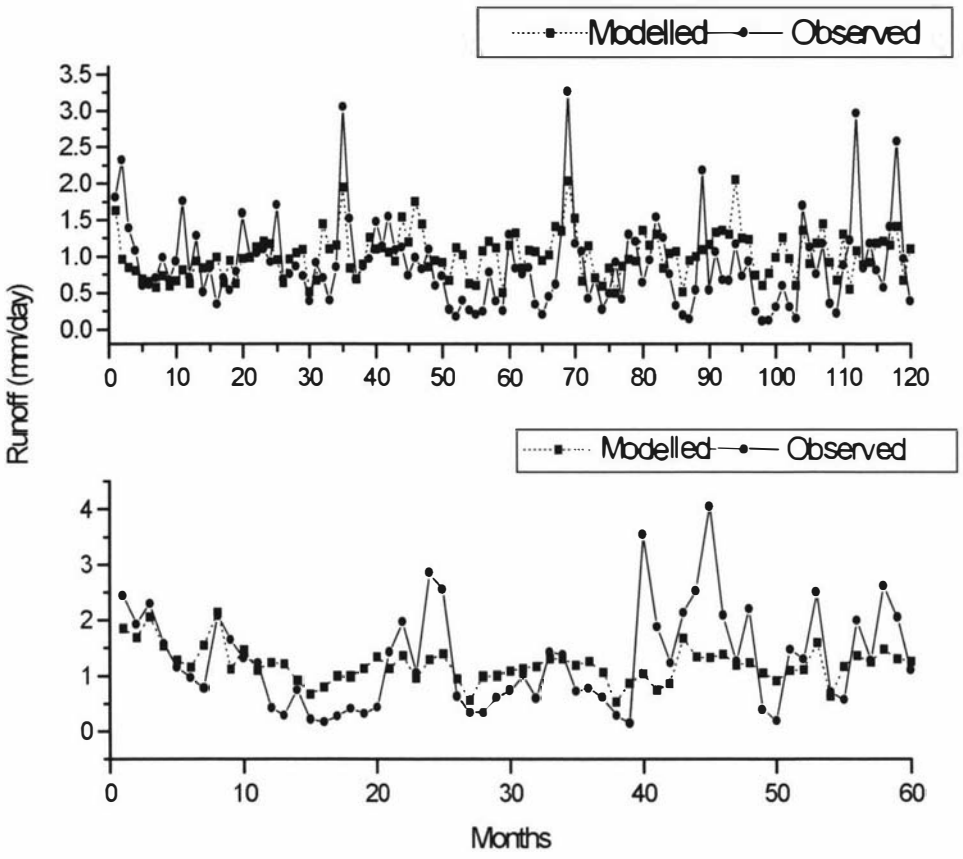

Figure A2 Observed versus modelled monthly runoff of the Opihi River at Saleyards Bridge for calibration (1965-1974) and validation (1975-1979) periods.